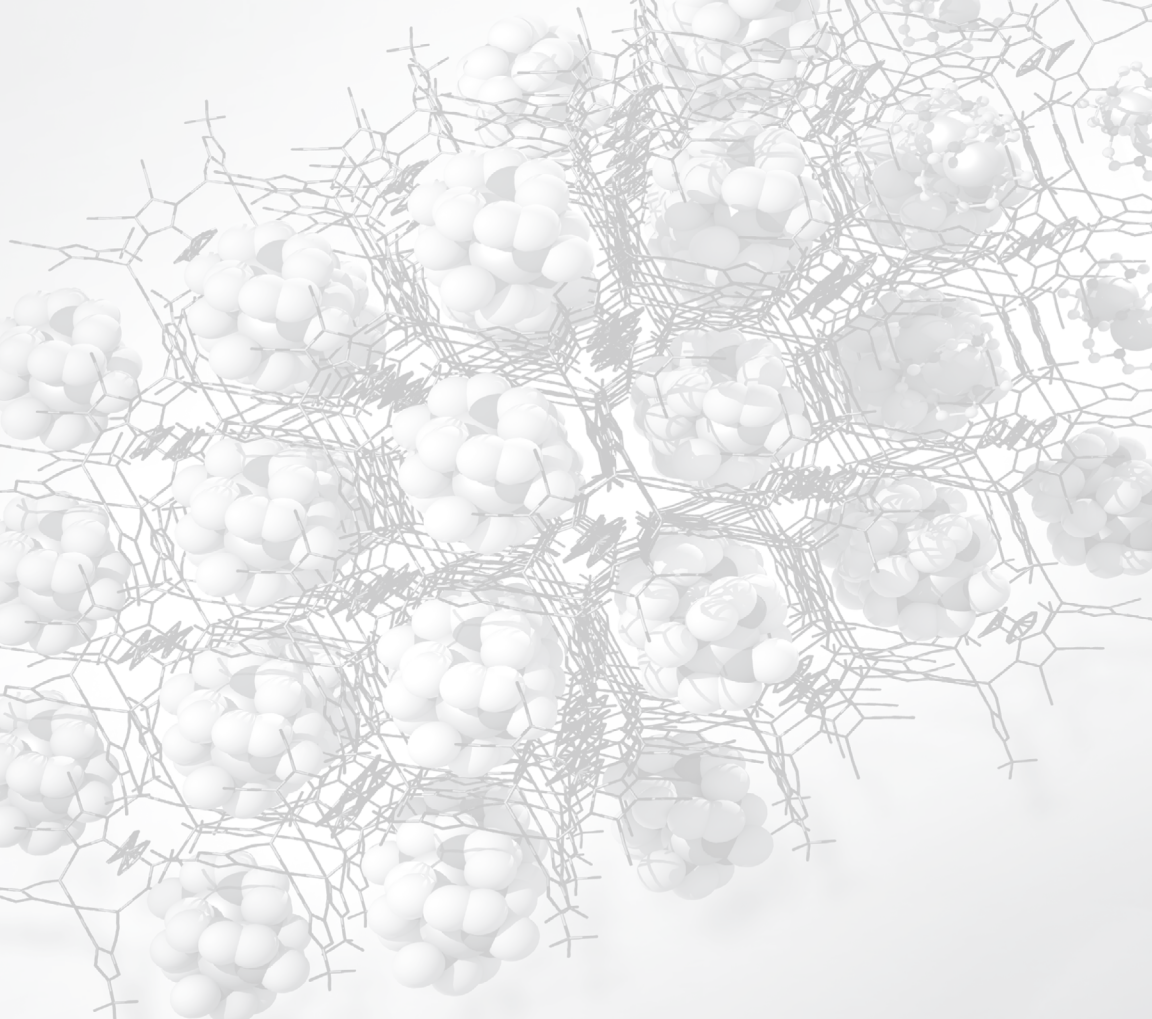


# Designing Electrolytes for Lithium-Ion and Post-Lithium Batteries

edited by  
**Władysław Wieczorek | Janusz Płocharski**





## Designing Electrolytes for Lithium-Ion and Post-Lithium Batteries



Taylor & Francis

Taylor & Francis Group

<http://taylorandfrancis.com>

# **Designing Electrolytes for Lithium-Ion and Post-Lithium Batteries**

**edited by**  
**Władysław Wieczorek**  
**Janusz Płocharski**



*Published by*

Jenny Stanford Publishing Pte. Ltd.  
Level 34, Centennial Tower  
3 Temasek Avenue  
Singapore 039190

Email: editorial@jennystanford.com  
Web: www.jennystanford.com

**British Library Cataloguing-in-Publication Data**

A catalogue record for this book is available from the British Library.

**Designing Electrolytes for Lithium-Ion and Post-Lithium Batteries**

Copyright © 2021 Jenny Stanford Publishing Pte. Ltd.

*All rights reserved. This book, or parts thereof, may not be reproduced in any form or by any means, electronic or mechanical, including photocopying, recording or any information storage and retrieval system now known or to be invented, without written permission from the publisher.*

For photocopying of material in this volume, please pay a copying fee through the Copyright Clearance Center, Inc., 222 Rosewood Drive, Danvers, MA 01923, USA. In this case permission to photocopy is not required from the publisher.

ISBN 978-981-4877-16-9 (Hardcover)  
ISBN 978-1-003-05093-3 (eBook)

# Contents

*Introduction: Challenges toward Designing Novel Electrolytes  
for Modern Lithium-Ion and Post-Lithium Batteries*

xi

*Janusz Płocharski and Władysław Wieczorek*

## PART I

### Novel Electrolytes for Lithium Batteries

<b>1 New Strategies in Designing Salts and Solutions for the New Generation of Electrolytes</b>	<b>3</b>
<i>Leszek Niedzicki and Marta Kasprzyk</i>	
1.1 Introduction	3
1.2 Anion Structure Impact	4
1.3 Requirements toward Electrolyte	8
1.4 Classes of Anions Investigated So Far	9
1.5 Properties of Anion Classes Investigated So Far	11
1.6 Properties of Commonly Used Salts	13
1.7 Strategy for New Anion Design	16
1.8 Anions Designed with the New Described Strategy	19
1.9 Other Concepts	22
1.10 Electrolyte Design: Solvent Effect	24
1.11 Electrolyte Design: Maximizing Parameters	27
1.12 Other Electrolytes for Li-Ion Cells	30
1.13 Anions for Post-Li-Ion Cells	33
1.14 Examples of Electrolytes for Li-Ion Cells	34
<b>2 X-Ray Crystallography in Developing New Electrolyte Systems Based on Heterocyclic Anions</b>	<b>43</b>
<i>Maciej Dranka and Janusz Zachara</i>	
2.1 Introduction	43

2.2	Aggregation Phenomena: Solid-State and Concentrated Liquid Electrolytes	45
2.3	Crystal Structure Analysis: Hints about the Properties of Heterocyclic Anions	46
2.4	Structural Studies of LiTDI Solvates with Glymes: Disproportionation Mechanism	51
2.5	Structural Studies of Sodium Salts with Heterocyclic Anions	57
2.6	Structural Studies of Lithium Salt Hydrates with Dicyanoimidazole Anions	61
2.7	Conclusions	64
<b>3</b>	<b>Overview of Polymer and Solid Electrolytes: Towards All Solid-State Batteries</b>	<b>71</b>
	<i>Michał Marzantowicz and Michał Struzik</i>	
3.1	Introduction	71
3.2	Classification of Polymer Electrolytes	72
3.3	Dissociation and Transport of Ions: Microscopic View	74
3.3.1	Dissociation	74
3.3.2	Ion Transport	76
3.4	Quantitative Models for Describing Ion Transport	79
3.4.1	Arrhenius Model	79
3.4.2	Vogel–Tammann–Fulcher Model	81
3.4.3	Conductivity of an Inhomogeneous Medium: Percolation Models	83
3.5	Lithium Transference Numbers	85
3.6	Polymer Electrolyte as an Element of the Cell: Electrolyte/Electrode Interface	88
3.7	Examples of Solid Polymer Electrolytes	91
3.7.1	Polymer with a Salt	91
3.7.1.1	Electrolytes based on PEO	91
3.7.1.2	Electrolytes based on other polymers	94
3.7.2	Organic/Inorganic Composite Systems	96
3.7.3	Polymer in a Salt and Systems with Ionic Liquids	101
3.7.4	Polyelectrolytes and Oligomeric Salts	107
3.8	Ceramic Electrolytes	110
3.8.1	NASICON-Type Conductors	112

3.8.2 Electrolytes with Perovskite Structure	114
3.8.3 Lithium Sulfides	116
3.8.4 Electrolytes with a Garnet Structure	118
 <b>PART II</b>	
<b>Electrolytes for Post-Lithium-Ion Systems</b>	
<b>4 Electrolytes for Sodium and Sodium-Ion Batteries</b>	<b>141</b>
<i>Marek Marcinek, Anna Bitner-Michalska, Anna Szczęsna-Chrzan, and Tomasz Trzeciak</i>	
4.1 Introduction	141
4.2 Electrolyte	146
4.2.1 Solvents and Systematics	147
4.2.1.1 Liquid electrolytes	147
4.2.1.2 Ionic liquid-based electrolytes	150
4.2.1.3 Gel systems	152
4.2.1.4 Polymer electrolytes	153
4.2.2 Salts	154
4.3 Summary	156
<b>5 Multivalent Cation Systems: Electrolytes for Magnesium Batteries</b>	<b>165</b>
<i>Janusz Płocharski</i>	
5.1 Electrolytes Evolved from Grignard Compounds	167
5.2 Electrolytes with Boron Compounds	168
5.3 Electrolytes with Hexamethyldisilazide Ions	173
5.4 Simple Inorganic Electrolyte	174
5.5 Electrolytes with TFSI Anion	176
5.6 Miscellaneous Electrolytes	182
5.7 Comparison of Various Electrolyte Systems	183
5.8 Problem of Dendrites	184
5.9 Summary	185
<b>6 Multivalent Cation Systems: Toward Aluminum, Zinc, and Calcium Batteries</b>	<b>191</b>
<i>Michał Piszcza and Maciej Siekierski</i>	
6.1 Introduction	191

6.2	Aluminum	195
6.2.1	Water-Based Electrolytes	196
6.2.2	Nonaqueous Systems	199
6.3	Calcium	203
6.4	Zinc	206
6.5	Conclusions	207
<b>7</b>	<b>Electrolytes for Metal-Air Batteries</b>	<b>215</b>
<i>Maciej Siekierski, Michał Piszcza, and Grażyna Żukowska</i>		
7.1	Introduction	215
7.2	Lithium-Air Systems	217
7.2.1	Organic and Polymeric Electrolytes	217
7.2.2	Aqueous	222
7.2.3	Ceramic and Glassy	227
7.2.4	Hybrid Systems	236
7.3	Sodium	242
7.4	Potassium	246
7.5	Magnesium	248
7.6	Calcium	251
7.7	Aluminum	251
7.8	Zinc	254
7.9	Miscellaneous	261
7.10	Conclusions	264
<b>8</b>	<b>Electrolytes for Lithium-Sulfur Batteries</b>	<b>293</b>
<i>Maciej Marczewski</i>		
8.1	Introduction	293
8.2	Electrolyte Requirements	296
8.3	Liquid Electrolytes	296
8.3.1	Carbonates	301
8.3.2	Ethers	302
8.3.3	Sulfones	303
8.3.4	Ionic Liquids	304
8.3.5	Concentrated Electrolytes	305
8.3.6	Novel Approach	305
8.4	Solid Electrolytes	306
8.4.1	Polymer Electrolytes	309

8.4.2 Ceramic Electrolytes	310
8.5 Additives	310
8.6 Summary	312
<i>Index</i>	319



Taylor & Francis

Taylor & Francis Group

<http://taylorandfrancis.com>

# Introduction: Challenges toward Designing Novel Electrolytes for Modern Lithium-Ion and Post-Lithium Batteries

Janusz Płocharski and Władysław Wieczorek

*Faculty of Chemistry, Warsaw University of Technology,  
Noakowskiego 3, 00-664 Warszawa, Poland*

Every electrochemical source of electric current is composed of two electrodes and a layer of electrolyte in-between. Since the storage capacity—the crucial appropriate property of such a device—depends predominantly on the composition and design of the electrodes, most of the research and development efforts have been focused on them and many review publications have been dedicated to this subject [1]. Considerably less attention has been paid to the electrolyte, the third basic component of a battery. This review attempts to fill this gap and give more information on the role of electrolytes in modern batteries, limitations of lithium-ion batteries resulting from nonoptimal properties of commercial electrolytes, and the scientific and engineering challenges related to novel electrolytes for improved lithium-ion as well as future post-lithium batteries.

An effective electrolyte must fulfill a series of requirements. The most basic ones are as follows:

- **Sufficient chemical and electrochemical stability:** Electrolyte solutions must be stable at highly oxidative potentials at a battery cathode and at highly reductive potentials at a battery anode during charging. Generally speaking, stronger bonds connecting the atoms result in higher stability of

molecules present in an electrolyte. In the case of electrochemical stability, it can be quantified as the highest occupied molecular orbital and the lowest unoccupied molecular orbital levels, which can be calculated for a given structure and observed experimentally as oxidation and reduction potentials, respectively. In practical cases, however, electrolyte stability is of a kinetic character since there are simply no polar solvents of sufficient thermodynamic robustness. Predictions of possible reactions leading to electrolyte degradation should also consider the presence of highly reactive electrolyte additives improving the durability and transport properties of interphase layers. These considerations should involve a particular environment in which the electrolyte components are designed to operate and their interactions with electrode materials at very low and/or very high electrical potentials. Another factor is that the electrode materials often have catalytic properties—graphite, carbon black, compounds of cobalt, manganese, nickel, and iron are known catalysts for organic reactions. Effects of this catalytic activity are more clearly visible in systems working at elevated temperatures. On top of that, electrolytes must not react with other components of a battery, like current collectors and casing, or these reactions would be hindered due to passivation processes. It is also highly recommended that electrolytes not react with compounds typically present in the environment, like oxygen and water.

- **High ionic conductivity:** Electrolytes should efficiently support the transport of ions migrating between electrodes in consecutive cycles of charging and discharging. Therefore, a high ionic conductivity is required within the whole range of operating temperatures. This is particularly important for systems designed for high current applications and short charging times. Ionic conductivity of electrolyte solutions depends obviously on the molecular structures of solvents and salts. To find optimal compositions and concentrations, viscosity measurements could be helpful since viscosity is inversely related to molar conductivity in many systems. Both parameters—viscosity and conductivity—are influenced

by the size and shape of an anion (type of cation is fixed in a given battery system). In fact, only the transport of active ions—lithium cations in the case of lithium-ion batteries—contributes to electricity generating processes. The dissociation of an electrolyte salt into simple cations as well as unfavorable neutral ionic pairs and higher charged agglomerates depends predominantly on the dissociation energy of the salt and its concentration. It is then recommended to measure a cation's transference number and its dependence on the salt concentration and temperature. So, even slightly lower total conductivity can be accepted if the related transference number is closer to unity. To calculate the value of ionic conductivity that actually yields energy over the continued discharge of the cell, one needs to multiply the cation transference number by the total ionic conductivity ( $\sigma_{\text{Li}^+} = \sigma T_{\text{Li}^+}$ ).

- **Fulfilling the demands of the economy:** The commercial success of a particular battery design can be achieved only when the full cost of all components is economically justified. The typical material cost of the electrolyte in a battery does not exceed 10% of the total cost of all its active and inactive components [2]. In addition, the material costs of the necessary components are only a small part of all the expenses of a ready-to-use battery pack, which must also include investment and operation costs of a production plant, marketing, cost of capital, etc. This is a clear reason for the observable inertia of the industrial companies reluctant to introduce new components if they offer only slightly improved properties in comparison to the existing solutions. It is worth mentioning here, as we write about electrolytes, that notable costs are related to electrolyte handling, for example, a controlled/protective atmosphere for storage, desiccation processes, and cell assembly.
- **Acceptable operational and environmental safety:** A battery must obviously be safe during its whole life and even in emergency situations. In particular, a battery should not catch fire, explode, or release toxic or corrosive gases even when it is damaged, unsealed, overheated, or improperly used. This is a

really tough requirement since a charged battery stores a lot of chemical energy and a typical electrolyte is made of flammable organic solvents containing compounds that generate toxic fumes. It is also critical to know what gaseous decomposition products can be released upon solid-electrolyte interphase (SEI) formation, thermal decomposition, and long-term exposure to high temperatures.

A battery should also be safe for the environment when discarded or recycled. The electrolytes in present use hardly fulfill this requirement. This kind of toxicity is mostly connected to fluorine, phosphorous, or arsenic content in electrolyte salts as well as in their thermal, chemical, or electrochemical decomposition products. Biological compatibility or ease of migration through the skin and/or cell membrane, as well as its carcinogenicity and/or mutagenicity, is also a potential risk factor if the salt or its decomposition products are toxic.

A short review of all the above requirements leads to the conclusion that there can be nothing like an ideal electrolyte. Instead we will rather search for a compromise to prepare "the least imperfect" electrolyte offering an acceptable combination of advantages and drawbacks.

- **Electrolytes in present use:** Today, almost all commercial lithium-ion batteries use the same electrolyte. This is 1.2 M solution of lithium hexafluorophosphate ( $\text{LiFP}_6$ ) in a mixture of ethylene carbonate and ethyl methyl carbonate. Typically, some additives, like vinylene carbonate (VC), are used in order to improve the formation of stable and ionically conductive passive layers on negative electrodes (the so-called SEI). This electrolyte has a conductivity slightly exceeding 10 mS/cm at room temperature; electrochemical stability of >4.8 V versus that of the Li/Li<sup>+</sup> redox pair, which is sufficient for the presently used cathodes based on  $\text{Li}_{1-x}\text{CoO}_2$ ; and does not create problems with other components of a battery system; detrimental corrosion of aluminum connectors is observed when some other electrolyte salts are used. On the other hand, the electrolyte undergoes decomposition above 70°C and is

very sensitive to traces of water—hydrolysis reactions take place, resulting in the emission of harmful hydrogen fluoride.

## Challenges

A comparison of the above requirements with the properties of electrolytes in use clearly indicates the fields of necessary development. The expected improvements are often real challenges and should be preceded by extensive fundamental research. In fact, the battery industry waits now for an effective replacement of the LiPF<sub>6</sub> salt. The new one should offer a comparable level of ionic conductivity and support passivation of typical current collectors. On top of that, the new compound should be chemically and thermally stable, which means inhibition of hydrolysis reactions and resistance against temperatures far above 100°C. The molecular weight of such a salt should be relatively low because high molar concentrations are typically required. In addition, the planned introduction of the so-called high-voltage cathodes operating at about 5 V versus Li/Li<sup>+</sup> requires electrolytes of enhanced endurance against oxidation. Then, an obvious need of the market is the long operation time of energy storage systems, which means that batteries should withstand many thousands of cycles of charging and discharging during many years of service. This awaited high cyclability is strongly related to the stability and properties of the passive layers that form on electrodes (on anodes in most cases) during controlled reduction (or oxidation in a few cases) of electrolyte components. In this situation VC and other commonly used additives are not sufficient anymore and a systematic search for newer compounds is recommended.

More difficult goals appear when new battery systems are considered. This applies to all-solid-state-batteries, being a battery version of the Holy Grail, because the fulfillment of various conflicting needs, like high conductivity, good mechanical properties, and electrochemical stability, is extremely challenging. However, a vision of a storage battery with metallic lithium and a flexible thin film electrolyte is worth investing research efforts in.

Considering the problems of presently investigated multivalent batteries and batteries with conversion cathodes brings us to the

conclusion that electrolytes are crucial for these systems. The success of magnesium-, calcium-, or aluminum-based cells depends very much on the elaboration of electrochemically stable electrolytes supporting reversible deposition of these metals. Perhaps even a more demanding electrolyte is needed for the very promising lithium-sulfur cells since it should support the easy diffusion of lithium cations and block the migration of sulfur.

## About the Book

As mentioned above, the challenges in front of researchers have different characters and, in particular, different time perspectives. Therefore, in order to organize the contents of this book in a logical way, it has been divided into two parts. Part I, “Novel Electrolytes for Lithium Batteries,” describes ideas that can be introduced into the industrial practice in the relatively near future since they do not require a very different technology—they can be treated as useful modifications of the existing lithium-ion batteries that result in a higher capacity or lifetime of not more than a few dozen percent. Part II, “Electrolytes for Post-Lithium-Ion Systems,” is addressed to riskier projects whose commercial implementation is still doubtful for many researchers but if successful could create a real breakthrough in the field of the electrochemical storage of electricity.

Thus, Chapter 1 describes strategies for designing electrolytes with new compositions capable of replacing the commonly used LiPF<sub>6</sub> keeping its high conductivity and good electrochemical stability but less prone to reactions with moisture and less harmful to the environment. It seems now that the developed electrolytes based on the newly designed and synthesized salts are close to commercial implementation. In addition, some concepts of electrolytes fulfilling their role at very high and very low temperatures are shown. These new ideas are complemented with a new approach presented in Chapter 2. It shows that crystallographic studies allow for a better understanding of the electrochemical properties of the proposed lithium salts comprising heterocyclic anions with electron-withdrawing groups. It turns out that crystalline structures

of these salts form a perfect basis to reveal real aggregation modes in concentrated liquid electrolytes. There is no doubt that solid-state structural studies have now become a powerful tool supporting the search for better electrolytes.

Since the very beginning of the search for better batteries the concept of replacing liquid electrolytes with solid ones was present. This is because it offers a more compact design, easier assembly, higher safety, and, which is perhaps the most important, partial suppression of lithium dendrite growth, opening the possibility of the application of lithium metal anodes. The “only” problem seems to be the too-low conductivity of solid electrolytes. However, due to the recent progress in reaching conductivities of 1 mS/cm, all-solid-state cells are not an illusion any more. Various aspects of solid electrolytes for lithium batteries are discussed in Chapter 3, including newly introduced classes of solid electrolytes. In addition, some properties of composite polymer electrolytes with inorganic fillers are discussed. The chapter also contains a concise description of mechanisms of ionic transport in solid and polymer electrolytes. This is justified by the fact that the related transport phenomena in solid phase are considerably different from ionic conduction mechanisms in liquid electrolytes and as such they are less familiar to the battery research community.

Part II of the book, as already mentioned, focuses on concepts for the more or less remote future. It starts with Chapter 4 reporting the recent progress in the research on electrolytes for sodium and sodium-ion batteries. A great demand for all kinds of lithium batteries finding applications both in stationary and mobile systems can result in a lithium shortage and an increase in its price. A natural candidate to replace lithium is sodium, which offers lower energy density but which due to its unlimited and scattered resources can be successful in less demanding products. In particular, sodium batteries can be applied as stationary storage facilities necessary for renewable energy sources and prosumer systems. As already proved by many research groups, sodium batteries cannot be manufactured by simply copying the known concepts taken from lithium systems; new chemistry, including new electrolytes, is required.

Chapters 5 and 6 cover the problem of electrolytes for the current multivalent cation batteries. The concept of such cells

is attractive due to their potentially higher volumetric capacity in comparison to lithium; a reported reduced tendency toward dendrite growth, allowing the application of metallic anodes; and abundance of resources. Unfortunately, reversible electrodeposition of magnesium, aluminum, or calcium with low overpotential is a problem that up to now has not been solved in full. The existing concepts as well as suggestions for future research will be discussed.

Batteries that potentially offer the highest energy densities and could be a real turning point in the energy supply for electric vehicles are reversible metal-air cells. Chapter 7 reviews recent achievements in and future strategies for the prospective but research-demanding metal-air systems, with particular attention paid to electrolytes for them.

Another idea to build a high-capacity battery relies on replacing graphite anodes and oxide intercalation cathodes by metallic lithium and elemental sulfur. The problems related to lithium-sulfur batteries are described in Chapter 8, the last chapter. At the moment, the biggest challenges for researchers in this field are to improve the cyclability and available current densities of cells as well as to counteract the rapid decrease in the cell capacity. The main reason for the unsatisfactory performance of the existing systems results from the uncontrolled migration of sulfur within the applied electrolyte. Select concepts to solve this problem are included in the chapter.

## Acknowledgements

This work was financially supported by the Warsaw University of Technology under the ID-UB Energytech-1 programme.

## References

1. X. Yuan, H. Liu, J. Zhang, *Lithium-Ion Batteries: Advanced Materials and Technologies*, CRC Press Taylor & Francis Group, 2011.
2. K. G. Gallagher, P. A. Nelson, Manufacturing costs of batteries for electric vehicles, in *Lithium-Ion Batteries: Advances and Applications*, Elsevier B.V., 2014, pp. 97–126.

**PART I**

**NOVEL ELECTROLYTES FOR  
LITHIUM BATTERIES**



Taylor & Francis

Taylor & Francis Group

<http://taylorandfrancis.com>

## **Chapter 1**

# **New Strategies in Designing Salts and Solutions for the New Generation of Electrolytes**

**Leszek Niedzicki and Marta Kasprzyk**

*Warsaw University of Technology, Faculty of Chemistry, Noakowskiego 3,  
00-664 Warszawa, Poland  
lniedzicki@ch.pw.edu.pl, mkasprzyk@ch.pw.edu.pl*

### **1.1 Introduction**

An electrolyte is by definition a substance that upon dissolving in a polar solvent forms a system in which there is freedom of ionic movement. Thus, ionic conductivity is possible. These days such a definition is too narrow, as we now know that not only polar solvents but also weakly polar solvents enable freedom of ionic movement. Polymer matrices can achieve it too, as well as molten salts. That is why in electrochemical or battery jargon, the whole system containing ions and in which ions can move freely is called an electrolyte. Thus, an electrolyte for lithium-ion (Li-ion) cells is not only the lithium salt but the whole system, including the solvent and/or the solvent mixture as well as possible additives.

---

*Designing Electrolytes for Lithium-Ion and Post-Lithium Batteries*

Edited by Władysław Wieczorek and Janusz Płocharski

Copyright © 2021 Jenny Stanford Publishing Pte. Ltd.

ISBN 978-981-4877-16-9 (Hardcover), 978-1-003-05093-3 (eBook)

[www.jennystanford.com](http://www.jennystanford.com)

An electrolyte in Li-ion cells compared to older rechargeable cell technologies plays many more functions than just its main role. The most important role of the electrolyte is the transport of lithium cations between electrodes, which affects the maximum current available for the cell [1]. However, other parameters of the cell are also influenced by the electrolyte parameters directly or indirectly, which are:

- Storage and operating temperatures, limited directly by the thermal stability of the electrolyte, both in the case of solvents and salts [2].
- Charge-discharge cycle efficiency (ratio between the energy taken in during charge and the energy retrieved during discharge), affected directly by electrolyte conductivity and lithium cation transference number and possibly affected by the solid-electrolyte interphase (SEI) layer resistance [3].
- Energy density, affected indirectly through limitations due to incompatibility of the electrolyte with new/better electrodes (thus restricting its use), either due to chemical incompatibility (no passivation or overreaction) or due to inability to reach high and/or low potentials required to achieve the full capacity of the electrode [4].
- Safety and environmental impact, affected directly by acute toxicity, long-term toxicity, and stability of the salt and also by solvent(s) and/or the influence of the electrolyte on the electrodes' stability [5].
- Cost (depending on the size of the cell and exact technology used, the electrolyte takes up to 15% of the components' costs in a Li-ion cell) [6].

## 1.2 Anion Structure Impact

The lithium salt affects all above-mentioned properties partially or exclusively. The anion of the salt is responsible for all of these, as most of the manufacturing costs, stability, and all performance parameters are rooted in the anion's properties. Some of these properties are as follows:

- Electrochemical and thermal stability is directly connected to the structure of the anion, as lithium cannot decompose under earth conditions. This involves used elements, the general structure of the anion (cyclic, complex-like, etc.), and types as well as strength of bonds that connect atoms composing the anion. The stability of the salt or the anion represented by its highest occupied molecular orbital and lowest unoccupied molecular orbital values originates from a few factors. In the case of organic anions, it depends on the presence of atoms that form polarized bonds with carbon and/or nitrogen. These include sulfur, oxygen, phosphorous, and hydrogen presence, which can be a point of substitution for other atoms or become acidic upon bond cleavage. Reactivity, and as such, lack of stability, is also increased by the presence of elements such as oxygen and hydrogen (acidity) of groups such as SO<sub>2</sub> (weakly bonding with other atoms), of unstable complexes of Lewis bases and acids, or of unstable bond formations. The last group includes reactive bonds, such as the P-F bond, or atoms constituting polarized (weak) bonds with carbon and nitrogen, such as oxygen, sulfur, fluorine, and phosphorous [7].
- Ionic conductivity is affected by the viscosity (inverse relationship), which in turn is strongly influenced by the anion size and shape—its cross-section area. Also, groups that increase the number of degrees of freedom also increase viscosity due to a bigger chance of interaction—the longer and/or branched the side chains, the higher the viscosity [8–10]. A salt's solubility in a given solvent may affect the maximum conductivity, so the binding energy between anion and cation is of particular importance here. This, in turn, is affected by the uniformity of charge distribution over the anion structure. The binding energy with the cation and the related association properties influence the agglomeration degree and as such the resulting viscosity change with increasing concentration of the salt in a solvent. Also, minute structure properties may affect the imbalance of the triplets formed—that there is no equal amount of positively and negatively charged triplets.

- The lithium cation transference number is influenced by the anion's affinity toward agglomeration (association and dissociation constants), the anion size, the solvation degree of the cation, the ratio between cation and anion mobility, and the interaction types between anion and cation (coordination sites for the lithium cation on the anion). The lithium cation transference number and lithium cation conductivity are improved by lower affinity toward agglomeration, a smaller anion size, better shielding of cation by the solvation layer, higher cation mobility over the anion one, and/or weaker interactions between anion and cation [11].
- SEI quality and salt compatibility with electrode active materials, electrode binder, electrode additives, solvent, current collectors, and container (can) are crucial for proper operation of the cell, that is, the charge-discharge process. The salt's compatibility depends mostly on the anion structure and optimal solvents used with it [12]. The anion structure and its reactions with electrode materials and solvent decomposition products, as well as secondary anion decomposition products, influence the thickness, resistance, and morphology of the SEI [13]. These are affected by the final products of the salt, solvents, and electrode reactions as they constitute the SEI. Particularly of interest is the ratio of the inorganic content to the organic content in the SEI. In the inorganic content, the most prominent is the LiF content—fluorine is present in most salts and most common additives—and the  $\text{Li}_2\text{CO}_3$  content, as the solvent mixture usually contains organic carbonates [14]. Other salt decomposition products and solvent decomposition products also affect the SEI properties. Among these are alcoholates, organic and inorganic-organic carbonates, oligo- and polycarbonates, and other polymers. The ability of polymeric products of electrolyte decomposition to cross-link is particularly important. Only after cross-linking is the SEI flexible enough to sustain mechanical stress at the electrode surface during multiple charge-discharge cycles. This stress is a result of electrode material grains changing their volume during charge or discharge and/or pressure from other components during cycling [15]. All of the above directly

depend on the anion structure, the anion decomposition route, and anion decomposition products' interactions with solvents and electrode components. Such interactions are influenced by the temperature and catalytic properties of electrode components—active materials such as transition metals and additives such as carbon black [12]. A separate problem is that of the compatibility of electrolytes with the binder, the separator, and the current collector. The first two are usually chemically inert, although should be taken into consideration, while the current collector, especially aluminum (cathode current collector), is a common subject to corrosion [16]. Most salts react with aluminum under at least some potentials within the Li-ion cell operating range. Thus, it is important for salt corrosion products to effectively passivate the aluminum surface without the formation of a thick salt layer. It is often suggested that for quick passivation the main product of the corrosion should be  $\text{AlF}_3$  [17]. However, there are other solutions as well. For instance, some novel salts do not form aluminum fluoride but still passivate aluminum [18].

- The safety of the cell, apart from electrode and solvent stability, is very much dependent on anion stability. Flammability is a critical property both for acute and long-term exposure to high temperatures but potentially also to side reactions catalyzed by transition metals or graphite [19]. Typical gaseous products of electrolyte decomposition in Li-ion cells are carbon dioxide, carbon monoxide, short alkanes (methane, ethane, propane, etc.), short alkenes (like ethylene propylene), nitrogen, and hydrogen. Depending on the exact anion structure these may be also hydrogen fluoride, fluorine, and other chlorinated or fluorinated compounds. Some gaseous products are toxic and have to be taken into account when batteries are stored or put away for waste disposal/recycling—such as HF, CO, and chlorinated or fluorinated organic compounds [20]. Others are flammable or explosive—alkanes, alkenes, and hydrogen [21]. High temperatures resulting from exothermic decomposition (temperature or SEI formation related), even on a very small scale, may start thermal runaway if the cathode active

material's decomposition temperature is exceeded. Transition metal oxides making the most of used cathode materials are susceptible to low-temperature thermal runaway. This is more than enough to be dangerous if locally in the cell the temperature exceeds 130°C–150°C [22].

- Manufacturing costs of the electrolyte are mostly affected by the anion price, as the lithium content is relatively low and the solvent prices are relatively stable and low in comparison to the salt price. The most important factors contributing to price are the elements used, the abundance and purity of the raw materials required for production, the required purity of the substrates and their availability on the market (number of suppliers), and the required catalysts or coupling agents (along with their market availability). Also important are the yield of the reaction, the complexity of synthesis (including the number of reaction steps), the amount of side products and waste, the environment of the synthesis (if an inert gas and/or a dry atmosphere required), the required final purity for the battery-grade salt, and the desiccation costs (if required).

### 1.3 Requirements toward Electrolyte

To use a given electrolyte in a Li-ion cell, it has to pass the minimum battery industry requirements [23]. Some of those are as follows:

- Ionic conductivity at the level of at least 1 mS/cm (in the case of solid electrolytes it is enough to be above 0.1 mS/cm)
- No electronic conductivity (not detectable)—to avoid self-discharge of the cell
- A lithium cation transference number above 0.3—to enable a high amount of charge transport
- Thermal stability in the typical operating temperature range for Li-ion-powered device applications with some the safe buffer (so at least in the -30°C to the +100°C range)
- Electrochemical stability at least between 2 V and 4.5 V versus Li (lithium anode Li/Li<sup>+</sup>) against all of the components of the cell (including the aluminum current collector)

- Chemical compatibility with other cell components, in both whole storage or operating temperature range and whole operating potential range
- Keeping low toxicity and low manufacturing cost, just like in the case of any other component

As the requirements for electrolyte and salt are established, let us look at the choice of salts to fulfill them. The following parts of this chapter will discuss the anions investigated so far.

## 1.4 Classes of Anions Investigated So Far

Over 30 years have passed since Li-ion cell research started. During this time, numerous research groups all over the world have tried to use existing salts or design and synthesize salts particularly for Li-ion cells using different strategies. As a result, over 200 different new salts have been introduced to electrolyte research in addition to the existing salts.

- Approximately 20 salts each from perfluoroalkylsulfonates, perfluoroalkylsulfonylimides [24] (containing a  $-SO_2-N-SO_2-$  block) (Fig. 1.1a) and perfluoroalkylsulfidearylsulfonates [25] (Fig. 1.1b) classes, where the most prominent examples are lithium trifluoromethylsulfonate ( $LiTf$ ), lithium bis(fluorosulfonyl)imide ( $LiFSI$ ) [26], lithium bis(trifluoromethylsulfonyl)imide ( $LiTFSI$ , also noted as  $LiNTf_2$ ) [27, 28], and lithium bis(pentafluoroethylsulfonyl)imide ( $LiBETI$ ) [29, 30] and numerous sulfonylimides with perfluoroalkyl substitutions of varied lengths (not limited to symmetric) to sulfonyl groups [31] (Fig. 1.1c)
- Approximately 15 salts each from perfluoroalkylphosphate (Fig. 1.1d), perfluoroalkylsulfonylphosphate [32] (Fig. 1.1e), and chelatephosphate [33] (Figs. 1.1f and 1.1g) classes, with the most important representative being lithium tris(pentafluoroethyl)trifluorophosphate ( $LiFAP$ ) [34, 35] (Fig. 1.1d)
- Approximately 30 salts from chelatoborates [36] (Fig. 1.1h), including fluorobenzenediolatoborate [37] (Fig. 1.1i), oxocarbonoborate, and triacetoxyarylborate [38] (Fig. 1.1j) classes,

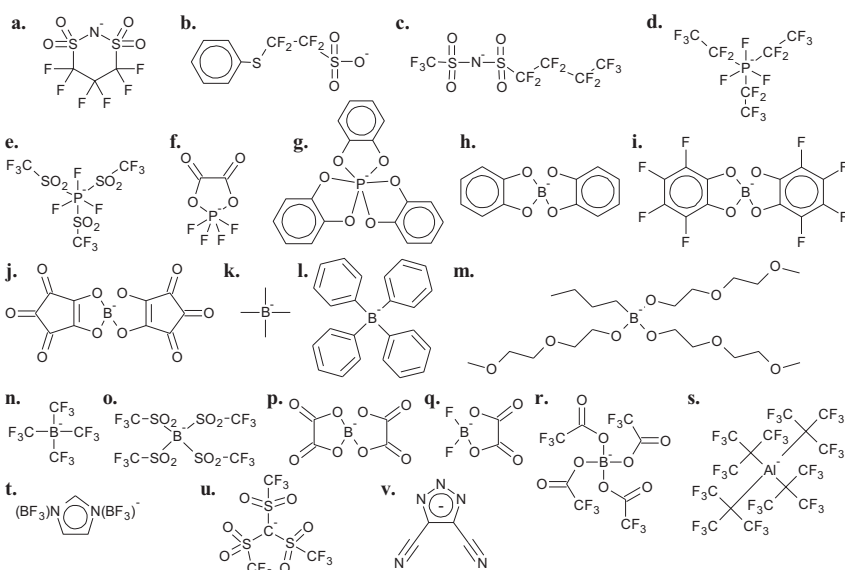


**Figure 1.1** Examples of anions from each class: (a) cyclohexafluoropropene-1,1-bis(sulfonyl)imide; (b) 1,1,2,2-tetrafluoro-2-phenylsulfanylethanesulfonate; (c) (trifluoromethylsulfonyl) (nonafluorobutylsulfonyl)imide; (d) tris(pentafluoroethyl)trifluorophosphate (FAP); (e) tris(pentafluoroethylsulfonyl)trifluorophosphate; (f) oxalatotetrafluorophosphate (TFOP); (g) tris[1,2-benzenediolato(2-)O,O']phosphate; (h) bis[1,2-benzenediolato(2-)O,O']borate; (i) bis[tetrafluoro-1,2-benzenediolato(2-)O,O']borate; (j) bis[croconato]borate (BCB); (k) tetramethylborate; (l) tetraphenylborate; (m) butyltris(methoxyethoxyethoxy)borate; (n) tetrakis(trifluoromethyl)borate; (o) tetrakis(trifluoromethylsulfonyl) borate; (p) bis(oxalato)borate (BOB); (q) difluoro(oxalato)borate (DFOB); (r) tetrakis(trifluoroacetoxy)borate (TFAB); (s) tetrakis[tris(trifluoromethyl)methyl]aluminate; (t) bis(trifluoroborane)imidazolate; (u) lithium tris(trifluoromethylsulfonyl)methide (TFSM); (v) dicyanotriazolate (DCTA).

and another about 60 salts from the borate classes, including alkylborates (Fig. 1.1k), arylborates [39] (Fig. 1.1l) and mixed ones, fluorinated alkylborates, alkyltrialkoxyborates [40] (Fig. 1.1m), perfluoroalkylborates (Fig. 1.1n), and perfluoroalkylosulfonylborates [41] (Fig. 1.1o), with the most prominent representatives being, for example, lithium bis(oxalato) borate [42] (Fig. 1.1p), lithium difluoro(oxalato)borate [43]

(Fig. 1.1q), and lithium tetrakis(trifluoroacetoxy)borate [44] (Fig. 1.1r)

- A few salts each from perfluorooxyaluminates [45] (Fig. 1.1s), boroimidazolides [10] (particularly containing  $\text{BF}_3$  moiety, Fig. 1.1t) and perfluorosulfonylmethides classes, with the notable example of lithium tris(trifluoromethylsulfonyl)methide ( $\text{LiTFSM}$ ) [46] (Fig. 1.1u), which is a member of the last of those classes
- A few salts from the azole (imidazoles, triazoles) aromatic ring class, with the most notable cases being lithium 4,5-dicyano-2-trifluoromethylimidazolide ( $\text{LiTDI}$ ) [47, 48] and lithium 4,5-dicyano-1,2,3-triazole ( $\text{LiDCTA}$ ) [49] (Fig. 1.1v)

Most of the salts from above-mentioned classes have turned out to be unstable either chemically (in contact with moisture, air, or other components of the cell), thermally, or electrochemically. Authors have stopped developing other technologies due to low conductivity of electrolytes based on new salts, problems with solubility of salts in typical battery solvents, or the inability to lower a salt's manufacturing costs. To sum it up, most of them failed to fulfill at least part of the minimum requirements for an electrolyte. Thus, only a few of those salts (mostly those mentioned by name) are available on the market and are used mostly for research purposes.

The previously existing salts used in Li-ion cell research include most notably lithium perchlorate ( $\text{LiClO}_4$ ), lithium tetrafluoroborate ( $\text{LiBF}_4$ ), lithium hexafluorophosphate ( $\text{LiPF}_6$ ), lithium hexafluoroarsenate, and lithium trifluoromethylsulfonate ( $\text{LiSO}_3\text{CF}_3$ , also called lithium triflate and often noted as  $\text{LiTf}$ ).

## 1.5 Properties of Anion Classes Investigated So Far

Let us look at the presented classes in detail.

Sulfonylimides are mostly corrosive to aluminum at potentials above 3.5 V versus Li, above which occurs electrochemical instability or the inability to passivate aluminum [29]. None of the salts of this class (including  $\text{LiFSI}$ ,  $\text{LiTFSI}$ , and  $\text{LiBETI}$ ) are stable against

aluminum in the full potential operating range of Li-ion cells. Even though small anion size allows LiFSI and LiTFSI to achieve high conductivity levels, they exhibit low lithium cation transference numbers ( $\sim 0.2$ ), as lithium strongly interacts with oxygen in  $\text{SO}_2$  groups [50]. Longer perfluoroalkyl chains also contribute toward higher viscosities and lower conductivities. The more asymmetric the perfluoroalkyl substituents used, the lower the conductivity of their salt solutions. This may be explained by the asymmetric structure and thereby stronger lithium-anion interaction, resulting in a lower dissociation degree, as previously explained. Also, most imides are hygroscopic and some undergo slow hydrolysis.

The chelatephosphates show quite low conductivities due to their incorporation of multiple benzene rings, which makes their size too big for them to achieve low viscosity in solutions. The same fate is shared by chelateborates, which employ multiple big groups, like benzene rings and/or  $\text{BF}_3$  groups. Poor electrochemical stabilities of both classes result from relatively weak P–O and B–O bonds. However, one prominent member of the group,  $\text{LiPF}_4(\text{C}_2\text{O}_4)$  is known to be well conducting as it is the smallest of its class and only semichelated. Its conductivity is close to that of  $\text{LiPF}_6$  (conductivity value of both is close to 10 mS/cm) [51]. It is also more thermally stable than  $\text{LiPF}_6$  [52] but cycles worse with the standard electrode materials [51].

Fluoroalkylphosphate and fluoroalkylsulfonylphosphate exhibit medium conductivities and average electrochemical stability with the notable exception of LiFAP. An FAP anion, due to its symmetric structure, shows similar conductivity to that of  $\text{LiPF}_6$  (their conductivity values are 7 and 10 mS/cm, respectively, in a 1:1 solvent mixture of ethylene carbonate (EC) and dimethyl carbonate (DMC) [53]). They have good stability over cell cycling but not very high stability and often have a high cost of manufacturing. LiFAP is an exception to the poor stability of the class, but not an exception when it comes to the high manufacturing cost [54].

All classes of borate salts share low electrochemical stability (often not enough to operate with the low-voltage cathode, like  $\text{LiFePO}_4$  at 3.7 V versus Li) as well as often poor solubility in typical battery solvents (lower than 1 mol kg<sup>-1</sup>) [55]. Low stability results

from weak B–O bonds (particularly at high potentials). Additionally, most borate salts suffer from very low conductivity due to their big sizes (mostly below 2 mS/cm), because in order to stabilize the charge, very big structures are employed, like benzene rings (also substituted with fluorine atoms) and benzenodiolate groups [56]. This also decreases their conductivity and often their solubility [57]. Boroimidazolides share their disadvantages with other borate classes.

Aluminates are most often chemically as well as electrochemically unstable. Anions containing Al–C bonds are usually extremely reactive and those containing Al–O bonds, due to their presence, are either electrochemically unstable or too strongly interact with lithium.

Methide salts are scarce, but all of them have worse electrochemical stability and conductivity than their imide counterparts or LiPF<sub>6</sub>. As an example, let us take conductivity values in a 1:1 solvent mixture of EC and diethyl carbonate (DEC) are as follows: LiTFSM, 4.5 mS/cm; versus LiPF<sub>6</sub>, 7.6 mS/cm [58]. It is due to electronic structure differences where the carbanion is much less stable than imide anion. Similarly, the dissociation of lithium salt is to a much lower degree in the case of the carbanion.

The azole family ranges from imidazoles, through triazoles, to tetrazoles. It recently garnered high interest due to some advantages over state-of-the-art salts. Although electrochemically, chemically, and thermally stable, they tend to have low conductivities due to already large sizes, a tendency toward association, as well as not a very high dissociation degree. For instance, LiDCTA exhibits conductivity of 1 mS/cm in propylene carbonate (PC) (LiPF<sub>6</sub> in PC exhibits a conductivity value of ~6 mS/cm). A notable exception to low conductivity is LiTDI salt, which has 50%–60% of LiPF<sub>6</sub> conductivity and almost twice as high a transference number, resulting in similar lithium conductivity values.

## 1.6 Properties of Commonly Used Salts

Now, let us discuss individually the most popular salts in the Li-ion cell scientific and industrial community.

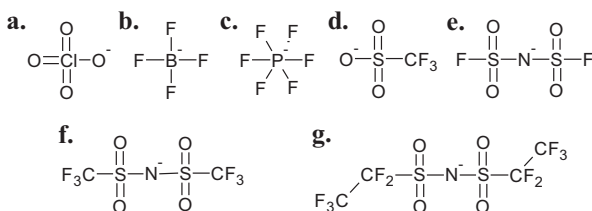


**Figure 1.2** Anions of commonly used lithium salts: (a) perchlorate; (b) tetrafluoroborate; (c) hexafluorophosphate; (d) trifluoromethylsulfonate; (e) bis(fluorosulfonyl)imide; (f) bis(trifluoromethylsulfonyl)imide; (g) bis(pentafluoroethylsulfonyl)imide.

$\text{LiClO}_4$  (Fig. 1.2a) is explosive in the presence of electrodes containing transition metals or acetylene black (a component of most cathodes) [59]. Upon exchanging the cation with a transition metal or when in the catalytic environment of the acetylene black, it easily undergoes exothermic decomposition—a temperature of  $\sim 100^\circ\text{C}$  is enough on its own. The salt itself also has low thermal stability [60].  $\text{LiClO}_4$ -based electrolytes have high conductivity values (10 mS/cm at room temperature in a 1:1 solvent mixture of EC and PC) and lithium cation transference numbers (0.6 in the case of 1 M  $\text{LiClO}_4$  in a 1:1 solvent mixture of EC and PC) [61]. Although in terms of electrochemical properties  $\text{LiClO}_4$  fulfills the basic requirements for electrolytes, it does not do so in terms of safety and stability.

$\text{LiBF}_4$  (Fig. 1.2b) salt dissolved in typical battery solvents yields low ionic conductivity (below 2 mS/cm for optimal concentration in a typical solvent mixture) [62] and forms interfacial layers on anodes that poorly conduct lithium cations [63], especially in temperatures above  $60^\circ\text{C}$  [64]. The main reason is its structure—a complex of  $\text{LiF}$  and  $\text{BF}_3$  that easily disconnects  $\text{LiF}$  and leaves  $\text{BF}_3$  moiety undergoing secondary reactions.

$\text{LiPF}_6$  (Fig. 1.2c) is the most commonly used salt in Li-ion cells on the market. Electrolytes containing this salt have very high conductivity, reaching  $\sim 10$  mS/cm in optimal battery mixtures [65].  $\text{LiPF}_6$  also forms a relatively stable SEI layer permeable to lithium cations with multiple cathodes and anodes. On the downside of the electrochemical properties is its average lithium

cation transference number of 0.25–0.35, depending on the solvent mixture. Unfortunately, LiPF<sub>6</sub> becomes thermally unstable just above ~70°C. The LiPF<sub>6</sub> salt always contains at least traces of hydrogen fluoride due to natural decomposition, LiPF<sub>6</sub> → LiF + PF<sub>5</sub> (decomposition to components of a complex), and it easily undergoes hydrolysis with ever-present traces of water (at the ppm level): PF<sub>5</sub> + H<sub>2</sub>O → POF<sub>3</sub> + 2HF [66, 67]. Hydrogen fluoride is toxic and caustic, so it can damage (corrode) other cell components from the inside of the cell. POF<sub>3</sub> formed due to the hydrolysis reaction is also a toxic compound [68]. This is why in Li-ion cells manufacturers often use additives that absorb moisture and hydrogen fluoride, and before the cell assembly all the components have to be dried to a very high extent. LiPF<sub>6</sub> salt is unstable even when cycled below 2.5 V or above 4.2 V versus the lithium anode in cells containing organic carbonates, which include almost every modern Li-ion cell [20]. Simultaneously, LiPF<sub>6</sub> is very demanding in terms of synthesis conditions, making it expensive—it requires a moistureless environment as well as very pure and very dry substrates. Regardless of all the above, LiPF<sub>6</sub> is still the most common salt in Li-ion cells as it is one of the first ones to have fulfilled most industry requirements and as such, most cell manufacturers are keeping to it.

LiTf (Fig. 1.2d), LiFSI (Fig. 1.2e), LiTFSI (Fig. 1.2f), and LiBETI (Fig. 1.2g) salts all cause aluminum corrosion [69, 29]. Even though all except LiTf exhibit good conductivity in liquid electrolytes (all above 6 mS/cm) [53], they also exhibit very low lithium cation transference numbers (~0.2). A small size is part of the deal in the presence of –SO<sub>2</sub>– groups, exposing four oxygen atoms in total, each of them being the preferred lithium coordination site. Due to possible rotation and chain movement, these anions have multiple degrees of freedom of movement and are not symmetric. Their instability is due to weak S–N bonds, but fluorine present only in –CF<sub>3</sub> groups makes it harder to passivate aluminum (preferably to AlF<sub>3</sub>). However, the main disadvantage of aluminum corrosion is the case only for lithium salt liquid solutions, while at least LiTFSI is stable in highly concentrated forms (solvent-in-salt, ionic liquids [ILs], etc.) as well as in solid polymer electrolytes in which there is no direct contact (or restricted one) between salt and current collector. Thus, in new generations of Li-ion cells, there might be place for this

class. Use of LiTf, LiFSI, LiTFSI, and LiBETI in liquid electrolytes is possible only upon use of additives that are inhibitors of aluminum corrosion, but using those additives results in a higher cost of cell manufacturing [70].

## 1.7 Strategy for New Anion Design

As all important salts in the field of Li-ion cells have various disadvantages, the search for new salts or solutions for electrolytes continues. Experiences with salts investigated so far—their advantages and disadvantages—forms some basis for what building blocks work the best for anions. That and the list of anion structure-influenced properties as well as the list of requirements for electrolytes (Sections 1.2 and 1.3) allow the creation of a general strategy on the design of new salts, including what elements not to be used, what building blocks to use, and general rules of what to do and not to do when designing salts (anions) to be used as electrolytes for Li-ion cells.

Elements should be restricted to those not forming very strong bonds with lithium. The less covalent in character they are, the weaker the coordination of lithium between anion and cation and the easier the charge distribution [71]. That is why carbon or nitrogen should be used. Also, fluorine can be used, if needed, as fluorine connected to an organic structure has relatively weak interaction with lithium when compared to fluoride anion. On one hand, fluorine usually increases the electrochemical stability but also increases the toxicity of most compounds compared to compounds containing hydrogen substitutes. On the other hand, fluorine is important to passivate aluminum current collector although it is not the only way to prevent aluminum corrosion [18]. Oxygen and sulfur, as both have very strong interactions with lithium regardless of their form, should be avoided. Hydrogen can form hydrogen bonds, which strengthen the association and interactions between the components of the electrolyte, in this way damaging the electrochemical properties important for Li-ion cells. Finally, hydrogen presence in organic compounds always bears the risk of detaching from the original structure and catalyzing decomposition

of electrolyte compounds and/or forming acids when within the extreme potentials of the Li-ion cell interior. Other elements should be avoided as well if they form strong bonds with lithium or weak bonds with other atoms in the anion. That is why the more covalent bonds between the atoms of the anion, the better, which suggests using multiple bonds and atoms of elements that can easily connect to each other. The last element rule is due to multiple situations in which the central atom is too reactive with its environment or possible impurities of the electrolyte. As it is the easiest to build structures with carbon, this is a good element for designing anions as well as atoms with similar electronegativity or affinity toward electrons, which means strong bond formation with each other, like nitrogen.

As a result of the already limited elements list, the broadest classes of possible structures for anions are carbanion and imide. Carbon and nitrogen atoms are good as an anion base as long as there are no atoms forming strongly polarized bonds with the main atom. Among organic structures, in order to keep anion atoms strongly bonded, it seems logical to use mostly double or aromatic bonds. Single bonds may be too weak, with the exception of the C–C bond, while triple bonds may attract cations too strongly with their electron cloud density. Similarly, double bonds may also be a strong cation attraction in certain structures. As an anion naturally has a large electron density, it would be obvious to uniformize the charge over its structure in order to keep the number of active sites on the structure down. In this way, the whole structure will interact with the lithium cation less strongly. To uniformize a charge over the anion, one may design the anion on the basis of the aromatic or heteroaromatic ring (preferably with nitrogen). It keeps the bonds strong and shares charge over all ring members. Symmetrical design of the anion increases the number of active sites that are equivalent, making each interact in a weaker manner with the lithium cation. For a symmetrical design, the structure may have multiple symmetry planes or axes.

More importantly, the presence of the electron-withdrawing groups help the charge to be better spread over the anion electronic structure, but it is limited to groups that do not possess oxygen or hydrogen. For instance,  $-C_nF_{2n+1}$  perfluoroalkyl groups ( $-CF_3$ ,

$-C_2F_5$ , etc.) or  $-C_nF_{2n}$  – perfluoroalkyl bridges are stable and stabilize the anion structure by their presence [72]. That is due to their strong electron-withdrawing properties and high stability of groups with C–F bonds, contrary to the  $-F$  fluoride group, which is also a poor electron-withdrawing group. Another very common building block is the  $SO_2$  sulfonyl group as a part of  $SO_2C_nF_{2n+1}$  perfluoroalkylsulfonyl—a very strong electron-withdrawing group. The  $SO_2$  group itself unfortunately increases instability and lowers the transference number of the lithium cation due to the  $>S=O$  moiety. Other typical electron-withdrawing groups are  $-CN$  nitrile. Avoiding building blocks of high electron densities that are not electron-withdrawing groups is also suggested as this strengthens the interaction with cations while not contributing to uniform charge distribution [71].

An anion that is too big contributes to high viscosity, as well as to a long atomic chain, which enforces spatial effects. Slowing down the anion at all costs, which was an object of multiple investigations and concepts in the past, also proved to be a disadvantage [1]. Examples of such concepts are polyanionic electrolytes, anion trap supramolecular structures, and using very big anions (including oligoanions). Due to the interaction of anion with cation, there will always be a connection between their mobilities. As the anion velocity reduces, even in salts with the lowest level of interactions it will affect cation mobility.

Finally, using building blocks (like groups and atoms) that react with water or oxygen is relatively common, but it makes handling salts with such anions difficult. Similarly, all groups unstable at potentials above  $-1$  V versus a standard hydrogen electrode (SHE, 2.04 V vs. Li) or below 1.5 V versus a SHE (4.54 V vs. Li) have to be avoided as such a group will quickly decompose in the operating range of Li-ion cells. It is also good to avoid groups that are unstable in the  $-3$  to  $-1$  V potential range versus SHE (0.04 V to 2.04 V vs. Li) in the unlikely case of cell voltage drop below the typical operating range.

The above-mentioned strategy has been used in recent years to tailor new salts for the new generation of Li-ion cells. Such salts and their properties will be presented in the following part of this chapter.

## 1.8 Anions Designed with the New Described Strategy

The salt family of imidazoles has been designed using the strategy explained previously in this chapter. The most important member of this family is LiTDI (Fig. 1.3a), but it also contains lithium 4,5-dicyano-2-pentafluoroethylimidazolide (LiPDI, Fig. 1.3b) and lithium 4,5-dicyano-2-(*n*-heptafluoropropyl)imidazolide salts. This imidazole family is chemically very stable, electrochemically stable up to 4.7 V versus Li, and thermally stable up to 250°C [73]. Ionic conductivity is not the highest (up to 6 mS/cm in optimal mixtures [74]), but its strength is in high lithium cation transference numbers, which reach values of 0.45–0.55 depending on the solvent mixture [75]. The effective conductivity of a lithium cation is then similar to that of LiPF<sub>6</sub>, which is the benchmark of the Li-ion field. Thus, it is one of the few salts fulfilling all the industrial requirements. The success of LiTDI is due to its uniformized charge distribution thanks to the heteroaromatic ring base and the use of various electron-withdrawing groups, while keeping the relatively size of the anion small. Here is a comparison: size: 13 atoms/cation in LiTDI, 7 atoms/cation in LiPF<sub>6</sub>, and 15 atoms/cation in LiTFSI; molecular mass: 185 u/cation in LiTDI, 145 u/cation in LiPF<sub>6</sub>, and 280 u/cation in LiTFSI. However, LiTDI is more like LiPF<sub>6</sub> in terms of structural stiffness (freedom of movement), but with more uniform charge distribution than in LiTFSI and a lower electron cloud density than in LiPF<sub>6</sub>. Thus, it weakly associates and has high mobility. LiTDI does not employ sulfur or oxygen atoms, thanks to which it

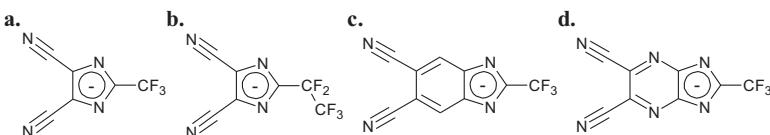


**Figure 1.3** Anions designed with the described strategy: (a) lithium 4,5-dicyano-2-trifluoromethylimidazolide (LiTDI); (b) lithium 4,5-dicyano-2-pentafluoroethylimidazolide (LiPDI); (c) lithium 5,6-dicyano-2-trifluorobenzimidazolide (LiTDBI); (d) lithium 4,5-dicyano-2-trifluoroimidazo-pyrazinium (LiTDPI).

is hard for lithium cation to find a good coordination site. X-ray diffraction and modeling show two bidentate sites for a lithium cation—between ring nitrogen and fluorine of the  $-CF_3$  group and between two nitrogen atoms from the  $-CN$  groups. Both sites have low dissociation energy [76]. Thanks to this, LiTDI exhibits a higher lithium cation transference number than other mentioned anions. Chemical, thermal, and electrochemical stability is achieved thanks to the stable ring on which anion is based and using only the most stable side chains for electron-withdrawing groups, such as perfluoroalkyl and nitrile groups. Finally, the structure has been chosen in such a way that synthesis would be relatively inexpensive (compared to most other anions in the field) and that salt handling would be easy. Chemical stability in this case means that LiTDI is one of the only salts in the Li-ion cell field that is stable in the presence of water, including forming water solutions. Additionally, it can be used with all commonly used electrode materials as well as with new generations of electrode materials that  $LiPF_6$  cannot due to the HF content—like silicon anodes or silicate cathodes. Again, a design that leaves only strong bonds between atoms of the anion allows for stability against air and moisture.

LiPDI is almost identical to LiTDI but contains a  $-CF_2-CF_3$  group instead of a  $-CF_3$  group. Although theoretically it should be less conductive due to its bigger size (16 atoms/cation, 235 u/cation), it contains a much stronger electron-withdrawing group. Even bigger freedom of movement does not harm good mobility and weak association properties. Thanks to this, the effects of uniform charge distribution and viscosity balance each other, yielding almost the same conductivity and lithium cation transference number values [77]. Most of the other properties of LiTDI and LiPDI are also identical or very similar.

By employing the described strategy, one can design anions that can maximize chosen parameters. Typically, the idea is to make the best anion possible, which means trying to reach the golden mean of all electrochemical and safety parameters (with stress on conductivity). However, another way, which may be more interesting for specialized applications, is to maximize selected parameters and keep the rest of the parameters at the level of

minimum requirements. Examples of such an approach are lithium 5,6-dicyano-2-trifluorobenzimidazolide (LiTDBI) and lithium 4,5-dicyano-2-trifluoroimidazopyrazinium (LiTDPI).

LiTDBI [78] (Fig. 1.3c) was designed with the same principles and strategy as LiTDI, but this time focusing on a high transference number. LiTDBI ionic conductivity due to the bigger size (19 atoms/cation, 235 u/cation) and shape is much worse (maximum is just over 1 mS/cm) than that of LiTDI, which was foreseen. However, it exhibits a lithium cation transference number value of 0.6–0.7, which shows visible improvement over that of LiTDI. Low lithium conductivity may not be an issue in some low-power applications where a high transference number is the most important factor. For instance, poor or scarce energy source for charging may be a reason for maximizing the charge-discharge cycle efficiency. This includes looking for a high lithium cation transference number, even at the cost of low maximum power (total ionic conductivity). However, ionic conductivity is the only trade-off here, as LiTDBI has similar thermal stability ( $\sim 270^\circ\text{C}$ ), identical electrochemical stability (up to 4.75 V vs. Li), and identical chemical stability (does not react with air or water and works with common electrode materials) as LiTDI. Better charge distribution thanks to the use of a double condensed aromatic ring as a base for the anion results in a higher lithium cation transference number. From the strategy point of view, there is one design flaw—there are two hydrogen atoms at the benzene ring. This flaw does not seem to affect any of the stability properties, as LiTDBI does not suffer in these terms in comparison to LiTDI. It may be so due to the fact that hydrogen atoms connected to aromatic ring carbon atoms are bonded stronger than in the case of any saturated aliphatic chain. However, removing those two hydrogens should improve the stability.

LiTDPI [79], (Fig. 1.3d), just like LiTDPI, was designed like LiTDI and LiTDBI, but with a focus on higher stability. To achieve it, two hydrogen atoms were removed and carbon atoms in the ring were substituted by nitrogen atoms. Its size (17 atoms/cation, 237 u/cation) and shape are the same as those of LiTDBI, although removing two hydrogen atoms improved the conductivity (to 3 mS/cm)—in fact it decreased the area of the anion cross section.

Removing two hydrogen atoms also proved that hydrogen actually decreases stability parameters. LiTDPI is stable thermally up to 350°C (improved by 80°C) and electrochemically up to 5.1 V versus Li (improved by 0.35 V). It is also still stable against moisture and air. The only disadvantage of LiTDBI is a lower lithium cation transference number value: 0.4. However, lithium conductivity in LiTDPI has improved to 1.2 mS/cm from 0.7 mS/cm of LiTDBI. Thus, it can be concluded that it is possible to tailor anions for particular applications and yields satisfactory effects.

## 1.9 Other Concepts

Multivalent anions tend to have a charge distribution more uniform than that in monovalent anions. Although obviously bigger than monovalent anions, they are designed with the hope of balancing lower conductivity with a higher lithium cation transference number. So far, most multivalent lithium salts made for Li-ion cell application have been members of the sulfonyl imide class [80, 81] (mostly oligomers based on the bis(trifluoromethylsulfonyl)imide [TFSI] building block, Fig. 1.4a) and as such are prone to all their disadvantages. Low conductivity is the main issue here (much below 0.1 mS/cm or lower than that of monovalent salts in solid polymer electrolytes), but expensive synthesis is also a problem. Due to

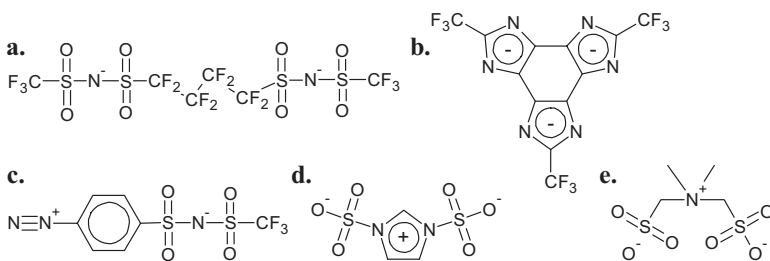


**Figure 1.4** Examples of anions with nonmonovalent concepts: (a) bis(trifluoromethylsulfonyl)octafluorobutyldiimide; (b) trolithium 2,2',2''-tris(trifluoromethyl)benzotris(imidazolide) (BTI); (c) (*p*-diazoniumbenzenesulfonyl)(trifluoromethylsulfonyl)imide; (d) 1,3-di(sulfonate) imidazolium; (e) *N,N*-dimethylsulfonate-*N,N*-dimethylammonium.

poor electrochemical parameters, no transference numbers were measured for this class, as even a value of 1 would not balance the decrease of conductivity compared to that of monovalent sulfonyl imides. Most experiments were performed with solid electrolyte polymers [82].

The only multivalent lithium salt so far that is nonoligomeric and also not based on TFSI is a TDI-derivative salt called trilithium 2,2',2''-tris(trifluoromethyl)benzotris(imidazolide) ( $\text{Li}_3\text{BTI}$ , Fig. 1.4b) [83]. It was synthesized to maximize the lithium cation transference number and has been designed employing the strategy explained in this chapter—in this case, using no oxygen, hydrogen, or sulfur atoms; keeping the size small (9 atoms/cation, 133 u/cation); and using an imide or heteroaromatic ring as a base, as well as a highly symmetric and planar structure.  $\text{Li}_3\text{BTI}$  has been tested in a typical battery solvent, yielding a lithium cation transference number of 0.73, which proves that the design has been successful in its main aim. A conductivity of 1 mS/cm at room temperature shows that even multivalent salts can conduct at the minimum required level and that the multivalent concept is not a dead-end.

Another concept similar to multivalent anions has been proposed. Pseudodelocalized zwitterion-type anions [84] are based mostly on sulfonate derivatives (Fig. 1.4c–e). As they have not yet been synthesized, not much can be said about their properties. The only zwitterions synthesized so far are cesium salts based on diazonium TFSI derivatives [85]. However, this proof of concept shows that the synthesis of such zwitterionic structures for alkali metal salts is possible.

The idea of using polyanions [86, 87] in order to increase the lithium cation transference number has been investigated for some time. Polyanions indeed possess cation transference numbers close to 1 (at least over 0.7, but usually 0.98–0.99, depending on the molecular mass of the anion), but at the cost of very low ionic conductivity—similar to or even lower than that of traditional solid polymer electrolytes [88]. Sulfonyl or perfluorosulfonyl electron-withdrawing groups have been the main building block also for polyanions.

## 1.10 Electrolyte Design: Solvent Effect

The modern technology of Li-ion batteries is still in need of new solvents and solvent mixtures. It is important for the solvent to be pure, dry, and aprotic. Various solvent parameters may significantly influence the electrolyte properties. That is why selecting the appropriate composition of the solvent or the solvent mixture of certain salts is critical. Among all solvent properties the most important are its dielectric constant ( $\varepsilon$ ), viscosity ( $\eta$ ), melting point or glass transition temperature, boiling point, flash point, vapor pressure, toxicity, electrochemical stability, and chemical stability versus those of Li or other electrode materials. But the main role of the solvent is still to provide the proper dissolution, solvation, and dissociation of a chosen salt.

While tailoring the perfect solution it is crucial to take into account all of the mentioned properties. Firstly, all solvents that are not stable in the 2.5–4.2 V potential range versus Li can be ruled out as this is a basic requirement. Secondly, solvents have to form a stable SEI on the typical electrode materials in the presence of lithium salts. Multiple solvents cannot meet this condition. Thirdly, solvents should not react violently or exothermally with any other cell component. Only after selecting solvents on the basis of such basic properties do other properties come into question. Only a few classes of solvents meet these conditions—carbonates, ethers, esters, nitriles, and sulfites. However, mostly carbonates are used as the main solvents in commercial Li-ion cells. The rest are usually used as additives, as part of specialized electrolytes, or for research purposes. Others might be used only after the addition of SEI-forming additives, which makes the cost of the electrolyte higher.

When the dielectric constant of the solvent/solvent mixture increases, then usually the salt solubility is higher. Furthermore, the ions will be better solvated by solvent molecules. The most popular solvent for Li-ion batteries that has a very high dielectric constant is EC (Fig. 1.5a). Its dielectric constant reaches 90.8 at 36°C [89] (in comparison water's dielectric constant is ~81 at 20°C). It is one of the most polar solvents, and it should be the ideal solvent for Li-ion batteries if not for its high melting point, which

is 36°C. That is why this solvent cannot be used alone and is always used mixed with other carbonates. One such mixture that keeps the dielectric constant high is the one with PC (Fig. 1.5b). PC exhibits a lower dielectric constant (~63), but its melting point is much lower (~43°C) [1]. A 1:1 (m/m) mixture of EC and PC may exhibit a dielectric constant of ~80 [90]. PC cannot be used alone as graphite used as an anode material in cells is exfoliated upon longer exposure to PC during cell cycling. It has been proved that some additives, like diglymes and EC, prevent the exfoliation and ensure good cyclability of the system [91].

The next important parameter is the viscosity of the solvent. As the electrolyte viscosity increases, the conductivity value drops. The following linear carbonates exhibit very low viscosity (data at room temperature): DMC (Fig. 1.5c), 0.59 mPa s; ethyl-methyl carbonate (EMC, Fig. 1.5d), 0.65 mPa s; and DEC (Fig. 1.5e), 0.75 mPa s [92]. Unfortunately, all of these solvents are nonpolar and their dielectric constants are quite low (2.82 for DEC and 3.09 for DMC [93]). These solvents are also very volatile. For instance, at ~42°C, DEC has a vapor pressure of 10 Pa and at 17°C, it has a vapor pressure of 1 kPa [93]. They are commonly used in solvent mixtures to lower the viscosity of the system and decrease the melting point of the mixture with EC. For instance, the mixture EC:DMC (1:1 m/m) has a dielectric constant of ~49.2 [94], viscosity of ~0.78 mPa s at 25°C [95], and a melting point of 5°C [96]. The total linear carbonates content in a mixture cannot be too high as the dielectric constant drops too low and it may cause a pressure increase in the battery due to its high vapor pressure at higher temperatures [93]. If the pressure in the battery system increases, it may puncture and damage the cell. That is why it is so important to design solvent mixtures in terms of their utilization, for instance, by establishing a range of operating temperatures [97]. Also, the battery construction itself may help to control and prevent cell damage [98].

The melting and boiling points of a solvent (solvent mixture) restrict the operating temperature range of the future electrolyte. It also depends on the thermal stability of the salt, as mentioned before. That is why differential scanning calorimetry measurement is needed to investigate the temperature stability of a given electrolyte.

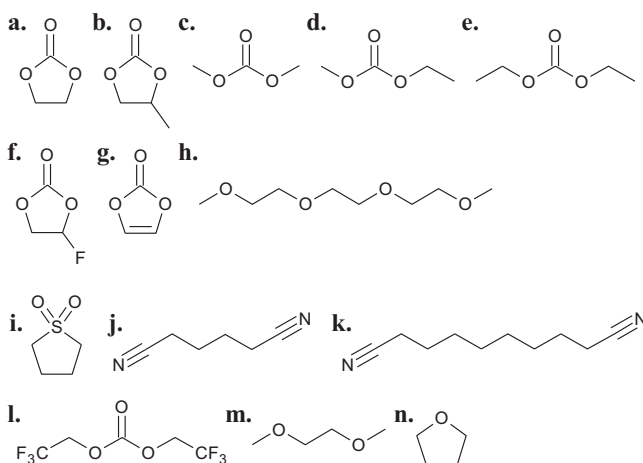


**Figure 1.5** Common Li-ion cell solvents and additives: (a) ethylene carbonate (EC); (b) propylene carbonate (PC); (c) dimethyl carbonate (DMC); (d) ethyl-methyl carbonate (EMC); (e) diethyl carbonate (DEC); (f) fluoroethylene carbonate (FEC); (g) vinylene carbonate (VC); (h) triethylene glycol dimethyl ether (triglyme); (i) sulfolane (SL); (j) adiponitrile (ADN); (k) sebaconitrile; (l) bis(2,2,2-trifluoroethyl)carbonate (TFEC); (m) 1,2-dimethoxyethane (DME); (n) tetrahydrofuran (THF).

Organic carbonates, as mentioned above, are not the only carbonates commonly used in solvent mixtures. There are also many solvents that are used as additives in solutions to stabilize the SEI formation during cycling. The most popular are fluoroethylene carbonate (FEC, Fig. 1.5f) and vinylene carbonate (VC, Fig. 1.5g) [14]. The amounts of 5%–15% in the case of FEC [99] and 1%–3% in the case of VC are usually enough [100] to achieve the stability and proper cyclability of the electrolyte [101].

Some of the solvents investigated in the Li-ion technology are known to be model solvents or are investigated as new solvents in Li-ion cells [102]. The most popular of this group of solvents are ethylene glycol ethers of the general formula  $R_1-(\text{CH}_2-\text{CH}_2-\text{O}-)_n-R_2$ . Depending on the chain endings there are methoxy ( $\text{CH}_3-\text{O}-$  and  $-\text{H}$ ) or dimethyl ( $\text{CH}_3-\text{O}-$  and  $-\text{CH}_3$ ) ethers. When the chains are short ( $n = 1$  to 4), then these solvents are called glymes (di-, tri-, or tetruglyme, depending on the value of  $n$ , Fig. 1.5h). These solvents

help to model the behavior of the polymer matrix in poly(ethylene oxide) membranes [103].

An additional group of solvents is used for high-voltage applications. As typically used carbonates are not fully stable in lithium salt solutions in the presence of high-voltage cathodes at high potentials (above 4.5 V), other classes of solvents are used. The most prominent examples are sulfur analogs of organic carbonates (e.g., sulfones and sulfites), like sulfolane (Fig. 1.5i) [104], and nitriles, like adiponitrile (Fig. 1.5j) or sebaconitrile (Fig. 1.5k) [105]. Fluorinated carbonates are another group good for this application, for example, FEC and bis(2,2,2-trifluoroethyl)carbonate (Fig. 1.5l) [106]. They are used often as the main solvents and for some applications as cosolvents/additives (up to 10%). These solvents, depending on ratios and the exact choice of the cosolvents, can be used up to 6 V versus Li [105].

## 1.11 Electrolyte Design: Maximizing Parameters

Battery usage at extreme temperatures requires special solvent mixtures to provide certain properties. If temperatures are high, then the maximum operating temperature will be the boiling point of the solvent or the cosolvent in the given mixture, in case one of solvents in the mixture may evaporate earlier than the rest. As usually it is the salt that limits the maximum operating temperature, a high vapor pressure at high temperatures also limits it, even if the solvent has a low vapor pressure at room temperature. On the other hand, at high temperatures, viscosity values are lower and conductivity values are higher, so some additional solvents are eligible for use in the cell for such a purpose. As a result, apart from choosing solvents with high boiling and decomposition points, one can also select solvents from oligomers—polymers that have no or negligible vapor pressure. Then, the whole mixture also has a low vapor pressure. Additionally, there is a possibility of using ILs as cosolvents [107]. However, for application temperatures above the 150°C–200°C range, mostly solid polymer or ceramic electrolytes are the only ones to use [108]. The downside of their use is that cells using them cease to operate properly at room temperature or below.

The minimum operating temperature shifts to 40°C–60°C in the case of polymer electrolytes [109, 110] and to 20°C–100°C in the case of ceramic materials—the range is wide, as there is a choice of ceramic material classes [111].

There are significant issues with battery operation at extremely low temperatures [112]. Most solvents and solvent mixtures crystallize between –40°C and 0°C [113]. That is why there are various methods to extend the operating temperature below this temperature range. The first method is to use traditional solvents (carbonates) to prepare a solvent mixture at the eutectic composition—for all components (usually two to four) [114, 115]. Also, there is a variant of this way—to use less common solvents but those that have very low melting points, for example, DME (1,2-dimethoxyethane, Fig. 1.5m) or tetrahydrofuran (Fig. 1.5n) [116]. In this way, it is possible to achieve electrolyte operating temperatures down to –40°C. The second method is to use specialized solvent mixtures containing oligomers and ethylene carbonate [117]. Such mixtures are fully amorphous (no melting point), and thus minimum operating temperatures drop to –70°C or even –80°C, below which point glass transition occurs. This comes at the cost of lower conductivities at room temperature (3–4 mS/cm) and lower conductivity at low temperatures compared to the first method. However, cell operation at a lower temperature is possible as long as the electrodes work at the given temperature. In the typical method, cells cannot be stored below the operation temperature of the electrolyte. Mechanical stress due to crystallization of the electrolyte in pores may damage the electrode. Thus, in the second method, there is an additional advantage. Even if the temperature drops below the operating temperatures, nothing will happen to the electrode structure as at glass temperature, there is no sudden density change.

A typical parameter to maximize for industrial purposes is ionic conductivity. To increase ionic conductivity, three variables need to be optimized: (1) which solvents are selected, (2) ratio between these solvents, and (3) salt concentration. One solvent has to be highly polar, and it is most commonly EC, but PC or FEC can be used instead as well. PC exfoliates most common graphite anodes, so unless other electrodes are used, PC cannot be considered. Even

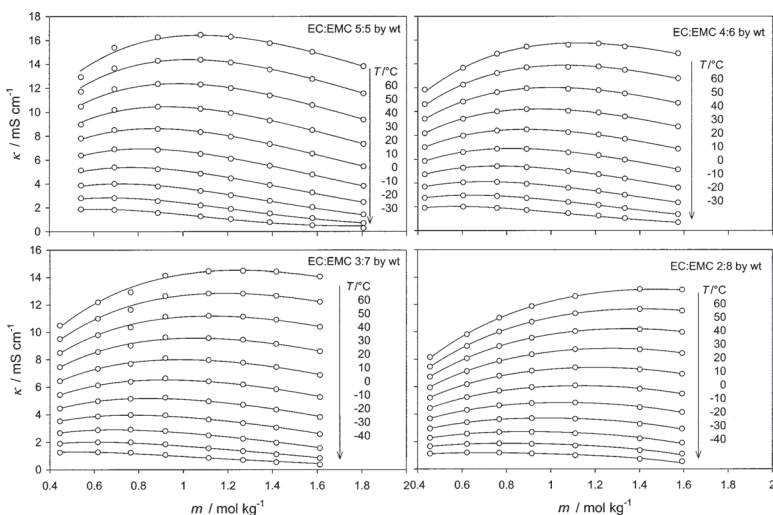


**Figure 1.6** Results of an exemplary optimization process of solvent ratio and lithium salt concentration [65]. Change of conductivity  $\kappa$  with salt content  $m$  at different temperatures  $T$  and solvent compositions EC:EMC for electrolytes of  $\text{LiPF}_6$  in a 1:1 mixture of EC and EMC. The dots represent experimental data, and the curves plot the fitting function.

if silicon or lithium titanate oxide anodes are used, PC still performs poorly in comparison because it has higher viscosity and lower dielectric constant than FEC or EC. As FEC is much more expensive than others and does not provide much better properties than EC, it is EC that is used in typical solvent mixtures. Both have high melting points (FEC at  $17^{\circ}\text{C}$  and EC at  $38^{\circ}\text{C}$ ) and high viscosity (FEC 4.1 mPa s and EC 1.9 mPa s at  $40^{\circ}\text{C}$ ) [118], so they need to be supported by at least one other solvent to lower their viscosity and melting points. From the conductivity point of view, as long as the minimum operating temperature is satisfactory, the higher the content of EC, the better. However, due to the high viscosity of EC (approximately 3 times the viscosity of DMC, DEC, or EMC) there is always some optimal range at which the viscosity is already low and the dielectric constant is still high. In terms of conductivity, this golden mean range is located usually somewhere between the ratios of 2:1 to 1:2, depending on the second solvent viscosity and the salt and its concentration. The salt concentration also cannot be too

high, as above some point, the increase in charge carriers does not balance the viscosity increase, so the typical optimal concentrations are in the 0.5–1.5 mol kg<sup>-1</sup> range. As for the viscosity of the second solvent, most commonly, the less viscous it is, the higher the amount of it should be used to prepare an optimal mixture. For instance, the optimal EMC range for LiPF<sub>6</sub>-based electrolytes is 1:1 to 1:2 (EC to EMC) while for DEC, it is 3:2 to 1:1 (EC to DEC). Figure 1.6 shows results of such an exemplary optimization process. Finally, the salt can also affect the optimal mixture, as the anion structure influences the viscosity of the solution, thus changing the solvent ratios for optimal viscosity. Even more complex optimization is required for a three- or four-component solvent mixture but may yield better results than those for two-component mixtures, or at least keep good conductivity and improve some other property.

## 1.12 Other Electrolytes for Li-Ion Cells

Use of ILs is one of the ways for avoiding the aforementioned disadvantages of liquid electrolytes. ILs consist only of ions and are actually molten salts with melting points below 100°C [119]. In the case of ILs for electrochemical purposes the ones that are used are selected from those the melting points of which are at least below room temperature, or even 0°C. ILs have very diverse compositions, as multiple organic and inorganic structures can be used for anions and cations for ILs. Both cations and anions need to be very weakly coordinating ones, as only weak interactions would allow for such a low melting point. Thanks to no measurable vapor pressure and no low-temperature decomposition or flash points, they are much safer as they are not flammable [120]. No solvent content in the electrolyte also broadens the cell's operating temperatures, as usually the IL decomposition temperature is higher than the typical solvent boiling point. On the other hand, ILs often limit the minimum operating temperature, as they tend to have high melting points. Getting rid of solvents also avoids the decomposition processes or side reactions connected to the instability of solvents upon contact with the electrodes at high or low potentials. The electrochemical stability of ILs is similar to that of anions, but cations also influence

and may limit that stability. However, due to a high concentration of ions—all of the volume is taken up by ions—the association degree is high, the agglomeration level is high (and agglomerates are big), and the viscosity is high as well. For instance, the viscosity value of 1-ethyl-3-methylimidazolium tetrafluoroborate ( $\text{EMImBF}_4$ ) IL without salt is 45 mPa s at room temperature. Upon addition of  $1.5 \text{ mol kg}^{-1}$   $\text{LiBF}_4$ , the viscosity increases to  $\sim 200$  mPa s [121]. Although the conductivity is also high, it drops substantially upon the addition of lithium salt, so the resulting electrolyte does not have so high a conductivity (the  $\text{EMImBF}_4$  conductivity of 17.2 mS/cm drops to 8.5 mS/cm after the addition of  $1.5 \text{ mol kg}^{-1}$   $\text{LiBF}_4$ ) [121]. Additionally, the lithium cation transference number is extremely low (below 0.1 for most systems) [122]. However, values can be flawed as there are limitations to methods used for measurements due to a complicated system composition. The anion range used in ILs for electrolyte applications is the same as in the case of lithium salts for Li-ion cells. That gives the possibility of using the same anion on both IL and lithium salt or a different one. However, apart from the poor electrochemical parameters, there may be also the issue of poor salt solubility. Usually, TFSI-based ILs tend to have good salt solubility of  $\text{LiTFSI}$  salt [123] as well as at least some solubility of other salts [124]. As for other salts, it may be an issue, although usually salts with the same anion as IL are soluble at least to a small degree. With other combinations, it may happen that the salt is completely insoluble. Although there are methods to affect this solubility [125], there is always some trade-off involved. For instance, the addition of a glyme may increase the salt solubility and electrolyte conductivity but decreases its electrochemical stability or may limit the maximum operating temperature [126].

Cations for ILs for electrochemical applications are selected from the list of typical classes. Their design or selection is based on the same general rules as for lithium salt anions, but with respect to their cationic nature. So instead of electron-withdrawing groups (acceptor groups), there should be donor groups, also used to achieve uniform charge distribution. The only important difference is that the cation should be asymmetrical, as the anion is usually symmetrical. It is due to the need for regularity disturbance, as structure regularity makes crystallization easier and increases the

melting point to a value above the one needed for the application of the IL as a solvent. So far at least a few hundred cations and a few dozen anions have been identified (and applied) that can be used to form ILs. However, not every combination can form an IL. The cation is usually selected to tailor the IL properties for a given anion. Due to the requirement of electrochemical stability, there are a few dozen cations and about a dozen anions typically used. Anions are usually chosen from the following list [127]:  $\text{ClO}_4^-$ ,  $\text{BF}_4^-$ ,  $\text{PF}_6^-$ ,  $\text{AsF}_6^-$ ,  $\text{BOB}^-$ ,  $\text{DFOB}^-$ ,  $\text{B}(\text{CN})_4^-$ ,  $\text{Tf}^-$ ,  $\text{FSI}^-$ ,  $\text{TFSI}^-$ ,  $\text{BETI}^-$ ,  $\text{TFSM}^-$ , and  $\text{FAP}^-$ . Also new anions can be used for that application and yield interesting results, like  $\text{TDI}^-$  [128]. For Li-ion research most commonly  $\text{TFSI}^-$ ,  $\text{FSI}^-$ ,  $\text{PF}_6^-$ ,  $\text{BF}_4^-$ ,  $\text{Tf}^-$ , and  $\text{FAP}^-$  are used as anions for ILs.

The cations with a potential for IL application in Li-ion cell electrolytes are [129] imidazolium (typically 1-alkyl-3-methylimidazole or 1-alkyl-2,3-dimethylimidazole, where the alkyl has 2–8 carbons, usually an even number), pyrrolidinium (e.g., 1-alkyl-1-methylpyrrolidine, where the alkyl can be a simple or branched chain), ammonium (asymmetric tetraalkylammonium or trialkylaloxonium), piperidinium (*N*-alkyl-*N*-methyl-piperidine), pyridinium (*N*-alkylpyridine, where the alkyl can be a simple or branched chain), and phosphonium (asymmetric tetraalkylphosphonium, where the alkyls are at least 4-carbon simple chains). The most frequently used cations for Li-ion research are imidazolium cations with a 2- to 6-carbon side chain and to a lesser extent also pyrrolidinium and piperidinium cations.

It is possible to use LiTFSI and other imide salts in liquid electrolytes thanks to the solvent-in-salt concept, which employs extremely high concentrations of lithium salts—above 5 mol dm<sup>-3</sup> [130]. As the idea is mostly developed for LiTFSI, other salts may also take advantage of the possibility. Thanks to high concentrations, the ratio between cation and solvent is so low that there is only a negligible number of solvent molecules in a nonsolvated form. In this way, the solvent-in-salt idea omits a lot of disadvantages connected to solvent reactions and/or catalytic properties upon contact with electrode and lithium salt.

There is also an actual attempt to use water as a solvent in Li-ion cells [131], as there are almost no “free” water molecules at the saturated-level concentrations. Electrolyte stabilities are much

widened [132], and although total ionic conductivity is not very high (0.8 mS/cm at room temperature in a 1,3-dioxolane:DME mixture), lithium cation transference numbers are substantially increased (above 0.7) [130].

On the other hand, only salts that are able to dissolve at such high concentrations may be used in this concept. So far, most applications of the solvent-in-salt concept have been limited to LiTFSI, LiFSI, and LiBETI salts but have yielded promising results for the conductivity and stability of water-in-salt systems with concentrations above 7 mol kg<sup>-1</sup> [133].

## 1.13 Anions for Post-Li-Ion Cells

Post-Li-ion cell technologies, by typical definition, are all new cell chemistries, such as lithium-air, sodium-ion, and magnesium-ion. However, depending on the definition, the range also includes advanced Li-ion cell technologies. These include Li-ion cells with solid polymer electrolytes (the so-called all-solid-state, by EU definition called “generation 4” or “generation 4a”), all-solid-state cells with lithium metal anodes (generation 4b), lithium-sulfur (often in generation 4), and lithium-air (if considered as Li-ion, then called generation 5). The common factor for advanced Li-ion and most post-Li-ion technologies is a similar basis of the operation. All share the concept of the rocking chair, which means the main ion movement between electrodes during charge and discharge being back and forth, with no charge transfer with the titular ion. This also means that the transport of ions in the electrolyte should undergo the same rules and behavior, as the same behavior and properties of the electrolyte are required. As a result, the same anions can be used for electrolyte design.

The Li-ion cell works in the widest operating range of all above-mentioned technologies, at least so far as the current state-of-the-art research goes. Thus, most of the anions used in Li-ion cells will be good for other technologies. The only limitations are possible different catalytic properties or reactivity of electrodes used for other technologies, as well as completely new properties required. However, compatibility with solvents, thermal and electrochemical

stability, conductivity, etc., should be similar. Also, solvents have to be different, which means the necessity to select the correct anion and with the correct concentration to allow the given metal salt to dissolve and dissociate in the dedicated solvent (solvent mixture) [134]. Finally, new challenges come with new cell technologies, such as requirement of good solubility or insolubility of the cell components. For instance, in a Li-S cell the solubility of sulfur and/or polysulfides is influenced by the salt anion and its concentration [135]. Another example is the Li-air cell, which requires electrolytes that allow adequate solubility of lithium oxides and oxygen.

Some similarities between Li-ion and post-Li-ion cells may be expected. For instance, in a Na-ion cell, both NaTFSI and NaPF<sub>6</sub> also exhibit very high conductivity (>10 mS/cm) [136]. However, NaTFSI still corrodes the aluminum current collector and NaPF<sub>6</sub> is still very unstable—both thermally and chemically [137]. Additionally, analogs of novel imidazolide tailored salts are available for post-Li-ion cells. For instance, NaTDI and NaPDI [138] can be used for Na-ion cells. New salts designed with the same strategy as TDI<sup>−</sup> are considered, including nonfluorine ones, like sodium 1,1,2,3,3-pentacyanopropenide [139]. However, research in all of the post-Li-ion cells is still in too early a stage to suggest any future possible predominance of any of the salts without any doubt.

## 1.14 Examples of Electrolytes for Li-Ion Cells

Here is a list of selected optimal electrolytes for particular applications/properties:

For general use, for high-power applications: 1 mol kg<sup>−1</sup> LiPF<sub>6</sub> in a 1:1 mixture of EC and DMC with the addition of 10% FEC and 2% VC [55]; the electrolyte is low in cost, with all requirements fulfilled.

For general use, nonflammable: 1 mol kg<sup>−1</sup> LiPF<sub>6</sub> in a 3:3:2 mixture of EC, PC, and DEC, respectively, with the addition of 20% trimethyl phosphate (TMP) [140]—TMP provides inflammability.

To use at high temperatures (>60°C): 1 mol kg<sup>−1</sup> LiTDI in a 3:7 mixture of EC and DMC, respectively, [141]—unlike LiPF<sub>6</sub>, there is no degradation of this electrolyte over time when cycled at 60°C.

To use at low temperatures ( $\leq 20^\circ\text{C}$ ): 1 mol  $\text{kg}^{-1}$  LiPF<sub>6</sub> in a 1:1:1:3 mixture of EC, DEC, DMC, and EMC, respectively, [92]—the best cycling is at  $-20^\circ\text{C}$  and below and the highest conductivity of the electrolyte is at low temperatures.

To use with a Si-C composite (50% Si) anode: 0.6 mol  $\text{kg}^{-1}$  LiTDI in a 1:2 mixture of EC and DMC, respectively, with the addition of 10% FEC and 2% VC [142, 143]—the electrolyte has a much longer life and a much higher capacity than in the case of LiPF<sub>6</sub>.

For the long life of the cell (with NMC, LTO, LFP, etc.): 0.6 mol  $\text{kg}^{-1}$  LiTDI in a 3:7 mixture of EC and DMC, respectively, with the addition of 2% FEC [144]—the electrolyte has better capacity retention over long cycling ( $> 500$  cycles).

For a better performance (with NMC/graphite) at both high and low temperatures: 1 mol  $\text{kg}^{-1}$  LiTDI in a 1:1:1 mixture of EC,  $\gamma$ -butyrolactone, and methyl propionate, respectively, with the addition of 2% FEC [145]—the electrolyte has better capacity retention and lower irreversible capacities during initial cycles of the cell.

For a low voltage drop near the end of the discharge (with a lithium cobalt oxide cathode): 0.6 mol  $\text{kg}^{-1}$  LiTDI in a 3:7 mixture of EC and DEC, respectively, [146]—in 3–4.2 V cycling cut-off limits, the cell voltage drops below 3.75 V for a LiPF<sub>6</sub>-based electrolyte at 14% and for a LiTDI-based electrolyte at 3% of the remaining capacity.

For high-voltage cathodes ( $> 4.2$  V): 1 mol  $\text{kg}^{-1}$  LiPF<sub>6</sub> in a 1:1:2 mixture of EC, DMC, and sebaconitrile, respectively, [105]—a high concentration of dinitriles (like adiponitrile and sebaconitrile) is required for achieving stability above 5 V versus Li—this particular mixture is stable close to 6 V versus Li.

## References

1. K. Xu, *Chem. Rev.*, **104** (2004) 4303.
2. E. Zinigrad, L. Larush-Asraf, J. S. Gnanaraj, H. E. Gottlieb, M. Sprecher, D. Aurbach, *J. Power Sources*, **146** (2005) 176.
3. Y. Wang, S. Nakamura, M. Ue, P. B. Balbuena, *J. Am. Chem. Soc.*, **123** (2001) 11708.
4. G. E. Blomgren, *J. Power Sources*, **81–82** (1999) 112.

5. M. M. Archuleta, *J. Power Sources*, **54** (1995) 138.
6. D. Chung, E. Elggqvist, S. Santhanagopalan, NREL/TP-6A20-66086, April 2016, CEMAC Technical Report (available on [www.manufacturingcleanenergy.org](http://www.manufacturingcleanenergy.org)).
7. D. Aurbach, *J. Power Sources*, **89** (2000) 206.
8. M. S. Ding, T. R. Jow, *J. Electrochem. Soc.*, **151** (2004) A2007.
9. R. K. Blundell, P. Licence, *Chem. Commun.*, **50** (2014) 12080.
10. T. J. Barbarich, P. F. Driscoll, S. Izquierdo, L. N. Zakharov, C. D. Incarvito, A. L. Rheingold, *Inorg. Chem.*, **43** (2004) 7764.
11. L. O. Valøen, J. N. Reimers, *J. Electrochem. Soc.*, **152** (2005) A882.
12. D. Aurbach, B. Markovsky, G. Salitra, E. Markevich, Y. Talyossef, M. Koltypin, L. Nazar, B. Ellis, D. Kovacheva, *J. Power Sources*, **165** (2007) 491.
13. D. Aurbach, *J. Power Sources*, **89** (2000) 206.
14. S. S. Zahng, *J. Power Sources*, **162** (2002) 1379–1394
15. V. A. Sethuraman, L. J. Hardwick, V. Srinivasan, R. Kostecki, *J. Power Sources*, **195** (2010) 3655.
16. H. Yang, K. Kwon, T. M. Devine, J. W. Evans, *J. Electrochem. Soc.*, **147** (2000) 4399.
17. M. Morita, T. Shibata, N. Yoshimoto, M. Ishikawa, *Electrochim. Acta*, **47** (2002) 2787.
18. I. A. Shkrob, K. Z. Pupek, J. A. Gilbert, S. E. Trask, D. P. Abraham, *J. Phys. Chem. C*, **120** (2016) 28463.
19. A. M. Andersson, K. Edström, *J. Electrochem. Soc.*, **148** (2001) A1100.
20. Gueguen, D. Streich, M. He, M. Mendez, F. F. Chesneau, P. Novak, E. J. Berg, *J. Electrochem. Soc.*, **163** (2016) A1095.
21. D. J. Xiong, L. D. Ellis, R. Petibon, T. Hynes, Q. Q. Liu, J. R. Dahn, *J. Electrochem. Soc.*, **164** (2017) A340.
22. M. Börner, A. Friesen, M. Grützke, Y. P. Stenzel, G. Brunklaus, J. Haetge, S. Nowak, F. M. Schappacher, M. Winter, *J. Power Sources*, **342** (2017) 382.
23. G.-A. Nazri, G. Pistoia, *Lithium Batteries: Science and Technology*, Kluwer Academic, MA, USA, 2004.
24. P. Murmann, P. Niehoff, R. Schmitz, S. Nowak, H. Gores, N. Ignatiev, P. Sartori, M. Winter, R. Schmitz, *Electrochim. Acta*, **114** (2013) 658.
25. F. Toulgoat, B. R. Langlois, M. Medebielle, J.-Y. Sanchez, *J. Org. Chem.*, **72** (2007) 9046.

26. C. Michot, M. Armand, J.-Y. Sanchez, Y. Choquette, M. Gauthier, Patent US 5916475 (1999).
27. A. Webber, *J. Electrochem. Soc.*, **138** (1991) 2586.
28. M. B. Armand, C. E. M. F. El Kadiri, Patent US 4505997 (1985).
29. L. J. Krause, W. Lamanna, J. Summerfield, M. Engle, G. Korba, R. Loch, R. Atanasoski, *J. Power Sources*, **68** (1997) 320.
30. W. M. Lamanna, L. J. Krause, Patent US 5652072 (1997).
31. L. Conte, G. P. Gambaretto, G. Caporiccio, F. Alessandrini, S. Passerini, *J. Fluorine Chem.*, **125** (2004) 243.
32. Komaru, T. Nirasawa, Patent JP 3642487B2 (2002).
33. M. Handa, M. Suzuki, J. Suzuki, H. Kanematsu, Y. Sasaki, *Electrochem. Solid-State Lett.*, **2** (1999) 60.
34. M. Schmidt, U. Heider, A. Kuehner, R. Oesten, M. Jungnitz, N. Ignat'ev, P. Sartori, *J. Power Sources*, **97–98** (2001) 557.
35. U. Heider, V. Hilarius, P. Sartori, N. Ignat'ev, Patent DE 19846636 (2000).
36. J. Barthel, R. Buestrich, H. J. Gores, M. Schmidt, M. Wuhr, *J. Electrochem. Soc.*, **144** (1997) 3866.
37. J. Barthel, R. Buestrich, E. Carl, H. J. Gores, *J. Electrochem. Soc.*, **143** (1996) 3572.
38. Z.-M. Xue, K.-N. Wu, B. Liu, C.-H. Chen, *J. Power Sources*, **171** (2007) 944.
39. H. H. Horowitz, J. I. Haberman, L. P. Kleemann, G. H. Newman, E. L. Stogryn, T. A. Whitney, *Proc. Electrochem. Soc.*, **81-4** (1981) 131.
40. E. Zygałdo-Monikowska, Z. Florjańczyk, K. Służewska, J. Ostrowska, N. Langwald, A. Tomaszewska, *J. Power Sources*, **195** (2010) 6055.
41. A. Ueda, K. Iwamoto, K. Sonoda, Patent JP 4843834B2 (2000).
42. W. Xu, C. A. Angell, *Electrochem. Solid-State Lett.*, **4** (2001) E1.
43. V. Aravindan, P. Vickraman, *Solid State Sci.*, **9** (2007) 1069.
44. H. Yamaguchi, H. Takahashi, M. Kato, J. Arai, *J. Electrochem. Soc.*, **150** (2003) A312.
45. I. Krossing, *Chem. Eur. J.*, **7** (2001) 490.
46. L. A. Dominey, V. R. Koch, T. J. Blakley, *Electrochim. Acta*, **37** (1992) 1551.
47. L. Niedzicki, M. Kasprzyk, K. Kuziak, G. Z. Żukowska, M. Armand, M. Bukowska, M. Marcinek, P. Szczęciński, W. Wieczorek, *J. Power Sources*, **192** (2009) 612.

48. M. Bukowska, P. Szczeciński, W. Wieczorek, L. Niedzicki, B. Scrosati, S. Panero, P. Reale, M. Armand, S. Laruelle, S. Grugeon, FR 2935382 (2008).
49. M. Egashira, B. Scrosati, M. Armand, S. Beranger, C. Michot, *Electrochim. Solid-State Lett.*, **6** (2003) A71.
50. P. Johansson, P. Jacobsson, *J. Power Sources*, **153** (2006) 336.
51. M. Xu, A. Xiao, W. Li, B. L. Lucht, *Electrochim. Solid-State Lett.*, **12** (2009) A155.
52. M. Xu, A. Xiao, W. Li, B. L. Lucht, *J. Electrochim. Soc.*, **157** (2010) A115.
53. O. V. Bushkova, T. V. Yaroslavtseva, Y. A. Dobrovolsky, *Russ. J. Electrochem.*, **53** (2017) 677.
54. H.-B. Han, S.-S. Zhou, D.-J. Zhang, S.-W. Feng, L.-F. Li, K. Liu, W.-F. Feng, J. Nie, H. Li, X.-J. Huang, M. Armand, Z.-B. Zhou, *J. Power Sources*, **196** (2011) 3623.
55. K. Xu, *Chem. Rev.*, **114** (2014) 11503.
56. W. Xu, C. A. Angell, *Electrochim. Solid-State Lett.*, **3** (2000) 366.
57. W. Xu, C. A. Angell, *Electrochim. Solid-State Lett.*, **4** (2001) E1.
58. P. Murmann, R. Schmitz, S. Nowak, N. Ignat'ev, P. Sartori, I. Cekic-Laskovic, M. Winter, *J. Electrochim. Soc.*, **162** (2015) A1738.
59. G. H. Newman, R. W. Francis, L. H. Gaines, B. M. L. Rao, *J. Electrochim. Soc.*, **127** (1980) 2025.
60. R. Jasinski, S. Carroll, *J. Electrochim. Soc.*, **117** (1970) 218.
61. N.-S. Choi, S.-W. Ryu, J.-K. Park, *Electrochim. Acta*, **53** (2008) 6575.
62. M. S. Ding, *J. Electrochim. Soc.*, **151** (2004) A40.
63. S. S. Zhang, K. Xu, T. R. Jow, *J. Electrochim. Soc.*, **149** (2002) A586.
64. A. M. Andersson, K. Edström, J. O. Thomas, *J. Power Sources*, **81–82** (1999) 8.
65. M. S. Ding, K. Xu, S. S. Zhang, K. Amine, G. L. Henriksen, T. R. Jow, *J. Electrochim. Soc.*, **148** (2001) A1196.
66. Z. Lu, L. Yang, Y. Guo, *J. Power Sources*, **156** (2006) 555.
67. H. Yang, G. V. Zhuang, P. N. Ross Jr., *J. Power Sources*, **161** (2006) 573.
68. M. Schmidt, U. Heider, A. Kuehner, R. Oesten, M. Jungnitz, N. Ignat'ev, P. Sartori, *J. Power Sources*, **97–98** (2001) 557.
69. T. Evans, J. Olson, V. Baht, S.-H. Lee, *J. Power Sources*, **269** (2014) 616.
70. Y. Abu-Lebdeh, I. Davidson, *J. Electrochim. Soc.*, **156** (2009) A60.
71. S. H. Strauss, *Chem. Rev.*, **93** (1993) 927.
72. J.-Y. Sanchez, F. Alloin, C. Iojoiu, *J. Fluorine Chem.*, **127** (2006) 1471.

73. L. Niedzicki, G. Z. Zukowska, M. Bukowska, P. Szczecinski, S. Grugeon, S. Laruelle, M. Armand, S. Panero, B. Scrosati, M. Marcinek, W. Wieczorek, *Electrochim. Acta*, **55** (2010) 1450.
74. L. Niedzicki, B. Brzozowski, P. Wieczorek, *Electrochim. Acta*, **174** (2015) 625.
75. L. Niedzicki, E. Karpierz, A. Bitner, M. Kasprzyk, G. Z. Zukowska, M. Marcinek, W. Wieczorek, *Electrochim. Acta*, **117** (2014) 224.
76. J. Scheers, L. Niedzicki, G. Z. Źukowska, P. Johansson, W. Wieczorek, P. Jacobsson, *Phys. Chem. Chem. Phys.*, **13** (2011) 11136.
77. M. Broszkiewicz, A. Zalewska, L. Niedzicki, *Ionics*, **25** (2019) 3651–3660.
78. L. Niedzicki, P. Oledzki, A. Bitner, M. Bukowska, P. Szczecinski, *J. Power Sources*, **306** (2016) 573.
79. L. Niedzicki, J. Korczak, A. Bitner, M. Bukowska, P. Szczecinski, *RSC Adv.*, **5** (2015) 101917.
80. O. E. Geiculescu, J. Yang, H. Blau, R. Bailey-Walsh, S. E. Creager, W. T. Pennington, D. D. DesMarteau, *Solid State Ionics*, **148** (2002) 173.
81. J. Nie, X. Li, D. Liu, R. Luo, L. Wang, *J. Fluorine Chem.*, **125** (2004) 27.
82. O. E. Geiculescu, Y. Xie, R. Rajagopal, S. E. Creager, D. D. DesMarteau, *J. Fluorine Chem.*, **125** (2004) 1179.
83. T. Trzeciak, L. Niedzicki, G. Groszek, P. Wieczorek, M. Marcinek, W. Wieczorek, *J. Power Sources*, **252** (2014) 229.
84. E. Jonsson, M. Armand, P. Johansson, *Phys. Chem. Chem. Phys.*, **14** (2012) 6021.
85. H. Mei, D. VanDerveer, D. D. DesMarteau, *J. Fluorine Chem.*, **145** (2013) 35.
86. M. Watanabe, H. Tokuda, S. Muto, *Electrochim. Acta*, **46** (2001) 1487.
87. R. Meziane, J.-P. Bonnet, M. Courty, K. Djellab, M. Armand, *Electrochim. Acta*, **57** (2011) 14.
88. S. Feng, D. Shi, F. Liu, L. Zheng, J. Nie, W. Feng, X. Huang, M. Armand, Z. Zhou, *Electrochim. Acta*, **93** (2013) 254.
89. R. P. Seward, E. C. Vieira, *J. Phys. Chem.*, **62** (1958) 127.
90. M. S. Ding, *J. Electrochem. Soc.*, **150** (2003) A455.
91. H.-Y. Song, T. Fukutsuka, K. Miyazaki, T. Abe, *J. Electrochem. Soc.*, **163** (2016) A1265.
92. M. C. Smart, B. V. Ratnakumar, L. D. Whitcanack, K. B. Chin, S. Surampudi, H. Croft, D. Tice, R. Staniewicz, *J. Power Sources*, **119–121** (2003) 349.

93. W. M. Haynes, ed., in Chapter 6, *Handbook of Chemistry and Physics*, 92nd Ed., CRC Press, Boca Raton, U.S., 2011.
94. J. Y. Kim, D. O. Shin, T. Chang, K. M. Kim, J. Jeong, J. Park, Y. M. Lee, K. Y. Cho, C. Phatak, S. Hong, Y.-G. Lee, *Electrochim. Acta*, **300** (2019) 299.
95. M. Dahbi, F. Ghamouss, F. Tran-Van, D. Lemordant, M. Anouti, *J. Power Sources*, **196** (2011) 9743.
96. M. S. Ding, K. Xu, T. R. Jow, *J. Therm. Anal. Calorim.*, **60** (2000) 177.
97. G. G. Eshetu, S. Grugeon, S. Laurelle, S. Boyanow, A. Lecocq, J.-P. Bertrand, G. Marlair, *Phys. Chem. Chem. Phys.*, **15** (2013) 9145.
98. T. M. Bandhauer, S. Garimella, T. F. Fuller, *J. Electrochem. Soc.*, **158**(3) (2011) R1.
99. V. Etacheri, O. Haik, Y. Goffer, G. A. Roberts, I. C. Stefan, R. Fasching, D. Aurbach, *Langmuir*, **28** (2012) 965.
100. C. C. Nguyen, B. L. Lucht, *J. Electrochem. Soc.*, **161** (2014) A1933.
101. H. Ota, K. Shima, M. Ue, J.-I. Yamaki, *Electrochim. Acta*, **49** (2002) 565.
102. D. Morales, R. E. Ruther, J. Nanda, S. Greenbaum, *Electrochim. Acta*, **304** (2019) 239.
103. G. J. Kearly, P. Johansson, R. G. Delaplane, J. Lindgren, *Solid State Ionics*, **147** (2002) 237–242.
104. J. Alvarado, M. A. Schroeder, M. Zhang, O. Borodin, E. Gobrogge, M. Olguin, M. S. Ding, M. Gobet, S. Greenbaum, Y. S. Meng, K. Xu, *Mater. Today*, **21** (2018) 341.
105. M. Nagahama, N. Hasegawa, S. Okada, *J. Electrochem. Soc.*, **157** (2010) A748.
106. K. Fridman, R. Sharabi, R. Elazari, G. Gershinsky, E. Markevich, G. Salitra, D. Aurbach, A. Garsuch, J. Lampert, *Electrochim. Commun.*, **33** (2013) 31.
107. N. Plylahan, M. Kerner, D.-H. Lim, A. Matic, P. Johansson, *Electrochim. Acta*, **216** (2016) 24.
108. I. Abrahams, E. Hadzifejzovic, *Solid State Ionics*, **134** (2000) 249.
109. F. Alloin, D. Benrabah, J.-Y. Sanchez, *J. Power Sources*, **68** (1997) 372.
110. H. Zhang, C. Li, M. Pisycz, E. Coya, T. Rojo, L. M. Rodriguez-Martinez, M. Armand, Z. Zhou, *Chem. Soc. Rev.*, **46** (2017) 797.
111. J. W. Fergus, *J. Power Sources*, **195** (2010) 4554.
112. M. C. Smart, B. V. Ratnakumar, S. Surampudi, *J. Electrochem. Soc.*, **149** (2002) A361.
113. H.-J. Gores, J. Barthel, *J. Solution Chem.*, **9** (1980) 939.

114. E. J. Plichta, M. Hendrickson, R. Thompson, G. Au, W. K. Behl, M. C. Smart, B. V. Ratnakumar, S. Surampudi, *J. Power Sources*, **94** (2001) 160.
115. M. S. Ding, K. Xu, S. Zhang, T. R. Jow, *J. Electrochem. Soc.*, **148** (2001) A299.
116. J.-P. Jones, S. C. Jones, F. C. Krause, J. Pasalic, M. C. Smart, R. V. Bugga, E. J. Brandon, W. C. West, *J. Electrochem. Soc.*, **164** (2017) A3109.
117. M. Kasprzyk, A. Zalewska, L. Niedzicki, A. Bitner, M. Marcinek, W. Wieczorek, *Solid State Ionics*, **308** (2017) 22.
118. M. Kobayashi, T. Inoguchi, T. Iida, T. Tanioka, H. Kumase, Y. Fukai, *J. Fluorine Chem.*, **120** (2003) 105.
119. H. Liu, H. Yu, *J. Mater. Sci. Technol.*, **35** (2019) 674.
120. A. Noda, K. Hayamizu, M. Watanabe, *J. Phys. Chem. B*, **105** (2001) 4603.
121. K. Hayamizu, Y. Aihara, H. Nakagawa, T. Nukuda, W. S. Price, *J. Phys. Chem. B*, **108** (2004) 19527.
122. S. Ferrari, E. Quartarone, P. Mustarelli, A. Magistris, S. Protti, S. Lazzaroni, M. Fagnoni, A. Albini, *J. Power Sources*, **194** (2009) 45.
123. J.-C. Lassegues, J. Grondin, D. Talaga, *Phys. Chem. Chem. Phys.*, **8** (2006) 5629.
124. M. Holzapfel, C. Jost, A. Prodi-Schwab, F. Krumeich, A. Wursig, H. Buqa, P. Novak, *Carbon*, **43** (2005) 1488.
125. R. Kido, K. Ueno, K. Iwata, Y. Kitazawa, S. Imaizumi, T. Mandai, K. Dokko, M. Watanabe, *Electrochim. Acta*, **175** (2015) 5.
126. E. Karpierz, L. Niedzicki, T. Trzeciak, M. Zawadzki, M. Dranka, J. Zachara, G. Z. Zukowska, A. Bitner-Michalska, W. Wieczorek, *Sci. Rep.*, **6** (2016) 35587.
127. A. Lewandowski, A. Swiderska-Mocek, *J. Power Sources*, **194** (2009) 601.
128. L. Niedzicki, E. Karpierz, M. Zawadzki, M. Dranka, M. Kasprzyk, A. Zalewska, M. Marcinek, J. Zachara, U. Domanska, W. Wieczorek, *Phys. Chem. Chem. Phys.*, **16** (2014) 11417.
129. M. Galinski, A. Lewandowski, I. Stepniak, *Electrochim. Acta*, **51** (2006) 5567.
130. L. Suo, Y.-S. Hu, H. Li, M. Armand, L. Chen, *Nat. Commun.*, **4** (2013) 1481.
131. V. A. Azov, K. S. Egorova, M. M. Seitkalieva, A. S. Kashin, V. P. Ananikov, *Chem. Soc. Rev.*, **47** (2018) 1250.
132. L. Suo, O. Borodin, T. Gao, M. Olguin, J. Ho, X. Fan, C. Luo, C. Wang, K. Xu, *Science*, **350** (2015) 938.

133. P. Lannelongue, R. Bouchal, E. Mourad, C. Bodin, M. Olarte, S. le Vot, F. Favier, O. Fontaine, *J. Electrochem. Soc.*, **165** (2018) A657.
134. R. Younesi, G. M. Veith, P. Johansson, K. Edström, T. Vegge, *Energy Environ. Sci.*, **8** (2015) 1905.
135. J. Chen, K. S. Han, W. A. Henderson, K. C. Lau, M. Vijayakumar, T. Dzwiniel, H. Pan, L. A. Curtiss, J. Xiao, K. T. Mueller, Y. Shao, J. Liu, *Adv. Energy Mater.*, **6** (2016) 1600160.
136. Ponrouch, D. Monti, A. Boschin, B. Steen, P. Johansson, M. R. Palacin, *J. Mater. Chem. A*, **3** (2015) 22.
137. L. Otaegui, E. Goikolea, F. Aguesse, M. Armand, T. Rojo, G. Singh, *J. Power Sources*, **297** (2015) 168.
138. A. Plewa-Marczewska, T. Trzeciak, A. Bitner, L. Niedzicki, M. Dranka, G. Z. Zukowska, M. Marcinek, W. Wieczorek, *Chem. Mater.*, **26** (2014) 4908.
139. A. Bitner-Michalska, G. M. Nolis, G. Zukowska, A. Zalewska, M. Poterala, T. Trzeciak, M. Dranka, M. Kalita, P. Jankowski, L. Niedzicki, J. Zachara, M. Marcinek, W. Wieczorek, *Sci. Rep.*, **7** (2017) 40036.
140. G. E. Blomgren, *J. Power Sources*, **119–121** (2003) 326.
141. D. W. McOwen, S. A. Delp, W. A. Henderson, *224th ECS Meeting*, Abstract #1182.
142. L. Niedzicki, P. Oledzki, P. Wieczorek, M. Marcinek, W. Wieczorek, *Synth. Met.*, **223** (2017) 73.
143. F. Lindgren, C. Xu, L. Niedzicki, M. Marcinek, T. Gustafsson, F. Björefors, K. Edström, R. Younesi, *ACS Appl. Mater. Interfaces*, **8** (2016) 15758.
144. S. Paillet, G. Schmidt, S. Ladouceur, J. Frechette, F. Baray, D. Clement, P. Hovington, A. Guerfi, A. Vijh, I. Cayrefourcq, K. Zaghib, *J. Power Sources*, **299** (2015) 309.
145. C. L. Berhaut, R. Dedryvere, L. Timperman, G. Schmidt, D. Lemordant, M. Anouti, *Electrochim. Acta*, **305** (2019) 534.
146. S. Paillet, G. Schmidt, S. Ladouceur, J. Frechette, F. Baray, D. Clement, P. Hovington, A. Guerfi, A. Vijh, I. Cayrefourcq, K. Zaghib, *J. Power Sources*, **294** (2015) 507.

## **Chapter 2**

# **X-Ray Crystallography in Developing New Electrolyte Systems Based on Heterocyclic Anions**

**Maciej Dranka and Janusz Zachara**

*Faculty of Chemistry, Warsaw University of Technology, Noakowskiego 3,  
00-664 Warszawa, Poland  
mdranka@ch.pw.edu.pl*

### **2.1 Introduction**

Fast and reliable estimation of the electrochemical parameters of salts enabling their optimization for the growing number of new systems is a problem. This is not always easy to achieve, especially for new salts comprising anions of specific or unusual coordination properties. Therefore, a comprehensive structure analysis performed on the basis of the X-ray diffraction studies of the crystalline solvates of the new salt seems to be a good approach at the preliminary stage of research. Crystallographic studies could reveal valuable information about the properties and molecular assembly of the compound, the coordination ability of the anions,

---

*Designing Electrolytes for Lithium-Ion and Post-Lithium Batteries*

Edited by Włodzimierz Wieczorek and Janusz Płocharski

Copyright © 2021 Jenny Stanford Publishing Pte. Ltd.

ISBN 978-981-4877-16-9 (Hardcover), 978-1-003-05093-3 (eBook)

[www.jennystanford.com](http://www.jennystanford.com)

the coordination sphere of the cation, and preferred aggregation modes and in consequence, help model the local structure of the electrolyte. However, the structural characterization of salts considered for employment in the next generation of electrolyte systems is often relegated to the background. The total number of published studies investigating the impact of the molecular structure retrieved from the crystalline phase on electrochemical properties of salts is rather small or these papers relate to purely theoretical research, rarely verified experimentally [1–4]. It is worth mentioning that literature describes the results of single-crystal X-ray diffraction measurements only for a few classes of salts other than heterocyclic that are tested in electrolytes: perchlorates [5], salts with  $\text{AF}_x$  anion (hexafluoroarsenate [6, 7] and tetrafluoroborates [8]), salts of perfluoroalkylsulfonic acids (e.g.,  $\text{LiCF}_3\text{SO}_3$ ) [9], and salts with bis(trifluoromethanesulfonyl)imide (TFSI) anions [10]. The authors have pointed out that crystal structures provide valuable information about the molecular interaction between cations, anions, and solvent donor centers. As such they can serve as models of solvates found in battery electrolytes [9, 11]; they can contribute to a better understanding of the ion transport mechanism in polymer electrolytes and to the optimization of their properties [6, 12]; they are useful as models for solvate structures in concentrated electrolyte mixtures and informative about the behavior of ionic association in solutions when coupled with vibrational spectroscopic and thermal analysis [5]; or they can be a good starting point for theoretical calculations [13].

Crystallographic studies allow for a better understanding of the electrochemical properties of heterocyclic salts. A comprehensive structure analysis of a crystalline material reveals valuable information about the coordination ability of the anions as well as the coordination sphere of the cation and provides the basis for developing the model of poly(ethylene oxide) (PEO) electrolytes and liquid systems. Results revealing new aggregation modes at high concentrations of lithium salts involving the release of cations by self-assembly of the anionic subnetwork are presented. Discovering and understanding the phenomena related to the organization of such systems in the solid state is crucial for the elaboration of novel

electrolytes and significantly reduces the time required to get the optimal composition of salt and solvent.

## 2.2 Aggregation Phenomena: Solid-State and Concentrated Liquid Electrolytes

Recently, it has been found that electrolytes containing highly concentrated solutions of lithium and sodium salts or based on molten lithium salts, and thus containing strongly aggregated structural motifs, possess a number of unique features. The most important advantages of concentrated electrolytes are increased safety of batteries, the possibility of using cheap aluminum charge collectors, increased stability of the solid-electrolyte interphase passivation layer on the surface of the electrodes, and increase in the electrochemical stability window by limiting the amount and decomposition of free solvent at the electrode [14, 15]. It should be emphasized that knowledge of the factors affecting the local electrolyte structure, and hence its supramolecular assembly and the formation of associates, is crucial to understanding the mechanism of ion transport, especially in a solid, and what is important in highly concentrated electrolytes. When the salt concentration increases, which results in association and aggregation processes, the number of charge carriers decreases and the viscosity increases, reducing the mobility of the ions. Information about the coordination sphere of the cation and the surrounding anions allows for the understanding of the solvation and association processes leading to the formation of aggregates [16]. Structural research allows one to determine the coordination ability of anions and their competitiveness in the coordination sphere of the cation in relation to solvent molecules [13]. Therefore, the correlation of structural studies with electrochemical parameters should be one of the main tasks to characterize new anions for battery applications. The observed aggregation modes and the degree of association, largely influencing the conductivity and cation transference numbers, strongly depend on the coordination properties of the anion, its ability to form hydrogen bond networks, and the match of its basic

properties with the acidic properties of the cation. Both in solid and liquid electrolytes one should expect the coexistence of many species, such as cations solvated exclusively by solvent molecules and isolated anions, ionic pairs in which the coordination sphere of the cation is completed with solvent molecules, and dimers and various aggregates in the form of coordination polymers with different salt-to-solvent molar ratios. Together with the increase in salt concentration and the decrease in the number of solvent donor centers one should observe a shift in the equilibria toward higher aggregates, up to systems with a polymeric structure in the form of chains, ribbons, layers, or 3D networks. The observed degree of aggregation should depend on both the coordination properties of the anion and the solvent used. In addition, as other authors have pointed out, the ionic and donor-acceptor interactions determining the crystalline structure of the salt also determine the local assembly of structural fragments in molten and concentrated solutions. Therefore, there is a necessity to determine the ability of new anions to bind in the coordination sphere of the cation in the presence of solvent molecules such as aliphatic carbonates, ethylene glycol dimethyl ethers, and crown ethers. Analyzing the structure of crystalline phases containing individual structural motifs can then provide fingerprints for subsequent studies on liquid and polymer systems. The leitmotiv of the research presented herein is to seek an answer to the question about the structure-properties relationship of new heterocyclic anions. Conclusions resulting from these studies allow for the modeling of the local electrolyte structure with these anions and enable the design of new solid and liquid electrolytes with desired parameters.

## 2.3 Crystal Structure Analysis: Hints about the Properties of Heterocyclic Anions

Alkali metal salts of imidazolates comprising heterocyclic anions have attracted attention for being capable of forming complexes with PEO, which is needed for the preparation of solid-state polymer electrolytes. However, electrolytes with lithium and

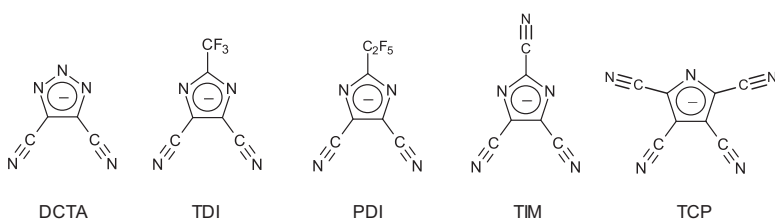


**Figure 2.1** Examples of heterocyclic anions tested for battery applications.

sodium salts of unsubstituted imidazole, benzimidazole, and 2-methylbenzimidazole dissolved in a PEO matrix are characterized by a low conductivity [17]. A similar problem occurs for other heterocyclic systems, for example, lithium 4,5-dicyano-1,2,3-triazolate (LiDCTA) [18]. In 2010, Armand suggested that salts such as lithium 2-trifluoromethyl-4,5-dicyanoimidazolate (LiTDI), that is, containing nitrile- and perfluoroalkyl-substituted heteroaromatic anions, should be electrochemically tested because of their promising properties for use in electrolytes [19, 20]. This group of anions contains a five-member aromatic *N*-heterocyclic ring substituted with nitrile groups. The dicyanoimidazolate anion has four nitrogen donor centers capable of coordinating metal cations. Moreover, the strong charge delocalization within both the imidazole ring and the nitrile groups causes this anion to behave as a weak base. Additionally, as shown in Fig. 2.1, the coordination ability of the anion can be modified by introducing more donor centers or other substituents. The lithium and sodium salts with such heteroaromatic anions, therefore, seem to be an interesting alternative to the currently used and tested compounds for battery applications. Indeed, the research on the electrochemical characterization and practical application of lithium and sodium salts with the 2-trifluoromethyl-4,5-dicyanoimidazolate (TDI) anion carried out by the group of Wieczorek has shown better electrochemical parameters of electrolytes with this type of anion than with dicyanotriazoles [21–24]. Moreover, salts containing the 4,5-dicyano-2-(trifluoromethyl)imidazolate anion ( $\text{TDI}^-$ ) are interesting because of the variety of crystalline structures formed. Simultaneously performed X-ray studies carried out in order to understand the coordination properties of heterocyclic

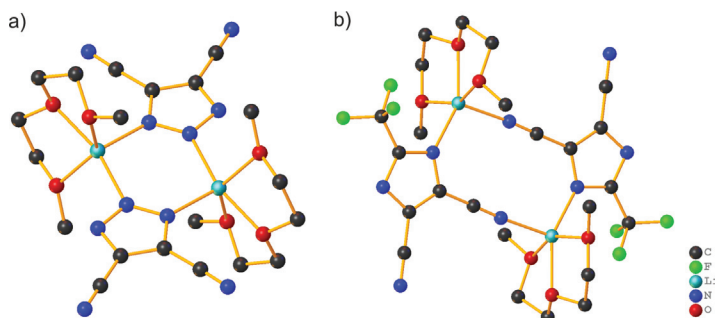


**Figure 2.2** Crystal structures of diglyme solvates of (a) LiDCTA (CSD Refcode ENULEG) and (b) LiTDI (CSD Refcode KADSIU).

4,5-dicyanoimidazole anions significantly help to understand the relationship between the structure of dicyanoimidazolates and their electrochemical parameters.

4,5-Dicyano-1,2,3-triazolate ( $\text{DCTA}^-$ ) and  $\text{TDI}^-$  anions are structurally very similar. An interesting question is why TDI-based electrolytes have noticeably higher conductivity values than electrolytes with DCTA salts. Crystal structure analyses performed on several solvates with these anions suggest that the exchange of a nitrogen atom in the  $\text{DCTA}^-$  anion with a  $\text{C}-\text{CF}_3$  group considerably decreases the lithium cation ionic association tendency of the anion [25]. A comparison of crystal structures retrieved from the Cambridge Structural Database (CSD) [26] for corresponding solvates of LiDCTA [25] and LiTDI [27] with diglymes shows two different types of dimers (Fig. 2.2).

LiDCTA and LiTDI form dimers with 6- and 10-member central rings, respectively. It is worth noticing that  $\text{Li}-\text{N}_{\text{imidazole}}$  bond lengths (2.094 Å and 2.097 Å) in a LiDCTA solvate are considerably shorter in comparison to the  $\text{Li}-\text{N}_{\text{imidazole}}$  bond length in LiTDI (2.211 Å). This suggests that the LiTDI complex may be more easily dissociated and therefore has better electrochemical parameters. Interestingly, the molecular structure of acetonitrile solvates of the formula  $[\text{Li}(\text{L})(\text{MeCN})_2]_2$  (where  $\text{L} = \text{TDI}^-$  or  $\text{PDI}^-$ ) with lithium salts having the imidazolate anion substituted with perfluoroalkyl groups are based on the same structural motif as that of a dimer with a double lithium bridge [28].

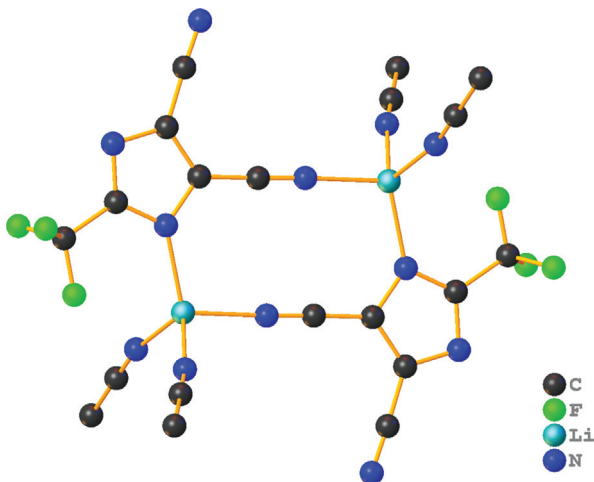


**Figure 2.3** Molecular structure of the  $[\text{Li}(\text{TDI})(\text{MeCN})_2]_2$  adduct (CSD Refcode GIBRIU).

Figure 2.3 presents an example of acetonitrile solvates of LiTDI in which TDI<sup>-</sup> anions bind asymmetrically to two lithium cations via the nitrogen atom of the imidazole ring and the nitrogen atom of the adjacent nitrile group. The remaining sites in the coordination sphere of cations are accomplished by solvent molecules, acetonitrile in this case. These heterocyclic anions are soft bases having a strongly delocalized charge and carry four donor centers whose basicity is lower than the basicity of nitrile groups in electrically neutral acetonitrile molecules. An analysis of the structural data, confirmed by further studies, showed that the basicity of the centers in such systems decreases in the series  $\text{N}_{\text{MeCN}} > \text{N}_{\text{CN}} > \text{N}_{\text{imidazole}}$ , while the similar arrangement of perfluoroalkyl groups in the crystals of these compounds is most likely the result of the weak interactions between fluorine atoms and lithium cations. Li...F contacts in the discussed structures are within the range of 2.70–2.78 Å. The intramolecular interaction of the cation with the fluorine atom from  $-\text{CF}_3$  groups completes the coordination sphere supporting the coordination of the anion through the nitrogen atom of the imidazole ring. The central, almost planar, 10-member Li(NCCN)<sub>2</sub>Li ring constituting the structure of

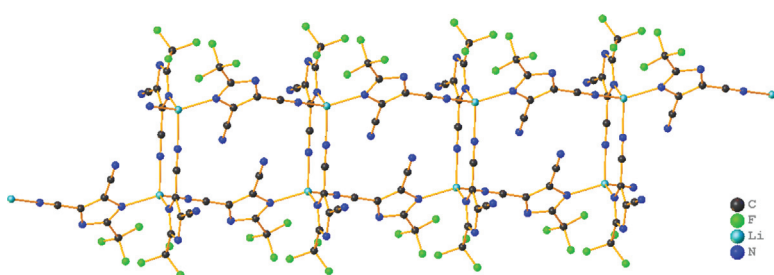


**Figure 2.4** Structure of the anionic coordination polymers of the formula  $[\text{Li}(\text{TDI})_2]_n^-$  observed in  $\text{Li}_{0.5}\text{BMIm}_{0.5}\text{TDI}$  salt (CSD Refcode BIXHEX). Imidazolium cations are omitted for clarity.

the dimer is, therefore, the basic structural motif that can be observed in crystalline structures of many other dicyanoimidazole solvates. For example, it can be distinguished in the crystal structure of polymeric anions found in LiTDI salt, in which there are also imidazolium cations besides the lithium cations [29]. Such systems can be obtained in a simple manner by dissolving LiTDI salt in ionic liquids of the general formula  $\text{XMIm}^+\text{TDI}^-$  acting as a solvent (where  $\text{XMIm}^+$  = *N,N*-methylpropyl imidazolium cation:  $\text{PMIm}^+$  or *N,N*-methylbutylimidazolium cation:  $\text{BMIm}^+$ ). Despite the promising ionic conductivity of the mixed imidazolium-lithium salts, the attempt to dissolve more LiTDI salt in the ionic liquid very quickly leads to a decrease in conductivity. A structural analysis revealed that such behavior of the system results directly from the binding of all the lithium cations in an aggregated polyanion. An analysis of the crystalline structure of the salt with the stoichiometry  $\text{Li}^+:\text{XMIm}^+:\text{TDI}^- = 1:1:2$  (where  $\text{XMIm}^+$  =  $\text{PMIm}^+$  or  $\text{BMIm}^+$ ) obtained from such a system showed the formation of very interesting structural motifs in the form of 1D polyanionic ribbons of the general formula  $[\text{Li}(\text{TDI})_2]_n^-$ , depicted in Fig. 2.4.

The lithium cations of the tetrahedral coordination sphere are connected by two bridging  $\text{TDI}^-$  ligands, forming the previously mentioned specific subunit with a 10-member  $\text{Li}(\text{NCCN})_2\text{Li}$  ring, which is then joined by subsequent  $\text{TDI}$  anions to form a negatively charged polymeric structure of the formula  $[\text{Li}(\text{TDI})_2]_n^-$ . The chains

in the crystal structure are arranged in a grid, forming gaps occupied by imidazolium cations.

## 2.4 Structural Studies of LiTDI Solvates with Glymes: Disproportionation Mechanism

The ability of the dicyanoimidazolate anions to form aggregated anionic subnetworks motivated broader systematic studies to search for analogous systems in which there will be lithium cations able to carry the charge in the electrolyte besides polyanions. This requires the use of an aprotic solvent with a suitable donor number that could compete with imidazolate anions for a place in the coordination sphere of the cation. The convenient choice was using polyethylene glycol dimethyl ethers (glymes) with polyether chains of different lengths (G1–G4), often tested as solvents in lithium-ion battery electrolytes, PEO, and additionally crown ethers [27, 30]. These results shed new light on the problem of the salt aggregation with heterocyclic anions and made it possible to determine the coordinating properties of dicyanoimidazolate anions toward lithium in the presence of polyglycol molecules as a solvent. Structural motifs founded in crystalline LiTDI solvates with glymes disclosed that the aggregation process progresses with a decrease in the number of available ether donor centers compared to the number of lithium cations in the direction indicated in Fig. 2.5 with an arrow. A detailed description of lithium cation environments and resultant aggregation modes for several solvates is summarized in Table 2.1.

The observed structural motifs appear to be dependent directly on the Li:O molar ratio and not on the chain length of the glymes used. This is supported, for example, by the occurrence of analogous structures of ionic pairs forming at the Li:O ratio equal to 1:4, where one triglyme molecule (G3) has been replaced by two molecules of monoglyme (G1) without any change in the coordination mode of the imidazolate anion to the lithium cation. A similar situation was observed for ribbons formed at a ratio of 1:2. It is worth noticing that at a Li:O ratio equal to or less than 1:2, lithium cations of different

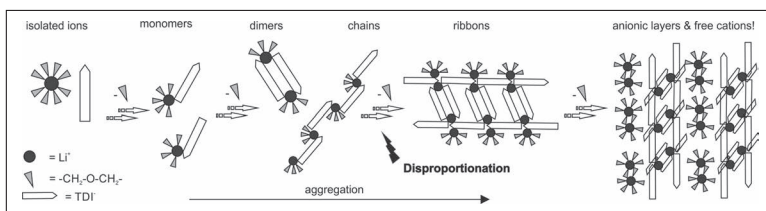


**Figure 2.5** Scheme of the aggregation process for LiTDI solvates occurring in the solid phase in the presence of dimethyl esters of polyethylene glycols (glymes) and crown ethers [27]. Reprinted with permission from Ref. [27]. Copyright (2015) American Chemical Society.

**Table 2.1** LiTDI-glyme solvates and description of the Li<sup>+</sup> coordination spheres

Average Li:O ratio	Molecular formula	Li coordination sphere	Molecular assembly
1:8	Li(12C4) <sub>2</sub> <sup>+</sup> TDI <sup>-</sup>	80	Isolated ions
1:5	Li(15C5)-TDI	50 + N <sub>CN</sub>	Monomer
1:4	Li(G1) <sub>2</sub> -TDI	40 + N <sub>Im</sub> + F	Monomer
1:4	Li(G3)-TDI	40 + N <sub>Im</sub> + F	Monomer
1:3	[Li(G2)-TDI] <sub>2</sub>	30 + N <sub>CN</sub> + N <sub>Im</sub> + F	Dimer
1:3	[Li(G2)-PDI] <sub>n</sub>	30 + N <sub>CN</sub> + N <sub>Im</sub>	1D chain
1:2	Li(G1)-TDI	<hr/> 2N <sub>CN</sub> + 2N <sub>Im</sub> + F <hr/> 40 + N <sub>Im</sub> + F	1D ribbon
1:2	Li(G3) <sub>0.5</sub> -TDI	<hr/> 2N <sub>CN</sub> + 2N <sub>Im</sub> + F <hr/> 40 + N <sub>Im</sub> + F	1D ribbon
1:1.67	[Li <sub>2</sub> (G4) <sub>2</sub> <sup>2+</sup> ] [Li <sub>4</sub> TDI <sub>6</sub> <sup>2-</sup> ]	<hr/> 2N <sub>CN</sub> + 2N <sub>Im</sub> + F <hr/> 50	2D anionic layers
1:1	Li(G1) <sub>0.5</sub> -TDI	<hr/> 2N <sub>CN</sub> + 2N <sub>Im</sub> + F <hr/> 20 + 2N <sub>Im</sub> + F	3D aggregate

Source: [27]

surroundings appear in the crystalline structures of LiTDI-glyme solvates. A detailed structural analysis helped draw a very important conclusion: at a sufficient deficit of ether donor centers, there is a disproportionation of acidic centers and a variation in the lithium cations' surroundings occurs in such a way that some cations are coordinated exclusively by the TDI<sup>-</sup> anions while the remaining Li<sup>+</sup> cations have more oxygen ligands in their environment [27]. The

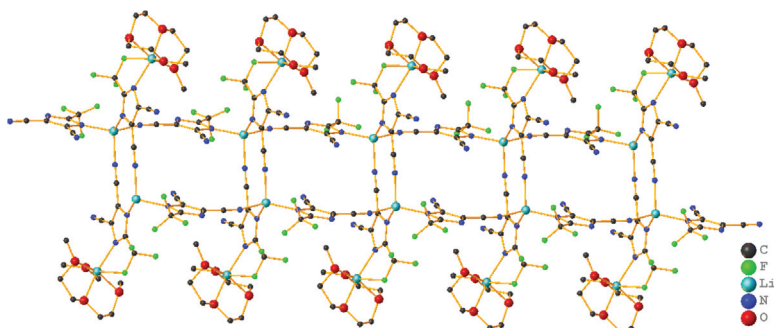


**Figure 2.6** The occurrence of two types of  $\text{Li}^+$  cations after suitable lowering of the Li:O molar ratio observed in the  $\text{Li}(\text{G}3)_{0.5}\text{TDI}$  solvate, (CSD Refcode KADTAN).

structure of the solvate with the formula  $\text{Li}(\text{G}3)_{0.5}\text{TDI}$ , shown in Fig. 2.6, may serve as a very good example of this phenomenon.

In the  $\text{Li}(\text{G}3)_{0.5}\text{TDI}$  structure one can distinguish the main structural motif in the form of a polyanionic ribbon identical to that found in the lithium salts  $\text{Li}_{0.5}\text{PMIm}_{0.5}\text{TDI}$  and  $\text{Li}_{0.5}\text{BMIm}_{0.5}\text{TDI}$  [29]. Here, polyanions are additionally decorated with lithium cations solvated by a molecule of G3. The terminal lithium cations having such a structure are supposed to dissociate more easily at the working conditions of the cell. Importantly, an analysis of the process of aggregation and disproportionation of LiTDI-GX systems ( $X = 1 - 4$ ) shows that in order to shift the equilibria toward a higher content of unbound lithium cations solvated only by polyether molecules, the molar ratio of lithium to oxygen donors should be reduced even more. Melting LiTDI salt with tetraglyme (G4), in which the Li:O molar ratio is equal 1:1.67, leads to the formation of an ionic compound with a very interesting crystalline structure, as shown in Fig. 2.7b [27].

The cations are in the form of dinuclear solvates in which two  $\text{Li}^+$  centers are bound to two helically twisted G4 molecules, while counterions are polyanions in the form of aggregated layers. This type of salt association for battery applications in which free cations capable of carrying charges are found at very high concentrations has been discovered for the first time. Until then, there was a common view that aggregation occurring at high salt

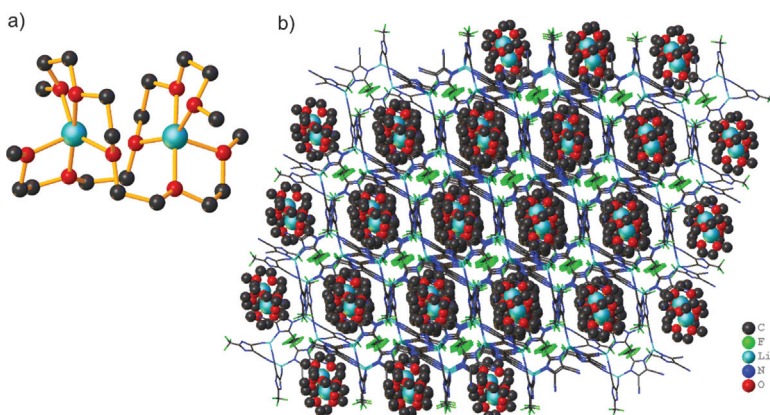


**Figure 2.7** (a) Dinuclear cation  $\text{Li}_2(\text{G}4)_2^{2+}$  present in the crystal structure of the tetraglyme ionic solvate formed in the process of acid-base disproportionation and (b) the molecular structure of  $[\text{Li}_2(\text{G}4)_2^{2+}] [\text{Li}_4\text{TDI}_6^{2-}]$ , (CSD Refcode KADTER).

concentrations always deteriorates the electrochemical parameters of the electrolyte. It should be emphasized that the discovered aggregation mechanisms associated with the disproportionation allow for obtaining systems with very good electrochemical parameters in the solid phase or at high concentrations of salts. It is worth stressing here that there is a significant difference with respect to the systems composed of concentrated lithium salt systems based on imidate anions such as TFSI called solvated ionic liquids, previously examined by the team of Watanabe [31]. In the aggregates of salts with heterocyclic anions, there is immobilization of anions resulting from the formation of an aggregated anionic subnetwork. This increases the transference number of the remaining lithium cations significantly, which is particularly important for solid electrolytes [32–34]. As a result, the obtained crystalline electroactive material has a higher conductivity at 30°C than electrolytes with a polymer matrix containing PEO and simultaneously exhibits very high transference number of the lithium cation  $t_+$  of about 0.8. Moreover, after the melting of such a crystalline solvate and its subsequent cooling to 30°C, a marked decrease in the conductivity of the new phase with respect to the starting crystalline complex is observed.

On the basis of further spectroscopic studies, it was confirmed that this is related to the reorganization of structural fragments and the creation of melt-down oligomeric forms with a chain structure. Conductivity returns to the initial value only after a few days, during which the previously molten phase gradually crystallizes by reproducing lithium dications solvated with ether. The presence of this type of cations significantly increases the conductivity of the entire electrolyte. An important result of the analysis of crystalline structures of solvates with LiTDI salt was also the distinction of eight unique types of lithium cation coordination to this anion [30]. Each of these motifs exhibits in the Raman spectrum a unique pattern of C–N stretching vibrations of nitrile groups ( $\nu_{\text{CN}}$ ) and an imidazolate ring ( $\nu_{\text{CN,Im}}$ ) and bending vibrations of the C–N–C group in the ring plane ( $\delta_{\text{NCN}}$ ). The positions of these bands registered for single crystals of solvates can be correlated with specific structural motifs. This allowed for a convenient determination of the coordination of the TDI anion and made insight into the structure of the phases formed in liquid systems [27, 30] and polymer matrices [30, 35] possible. For example, the analysis of TDI-specific bands in the Raman spectra along with appropriate attribution of structural fragments led to the conclusion that in concentrated polyglycol solutions there is limited progress of the aggregation with increasing concentration, which results in the formation of solvates only in the form of ionic pairs, dimers, and chains [30]. The same method can be applied for analyzing the coordination environment of the anion in order to determine the structure of the phases that make up the solid electrolytes obtained by dissolving LiTDI salt in the PEO polymer matrix. This type of study for complicated multiphase systems is a big challenge. Temperature studies carried out by means of differential scanning calorimetry on samples of polymer membranes with different salt contents showed that their structure includes both the crystalline PEO phase and two solvate phases of LiTDI salts with PEO denoted as  $\alpha$  and  $\beta$  [30]. The structural analysis supported by spectroscopic studies based on real structural fragments specific for a given coordination environment of the anion showed that in the  $\alpha$  phase structure, the TDI anions are coordinated to lithium cations via the nitrogen atom of the imidazole ring only and thus according to the structural motif correspond

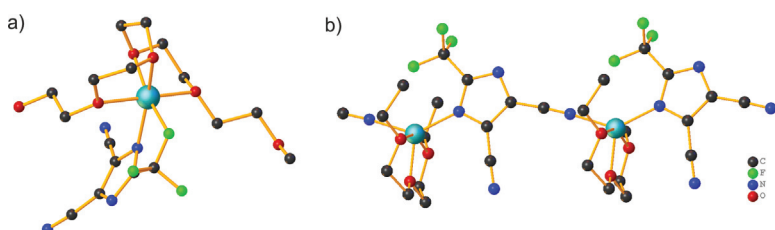


**Figure 2.8** Structural fragments showing theoretically calculated models of the anion and cation environments in (a)  $\alpha$  and (b)  $\beta$  phases found in the LiTDI-PEO system [35].

to ionic pairs. The remaining places in the coordination sphere of the lithium cation are supplemented by oxygen atoms from a helically arranged chain of PEO. On the other hand, on the basis of a structural analysis carried out, it was found that in the construction of the more strongly aggregated  $\beta$  phase, most likely there are chain coordination polymers formed of TDI anions coordinated by one of the nitrogen atoms of the imidazole ring and the nitrogen atom opposite the nitrile group. The proposed structures of the  $\alpha$  and  $\beta$  phases were further verified and optimized using quantum mechanical calculations and the density functional theory method (Fig. 2.8) [35].

The models of lithium salt solvates with PEO obtained on the basis of theoretical calculations, in which the method of coordination was proposed based on the structural motifs of model solvates with low-molecular glymes, seem to reflect well the structure of local fragments of the polymer membrane structure. What is interesting is that during the melting of the  $\alpha$  phase the formation of a larger amount of the aggregated  $\beta$  phase with the simultaneous formation of a pure PEO phase, the presence of which was initially not detected in the membrane, is observed. This effect is detected on the conductivity diagram for the highest LiTDI salt content in the membrane at a temperature of about 40°C and is probably caused by the disproportionation mechanism observed previously for glyme solvates [35].

The results of research on solvates of lithium salts with heterocyclic anions and the exact knowledge of their structure in the solid phase and concentrated solutions were a very good

starting point for theoretical simulations. The disproportionation process combined with the formation of aggregated polyanionic structures was analyzed using theoretical modeling by molecular dynamics, which allowed the experimental results to be supported by theoretical analysis [36]. Simulations conducted for electrolytes in the LiTDI-G4 system with an increasing salt concentration, where the Li:O ratio varied from 1:9 to 1:1, confirmed the existence of the disproportionation process consistent with the results of structural studies based on X-ray measurements. On the basis of the distribution analysis of ether donor centers in the lithium coordination sphere, it was possible to show that the formation of aggregated polyanions is directly related to the release of lithium cations solvated only by polyether molecules. Importantly, the system based on imidate TFSI anions (commonly studied in battery applications) selected as a reference point, did not show such behavior.

## 2.5 Structural Studies of Sodium Salts with Heterocyclic Anions

In parallel to the research on the structure of solvates of lithium salts, structural studies of heterocyclic sodium salts in the context of electrochemical application have been conducted. The first crystal structures were obtained for sodium salts with dicyanoimidazolate anions containing trifluoromethyl (NaTDI) and pentafluoroethyl substituent (NaPDI) with propylene carbonate (PC) as a solvent [37]. Studies of NaTDI and NaPDI salt solutions using Raman spectroscopy showed that in diluted solutions there are uncoordinated heterocyclic anions and sodium cations solvated with a solvent. The increase in the salt concentration results in the association of ions and, as a result, the formation of ion pairs and dimers. However, the crystallization of the sodium salt solvate from the PC solution, regardless of the conditions used, always led to the formation of more aggregated compounds. For example, TDI-sodium salt crystallizes as a solvate with the composition  $\text{Na}^+:\text{TDI}^-:\text{PC} = 1:1:1$  (Fig. 2.9a).

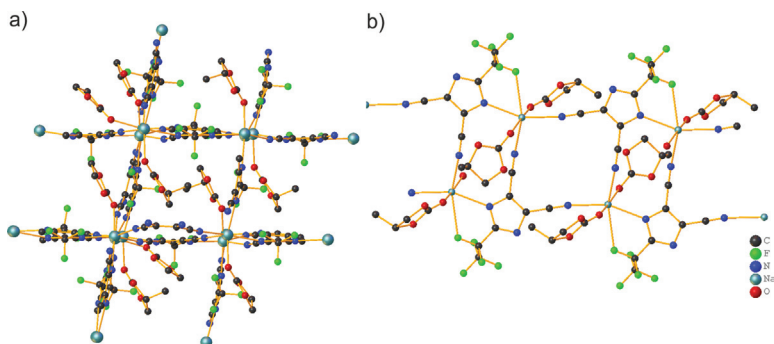


**Figure 2.9** (a) View of the 3D crystal lattice created by the NaTDI-PC solvate and (b) the structural motif found in the solvated structure with the NaPDI-2PC stoichiometry [37].

The coordination sphere of the sodium cation contains four TDI anions and one carbonate molecule coordinated by a carbonyl group. Two of the TDI anions are coordinated by the nitrogen atoms of the imidazole ring and the other two by nitrogen atoms of the nitrile groups. In this structure, the dicyanoimidazolate anions connect neighboring sodium cations and together form a 3D network. In the case of salts with PDI anions, however, a solvate of different stoichiometry crystallized, containing two PC molecules coordinated to one sodium cation ( $\text{Na}^+:\text{PDI}^-:\text{PC} = 1:1:2$ ) (Fig. 2.9b). The determined structure is in the form of an electroneutral ribbon-like coordination polymer [37]. Promising results of electrochemical measurements of the electrolytes created on the basis of discussed sodium salts and PC led to the thesis that the TDI anion can be used to design future sodium-ion batteries. The monodentate solvent, which is PC, unfortunately, did not allow for the isolation of more structural motifs formed in adducts with the NaTDI salt. Therefore, the structure of a series of NaTDI sodium solvates with glymes of different lengths of polyether chains and crown ethers have been analyzed [38]. Similarly to lithium salts the change in the mode of anion coordination by sodium cations changes with the change in the number of available solvent donor centers, and in the case of strongly aggregated structures, the diversity of the donor centers' environment due to disproportionation can be seen.

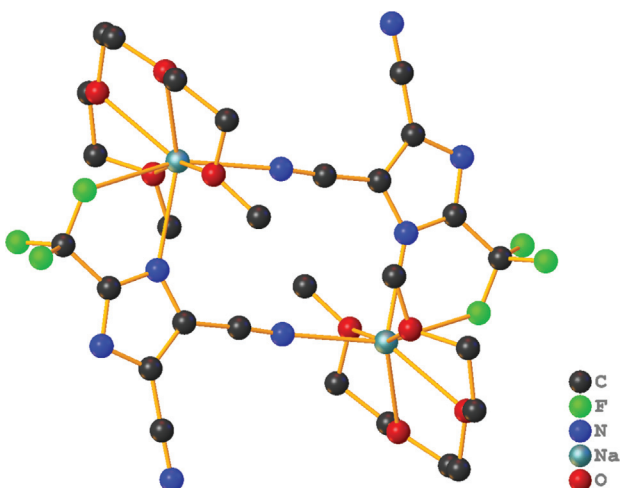


**Figure 2.10** Crystal structure of the NaTDI-G3 solvate, (CSD Refcode AGOWEB).

However, the larger average coordination number (AOCN) of sodium (6.4) compared to lithium (4.9) results in solvates with the same level of structural complication being realized in the presence of a larger number of solvent donor centers. For example, for stabilizing an isolated dimer in TDI lithium salts, G2 containing three oxygen atoms in the ether chain suffices (Fig. 2.2b), whereas for sodium salt, as shown in Fig. 2.10, this motif is realized only by G3 containing four ether donor centers in its structure.

This type of difference observed in the structures of compounds with different cations can be interpreted on the basis of the valence-matching principle given by Brown, saying that the most stable structures are formed when the acidity strength of the cation ( $S_a$ ) corresponds to the basic strength of the anion ( $S_b$ ) [39]. The acidity strength of sodium and lithium cations estimated on the basis of the AOCN is 0.16 and 0.21 v.u [40]. In contrast, the basic strength of TDI<sup>-</sup> anions, which can be considered as ligands having four nitrogen donor centers, can be estimated at 0.25 v.u. The poorer match of the TDI<sup>-</sup> anion to the sodium cation means that a greater number of oxygen centers are required to maintain the same level of aggregation. As a result, highly aggregated electroneutral

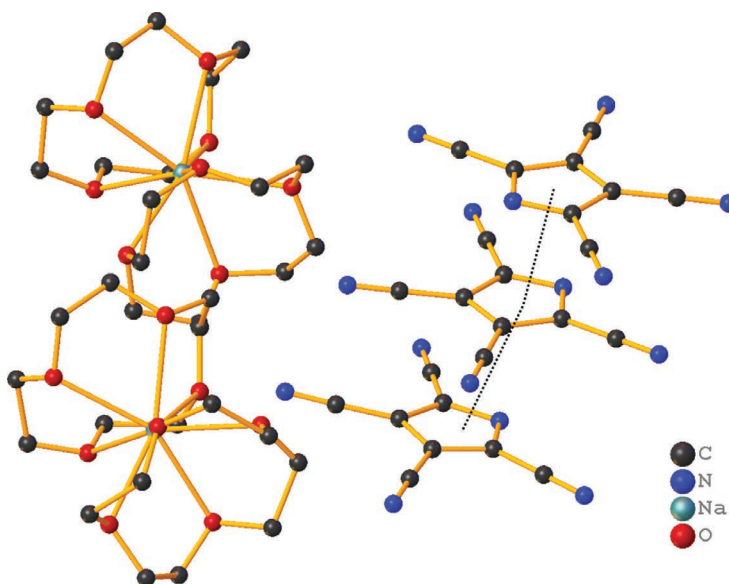


**Figure 2.11** Structural fragment of the NaTCP-12C4 solvate, (CSD Refcode RAKMOI).

structures are formed instead of disproportionated polyanions and free unsolvated cations. The solution to this problem seems to be to lower the  $S_b$  parameter of the anion by increasing the number of nitrile nitrogen donor centers. This can be achieved by introducing additional groups into the heterocyclic ring constituting new subclass of “fluorine-free” heterocyclic anions. Sodium salts with 2,4,5-tricyanoimidazole anions and tetracyanopyrrole anions (TCP) have been recently used to create solid polymer electrolytes, showing very promising electrochemical and mechanical parameters of the obtained membranes [41]. In addition, analysis of the crystalline structure of the tetracyanopyrrole sodium solvate (NaTCP) with 12C4 crown ether, depicted in Fig. 2.11, showed that there are  $\pi$ -stacking interactions between TCP anions.

Importantly, this type of association of anions through weak noncovalent interactions has neither been observed until now nor been considered in the theoretical modeling of electrolytes. This phenomenon may lead to a favorable immobilization of anions in

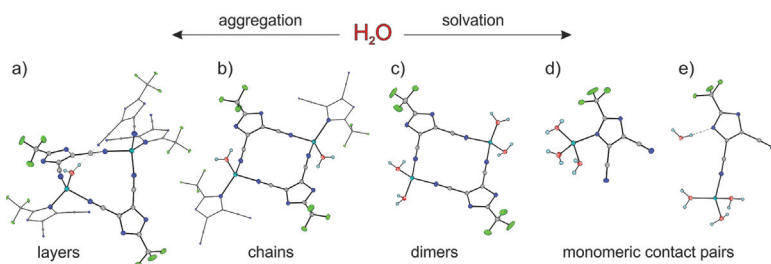
the polymer matrix and to an increase in the cation transference number.

## 2.6 Structural Studies of Lithium Salt Hydrates with Dicyanoimidazole Anions

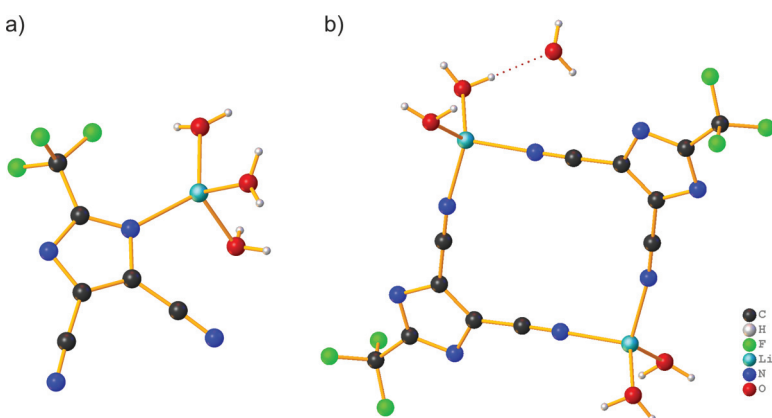
A crystal structure analysis carried out on a series of hydrates obtained from gradual, stepwise hydrolysis of LiTDI salt proved to be a useful source of knowledge regarding the evaluation of the suitability of this salt for hydrated electrolytes, investigation of the impact of moisture on heterocyclic salts, and the structural role of water in the formation of hydrates in electrolytes [42]. This issue is particularly important due to the rapidly growing interest in applications of safe and ecological water electrolytes for lithium-ion batteries [43–45] as well as to obtain important information on the durability of batteries constructed with anhydrous electrolytes on exposure to humidity. It has been shown that water competes with the TDI anions in the coordination sphere of lithium, causing desolvation of the TDI anions and reorganization of the solvated structure, as shown in Fig. 2.12 [42].

Figure 2.13 presents in detail crystal structures having two most characteristic motifs identified during research on hydrates [42].

The gradual replenishment of the lithium coordination sphere with water molecules leads at the last stage to obtaining trihydrates



**Figure 2.12** Coordination modes identified in the LiTDI-glyme-water system. Reprinted with permission from Ref. [42]. Copyright (2018) American Chemical Society.



**Figure 2.13** Two of the most stable hydrates of LiTDI characterized by X-ray diffraction technique, (a) trihydrate  $\text{Li}(\text{H}_2\text{O})_3\text{TDI}$ , (CSD Refcode OGEGEP) and (b) dihydrate of composition  $[\text{Li}(\text{H}_2\text{O})_2\text{TDI}]_2 \cdot 2\text{H}_2\text{O}$ , (CSD Refcode OGEGOZ).

in the form of ionic pairs of composition  $\text{Li}(\text{H}_2\text{O})_3\text{TDI}$ . A crystal structure analysis reveals that the  $\text{Li}^+$  cation is coordinated by three  $\text{H}_2\text{O}$  molecules and one molecule of the TDI anion through the nitrogen atom of the imidazole ring or nitrile group. The first mode of coordinating the anion, which is depicted in Fig. 2.12a, is preferred at room temperature, while the latter mode exists at temperatures below  $10^\circ\text{C}$ . Raising the temperature to a value above  $80^\circ\text{C}$  leads to partial dehydration of the trihydrate compound with the simultaneous formation of a dihydrate of the formula  $[\text{Li}(\text{H}_2\text{O})_2\text{TDI}]_2$ , depicted in Fig. 2.12b. The detailed process of dehydration is shown in Fig. 2.14.

A very important result of the research was the discovery that a dimeric unit in which the lithium cations are coordinated through the nitrile groups of the  $\text{TDI}^-$  anions is remarkably thermally stable [42]. It dehydrates just above  $300^\circ\text{C}$ , and the process is accompanied by the simultaneous decomposition of the compound. For this reason, the production of an anhydrous LiTDI salt for LiB application requires necessarily the use of reduced pressure during drying. On the other hand, the formation of an electroneutral stable hydrate can be applied to improving the electrochemical

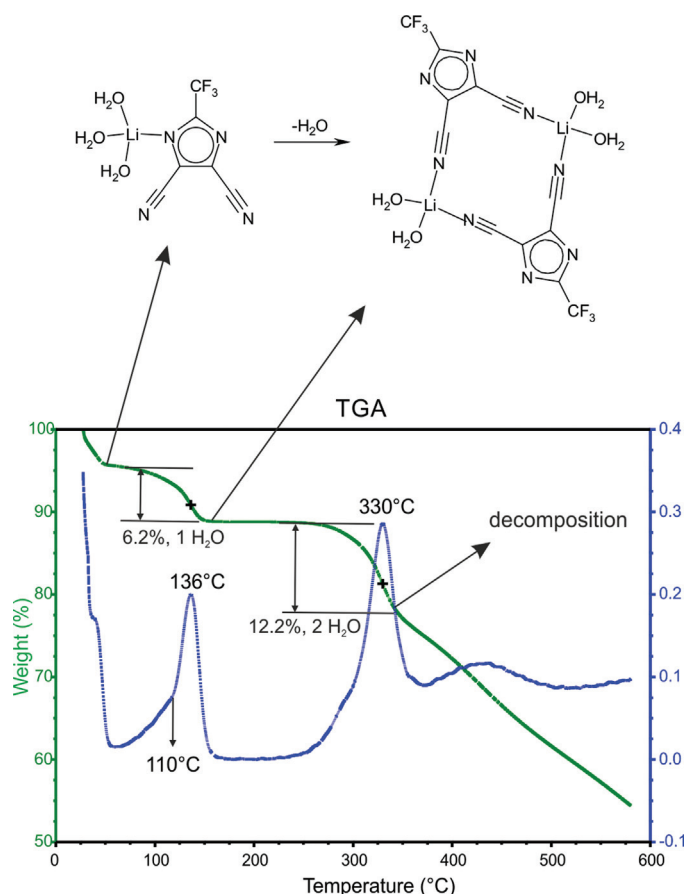


**Figure 2.14** TGA and DTGA curves for the dehydration of LiTDI·3H<sub>2</sub>O. Adapted with permission from Ref. [42]. Copyright (2018) American Chemical Society.

parameters of commercial electrolytes containing LiPF<sub>6</sub> salt. Lithium dicyanoimidazolate salt turned out to be a promising additive acting as a moisture scavenger [46]. Determining the structure and investigating complicated transformations of LiTDI salt hydrates show very well the high potential of the developed approach using single-crystal X-ray diffraction as a convenient tool for studying the local electrolyte structure [42]. It seems that understanding of solvation phenomena of heterocyclic lithium salts

in the presence of water is the first step in developing highly concentrated and solid hydrated electrolytes for battery application.

## 2.7 Conclusions

Conclusions resulting from X-ray structural analysis carried out on lithium and sodium salts with perfluoroalkyl-substituted dicyanoimidazolato salts have made a significant contribution to the development of electrolytes based on heterocyclic anions. Structural research oriented toward basic research focused on the detailed understanding of the coordination properties of new anionic heterocyclic ligands was carried out in three main areas: the structural analysis of solvates of lithium salts, that of sodium solvates, and that of lithium salts hydrates. On the basis of single-crystal X-ray diffraction studies, which were correlated with the results of spectroscopic and temperature studies, a method to gain structural information of cation coordination spheres, as well as the anion surroundings in dicyanoimidazolate salts, was developed. A systematic structural analysis revealed that heterocyclic salts dissolved in aprotic solvents such as acetonitrile or glymes tend to form coordination polymers. The association taking place along with the increase in salt concentration leads to the formation of aggregated structures in the form of dimers, chains, ribbons, and 3D structures comprising the same characteristic dimeric structural motif with a double lithium bridge. The observed level of complexity depends directly on the molar ratio of metal cations to the number of solvent donor centers. The unique feature of dicyanoimidazole anions, which was discovered, is their ability to form polyanionic aggregates. At a low molar ratio of  $\text{Li}^+:\text{O}$  or  $\text{Na}^+:\text{O}$  the unexpected phenomenon of disproportionation of acidic centers ( $\text{Li}^+$  and  $\text{Na}^+$ ) occurs, resulting in the formation of solid electrolytes in which, next to the aggregated polyanions, isolated lithium or sodium cations coordinated only with a solvent are present. This process has a significant impact on the improvement of observed electrochemical parameters such as electrical conductivity or cation transference numbers. It was shown that similar processes occur also in solid electrolytes with a polymer matrix. The developed method of

examining the local electrolyte structure using the correlation of the identified structural motifs obtained for a number of model solvates with the results of spectroscopic studies made it possible to use the crystallographic studies for describing the structure of liquid and solid phases in electrolytes with heterocyclic anions. As a consequence, a better understanding of the relationship between the structure of new salts and their electrochemical parameters is available, enabling the characterization of new heteroaromatic salt systems. It is possible, for example, to study the coordination properties of heterocyclic anions, such as percyano anions, which, due to the greater number of nitrile groups and other donor centers, form much more complex systems and thus are difficult to interpret. The correlation of the crystalline structure of lithium and sodium heterocyclic salt solvates and their spectroscopic characteristics on the basis of a large number of isolated and characterized structural motifs allows one to retrieve valuable information about cation-anion interactions in both solid electrolytes with a polymer matrix and in liquid electrolytes. A significant problem in theoretical calculations is the correct description of the salt interactions with solvent molecules at higher concentrations when larger aggregates start to appear, and the form of these aggregates itself has remained elusive so far. The possibility to apply structural models in the form of fragments of crystalline structures allows the modeling of the conditions prevailing in the electrolyte, particularly in systems with high salt concentrations, and it is an innovative approach to understanding the processes and the way of materials self-organization in real systems. Understanding factors governing the self-organization of such systems in the solid phase is crucial in the characterization of electrolytes and it is necessary for further development in this field, offering the possibility to rationally plan research aimed at finding compounds with expected properties. Undoubtedly, an important contribution to the development of research on concentrated and solid electrolytes is the discovery of a completely new aggregation process accompanying the disproportionation of acidic centers. Determination of coordination properties of heterocyclic anions toward cations with weak acidic properties made, as a consequence, understanding the aggregation processes occurring in the electrolytes possible, including the processes' impact on the

measured electrochemical parameters resulting from an increased number of free lithium cations in solid electrolytes. Formulated conclusions regarding this process are relevant for designing new electrolytes in lithium-ion and sodium-ion batteries containing heterocyclic salts. A detailed structural analysis of the sodium salts correlated to the structure of analogous lithium salts has suggested modifying the heterocyclic anions by introducing additional nitrile groups to the aromatic ring in order to properly match the acidic properties of sodium cations to heterocyclic anions. Analysis of the hydration process of LiTDI salt and the crystal structures of a series of hydrates having different degrees of hydration enables one to disclose a mechanism of improving the electrochemical parameters of commercial electrolytes containing LiPF<sub>6</sub> salt by using LiTDI salt as an additive.

## References

1. M. G. Davidson, P. R. Raithby, A. L. Johnson, P. D. Bolton, Structural diversity in Lewis-base complexes of lithium triflamide. *Eur. J. Inorg. Chem.*, **2003**(18) (2003) 3445–3452. 10.1002/ejic.200300372.
2. W. A. Henderson, F. McKenna, M. A. Khan, N. R. Brooks, V. G. Young, R. Frech, Glyme–lithium bis(trifluoromethanesulfonyl)imide and glyme–lithium bis(perfluoroethanesulfonyl)imide phase behavior and solvate structures. *Chem. Mater.*, **17**(9) (2005) 2284–2289. 10.1021/cm047881j.
3. K. Matsumoto, R. Hagiwara, O. Tamada, Coordination environment around the lithium cation in solid Li<sub>2</sub>(EMIm)(N(SO<sub>2</sub>CF<sub>3</sub>)<sub>2</sub>)<sub>3</sub> (EMIm=1-ethyl-3-methylimidazolium): structural clue of ionic liquid electrolytes for lithium batteries. *Solid State Sci.*, **8**(9) (2006) 1103–1107. 10.1016/j.solidstatesciences.2005.12.017.
4. Q. Zhou, K. Fitzgerald, P. D. Boyle, W. A. Henderson, Phase behavior and crystalline phases of ionic liquid-lithium salt mixtures with 1-alkyl-3-methylimidazolium salts. *Chem. Mater.*, **22**(3) (2010) 1203–1208. 10.1021/cm902691v.
5. W. A. Henderson, N. R. Brooks, W. W. Brennessel, V. G. Young, LiClO<sub>4</sub> electrolyte solvate structures. *J. Phys. Chem.A*, **108**(1) (2004) 225–229. 10.1021/jp035836d.

6. C. Zhang, S. J. Lilley, D. Ainsworth, E. Staunton, Y. G. Andreev, A. M. Z. Slawin, et al., Structure and conductivity of small-molecule electrolytes  $[\text{CH}_3\text{O}(\text{CH}_2\text{CH}_2\text{O})_n\text{CH}_3]:\text{LiAsF}_6$  ( $n = 8-12$ ). *Chem. Mater.*, **20**(12) (2008) 4039–4044. 10.1021/cm8005327.
7. C. Zhang, D. Ainsworth, Y. G. Andreev, P. G. Bruce, Ionic conductivity in the solid glyme complexes  $[\text{CH}_3\text{O}(\text{CH}_2\text{CH}_2\text{O})_n\text{CH}_3]:\text{LiAsF}_6$  ( $n = 3, 4$ ). *J. Am. Chem. Soc.*, **129**(28) (2007) 8700–8701. 10.1021/ja073145f.
8. C. Zhang, Y. G. Andreev, P. G. Bruce, Crystalline small-molecule electrolytes. *Angew. Chem. Int. Ed.*, **46**(16) (2007) 2848–2850. 10.1002/anie.200604934.
9. W. A. Henderson, N. R. Brooks, W. W. Brennessel, V. G. Young, Triglyme–Li<sup>+</sup> cation solvate structures: models for amorphous concentrated liquid and polymer electrolytes (I). *Chem. Mater.*, **15**(24) (2003) 4679–4684. 10.1021/cm034351z.
10. J. D. Holbrey, W. M. Reichert, R. D. Rogers, Crystal structures of imidazolium bis(trifluoromethanesulfonyl)imide ‘ionic liquid’ salts: the first organic salt with a cis-TFSI anion conformation. *Dalton Trans.*, (15) (2004) 2267–2271. 10.1039/B405901H.
11. W. A. Henderson, N. R. Brooks, V. G. Young, Tetraglyme–Li<sup>+</sup> cation solvate structures: models for amorphous concentrated liquid and polymer electrolytes (II). *Chem. Mater.*, **15**(24) (2003) 4685–4690. 10.1021/cm034352r.
12. W. A. Henderson, N. R. Brooks, V. G. Young, Single-crystal structures of polymer electrolytes. *J. Am. Chem. Soc.*, **125**(40) (2003) 12098–12099. 10.1021/ja036535k.
13. D. M. Seo, P. D. Boyle, O. Borodin, W. A. Henderson, Li<sup>+</sup> cation coordination by acetonitrile—insights from crystallography. *RSC Adv.*, **2**(21) (2012) 8014–8019. 10.1039/C2RA21290K.
14. Y. Yamada, Developing new functionalities of superconcentrated electrolytes for lithium-ion batteries. *Electrochemistry*, **85**(9) (2017) 559–565. 10.5796/electrochemistry.85.559.
15. J. Zheng, J. A. Lochala, A. Kwok, Z. D. Deng, J. Xiao, Research progress towards understanding the unique interfaces between concentrated electrolytes and electrodes for energy storage applications. *Adv. Sci.*, **4**(8) (2017) 1700032–n/a. 10.1002/advs.201700032.
16. D. M. Seo, J. L. Allen, L. A. Gardner, S.-D. Han, P. D. Boyle, W. A. Henderson, Electrolyte solvation and ionic association: cyclic carbonate and ester-LiTFSI and -LiPF<sub>6</sub> mixtures. *ECS Trans.*, **50**(26) (2013) 375–380. 10.1149/05026.0375ecst.

17. J. P. Voss, S. V. Batty, J. P. Patel, P. V. Wright, Conductivities of poly(ethylene oxide)-alkali salts with aromatic and heterocyclic anions. *Solid State Ionics*, **60**(1) (1993) 93–97. 10.1016/0167-2738(93)90280-G.
18. M. Egashira, B. Scrosati, M. Armand, S. Béranger, C. Michot, Lithium dicyanotriazolate as a lithium salt for poly(ethylene oxide) based polymer electrolytes. *Electrochim. Solid-State Lett.*, **6**(4) (2003) A71–A73. 10.1149/1.1558352.
19. C. Michot, M. Armand, M. Gauthier, Y. Choquette. Pentacyclic anion salts or tetrazapentalene derivatives and their uses as ionic conducting materials. US6835495 B2, December 28, 2004.
20. M. Armand, S. Grugeon, S. Laruelle, M. Bukowska, P. Szczecinski, W. Wieczorek, et al., Pentacyclic anion salt and use thereof as an electrolyte. US20110311884 A1, December 22, 2011.
21. L. Niedzicki, G.Z. Žukowska, M. Bukowska, P. Szczeciński, S. Grugeon, S. Laruelle, et al., New type of imidazole based salts designed specifically for lithium ion batteries. *Electrochim. Acta*, **55**(4) (2010) 1450–1454. 10.1016/j.electacta.2009.05.008.
22. L. Niedzicki, E. Karpierz, A. Bitner, M. Kasprzyk, G. Z. Zukowska, M. Marcinek, et al., Optimization of the lithium-ion cell electrolyte composition through the use of the LiTDI salt. *Electrochim. Acta*, **117** (2014) 224–229. 10.1016/j.electacta.2013.11.134.
23. L. Niedzicki, S. Grugeon, S. Laruelle, P. Judeinstein, M. Bukowska, J. Prejzner, et al., New covalent salts of the 4+V class for Li batteries. *J. Power Sources*, **196**(20) (2011) 8696–8700. 10.1016/j.jpowsour.2011.06.030.
24. J. Scheers, L. Niedzicki, G. Z. Zukowska, P. Johansson, W. Wieczorek, P. Jacobsson, Ion-ion and ion-solvent interactions in lithium imidazolide electrolytes studied by Raman spectroscopy and DFT models. *Phys. Chem. Chem. Phys.*, **13**(23) (2011) 11136–11147. 10.1039/C1CP20063A.
25. D. W. McOwen, S. A. Delp, E. Paillard, C. Herriot, S.-D. Han, P. D. Boyle, et al., Anion coordination interactions in solvates with the lithium salts LiDCTA and LiTDI. *J. Phys. Chem. C*, **118**(15) (2014) 7781–7787. 10.1021/jp412601x.
26. C. R. Groom, I. J. Bruno, M. P. Lightfoot, S. C. Ward, The Cambridge structural database. *Acta Crystallogr. Sect. B*, **72**(2) (2016) 171–179. 10.1107/S2052520616003954.
27. P. Jankowski, M. Dranka, G. Z. Žukowska, J. Zachara, Structural studies of lithium 4,5-dicyanoimidazolate-glyme solvates. 1. From isolated free

- ions to conductive aggregated systems. *J. Phys. Chem. C*, **119**(17) (2015) 9108–9116. 10.1021/acs.jpcc.5b01352.
28. M. Dranka, L. Niedzicki, M. Kasprzyk, M. Marcinek, W. Wieczorek, J. Zachara, An insight into coordination ability of dicyanoimidazolato anions toward lithium in presence of acetonitrile. Crystal structures of novel lithium battery electrolyte salts. *Polyhedron*, **51** (2013) 111–116. <https://doi.org/10.1016/j.poly.2012.12.022>.
29. L. Niedzicki, E. Karpierz, M. Zawadzki, M. Dranka, M. Kasprzyk, A. Zalewska, et al., Lithium cation conducting TDI anion-based ionic liquids. *Phys. Chem. Chem. Phys.*, **16**(23) (2014) 11417–11425. 10.1039/C3CP55354J.
30. P. Jankowski, M. Dranka, G. Z. Żukowska, Structural studies of lithium 4,5-dicyanoimidazolate–glyme solvates. 2. Ionic aggregation modes in solution and PEO matrix. *J. Phys. Chem. C*, **119**(19) (2015) 10247–10254. 10.1021/acs.jpcc.5b01826.
31. K. Ueno, K. Yoshida, M. Tsuchiya, N. Tachikawa, K. Dokko, M. Watanabe, Glyme–lithium salt equimolar molten mixtures: concentrated solutions or solvate ionic liquids? *J. Phys. Chem. B*, **116**(36) (2012) 11323–11331. 10.1021/jp307378j.
32. Q. Li, J. Chen, L. Fan, X. Kong, Y. Lu, Progress in electrolytes for rechargeable Li-based batteries and beyond. *Green Energy Environ.*, **1**(1) (2016) 18–42. 10.1016/j.gee.2016.04.006.
33. J. L. Schaefer, D. A. Yanga, L. A. Archer, High lithium transference number electrolytes via creation of 3-dimensional, charged, nanoporous networks from dense functionalized nanoparticle composites. *Chem. Mater.*, **25**(6) (2013) 834–839. 10.1021/cm303091j.
34. K. M. Diederichsen, E. J. McShane, B. D. McCloskey, Promising routes to a high Li<sup>+</sup> transference number electrolyte for lithium ion batteries. *ACS Energy Lett.*, **2**(11) (2017) 2563–2575. 10.1021/acsenergylett.7b00792.
35. P. Jankowski, G. Z. Żukowska, M. Dranka, M. J. Marczewski, A. Ostrowski, J. Korczak, et al., Understanding of lithium 4,5-dicyanoimidazolate–poly(ethylene oxide) system: influence of the architecture of the solid phase on the conductivity. *J. Phys. Chem. C*, **120**(41) (2016) 23358–23367. 10.1021/acs.jpcc.6b07058.
36. P. Jankowski, M. Dranka, W. Wieczorek, P. Johansson, TFSI and TDI anions: probes for solvate ionic liquid and disproportionation-based lithium battery electrolytes. *J. Phys. Chem. Lett.*, **8**(15) (2017) 3678–3682. 10.1021/acs.jpclett.7b01160.

37. A. Plewa-Marczewska, T. Trzeciak, A. Bitner, L. Niedzicki, M. Dranka, G. Z. Źukowska, et al., New tailored sodium salts for battery applications. *Chem. Mater.*, **26**(17) (2014) 4908–4914. 10.1021/cm403349t.
38. M. Dranka, G. Z. Źukowska, P. Jankowski, A. Plewa-Marczewska, T. Trzeciak, J. Zachara, Coordination abilities of 4,5-dicyano-2-(trifluoromethyl)imidazolate anion toward sodium cation: structural and spectroscopic studies of solid and liquid glyme-solvated electrolyte systems. *J. Phys. Chem. C*, **121**(48) (2017) 26713–26721. 10.1021/acs.jpcc.7b09705.
39. I. D. Brown, What factors determine cation coordination numbers? *J. Am. Chem. Soc.*, **44**(6) (1988) 545–553. 10.1107/S0108768188007712.
40. I. D. Brown, *The Chemical Bond in Inorganic Chemistry: The Bond Valence Model*, 2nd Ed. Oxford University Press, Oxford, New York, 2016.
41. A. Bitner-Michalska, G. M. Nolis, G. Zukowska, A. Zalewska, M. Poterala, T. Trzeciak, et al., Fluorine-free electrolytes for all-solid sodium-ion batteries based on percyano-substituted organic salts. *Sci. Rep.*, **7** (2017) 40036. 10.1038/srep40036.
42. M. Dranka, P. Jankowski, G. Z. Źukowska, Snapshots of the hydrolysis of lithium 4,5-dicyanoimidazolate-glyme solvates. impact of water molecules on aggregation processes in lithium-ion battery electrolytes. *J. Phys. Chem. C*, **122**(6) (2018) 3201–3210. 10.1021/acs.jpcc.7b11145.
43. H. Kim, J. Hong, K.-Y. Park, H. Kim, S.-W. Kim, K. Kang, Aqueous rechargeable Li and Na ion batteries. *Chem. Rev.*, **114**(23) (2014) 11788–11827. 10.1021/cr500232y.
44. Y. Yamada, K. Usui, K. Sodeyama, S. Ko, Y. Tateyama, A. Yamada, Hydrate-melt electrolytes for high-energy-density aqueous batteries. *Nat. Energy*, **1** (2016) 16129.
45. Y. Wang, J. Yi, Y. Xia, Recent progress in aqueous lithium-ion batteries. *Adv. Energy Mater.*, **2**(7) (2012) 830–840. 10.1002/aenm.201200065.
46. C. Xu, S. Renault, M. Ebadi, Z. Wang, E. Björklund, D. Guyomard, et al., LiTDI: a highly efficient additive for electrolyte stabilization in lithium-ion batteries. *Chem. Mater.*, **29**(5) (2017) 2254–2263. 10.1021/acs.chemmater.6b05247.

## **Chapter 3**

# **Overview of Polymer and Solid Electrolytes: Towards All Solid-State Batteries**

**Michał Marzantowicz and Michał Struzik**

*Faculty of Physics, Warsaw University of Technology, ul. Koszykowa 75,  
00-662 Warszawa, Poland  
michal.struzik@pw.edu.pl*

### **3.1 Introduction**

Rapid development of mobile electric devices, ranging from microscale sensors to buses and boats, stimulates the search for efficient, safe, and compact energy sources. While most of the production costs of lithium batteries are generated by cathode and anode materials, the proper selection of electrolyte often becomes the key factor that determines the safety and longevity of the device.

Achieving a high energy density requires the electrolyte to be lightweight and possibly thin. Less thickness of the electrolyte layer also decreases the internal resistance of the battery and improves its efficiency. However, at the same time, the electrolyte must prevent the electrodes from short-circuiting and compensate for the changes

---

*Designing Electrolytes for Lithium-Ion and Post-Lithium Batteries*

Edited by Władysław Wieczorek and Janusz Płocharski

Copyright © 2021 Jenny Stanford Publishing Pte. Ltd.

ISBN 978-981-4877-16-9 (Hardcover), 978-1-003-05093-3 (eBook)

[www.jennystanford.com](http://www.jennystanford.com)

in the electrode dimensions caused by intercalation/deintercalation processes. A soft electrolyte is also preferred during the cell manufacturing process, which may include bending or folding of the layered structure. When the safety of the cell is concerned, compatibility with the electrode material and electrochemical stability become important issues. Finally, as most battery manufacturers extend the warranty period to several years and thousands of charge-discharge cycles, the electrolyte must also be resistant to aging. In modern cell designs, two different classes of materials are considered as appropriate in terms of the above-mentioned properties: polymer electrolytes and “all solid state” inorganic compounds.

## 3.2 Classification of Polymer Electrolytes

Using a polymer as a component of an electrolyte allows one to focus on high conductivity, mechanical flexibility, and reliability. The first publications on the successful application of a polymer as a solid solvent for lithium salts date to the 1970s. Systems based on poly(ethylene oxide) (PEO) were pioneered by the groups of Wright [1] and Armand [2]. Initially, the polymer electrolytes, usually prepared by the solvent-cast method, comprised only high-molecular-weight polymers and low amounts of lithium salts. With further modifications, the family of polymer electrolytes evolved and now contains several different categories (see Fig. 3.1). In many of these systems, the polymer is merely an additive to the electrolyte and does not constitute the main weight or volume fraction.

The “solid” side of the diagram is occupied by systems described as composite polymer electrolytes, composed of both organic and inorganic fractions. The addition of a small amount of inorganic filler is known to improve the ionic conductivity of polymer electrolytes, which is usually attributed to the interaction of the surface groups of such fillers with charge carriers [3]. Recent works show that ion transport can be improved further by the addition of ordered structures of high aspect ratios—whiskers or nanosized wires [4]. Interesting results were obtained also for materials with the opposite topology—inorganic porous structures in which polymer

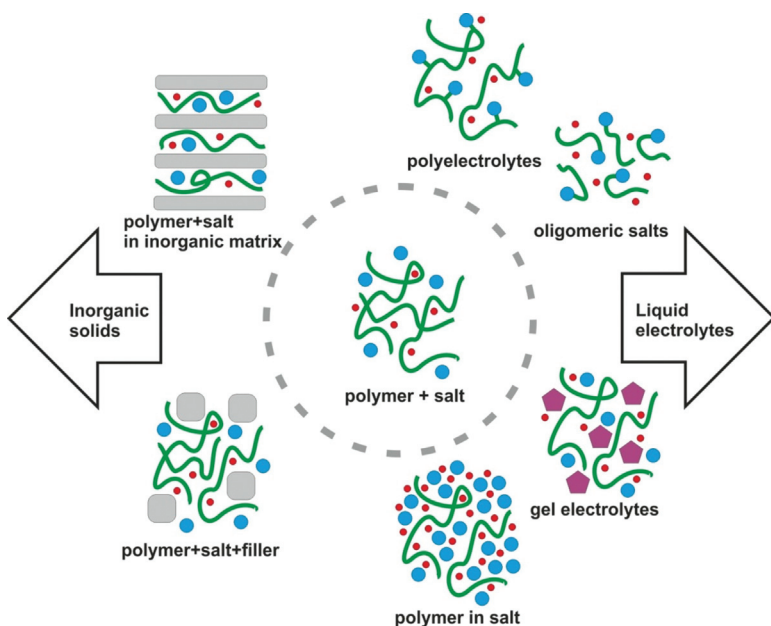


**Figure 3.1** Diagram showing major types of polymer electrolytes.

electrolytes act as conductive fillers [5]. Polymers can be also used as a binder between grains of crystalline materials in order to improve mechanical properties and preserve the continuity of conduction paths.

In most commercially available Li-ion cells, the polymer electrolyte also contains an additional low-molecular-weight organic solvent. Such systems, which represent the “liquid” side of the diagram are described as gel electrolytes. The addition of a solvent allows the achievement of high ionic conductivity but may contribute to safety issues in Li-ion cells. The organic solvent is flammable, and its molecules may also take part in anode and cathode degradation processes [6]. Semiliquid polymer electrolytes may also be formed by soaking the polymer matrix in a conductive salt of low melting point, called an ionic liquid. In this case, the role of polymer chains may be limited to providing a structure in which the conductive medium is stored. Another kind of electrolyte in which the properties of lithium salt determine the ionic conductivity is a

“polymer in salt,” in which the weight and the volume fraction of the salt surpass those of the polymer.

In most polymer electrolytes, a significant fraction of the charge is carried by anions, despite their large size and high molecular weight. Unlike lithium ions, the anions cannot be intercalated into the electrode and they accumulate at the interface, which is not favorable for the functioning of the Li-ion cell. This problem can be addressed either by immobilization of anions by attaching them to long polymer chains or by extending the anion structure with short oligomeric polymer chains. Unfortunately, the conductivity of these electrolytes—polyelectrolytes, ionomers, and oligomeric lithium salts—is usually much lower than that of traditional electrolytes with two mobile ionic species [7].

### 3.3 Dissociation and Transport of Ions: Microscopic View

Ionic conductivity is one of the key factors that determine the possibility of applying a polymer electrolyte in a Li-ion cell. The goal of  $10^{-3}$  S/cm at room temperature is easily achieved in liquid electrolytes but represents a challenge for polymeric materials. Understanding the origins of this problem requires both microscopic and macroscopic approaches to the conduction process.

#### 3.3.1 Dissociation

For a “polymer + salt” electrolyte the polymer acts as a solid solvent for lithium salt. The macromolecular chain comprises molecular dipoles and provides sites for coordination bonds with lithium ions. However, the dielectric constants of polymers are relatively low in comparison to those of commonly used liquid organic solvents with low molecular weights. For example, the reported dielectric constant of PEO is between 5 and 7 [8, 9], which is 5–7 times less than the dielectric constant of acetonitrile. To achieve good solubility, lithium salts with high delocalization of the anion charge are preferred. After the dissociation process, the released lithium ion may form an

aggregate with another anion. This effect can be prevented by using polymers that shield the cation from interactions with anions.

Even proper selection of salt and polymer does not guarantee that a homogeneous membrane will be formed. Effective dissolution of large crystals of salt requires elevated temperatures, and most polymers are semicrystalline at room temperature. Moreover, many polymers form stoichiometric crystalline complexes with lithium salts [10]. Any initial inhomogeneity may lead to the division of the electrolyte into areas with different concentrations of salt and of different structures [11]. Therefore, the preparation of polymer electrolytes on a laboratory scale usually involves the solvent casting method. In this process, polymer and salt are dissolved in a large amount of organic solvent, which is later removed by vacuum drying. An alternative method is hot pressing. A foil is formed from a premixed powder of polymer and lithium salt, using moderate pressure (usually single tons/cm<sup>2</sup>) and an elevated temperature [12, 13]. Although the homogeneity of the electrolytes may depend on the initial processing of the powders and the polymer's viscosity, the hot-pressing method seems to be better suited for industrial-scale production.

In other groups of polymer electrolytes, the role of the polymer as a solid solvent may be limited. Gel electrolytes permanently contain organic solvents, which promotes dissociation. In an electrolyte with an ionic liquid the dissociation occurs via ion-ion interactions, and the presence of a polymer matrix may only provide additional support to this process. In composite electrolytes, surface groups of inorganic fillers may promote dissociation. Surface sites representing Lewis acid interactions attract anions [14, 15], which results in a decrease in the number of ion pairs and an increase in the number of free charge carriers [16]. In a similar way, Lewis-base sites on the inorganic fraction surface provide coordination bonds for lithium cations. The dissociation process can be further supported by the application of fillers with high dielectric constants, such as lead zirconium titanate [17], BaTiO<sub>3</sub>, PbTiO<sub>3</sub>, and LiNbO<sub>3</sub> [18]. However, strong interactions may also bind a significant fraction of the charge carriers onto the grain surface.

### 3.3.2 Ion Transport

For “salt in polymer” electrolytes, the transport of ions is the most effective in an amorphous state and requires the rearrangement of the macromolecular chains. These segmental motions are strongly dependent on temperature: below the glass transition temperature  $T_g$ , the time required for the rearrangement of segments of polymer chains becomes so long (above 100 s) that the material can be regarded as “frozen” [8]. An ideal glass transition temperature  $T_0$ —usually about 50° lower—is the temperature at which the segmental motions freeze completely [19].

In the microscopic picture, segmental motions of polymer chains do not only allow the material to remain flexible but may also provide new hopping sites for ions and form conduction pathways. Transport to the next site is assisted by movements of the polymer chain, which support breaking and renewal of coordination bonds and significantly decrease the energy barrier of the transfer process [20]. This mechanism is quite effective at high temperatures, but the conductivity of the electrolyte decreases sharply as the temperature decreases and approaches the glass transition temperature. In a frozen, rigid polymer matrix, the high activation energy required for jumps between conduction sites hinders ionic conductivity.

A similar problem affects semicrystalline polymer electrolytes: chains closely packed in the crystalline lamellae cannot perform segmental motions. Therefore, the ionic transport relies on preserving the continuity of disordered, amorphous regions between the crystallites. Breaking the continuity of these pathways decreases the conductivity even by several orders of magnitude [21, 22]. There are only a few known exceptions to this rule: for lithium salts with the general formula of  $\text{LiXF}_6$ , the crystalline complexes of PEO and salt may form conduction channels for  $\text{Li}^+$  ions [23]. Conductivity pathways can also be formed by ordering of the polymer chains. Conductivity of stretched polymers, as well as foils cast under a magnetic field, is considerably higher than that of the bulk systems [24]. Unwanted crystallization induced by ordering of macromolecules can be avoided by the application of polymer blends or copolymers in which a rigid “skeleton” prevents the crystallization of the “soft” ion-conductive segments [25].

Some systems, like polymer-in-salt electrolytes and electrolytes with ionic liquids, can also be formed on the basis of polymers with high glass transition temperatures. At the intended operation temperature, the polymer matrix is rigid and provides a structural skeleton filled with a conductive medium of lithium salts. The conduction process includes ion-ion interactions and may take place either within the clusters of amorphous salt or along the polymer-salt boundaries [26]. In contrast to what has been described above for “salt in polymer” electrolytes, the transport of ions becomes partially decoupled from the motions of polymer chains. Another class of materials with conductivity decoupled from segmental motions of the polymer chains is gel polymer electrolytes. Molecules of the solvent support the dissociation of the salt and provide additional conduction sites [27]. The solvent also softens the polymer matrix, introduces structural disorder, and prevents crystallization of the polymer.

The positive influence of inorganic fillers on the ionic conductivity of polymer electrolytes is generally attributed to several factors. The presence of the filler grains usually prevents the growth of regular crystalline lamellae, leaving a shell of amorphous polymer around the filler. In this shell layer, the dynamics of the polymer chain motion may be affected by the proximity of the filler surface groups. The best results have been obtained for nanosized fillers [28], especially for materials with Lewis-acid sites, which coordinate cations [14]. According to these reports, it may be concluded that a significant improvement in ion transport between electrodes can be achieved if the shell layers of the grains form continuous paths through the bulk electrolyte. For nanosized fillers, this condition may be fulfilled even for the inorganic fraction of a few percent of the total electrolyte weight. For nonconductive fillers, a further increase in the amount of the filler may eventually result in a decrease in the conductivity by a reduction in the cross section available for ion transport.

Promising results were also obtained for electrolytes formed by filling a rigid structure with an amorphous polymer [29]. In both cases, improvement in the transport of lithium ions through the electrolyte may be obtained by ordering of the inorganic structures in a direction perpendicular to the electrodes [30]. At

first look, trapping of polymer chains between inorganic structures does not seem favorable for their segmental motion. However, the glass transition temperature of confined polymers may be lower than that of bulk systems and the frequency of the segmental motions of polymer chains is usually similar or greater [31]. Ordering of the macromolecules by the surrounding inorganic structures is also beneficial for charge transport [32]. This effect is similar to the enhancement of conductivity observed for stretched polymer foils, in which polymer chains become aligned along the stretching direction [33]. In the case of a composite organic-inorganic electrolyte, conductivity pathways may form along single or multiple neighboring polymer chains, as well as along the polymer-inorganic shell layers.

The degree of coupling of charge transport with motions of the polymer chain can be described quantitatively, as proposed by Angell and Martin [34]. The logarithmic decoupling index is based upon the value of ionic conductivity at the glass transition temperature

$$\log R_{\tau}^* = 14.3 + \log \sigma_{T_g}.$$

In the case of a “polymer + salt” electrolyte, the value of conductivity obtained at the glass transition temperature of the polymer is usually below  $10^{-12}$  S/cm, which is far too low for practical applications. For such systems, the logarithmic decoupling index is close to 1, which means that the lithium ions are strongly coupled to the polymer chain by coordination bonds. The transport of lithium ions is based on both movement along a single chain as well as hopping between the chains [35].

For electrolytes in which ion-ion interactions play an important role in the conduction process, including gel-type polymer electrolytes, polymers with ionic liquids, and polymers in salts, the values of the decoupling index are much higher. In these materials, ion transport may proceed even if the polymer matrix is frozen, as in the case of ion conductive glasses. Movements of the polymer chain may support the charge transport process, making it more effective, but they no longer determine the temperature dependence of conductivity.

## 3.4 Quantitative Models for Describing Ion Transport

In the first approximation, the temperature dependence of ionic conductivity can be quantitatively described using either the Arrhenius or the Vogel–Tammann–Fulcher (VTF) model. The Arrhenius approach is suited for systems with immobile matrixes in which charge transport occurs as the charge hops between sites separated by energy barriers of a certain height. It is usually applicable for crystalline solids with long-range structural order and materials in a frozen glassy state. The VTF model assumes a mobile matrix, in which the topology of conduction pathways is subjected to dynamic changes. It is applicable to polymer electrolytes with strong coupling between the segmental movements of polymer chains and the transport of ions.

For many polymer electrolytes, the above-mentioned models are not satisfactory or can be applied only in a narrow temperature range. The transport of charge may rely on two or more processes, each representing a different conduction mechanism. The transport of ions between the electrodes of the cell relies not only on elemental hopping between sites but also on the preservation of a network of continuous conductivity paths between the opposite interfaces of the electrolyte.

### 3.4.1 Arrhenius Model

A generally accepted model of ionic transport in an ordered, crystalline solid is based on hopping between neighboring sites separated by energy barriers of equal height. The conductivity pathways are formed by defects in the crystalline lattice—vacancies or interstitial sites. The frequency of successful jumps through the energy barrier decreases exponentially with the barrier height  $U_B$ :

$$\Gamma = v_0 \exp\left(-\frac{U_B}{k_B T}\right)$$

The presence of an external field increases the energy barrier in the direction opposite to the field and decreases the energy barrier in the direction of the field (see Fig. 3.2). The frequency of jumps in

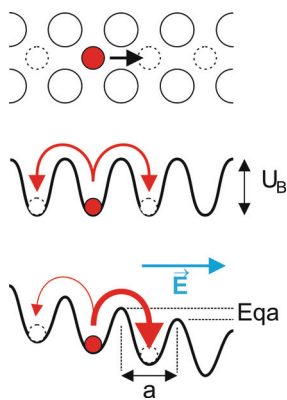


**Figure 3.2** In the Arrhenius model, the available conduction sites in the crystalline lattice (top) are separated by energy barriers (middle). An external electric field favors jumps in one direction (bottom).

the direction favored by the external field becomes greater than the frequency of jumps in the opposite direction. Under such conditions, the drift velocity of the charge carriers can be expressed as

$$v_d = \frac{Eq a^2}{2k_B T} c_v v_0 \exp\left(-\frac{U_B}{k_B T}\right).$$

The expression  $Eqa/2$  describes the additional energy that the charge carrier obtains in the external field, and the factor  $c_v$  denotes the probability of finding a free site in the desired direction of movement. Recalculation of the drift velocity to the charge carrier mobility  $\mu$  leads to the formula that describes the conductivity

$$\sigma = nq\mu = \frac{q^2 a^2}{2k_B T} n c_v v_0 \exp\left(-\frac{U_B}{k_B T}\right).$$

The formula can be divided into two parts: (i) a pre-exponential factor (often denoted as  $A/T$ ), which is sensitive to the concentration of charge carriers and available conduction sites and inversely proportional to the temperature, and (ii) exponential type dependence, which relies on the height of the barrier  $U_B$ , also called activation energy. If plotted in the so-called Arrhenius representation—logarithm of  $\sigma T$  on the vertical scale and  $1000/T$  on the horizontal scale—this dependence is expected to be linear and the activation energy can be calculated from the slope of a fitted linear function.

### 3.4.2 Vogel–Tamman–Fulcher Model

The temperature dependence of conductivity of electrolytes, in which the transport of ions is strongly coupled to segmental motions of polymer chains, can be described by the VTF model. This model, originally developed to describe temperature changes of viscosity, is applicable to all amorphous materials that can be obtained in a disordered glassy state.

Relocation of molecules or segments of polymer chains is possible if the energy of thermal vibrations is sufficient to overcome the pressure exerted by neighboring molecules and creates free volume slightly larger than the own volume of the moving object [36]. The probability of relocation depends exponentially on the ratio of the critical volume needed for the process ( $v_c$ ) to the average free volume available in the system:

$$P \sim \exp(-v_c/v_f)$$

If we define an ideal glass transition temperature  $T_0$  as a point at which the free volume is equal zero, the increase in the free volume with temperature can be related to the macroscopic thermal expansion coefficient  $\alpha$ :

$$v_f = \alpha (T - T_0) v_0$$

Thus, the probability of relocation can be expressed as

$$P \sim \exp\left(\frac{-B}{(T - T_0)}\right), \text{ where } B = v_c/\alpha v_0.$$

For polymers the formula that expresses the temperature dependence of conductivity contains two sections: (i) exponential type dependence related to the probability of relocation described above and (ii) the pre-exponential function  $A$  [37, 38]:

$$\sigma(T) = \frac{A}{T} \exp\left(-\frac{B}{(T - T_0)}\right)$$

In practice, the pre-exponential part is often assumed to be temperature independent [39], as the range of temperature in which polymer electrolytes are studied is usually limited. In some publications, a  $T^{-1/2}$  dependence is given [40].

The process of relocation based on free volume is schematically depicted in Fig. 3.3a. A jump to the next available conductivity site

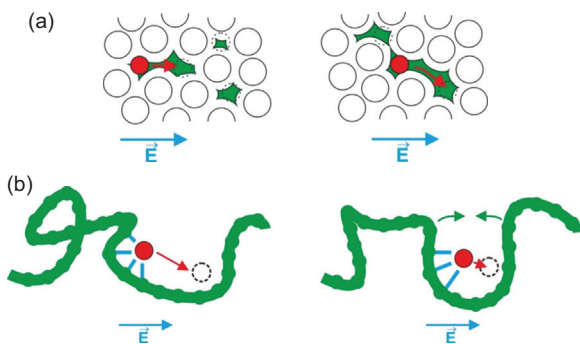


**Figure 3.3** Illustrations of the VTF model: (a) redistribution of free volume and (b) movements of the chain actively support the transport process by decreasing the distance between the sites.

requires large free volume bridging the two sites. For some of the charge carriers within the material, the volume allows only limited movements around the current position. In a glassy (frozen) matrix, the ions driven by the external field may reach a position in which they cannot “squeeze” through the passage to the next site. If the material is heated to a value above the glass transition temperature, the matrix becomes mobile and redistributes free volume. New conduction sites and continuous bridges between the sites are formed. In polymer electrolytes, such a model may refer directly to the transport of anions. Movement of usually bulky molecules requires adequate volume and cannot proceed effectively in a frozen polymer matrix.

For most “polymer + salt” electrolytes, the lithium cation is linked to the polymer chain by several coordination bonds. This often requires the chain to “wrap” around the ion, like in the case of PEO [41]. Travelling to the next position along the same chain requires a complex sequence of breaking and renewal of bonds, related to an elevated energy barrier. Inter-chain hopping may require even higher energy. Therefore, for a lithium cation the conduction process is not always directly obstructed by the volume occupied by the polymer macromolecules, but rather by an unfavorable arrangement of those molecules. Movements of the polymer chain lower the energy barrier related to transport

by decreasing the distance between coordination sites (Fig. 3.3b). Experimental evidence of this model is that similar values of glass transition temperatures are obtained for temperature dependence of segmental relaxation times and values of ionic conductivity [42].

An alternative model that explains temperature dependence of conductivity of polymers is the dynamic percolation approach [43]. In this model, the electrolyte can be treated as a constantly changing maze of connections between conductive sites. Although one moment the surrounding of the ion may not allow moving to the next position, the next moment reconfiguration of the chain may create the proper environment for such transport. If the ion driven by the external field becomes trapped in a “dead end” of the maze, it must await reconfiguration of the structure to advance to the next site. When the temperature rises, the reconfiguration events become more frequent.

### 3.4.3 Conductivity of an Inhomogeneous Medium: Percolation Models

Many polymer electrolytes contain fractions with different physical properties. For some systems, like composite electrolytes, this effect is a consequence of the presence of an inorganic compound. This compound may be either purely insulating, insulating with a conductive shell, or ionically conductive (active filler). For other electrolytes, inhomogeneity may result from the partial crystallization of the polymer matrix, from polymer-salt complexes, or from the fractionation of the electrolyte into areas of different compositions. Also polymer-in-salt systems exhibit structural inhomogeneity, as they are composed of domains of amorphous salt dispersed between polymer chains.

For all inhomogeneous electrolytes, the value of conductivity depends strongly on the continuity of pathways between the electrodes. If the domains of the poorly conducting fraction are scattered within the electrolyte and do not form continuous obstacles for the ions, they decrease only the volume and intersection available to the conduction process. With an increase in the fraction of the poorly conductive phase, its shape starts to play an important role in the model of charge transport. For example, large surfaces

perpendicular to the applied field may block charge carriers, leading to their accumulation and resulting in a Maxwell–Wagner–Sillars type polarization process.

The influence of inhomogeneity on the value of ionic conductivity can be described by percolation models. The most important parameter of these models is the percolation threshold  $\varphi_c$ , defined as the lowest volume fraction of the conductive phase that allows continuous clusters of that phase. This value depends greatly on the topology and microstructure of the material—for example, for a morphology typical of semicrystalline polymers in which the conductive domains are “squeezed” between the walls of large crystalline structures, the percolation threshold can be as low as 3% [44]. With decreasing volume fraction of the conductive phase, the conductivity depends on the distance from the percolation threshold

$$\sigma(\varphi) \sim (\varphi - \varphi_c)^t.$$

An identical model can be applied to describe approaching the percolation threshold from “below”—when the initial fraction of the conductive phase is lower than the percolation threshold

$$\sigma(\varphi) \sim (\varphi_c - \varphi)^{-s}.$$

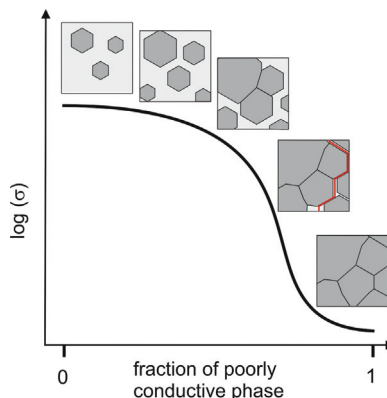


**Figure 3.4** A schematic plot of conductivity upon transition from a well-conductive phase to a poorly conductive phase. The red line marks the continuous conduction pathway near the percolation threshold.

The exponents  $t$  and  $s$  depend on the topology of the percolation system. This dependence, plotted on the logarithmic scale, gives a sigmoidal-type curve, which is a good approximation of results obtained for real polymeric systems (Fig. 3.4).

Percolation models have been successfully applied to describe the conductivity of semicrystalline polymers, in which conductivity occurs in the amorphous phase [45]. Other examples include polymer-in-salt systems, in which conductivity relies on the inter-connectivity of salt clusters [46], or systems with fillers, in which a peak of conductivity is observed at a certain filler amount [47, 48]. As most commercially applied polymer electrolytes comprise several components of different electrical properties, percolation models may aid the development process and indicate the optimum composition.

### 3.5 Lithium Transference Numbers

The lithium transference number  $t^+$  is expressed as the ratio of charge carried by lithium ions to the total electric charge transferred through the cell. In a rechargeable cell, the transport of anions may lead to a number of unwanted phenomena, like precipitation of salt at the anode and depletion of electrolyte at the cathode [49]. The transference number has a significant impact on the efficiency of the cell: according to the practical application goals set by United States Advanced Battery Consortium (USABC), the required conductivity of the electrolyte conducting single ionic species is  $10^{-4}$  S/cm, whereas for electrolytes conducting two or more species the limit is 10 times higher [50].

Unfortunately, for most electrolytes based on polymers with dissolved lithium salts, the amount of charge carried by anions is similar to or even higher than that carried by the cations. For polyether-type electrolytes with low concentrations of lithium salts, the anion does not interact with the polymer matrix and, therefore, its movement requires only free volume. Although the lithium cation has a much smaller radius and molecular weight, in a polymer matrix it is coordinated by several bonds with the macromolecular chain, which limit its mobility. Moreover, transport of cations in

a disordered and unaligned polymer matrix requires interchain jumps, also related to breaking and renewal of coordination bonds. Therefore, in dilute electrolytes, the lithium transference numbers are exceptionally low and lithium ions carry only up to 20% of the total charge [51].

Exemplary strategies leading to an increase in the lithium transference number are:

- Partial or full decoupling of lithium transport from the polymer matrix: High lithium transference numbers were achieved in polymers that coordinate alkaline cations much more weakly than polyethers, such as polycarbonate [52] and poly(*e*-caprolactone) with carbonate units incorporated in the polymer backbone [53]. A similar result can be obtained by the introduction of another conduction mechanism that competes with transport along polymer chains, such as ion-ion interactions. For polymer-in-salt electrolytes and ionic liquids, transport of lithium cations involves ionic clusters [54]. When transport occurs inside the cluster of an amorphous salt or at the cluster/polymer border, lithium is expected to exhibit higher mobility than the anions.
- Trapping of the anions in order to reduce anion mobility: Polymeric hosts with anion-trapping ability have been widely investigated, mostly involving acidic borate groups [55, 56]. Another example of successful enhancement of lithium transference numbers is of systems obtained by the addition of calix[6]pyrrole [57, 58]. Anion trapping may also be achieved in composite inorganic/organic electrolytes. Lewis-acid surface groups on the surface of the inorganic fraction can significantly reduce the mobility of anions. Enhancement of lithium transference numbers has been obtained for inorganic anion-trapping fillers [15] as well as polymer electrolytes in an inorganic host [59]. Anion-trapping organic groups can also be grafted in the shell layer of the inorganic filler [60].
- Formation of a composite organic-inorganic system comprising a large fraction of lithium conductive inorganic material or filling a porous ceramic structure with polymer (“polymer

in ceramic" systems): As an inorganic lithium-ion conductor usually transports only  $\text{Li}^+$ , it acts as a selective barrier, blocking the transfer of anions.

For some electrolytes, a combination of the effects described above can be observed. For example, our measurements have shown that in PEO-based systems, the lithium transference number initially decreases with increasing concentration of lithium salt but then eventually increases, even up to 0.8, when the weight fraction of lithium salt greatly surpasses that of polymer [51]. In this case, a high concentration of salt promotes ion-ion interactions, which aids the transport of lithium ions (especially interchain hopping). Additionally, as certain lithium salts form stoichiometric complexes with PEO, the anions of the salts become trapped within the structure of such complexes.

Complete immobilization of anions is possible in polyelectrolytes, in which the lithium salt is incorporated in the polymer chain at the synthesis stage and can participate in the ion conduction process only as an additional coordination site. Unfortunately, for nearly all studied systems, a high lithium transference number comes at the cost of low ionic conductivity [61]. Probably, a significant fraction of lithium ions becomes temporarily excluded from the charge transport as they become reattached to the anionic groups. Coordination of one lithium ion by two such groups from neighboring polymer chains can also cause cross-linking, which reduces the mobility of the whole polymer matrix [62]. Such combination of these two processes is rather unfortunate because segmental movements of the chains are needed in order to create new coordination bonds and redissociate the trapped cations. Lithium salts based on oligomeric anions may provide a solution to this problem—short polymer chains attached to anionic groups limit the mobility of the molecule and may themselves provide coordination sites for lithium cations.

Various experimental methods have been developed in order to estimate the share of lithium cations in overall charge transport. They can be divided into those that directly refer to the amount of charge carried by ions of a given type (transference number) and those that probe the diffusion coefficient of lithium, whether

charged or neutral (with the resulting quantity described as the transport number). In an ideal case, with only two kinds of charge carriers, the results obtained by different methods should be comparable. However, in many polymeric systems, a simple model involving only anions and cations cannot fully describe complex transport processes [63, 64]. For example, many polymers contain low-molecular-weight additives, which move along with the external field. An even more pronounced distortion of the transference number may come from the presence of ionic aggregates. Undissociated ion pairs are neutral and do not move in the direction of the external electrical field. For an electrolyte based on PEO and lithium bis(trifluoromethanesulfonyl)imide (LiTFSI) salt, which is relatively easy to dissociate, about a quarter of the lithium ions is contained within such pairs [65]. Triplets comprising two anion molecules and a lithium cation can give negative contribution to the lithium transference number, as the lithium travels in a direction opposite to the external field. Therefore, for electrolytes with a large share of ionic aggregates, even the total lithium transference numbers can be negative [66].

### 3.6 Polymer Electrolyte as an Element of the Cell: Electrolyte/Electrode Interface

Proper functioning of the cell requires maintaining good contact between electrolyte and electrode material. Many electrode materials are formed as micro- or nanosized grains. Such morphology allows the achievement of materials with unique properties, for example, composed of grains with a high-capacity core and a high-stability surface [67], or with ionic conductivity several orders of magnitude higher than that of the bulk material [68]. However, it also creates an extended surface area, which can be difficult to penetrate for macromolecules of high viscosity. Moreover, some electrode materials, like graphite, show only minor changes of volume upon intercalation with lithium (up to 10%), whereas for silicon compounds, the volume can increase by more than 3 times [69]. The electrolyte has to compensate for such changes, providing

the flexible “core” of battery structure. From this point of view, semiliquid electrolytes that also provide proper wetting of the electrode surface may be preferred.

On the other hand, the electrolyte has to separate electrodes and prevent self-discharge. A dense structure of the polymer matrix hinders many unwanted processes: the formation of dendrites, uncontrolled expansion of the solid-electrolyte interphase (SEI) layer, precipitation of lithium salts, and other forms of phase segregation. However, increasing the mechanical strength of polymer foil often results in the formation of a stiff, uneven, or porous surface on the electrolyte. As shown in experiments with flat blocking electrodes, such a surface may decrease the measured cell conductivity even by more than an order of magnitude [70] and heavily influence the properties of the interfacial layer.

To achieve a compromise between the two above-mentioned requirements, many polymer electrolytes contain two fractions: a rigid one, which provides membrane support, and a soft one, which adapts to the interface. Such an effect may be obtained by mixing two different polymers (heterogeneous or homogeneous blends) [71–74] or incorporating different monomers within the polymer structure (copolymers) [75, 76]. Another type of electrolyte with rigid and soft compounds is a polymer membrane soaked in an ionic liquid [77]. The ionic liquid guarantees proper wetting of the electrode surface, even for surfaces with granular or porous morphology. Further improvement in electrode contact is possible by the addition of low-molecular-weight solvents, which penetrate the electrode surface. However, not only are these organic solvents flammable, they can also co-intercalate into the structure of the graphite anode, which eventually leads to the cracking and detachment of graphene layers.

The SEI layer, which forms in the contact region of the electrolyte, is often considered an unwanted phenomenon, which creates an additional barrier limiting ion transport and thus increases the internal resistance of the cell. The SEI layer may bind and trap certain constituents of the electrolyte, including charge carriers, and can be responsible for reducing the cell capacity by as much as 50% [78]. However, a properly formed SEI prevents the transfer of electrons and further degradation of electrolyte and electrode

materials. Controlled growth of a stable SEI seems to be the best strategy for the development of stable Li-ion cells [79, 80].

The first model of SEI formed between lithium electrode and solid electrolyte dates back to 1979 [81]. Initially, the layer is formed by insoluble products of reactions, mainly caused by incompatibility between the electrode potential and the stability window of the electrolyte or its components [82]. On the anode side, reduction occurs if the lowest unoccupied molecular orbital of the electrolyte is positioned lower on the energy scale than the Fermi energy of the anode. On the cathode side, the electrolyte is oxidized if the highest occupied molecular orbital of the electrolyte is positioned higher than the Fermi energy of the electrode material. For polymer electrolytes composed of different fractions, the SEI often comprises heterogeneous layers or grains [83]. The reported thicknesses of the SEI vary from 1 nm to 100 nm.

The interphase layer represents a dynamic system, as the conditions at the electrolyte/electrode interface change during charge and discharge cycles. For example, in polymer electrolytes, mobile anions accumulate at the cathode upon charging of the cell, creating a salt-rich region and a significant concentration gradient. Volume expansion of the electrode material may result in cracking or even exfoliation of the SEI layer. In aged cells, the SEI usually contains small fragments of electrode material: graphene sheets for the carbon anode and detached grains of the cathode material. Investigation of the properties of the SEI layer usually involves “post mortem” decomposition of a cell subjected to several charge and discharge cycles [84].

The structure and composition of the SEI depends both on the composition of the polymer electrolyte and the composition and structure of the electrode. In simple “polymer + salt” systems, for which PEO and LiTFSI salt may serve as a model example, the SEI contains mainly hydrocarbons related to the polymer and compounds formed during decomposition of lithium salt. Even a trace amount of water and other additives present in commercially available polymers may significantly affect the properties of the SEI layer [85]. The accumulation of anions at the interface, which speeds up the formation of the SEI, may be avoided by the application of polyelectrolytes [86]. Also composite polymer electrolytes exhibit

improved stability of the interfacial layer, which can be attributed to the absorption of impurities on the filler surface, as well as restriction of the transport of unwanted low-molecular-weight molecules to the electrode [87]. In composite electrolytes in which the inorganic structure is soaked in the organic polymer electrode, the presence of an inorganic skeleton restricts the growth of the SEI layer. Electrolytes with inorganic reinforcement can be applied also in a cell's metallic lithium anode, as the inorganic fraction prevents the formation of lithium dendrites [88].

Commercially applied gel-type electrolytes introduce the risk of multiple unwanted electrode reactions and may result in uncontrolled growth of an SEI. For example, propylene carbonate is known to cause exfoliation of the outer layer of graphite anodes [89]. Also on the cathode side, the presence of solvents may represent a threat to cell safety. The surface layers of the widely used nickel-rich lithium nickel manganese cobalt oxide and lithium nickel cobalt aluminum oxide cathodes become less stable in a delithiated state, resulting in oxygen release, which may cause exothermic reactions with the solvent [90].

## 3.7 Examples of Solid Polymer Electrolytes

### 3.7.1 Polymer with a Salt

In an electrolyte formed by the dissolution of a small amount of lithium salt in a polymer, the polymer chain should incorporate atoms capable of creating coordination bonds with the lithium cations, situated within a distance that allows the transfer of cations to the next site. As conductivity is aided by segmental movements of the chains, flexible polymers with low glass transition temperatures and low crystallinity are preferred.

#### 3.7.1.1 Electrolytes based on PEO

PEO was one of the first candidates for polymer electrolyte matrixes [1] and can still be treated as a model example. The chain unit includes an oxygen atom, which provides the cation coordination

site and is responsible for relatively high dielectric constants. The PEO chain is known to wrap around the lithium cation, shielding it from interactions with anions. The glass transition temperature of high-molecular-weight PEO is about  $-56^{\circ}\text{C}$ , which is much below the intended operating temperature range of Li-ion cells. Proper selection of lithium salts for PEO-based systems allows the achievement of considerably high ionic conductivity. For lithium perchlorate ( $\text{LiClO}_4$ ), frequently used in commercial cells, the reported values of room-temperature conductivity were about  $10^{-6}$  S/cm [91]. Higher values, of around  $10^{-5}$  S/cm, were obtained for salts that plasticize the polymer matrix, such as  $\text{LiTFSILiN}(\text{CF}_3\text{SO}_2)_2$  [92] and  $\text{LiBETILiN}(\text{C}_2\text{F}_5\text{SO}_2)_2$  [93].

The major drawback of electrolytes based on unmodified PEO is the presence of a crystalline phase at the intended cell operating temperature range. The conductivity of a semicrystalline electrolyte can be even 3 orders of magnitude lower than that of an amorphous one. For a number of salts, like LiTFSI, the “crystallization gap” effect has been reported for selected electrolyte compositions and polymer chain lengths [94]—however, detailed studies have revealed that sluggish crystallization processes eventually lead to a decrease in the conductivity [95]. In recent years, various efforts have been made in order to completely inhibit the crystallization of PEO.

One of the methods that help suppress crystallization of a polymer is branching of the chains. The side chains disturb the regular alignment of the polymeric chains into lamellae during crystallization, therefore creating more disordered amorphous regions. Reasonable values of conductivity ( $1 \times 10^{-4}$  S/cm at  $30^{\circ}\text{C}$ ) were observed, for example, for branched PEO synthesized using boron compounds [96].

A detailed study of star-branched PEO-based electrolytes performed by the authors of this chapter [97, 98] revealed that although the branching did not prevent crystallization of pure PEO, it inhibited the growth of a crystalline phase of PEO:LiTFSI salt complexes. The branched electrolytes were initially based on a diepoxide core (Fig. 3.5a), which in the course of further studies has been replaced by a polyglycerol one.

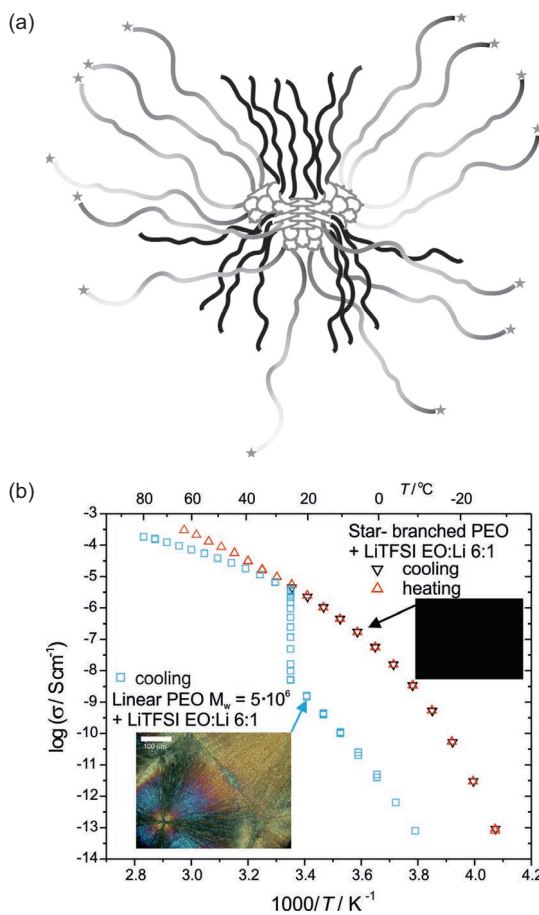


**Figure 3.5** Branching of PEO by attaching several polymeric arms to a diepoxide core (a, original drawing by G. Lapenis) suppresses the formation of crystalline PEO:salt complexes. This greatly improves the ionic conductivity of electrolytes below the melting point of the PEO:LiTFSI 6:1 crystalline complex (b).

Inhibition of growth of PEO:salt complexes helped obtain amorphous electrolytes with ionic conductivity comparable to that of overcooled amorphous electrolytes based on linear PEO, electrolytes that were stable regardless of the electrolyte thermal history. An example is depicted in Fig. 3.5b: for an electrolyte based on linear

PEO and LiTFSI salt, crystallization of the PEO:LiTFSI 6:1 stoichiometric complex at around 20°C causes a tremendous decrease in conductivity (by more than 500 times). A dense crystalline structure (pictured by a polarizing microscope) does not provide continuous conduction pathways and blocks the charge transport process. For star-branched PEO, branching inhibits the crystallization of the PEO:salt complex with a 6:1 EO:Li stoichiometry, and therefore the electrolyte remains amorphous in the whole studied temperature range.

Branched polymers can also be used as additives to polymeric systems. For an electrolyte in which a PEG-borate ester was used as the plasticizer of an electrolyte composed of poly(ethylene glycol) methacrylate and LiTFSI salt [99], crystallization was completely suppressed and the conductivity value ( $3 \times 10^{-4}$  S/cm at 30°C) resembled that obtained for overcooled amorphous electrolytes based on linear PEO with comparable lithium salt content. Promising values were reported also for polymer blends, in which a heterogeneous branched polymer structure was added to linear PEO [100]. Another class of branched structures is polymers with side chains added to the main polymer backbone. The movements of the side chains, faster than motions of the polymer backbone, can enhance ion transport through the matrix, as well as the charge transfer reaction rate at the lithium/electrode interface. In comb-shaped polyether electrolytes based on a matrix of PEO and 2-(2-methoxyethoxy)ethyl glycidyl mixed with LiTFSI salt, the ionic conductivity reached a maximum value of  $3.3 \times 10^{-4}$  S/cm at 30°C [101].

### 3.7.1.2 Electrolytes based on other polymers

A number of polymers can be considered as substitutes for PEO. An example is poly(propylene oxide) (PPO), which also exhibits a favorable glass transition temperature of about -60°C. Unfortunately, the ionic conductivity of electrolytes with this polymer is considerably lower than that of similar PEO-based systems despite the fact that it also contains oxygen atoms capable of coordinating lithium within the macromolecule [102]. The difference may arise from the greater distance and lower concentration of the cation

coordination sites. Therefore, PPO is used mainly as a plasticizer of PEO-based systems, forming a blend that introduces the disorder needed for the preservation of the amorphous character of the system [103]. Cross-linked systems based on PEO and PPO were also reported to remain in an amorphous state [104, 105].

Another amorphous polymer that could be considered is poly(methyl methacrylate) (PMMA). The carbonyl groups that coordinate lithium via the oxygen atom are not situated within the polymer backbone but are linked to the main chain as pendant side groups. For this polymer, the main problem is its rigidity and the brittleness of the obtained foils, which is related to an elevated glass transition temperature (above 100°C, depending on the exact polymer structure and the preparation method) [106]. Some ways to avoid this problem have been proposed, such as in situ polymerization inside the cell by irradiation [107]—however, even if the membrane is formed within the cell, the system may be troubled by inadequate flexibility and possible loss of contact with electrodes. Lack of support of ion transport by segmental motions of the chain limits values of ionic conductivity—the reported values of  $7 \times 10^{-5}$  S/cm at 100°C cannot be described as satisfactory [108]. The addition of inorganic fillers, which allows an electrolyte to stay within the “solid” regime, brings only temporary improvement in the electrical properties of PMMA-based electrolytes, which rapidly deteriorate over time [109]. Therefore, this polymer matrix polymer is used mainly for polymer-gel systems [110–112] in which its electrochemical stability and ability to prevent dendrite formation represent advantages and the rigid structure is softened by solvents.

Another alternative to PEO may be poly(vinylidene fluoride) (PVDF), which contains strong electron-withdrawing fluorine atoms [113]. These lithium coordination sites facilitate the dissociation of lithium salts [114]. The PVDF polymer matrix exhibits convenient mechanical properties and ensures separation of cell electrodes but at the temperature range of application is semicrystalline (melting point of around 170°C) [115]. Although the matrix exhibits a reasonable glass transition temperature of about –40°C, the low content of a well-conductive amorphous phase seems to be the main factor that limits the value of ionic conductivity. Therefore, the PVDF matrix is often used in gel-type systems, in which solvents act as plasticizers

[116–118]. The PVDF chains may also provide mechanical strength in copolymer polymeric membranes. One of best-known examples of such systems is the PVDF-hexafluoropropylene (HFP) copolymer [119, 120]. In such a system, amorphous and flexible HFP fragments provide the necessary pathways for ion transport.

Effective dissociation of lithium salts is possible also by nitrogen atoms from nitrile groups [121]. A representative of this family of polymers is poly(acrylonitrile) (PAN). This matrix represents good electrochemical stability toward oxidation, but the elevated glass transition temperature (125°C) and a melting point situated above 300°C practically exclude polymer chains from active support of ionic conductivity [122]. Moreover, lithium cations strongly coordinated by the polymer chain may in fact become immobile. PAN-based electrolytes obtained by the solvent casting method have exhibited promising values of conductivity [123, 124], but this effect can be attributed to the residual solvent left from the synthesis process. Solvent-free electrolytes have rather low conductivity [125]. PAN is often used as a structural skeleton for other classes of polymer electrolytes, such as polymer-in-salt or polymer-in-gel electrolytes.

The short review presented above shows that among all solid polymeric solvents, the performance of polyethers such as PEO is still unmatched by other polymers. Among recent publications, two trends emerge: modification of polyethers in order to avoid unwanted crystallization and using the polymer matrix merely as a structural skeleton for the conductive medium, usually comprising a solvent. While the first approach seems to provide a more elegant solution from the scientific point of view, sophisticated synthesis processes may be difficult to perform on an industrial scale. Therefore, commercialization of “true” solvent-free electrolytes based on a polymer with a small amount of lithium salt may still need several years of research.

### **3.7.2 Organic/Inorganic Composite Systems**

The term “composite” covers a wide range of systems, from nanosized inorganic granules suspended in polymers to polymers confined to the pores of an inorganic host. According to the

proportions of the inorganic and organic fractions and the functions of both constituents, composite electrolytes may be divided into three categories:

**Polymer with an inorganic filler:** The filler constitutes only a minor fraction of the electrolyte weight, usually much less than 10%. Interactions of filler with the electrolyte occur at the particle surface, and therefore nanometric grain sizes are preferred in order to increase the active surface area. These surface groups can create new conduction sites for cations or immobilize anions. The filler also introduces structural disorder, plasticizes the polymer matrix, and improves electrode compatibility. In this category of composite electrolytes, there does not seem to be a significant difference between lithium conductive and nonconductive fillers. This is due to the fact that isolated grains do not form continuous paths through the bulk. For inert fillers, the conductivity usually increases only up to a certain filler concentration—a higher content of the filler may cause agglomeration or sedimentation of particles, generating obstacles for ion transport.

Nonconductive oxides, such as  $\text{Al}_2\text{O}_3$ ,  $\text{TiO}_2$ ,  $\text{ZrO}_2$ , and  $\text{SiO}_2$ , constitute the most frequently studied group of fillers. These materials can be obtained in the form of micro- or nanosized granules, and progress in their preparation techniques have helped obtain grains of well-defined sizes and shapes. Some of these materials, like alumina, have been successfully applied in polymer electrolytes for many decades [126, 127]. Initially, these fillers were intended to improve the interfacial stability and mechanical properties of electrolytes. With the decrease in the grain size and increase in the relative surface area, other properties of the fillers were revealed—that they hinder polymer crystallization [15] and provide Lewis acid–base interactions [128, 129], allowing either anion trapping or coordination of lithium cations. Strongly acidic or basic filler surface groups provide additional “boost” to ionic conductivity and transference numbers. The influence of filler surface groups on electrical properties of the system was studied not only for PEO and other polyethers but also for other types of polymers, for example, PAN [130] and PVDF [131]. While in the case of PVDF, the increase in conductivity can be partially attributed to the larger content of the amorphous phase, for the PAN matrix, the

presence of fillers was reported not only to aid in the dissociation of lithium salt but also to promote the release of lithium ions bonded to the stiff and immobile polymer matrix. Additional interactions between filler and ions may come from spontaneous polarization of ferroelectric materials, such as BaTiO<sub>3</sub> [132].

Lithium-conductive fillers introduced as an additive into polymer electrolytes include materials with a perovskite structure Li<sub>3x</sub>La<sub>2/3-x</sub>TiO<sub>3</sub> (LLTO), a garnet structure Li<sub>7</sub>La<sub>3</sub>Zr<sub>2</sub>O<sub>12</sub> (LLZO) [133], and LLZTO [134], as well as the sodium superionic conductor (NaSICON) [135]. The obtained values of conductivity were usually similar to those for inert fillers. Further improvement of electrical properties of composite electrolytes was possible by the application of inorganic structures with a high aspect ratio (whiskers or flakes), which enable ordering of lithium transport pathways at the polymer/inorganic interfaces. It has been demonstrated that the addition of 5–20 wt.% of magnetically oriented montmorillonite flakes helps improve the conductivity of a PEO-based system with respect to the randomly aligned filler and bulk polymer system [136]. Structures with a very high aspect ratio, such as nanowires, may form continuous conduction paths. It has been shown [30] that nanowires of lithium-conductive LLTO immersed in a PAN-LiClO<sub>4</sub> electrolyte positioned across interdigitated electrodes help achieve ionic conductivity significantly greater than that of a filler-free polymer electrolyte and also that of the bulk LLTO if a very small cross section of the nanowires is taken into account. A moderate increase in the conductivity has been also observed for nonconductive nanowires [137].

**Polymer mixed with an inorganic compound:** The weight fraction of an inorganic compound is comparable to that of a polymer. The dominant morphologies of the inorganic fraction are either nanometric granules or elongated whiskers and fibers. The inorganic fraction improves the mechanical properties of the electrolyte and enhances the ionic conductivity of the organic part. The most interesting results were obtained for electrolytes in which the inorganic phase exhibited lithium cation conductivity. In such systems, the interconnectivity of domains of both constituents of the electrolyte (organic and inorganic) can be maintained, allowing parallel transport of ions.

Systems with a granular morphology were reported to exhibit good mechanical properties, stability, and ionic conductivity. The effects related to the transition from “polymer + filler” to a mixed polymer-inorganic system have been recently studied by the group of Goodenough [138]. In a system consisting of a PEO:LiTFSI polymer electrolyte and conductive LLZTO ceramics, the compositions with inorganic content up to 80% were studied. Although it turned out that the filler content optimal for achieving high conductivity is only about 10%, the electrolyte with a high content of ceramic conductor exhibited better selectivity of cation transport and enhanced electrode stability. Promising results were obtained also for other lithium-conducting ceramic nanopowders [139]. High ionic conductivity can be attributed partially to a convenient topology of the conduction channels: in a system with 60% inorganic compound, the percolation threshold is probably met for all possible kinds of conductive phases: polymer, inorganic, and organic/inorganic grain boundaries. The inorganic fraction also contributes to blocking anion transport and improving the cation transference number. The leading role of grain boundaries in the ionic conductivity of a mixed organic-inorganic system was also postulated for  $\text{LiAlO}_2:\text{LiI:P(EO)}_{3+x}$  electrolytes formed by electrophoretic deposition [140]. The ionic conductivity of this system of  $5 \cdot 10^{-4}$  S/cm seems close to the needs of rechargeable cells, and the weak temperature dependence of conductivity on temperature represents a strong advantage.

Aligned wires or nanowires of inorganic conductors surrounded by a polymer form ordered channels of ionic conductivity in both phases. Such structures can be used to produce conducting textiles [141], which greatly enhances the design possibilities of solid-state cells. In electrolytes with aligned fillers, the conductivity percolation threshold can be achieved using a relatively low filler content [142]. Systems in which the inorganic fraction forms a 3D network have also been studied. One of the recent examples of such systems is an electrolyte composed of garnet-type lithium conductor  $\text{Li}_{6.4}\text{La}_3\text{Zr}_2\text{Al}_{0.2}\text{O}_{12}$  nanowires soaked in a PEO-LiTFSI polymer electrolyte [143]. As both conducting constituents meet the percolation threshold needed for ion transport, the performance of the electrolyte is not limited by the problems related to the

transfer of Li<sup>+</sup> cations between the inorganic and organic fractions. 3D garnet structures provide enhanced thermal and electrochemical stability and low interfacial resistance in contact with metallic lithium electrodes [144].

**Inorganic structure soaked in a polymer:** A polymer electrolyte is confined to a layered or porous inorganic matrix, which constitutes the major weight fraction of the system. Confinement of polymer chains prevents crystallization and usually improves the conductivity by ordering of conduction pathways. Even in systems in which the inorganic part does not participate in transport lithium ions, enhancement with respect to the “bulk” unconfined polymer can be achieved.

A good example of enhancement of ionic conductivity by confining a polymer in an inorganic host is a system formed by soaking lithiated CdPS<sub>3</sub> in poly(propylene glycol) [145]. The host material has a layered structure, which allows the expansion of the lattice to accommodate the polymer macromolecules between the layers. Confinement of the polymer results in lowering of the glass transition temperature with respect to the bulk PP-based electrolytes, as well as the enhancement of conductivity. A single ion conductor is been formed with good stability and compatibility with most electrode materials. Also electrolytes formed by soaking nonconductive Al<sub>2</sub>O<sub>3</sub> material in PEO dimethyl ether were reported to exhibit high conductivity and excellent long-term stability toward lithium electrodes [146]. The inorganic host featured micro- and nanometric pores, and most promising results were obtained in samples with 60% porosity.

It is worth noticing that inorganic structures soaked in a polymer represent a concept close to nonconductive organic membranes filled with a conductive polymer. Also in such systems, confinement of the conductive polymer in the porous structure has proven to be beneficial for ionic conductivity. For example, for a PEO-based electrolyte confined to an organic, nonconductive polycarbonate membrane with cylindrical pores ranging between 30 and 400 nm in diameter, the conductivity of the material oriented in the conduction direction is 2 orders of magnitude higher than that of the bulk “polymer + salt” electrolyte with a similar composition [29].

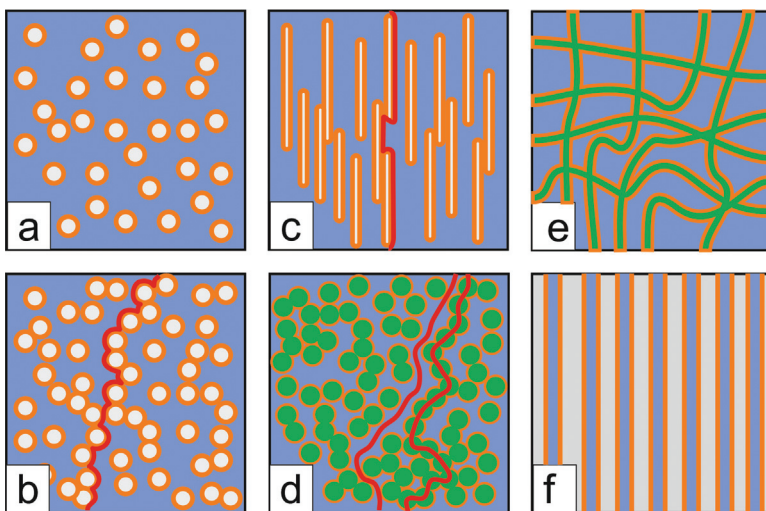


**Figure 3.6** Different topologies of composite systems: (a) A polymer with a small amount of filler. (b) A polymer with a filler; the percolation threshold for grain boundary conductivity has been reached. (c) A polymer with oriented nonconductive whiskers; conductivity along boundaries. (d) A polymer mixed with conductive inorganic conduction channels in both phases. (e) 3D lithium conductive nanowires immersed in a polymer. (f) An oriented inorganic structure soaked in a polymer.

From application and production point of view, it is relatively easy to add fillers, and therefore composite electrolytes can already be found in industrial patents and commercialized cells. Adding a small amount of filler is usually beneficial for the conductivity and stability of the electrolyte, leaving only one concern—that of decreasing energy density. Tailoring 3D inorganic structures filled with organic electrolyte is a much more challenging task. Increasing safety requirements for Li-ion batteries and need for power sources for critical applications may provide a boost for the development of these materials.

### 3.7.3 Polymer in a Salt and Systems with Ionic Liquids

The concept of salt-rich systems, in which conductivity is based on ion-ion interactions and only supported by motions of the polymer

chain, was first introduced by the group of Angell [147, 148]. The salt-rich systems were reported to exhibit a number of advantages, such as high lithium transference numbers and mild temperature dependence of ionic conductivity.

Salt-rich systems allow a wider range of polymer hosts as the conductivity does not necessarily require the polymer chains to be flexible. Ion transport occurs mainly in ionic clusters formed by the salt. The value of conductivity depends on the continuity of such clusters through the bulk electrolyte [149, 150]. However, there seems be only a thin border between achieving sufficient topology of nanosized ionic clusters and large-scale phase separation, which leads to the precipitation of lithium salts. In results obtained by other authors, promising values of conductivity were obtained for polymers that include EO units in the structure, such as polysiloxanes [151]. The studies also involved rigid polymers, such as PAN [136, 152]. The PAN matrix has a much higher glass transition temperature than PEO (above 80°C) and therefore would not be suitable for a traditional electrolyte with a low concentration of lithium salt. Another “stiff” polymer matrix that has been applied in salt-rich systems is chitosan [153]. Salt-rich electrolytes can also be prepared using nonpolar polymer hosts such as polystyrene [154] if proper additives are introduced to the system, such as fillers that provide Lewis acid-base interactions.

Studies performed by our research group on different salt-rich systems [11, 26, 98] revealed that even if the average salt concentration is below the solubility limit, the formation of local salt-rich domains that can start the phase segregation process is still possible. For electrolytes based on linear PEO and LiTFSI salt [11], the samples behaved in a relatively stable manner for up to 76.5 wt.% of the salt (molar ratio EO:Li = 2:1). Effects related to phase segregation upon crystallization of stoichiometric PEO:salt complexes were observed, but these processes had a local and reversible character. Upon increasing the content of LiTFSI to a value above 77 wt.%, the first precipitates of salt were observed. Initially, domains of crystalline salt appeared between the lamellae of the crystalline PEO:salt complex. Upon crystallization, the crystallites of the PEO:salt complex expelled the excess salt into the surrounding melt, thus locally increasing the concentration of the salt beyond

the solubility limit. This caused the appearance of thin, needle-like crystals of salt. Upon successive heating and cooling cycles, these small areas rich in salt systematically merged into larger domains, irreversibly turning the electrolyte into an inhomogeneous mixture.

Replacing linear PEO with star-branched PEO allowed increasing the content of the salt in the electrolytes [98]. As already mentioned, branching of PEO suppressed the formation of crystalline PEO:salt complexes. Without crystallites of these complexes, the crystallization-induced mechanism of phase segregation was excluded. Electrolytes with a salt content of up to 87 wt.% were obtained by the solvent-casting method, which homogenized the mix and prevented the precipitation of the salt. Measured freshly after preparation, these systems showed promising electrical properties: relatively high ionic conductivity was accompanied by a mild temperature dependence of the conductivity—a characteristic of electrolytes with ion-ion interactions. As a consequence, at a temperature range below 0°C, the conductivity surpassed the best results obtained for “salt in polymer” electrolytes with similar lithium salts. However, after several months, the ionic conductivity of the electrolytes started to decrease. The observed changes could not be reversed by heating the electrolytes to a value above the melting point of the salt—subsequent heating and cooling cycles only speeded up the process.

A comparison of polymer-in-salt systems based on PEO with electrolytes based on a copolymer of acrylonitrile and butyl acrylate [26] showed that for the latter electrolytes, even samples with 35 wt.% of LiTFSi salt exhibit a significant decrease in ionic conductivity upon prolonged storage. In fact, most dramatic changes in conductivity, by more than 4 orders of magnitude, were recorded mainly for electrolytes representing a medium content of salt, between 35 wt.% and 65 wt.%. It is remarkable that these changes were not related to the formation of salt precipitates, which were not observed in the system with up to 91 wt.% of LiTFSI salt, even after prolonged storage. A possible explanation may come from studies of the coordination environment of lithium cations. It seems that initially mobile charge carriers gradually become bonded in structures that either provide coordination by two or more groups from polymer chains or involve four molecules of lithium salt. In

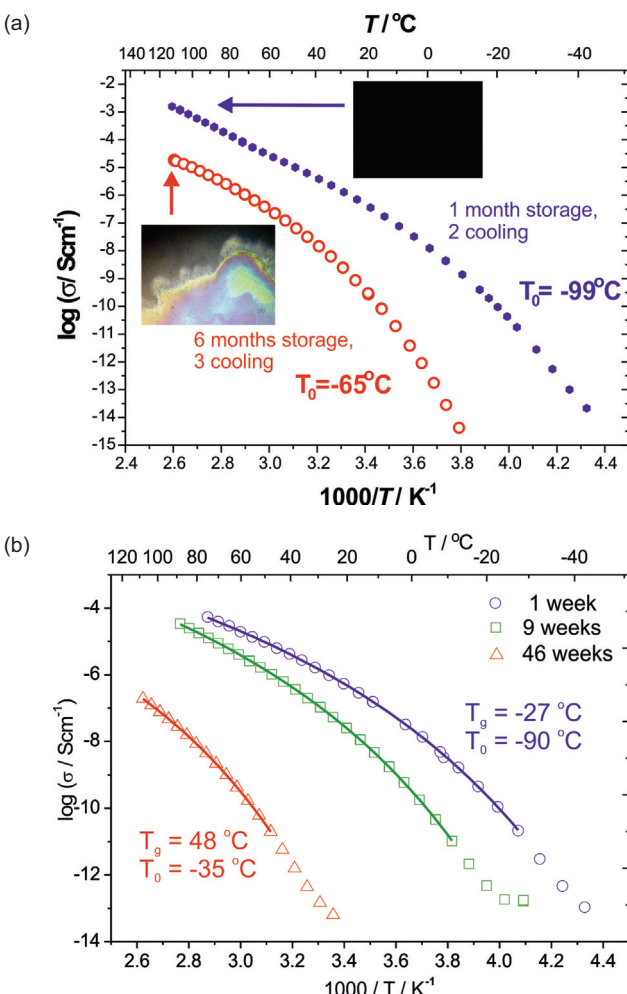


**Figure 3.7** Changes in ionic conductivity due to aging: (a) for a polymer-in-salt electrolyte with 87 wt.% of LiTFSI salt and 13 wt.% of branched PEO (polarizing microscope photos as inserts); (b) for an electrolyte with 65 wt.% of LiTFSI salt and 35 wt.% of AN-BuA copolymer.

either case, the mobility of lithium is restricted, as it is attached to a rigid polymer or positioned within a poorly conductive cluster of salt. A “microscopic” segregation process such as this can exhibit

an even more pronounced effect on the topology of the conduction channels than the occurrence of salt precipitates.

Conductivity based mainly on ion-ion interactions is also observed in electrolytes comprising polymer and ionic liquids. In such materials, both lithium coordinating and inert polymers can be applied, as the ionic liquid promotes the lithium salt dissociation process and provides sites for ion transport. The role of the polymer may be limited to providing a mechanical skeleton for the system and improving the electrochemical stability of the electrolyte/electrode interface with respect to the bulk ionic liquid.

Ionic liquids used in polymer electrolytes are based on organic cations. Exemplary families of compounds are imidazolium, pyridinium, pyrrolidinium, alkylammonium, alkylphosphonium, and alkylpyrrolidinium. Usually, the cation molecules have rather bulky and asymmetrical in structure [155], although examples of smaller cations, like phosphonium, can also be found [156]. Anions include those applied in lithium salts for Li-ion cells:  $\text{TFSI}^-$ ,  $\text{FSI}^-$ ,  $\text{Tf}^-$ ,  $\text{BF}_4^-$ ,  $\text{PF}_6^-$ . The lithium salt added to the system is typically of the same type of anion as the ionic liquid [157]. An ionic liquid-polymer system can be synthesized using various approaches: the solvent casting method, in which the polymer is mixed with an ionic liquid and a proper solvent (or the polymer is soaked in an ionic liquid-solvent solution), and the *in situ* polymerization of monomers dispersed in an ionic liquid [158]. In the case of solvent casting methods, the removal of trace amounts of solvents may be difficult as it becomes bonded to the ionic liquid molecules.

Conductivities of electrolytes comprising ionic liquids and PEO were reported to be 1 or 2 orders of magnitude higher than those of electrolytes comprising only lithium salt [159]. In this case, the electrolyte involved an ionic liquid representing the imidazolium family of compounds 1-ethyl-3-methylimidazolium TFSI as well as difluoro(oxalato)borate salt as a source of lithium ions and high-molecular-weight PEO. The enhancement of conductivity can be attributed partially to the much lower crystallinity of the electrolyte with an ionic liquid, as well as a low glass transition temperature, not significantly higher than that of pure PEO. Such an improvement of properties requires a fraction of about 40 wt.% of ionic liquid. A similar behavior was observed

for other ionic liquids: the addition of 32 wt.% of *N*-methyl-*N*-propylpiperidinium TFSI to PEO-LiTFSI helped increase the conductivity of the PEO-LiTFSI system by 2 orders of magnitude [160]; room-temperature conductivity of  $10^{-4}$  S/cm and excellent electrochemical stability have been reported for PEO-LiTFSI electrolytes with the addition of *N*-methyl-*N*-propylpyrrolidinium TFSI [161]. In the case of PEO-based systems, it was possible to surpass  $10^{-3}$  S/cm at room temperature by addition of solvents (ethylene carbonate) [162].

As already mentioned above, in the case of ionic liquids polyethers such as PEO may not be the optimum choice as they bind charge carriers involved in a less effective mechanism of ion transport along the polymer chain. Other types of polymers investigated as a matrix for ionic liquids include PVDF-HFP copolymers. For electrolytes with a mixture of hydrophilic 1-ethyl-3-methylimidazolium  $\text{BF}_4^-$ , 1-ethyl-3-methylimidazolium triflate, and hydrophobic 1-(1-butyl)-3-methylimidazolium  $\text{PF}_6^-$ , high conductivities, surpassing the  $10^{-3}$  S/cm limit, have been obtained [163]. A comparison of electrolytes that contained the same ionic liquid (1-*n*-propyl-2,3-dimethylimidazolium  $\text{BF}_4^-$  and 1-*n*-propyl-2,3-dimethylimidazolium  $\text{PF}_6^-$ ) but were prepared using either PEO or PVDF-HFP showed that generally PVDF-HFP helps achieve higher conductivity [164, 165]. According to the author, limiting interactions between ions and polymer matrix facilitated the formation of conduction channels in the ionic liquid, which constituted 30 wt.% of the electrolyte. In many other reports, the polymer acts merely as a mechanical support for the ionic liquid, which constitutes up to 90 wt.% of the electrolyte. Such systems have been prepared using, for example, block copolymers of polystyrene and PEO [166]. In terms of electrical properties, like conductivity and electrochemical stability, those electrolytes resemble ionic liquids.

Among the two classes of materials described above, polymers with ionic liquids are a better prospect in terms of commercialization as electrolytes in Li-ion cells. The issues of aging and phase segregation for polymer-in-salt systems have not been resolved yet. Ionic liquids have been studied extensively and are already routinely applied in prototype or laboratory cells. In some cases, the possibility of application by simply soaking the polymer membrane

in liquid salt instead of using the solvent casting method is an important advantage.

### 3.7.4 Polyelectrolytes and Oligomeric Salts

In most polyelectrolytes, the chain host groups are capable of releasing lithium cations, leaving the anions permanently bonded to the electrolyte matrix. Designed as single-ion conductors, these systems do not deal with problems such as accumulation of anions at the electrode and the corresponding concentration gradient. According to the USABC, the conductivity threshold that allows practical application of the electrolytes is 10 times lower than for traditional systems ( $1 \times 10^{-4}$  S/cm vs.  $1 \times 10^{-3}$  S/cm at room temperature) [50]. However, results published so far indicate that ionic conductivity values of polyelectrolytes are generally much lower than those of traditional systems. The main problems behind this effect are insufficient dissociation of anions and cations, trapping of already released charge carriers, and cross-links that form between the charged groups and restrict the movement of the chains.

Many polyelectrolytes contain oxyethylene units in their structure, which assist in the dissociation of lithium cations. Examples include PEO-based polyurethanes [167], short-chained poly(ethylene glycols) (PEGs) with lithium functional groups situated at the chain end, and additional PEG chains added as plasticizers [168], as well as copolymers of PEO and poly(epichlorohydrin) in which epichlorohydrin functional groups were substituted by a sulfate functional group [169]. For all these cases, the concentration of Li ions and the molecular ratio Li:EO were rather low. Assuming additional problems related to the incomplete dissociation of ionomers, this partially explains the low conductivity of these systems, which did not exceed  $10^{-6}$  S/cm at room temperature. Considerably higher values were obtained for polyelectrolytes with a star-branched structure, based on a polyglycerol core, studied by the group of authors of this chapter [170]. Placing lithium-releasing  $\text{P}(\text{=O})(\text{OLi})_2$  functional groups at the end of each of the 18 PEO arms helped achieve conductivities up to  $8 \times 10^{-6}$  S/cm, considerably higher than for the other functional groups that were studied. This

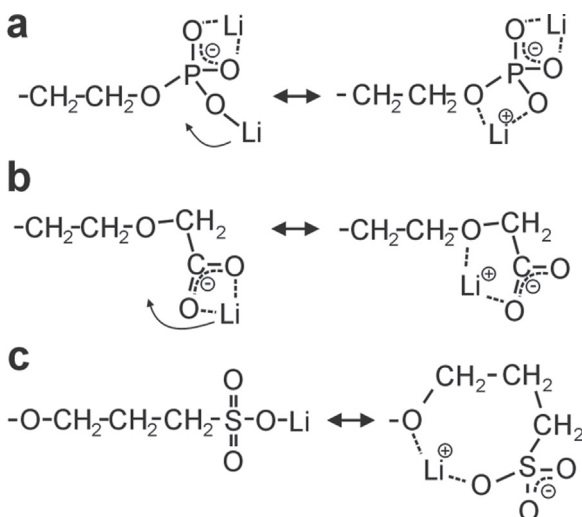


**Figure 3.8** The superior conductivity of an electrolyte with  $\text{P}(=\text{O})(\text{OLi})_2$  groups is related to the facile transfer of lithium onto the polymer chain (a). In the case of other groups (b, c), this process requires a sequence of breaking and renewal of bonds [170].

effect has been attributed mainly to the facile process of the transfer of lithium from the functional group to one of either oxygen atoms in the chain, which demonstrates the importance of the dissociation process in polyelectrolytes.

PEO can also act as a matrix to which heterogeneous ionomers have been added as a source of ions. An anion of very low mobility can be obtained, for example, by adding polystyrene chains to the  $\text{TFSI}^-$  group [171]. In such systems, as in the case of “polymer + salt” systems, PEO chains of the host are involved in the dissociation process. In polyelectrolytes that do not involve oxyethylene units, the issue of lithium dissociation becomes critical. For random copolymers, in which only one type of polymer units can release lithium, the conductivity did not increase proportionally to the increasing concentration of lithium donors [172, 173] but was rather found to be limited by the dissociation of lithium. Such interactions may come from other units of the copolymer, as well as from solvents, zwitterionic molecules, ionic liquids, and fillers. Following this approach, systems with conductivity as high as

$10^{-3}$  S/cm at room temperature can be prepared [174]. However, these are gel-type electrolytes, in which the transport of cations is strongly coupled to the mobility of the solvent molecules.

The concentration of lithium ions can be increased by shortening the polymer chains to only a few units. Such systems are often described as oligomeric salts or ionic melts. Oligomeric systems based on EO units can be obtained in an amorphous state up to a certain chain length. This can be partly attributed to the influence of added end groups [175–177]. For such salts formed by replacing either one or two end units of the PEO chain by  $\text{SO}_3\text{Li}$  groups [160], the highest values of room-temperature ionic conductivity were recorded for molecules with single functional groups and containing about 8–12 EO units. Conductivity values reaching  $10^{-5}$  S/cm at room temperature and high cation transference numbers of 0.8 have been obtained for oligomeric salts formed using a benzene ring “linker” between the oligomer chain and the  $\text{SO}_2\text{NSO}_2\text{CF}_3\text{Li}$  group [178]. Branched oligomeric salts containing more than one polymer chain were also studied. Lithium aluminates with two oligoether groups, with up to 12 EO units each, and two electron-withdrawing groups— $\text{CF}_3\text{CO}_2$ ,  $\text{CF}_3\text{SO}_3$ ,  $(\text{CF}_3\text{SO}_2)_2\text{N}$ , or  $\text{C}_6\text{F}_5\text{O}$ —were obtained in an amorphous state and exhibited promising values of ionic conductivity, up to  $10^{-4}$  S/cm for the system with  $(\text{CF}_3\text{SO}_2)_2\text{N}$  groups [179]. Improvement in the ionic conductivity of oligomeric salts can also be achieved by mixing these salts with oligomeric molecules of similar lengths. In the case of ionic liquids with  $\text{CH}_3\text{O}-(\text{EO})_{11}\text{CF}_2\text{CFHOCF}_2\text{CF}_2\text{SO}_2\text{N}-\text{SO}_2\text{CF}_3^-$  anion addition of low-molecular-weight PEG increased the ionic conductivity of the system by about 10 times with respect to the conductivity of pure oligomeric salt [180]. The additional molecules plasticize the system and provide vehicular-type transport of cations. Generally, for all oligomeric systems, the value of the cation transference number systematically decreases with a decreasing length of the oligomeric groups, so increasing the concentration of lithium cations can lead to lowering of cation transference numbers.

Considering the limited progress in the improvement of the ionic conductivity of polyelectrolytes, oligomeric salts may provide an alternative path of development for this group of materials. The problem of a nonunity lithium transference number can

be possibly resolved by imposing further restrictions onto the transport of anionic molecules, that is, by adding a structural “skeleton” composed of either a high-molecular-weight polymer or an inorganic network.

### 3.8 Ceramic Electrolytes

As already discussed in previous sections, achieving a solvent-free system with sufficient ionic conductivity represents a challenging task. The increase in ionic conductivity comes at the cost of either mechanical properties, safety, reliability, or stability. Therefore, most commercially applied polymer electrolytes contain flammable and volatile organic solvents to enhance their stability, with high ionic transport available at the same time. To exemplify, gel-type systems have achieved great commercial success. However, they suffer from critical safety issues, originating from the corrosive character of the electrolyte material, danger of leakage, a narrow thermal stability window (below 80°C), and high flammability. These limitations impose a number of restrictions on the battery cell operation conditions and its design.

One of the strategies for addressing these limitations is to replace the semiliquid organic components with their inorganic crystalline counterparts, known as “solid state” or “ceramic.” Inorganic solid electrolytes show slower reactivity when compared with liquids. Therefore, superior thermal and aging stability leading to a longer battery lifetime can be expected for solid-state devices. Ceramic electrolytes have a wide temperature operation window, allowing them to operate at temperatures below –50°C, where conventional liquid electrolytes would freeze, as well as at temperatures above 100°C without the risk of decomposition. In addition, inorganic solid electrolytes usually show wide electrochemical stability window, which allows for their safe application in cells with a high potential difference between electrode materials as well as operation with high-capacity anodes, such as metallic Li<sup>0</sup>, indicating the possibility of the development of lithium-air batteries. Unlike polymeric systems, solid-state electrolytes can block or significantly limit the growing rate of the lithium dendrites, which together with their

inherent nonflammability, results in enhanced safety of the solid-state-based devices. Moreover, most inorganic crystalline materials are single-ion conductors with predominantly ionic transport, usually following the hopping model. Ionic conductivity is, therefore, thermally activated and follows the Arrhenius dependence. Therefore, for achieving a desired weak temperature dependence of conductivity, the activation energy of ion transfer should be kept low and the amount of charge carriers high. With the above-mentioned features solid-state electrolytes bring the prospect of significantly enhanced energy density of solid-state-based energy storage devices.

Although for a long time, compared to their organic counterparts, inorganic conductors were considered unsuitable for application in low-temperature cells due to the poor ionic conductivity at room temperature, recent findings reveal that it is possible to overcome this limitation. Moreover, the introduction of inorganic solid-state electrolytes opens new avenues for further battery cell miniaturization, novel cell designs, 3D stacking, and deep integration with complementary metal-oxide semiconductor-based electronic circuits.

Despite the undeniable advantages of solid-state electrolytes, their commercial success still requires intensive research effort toward stabilization of the solid-state interfaces and maintenance of good physical contact upon cycling. Because the solid-state electrolytes technology is relatively recent, many factors, such as the electrolytes' mass-production costs and methods, integration into battery cells and stacks, long-term stability, and impact on the environment, still need to be researched.

In recent years, considerable attention has been devoted to new classes of ceramic materials, based primarily on oxides, exhibiting fast ionic conductivity, comparable with the conductivity of polymeric materials. In Fig. 3.9, we compare the ionic conductivities of representative organic electrolytes with those of new ceramic materials that are considered to be prospective candidates for all solid-state lithium-ion battery development. In the following paragraphs we deliver a brief description of the key features of these materials in the context of the development of new, safe, and efficient energy storage devices.

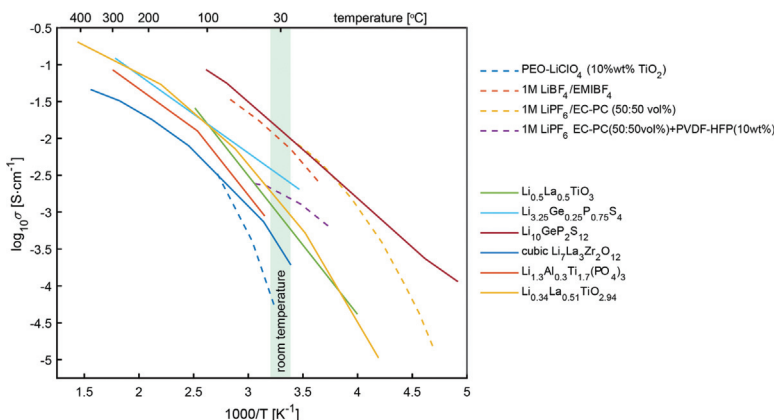


**Figure 3.9** A comparison of ionic conductivity as a function of temperature for selected classical polymer organic electrolytes (dashed lines) with ceramic solid-state electrolytes (solid lines).

### 3.8.1 NASICON-Type Conductors

Solid electrolytes of the NASICON-type structure show high ionic conductivity and considerable stability against air, making them an interesting candidate for electrolyte materials for solid-state batteries. They originate from their sodium-conducting counterparts of a general formula  $\text{NaM}_2(\text{PO}_4)_3$ , where sodium cations are replaced by  $\text{Li}^+$  [181, 182]. Among them  $\text{LiTi}_2(\text{PO}_4)_3$  shows the highest ionic conductivity, reaching  $10^{-6}$  S/cm, and low activation energy of  $\sim 0.30$  eV [183]. Their chemical stability and ionic conductivity can be enhanced using a doping strategy [184–186], resulting in high conductivity values of  $7 \times 10^{-4}$  S/cm at  $25^\circ\text{C}$  for  $\text{Li}_{1+x}\text{Al}_x\text{Ti}_{1-x}(\text{PO}_4)_3$  for  $x = 0.3$  [187].  $\text{Li}_{1.3}\text{Al}_{0.3}\text{Ti}_{1.7}(\text{PO}_4)_3$ , often designated as LATP, owes its fast ionic transport to its specific crystal structure, shown in Fig. 3.10, consisting of a rigid framework of  $\text{PO}_4$  tetrahedrons connected through  $\text{TiO}_6$  octahedrons, forming a 3D migration pathway for mobile cations [188]. Further, it was demonstrated that the glassy phase of  $\text{Li}_{1.3}\text{Al}_{0.3}\text{Ti}_{1.7}(\text{PO}_4)_3$  shows even higher lithium conduction, up to  $1.5 \times 10^{-3}$  S/cm at room temperature, making this material an interesting electrolyte candidate for solid-state batteries [189].

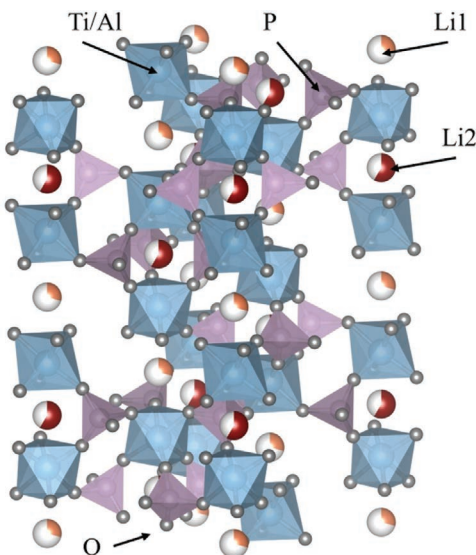


**Figure 3.10** Crystal structure of a NASICON-type  $\text{Li}_{1.3}\text{Al}_{0.3}\text{Ti}_{1.7}(\text{PO}_4)_3$  solid electrolyte.

Although glassy  $\text{Li}_{1.3}\text{Al}_{0.3}\text{Ti}_{1.7}(\text{PO}_4)_3$  shows one of the highest ionic conductivities among ceramic lithium conductors as well as excellent stability against air, its electrochemical stability window is limited by a low redox potential [190]—around 2.5 V versus  $\text{Li}/\text{Li}^+$ .  $\text{Ti}^{4+}$  reduces to  $\text{Ti}^{3+}$ , which induces electronic conductivity leading to short-circuiting of the battery cell [191, 192]. Therefore, lithium titanium phosphates should not be utilized with low-potential electrode materials, including metallic lithium. It was, however, demonstrated that NASICON-type lithium-conducting electrolytes can be successfully utilized in potentiometric gas sensors for tracking  $\text{NO}_x$  levels, mainly due to their extraordinary stability in air [193].

One of the successful strategies for extending the stability window of NASICON-type lithium-ion conductors is to replace titanium cations with  $\text{Ge}^{4+}$ . Glassy-ceramic  $\text{Li}_{1+x}\text{Al}_x\text{Ge}_{2-x}(\text{PO}_4)_3$ , where  $\text{Ti}^{4+}$  has been fully replaced by  $\text{Ge}^{4+}$ , reaches conductivities of  $4 \times 10^{-4}$  S/cm at room temperature [194]. With this, the electrochemical stability window has been significantly extended,

ranging from 0.85 to 7 V versus Li/Li<sup>+</sup>, which is technological enabled to utilize this material with low-potential anodes, except lithium [195].

### 3.8.2 Electrolytes with Perovskite Structure

Another group of prospective ceramic electrolyte materials that have attracted considerable attention due to their high lithium conductivity is that of lithium lanthanum titanates. The crystal structure of materials of general formula of  $\text{Li}_{3x}\text{La}_{2/3-x}\text{TiO}_3$  (LLTO) is strongly related to the lithiation state defined by the value of  $x$  parameter. A highly conductive perovskite structure is stabilized for  $0.04 < x < 0.17$ , with the maximum ionic conductivity of  $1 \times 10^{-3}$  S/cm for  $x = 0.11$ , for the compound  $\text{Li}_{0.34}\text{La}_{0.51}\text{TiO}_{2.94}$  [196, 197].

The ideal cubic perovskite of a general formula  $\text{ABO}_3$  is described within the space group  $Pm\bar{3}m$ , where La cations occupy the central A-sites, the Ti cations occupy the corner B-sites, while the oxygen atoms are at the face center positions (Fig. 3.11). Lithium ions are

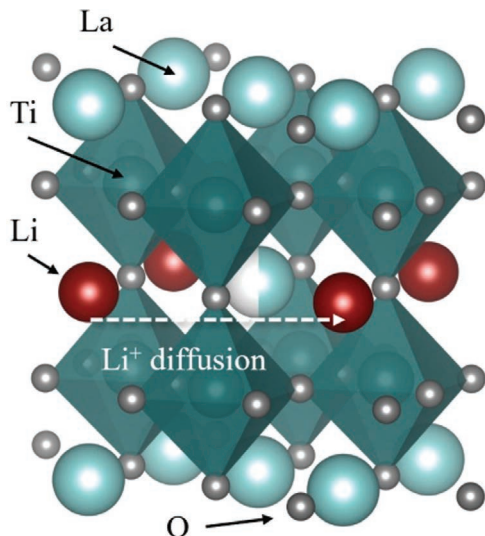


**Figure 3.11** Crystal structure of perovskite-type solid electrolytes  $\text{Li}_{3x}\text{La}_{2/3-x}\text{TiO}_3$ .

introduced in the perovskite structure through aliovalent doping on the 12-fold coordinated A-site. Li cations can diffuse through the structure by jumping along the *ab* plane through a square planar bottleneck made of oxygen anions. The size of the bottleneck can be tuned by changing the lattice parameter. Introducing larger cations into the structure expands the unit cell as per Vegard's law, and opening of the bottleneck improves lithium mobility and results in enhanced ionic conductivity. On the other hand, a slight variation in the Li concentration on the perovskite A-site leads to the distortion of the lattice and lowering of the symmetry, which results in lower conductivity values [198, 199].

Despite its high ionic conductivity originating from its unique crystal structure, utilization of LLTO as a solid electrolyte may be quite limited due to its narrow electrochemical stability window. From computational and experimental reports, it is evident that lithium lanthanum titanate shows instabilities at potentials below 1.78 V versus Li/Li<sup>+</sup>, with possible Li ion insertions/extractions at about 1.8–1.1 V and 0.6–0 V versus Li/Li<sup>+</sup>, accompanied by phase transitions [200]. Such ionic exchange through the electrolyte layer on cycling is caused by a change in the oxidation state of the titanium cation and its reduction from Ti<sup>4+</sup> to Ti<sup>3+</sup>. The limitation of the electrochemical stability window at low potentials means that this material should not be utilized with low-voltage electrode materials, including metallic lithium, and in consequence, it cannot be directly used for future high-capacity lithium-air batteries. Despite a number of attempts to extend the electrochemical stability window of LLTO using the doping strategy, it was found that although the total conductivity can be improved when LLTO is doped with Ge<sup>4+</sup> or Mn<sup>4+</sup>, the stability issue remains a key challenge [201].

As a result of the search for alternative solid electrolytes with a perovskite structure showing improved stability against lithium and acceptable conductivity, LiSr<sub>1.65</sub>Zr<sub>1.3</sub>Ta<sub>1.7</sub>O<sub>9</sub> and Li<sub>0.375</sub>Sr<sub>0.4375</sub>Ta<sub>0.75</sub>Hf<sub>0.25</sub>O<sub>3</sub> have been proposed. Although they show conductivities of  $2 \times 10^{-4}$  S/cm and  $3.8 \times 10^{-4}$  S/cm, respectively (lower than that of LLTO), they also have a wide electrochemical stability window, ranging from 1.4 V to 4.5 V versus Li/Li<sup>+</sup> in the case of Hf-containing compounds [202–205]. Although their conductivity is significantly lower than the conductivity of liquid-

based electrolytes, these perovskites still could be used in battery cells if applied as thin film electrolytes.

A common drawback of perovskite-based solid electrolytes is the high processing temperature required for their densification, reaching a value of 1300°C. At such high temperatures, additional measures preventing lithium loss and lithium concentration variations within the bulk sample must be taken. In addition, such high temperatures exceed the thermal stability window for most electrode materials, constraining the cell assembly techniques and design. It also has been shown that perovskite-based electrolytes suffer from interfacial instabilities, common to most Li-containing materials [206].

### 3.8.3 Lithium Sulfides

Although oxide-based ceramic electrolytes show a wide electrochemical stability window and appreciable ionic transport through the structure, reaching  $1 \times 10^{-3}$  S/cm, the record belongs to another group of solid electrolytes, where the oxygen anions have been replaced by  $S^{2-}$ . The electrolyte  $Li_{10}GeP_2S_{12}$  shows extremely high lithium-ion conductivity of  $1.2 \times 10^{-2}$  S/cm at room temperature, which is comparable to those of liquid electrolytes.  $Li_{10}GeP_2S_{12}$  has a tetragonal unit cell in the  $P4_2/nmc$  space group. Its unit cell, shown in Fig. 3.12, consists of a 3D framework of  $(Ge_{0.5}P_{0.5})S_4$  tetrahedrons,  $PS_4$  and  $LiS_4$  tetrahedrons, and  $LiS_6$  octahedrons. Ge cations share 4d tetrahedral sites with P, while smaller 2d tetrahedral sites are occupied solely by P. These  $(Ge_{0.5}P_{0.5})S_4$  tetrahedrons are connected through the edge with  $LiS_6$  octahedrons to form 1D chain along  $c$  axis. Chains are connected through the corners with smaller  $PS_4$  tetrahedrons to form an interstitial space filled with Li sites. There are three sites available for lithium cations—octahedral 4d, which forms the skeleton structure, and two tetrahedral 16h and 8f sites [207]. The anion sublattice has been found to be body-centered cubic, in which  $Li^+$  diffuses in a series of jumps between one tetrahedral side to the other face-shared tetrahedral site [208]. Such a pathway has a low activation barrier for lithium-ion migration, which together with weaker interaction between Li and S than Li and O results in fast migration of  $Li^+$  [209].

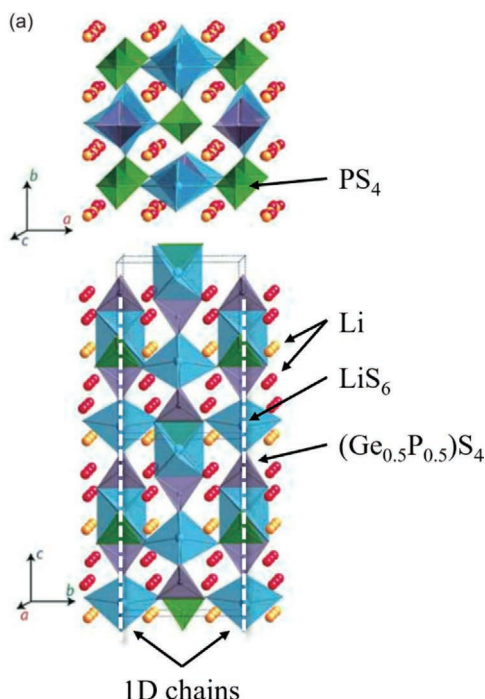


**Figure 3.12** Crystal structure of  $\text{Li}_{10}\text{GeP}_2\text{S}_{12}$ . 3D framework structure of  $(\text{Ge}_{0.5}\text{P}_{0.5})\text{S}_4$  tetrahedrons connected through  $\text{LiS}_6$  octahedrons to form space for Li-ion diffusion. Reproduced with permission from Ref. [207], Copyright © 2011 Nature Publishing Group.

There are two possible migration pathways for Li ions in  $\text{Li}_{10}\text{GeP}_2\text{S}_{12}$  shown using first-principle calculations. Fast ionic transport, up to  $4 \times 10^{-2} \text{ S/cm}$  at room temperature, occurs along the  $c$  axis and involves jumps from one tetrahedral position to another. Mo et al. showed that migration in the  $ab$  plane is also possible through the  $\text{Li}_6$  octahedral position. Although conductivity in the  $ab$  plane is 2 orders of magnitude lower than the fast path, it plays a significant role in the overall ionic transport as it allows Li ions to cross over between channels lying along the  $c$  axis [210].

Despite very high ionic conductivity,  $\text{Li}_{10}\text{GeP}_2\text{S}_{12}$  shows a very narrow electrochemical stability window between around 1.7 V

and 2.15 V [211]. Outside this narrow range, decomposition occurs, with  $\text{Li}_2\text{S}$  or  $\text{P}_2\text{S}_5$  being formed in the interfaces between solid electrolyte and electrode. Attempts to extend stability by introducing Si, Sn, or Al cations at Ge sites or partial oxidation were unsuccessful [212–214]. In addition,  $\text{Li}_{10}\text{GeP}_2\text{S}_{12}$  shows significant chemical instability upon exposure to ambient atmosphere, leading to structural collapse and formation of  $\text{H}_2\text{S}$  [215].

Despite the above-mentioned challenges,  $\text{Li}_{10}\text{GeP}_2\text{S}_{12}$  is still one of the best Li-ion conductors and attracts a lot of attention in the battery community, mainly due to its prospective application in Li-S batteries.

### 3.8.4 Electrolytes with a Garnet Structure

Currently, lithium-ion conductors with a garnet structure seem to be one of the most promising candidates for electrolytes for all solid-state batteries. Their development started in the 2000s, when Thangadurai et al. reported rather moderate lithium-ion conductivity of  $\sim 10^{-6} \text{ S/cm}$  at room temperature in  $\text{Li}_5\text{La}_3\text{M}_2\text{O}_{12}$  ( $\text{M} = \text{Ta}^{5+}, \text{Nb}^{5+}$ ) [216]. What attracted scientific attention was their desirable stability against metallic lithium, indicating the possibility of the utilization of metallic Li as the anode in combination with Li garnets. Using the common doping strategy led to enhanced lithium conductivity of  $4 \times 10^{-5} \text{ S/cm}$  and an extended electrochemical stability window of up to 6 V versus  $\text{Li}/\text{Li}^+$  for  $\text{Li}_6\text{BaLa}_2\text{Ta}_2\text{O}_{12}$  [217, 218].

In 2007, Murugan et al. reported the second generation of Li garnets, based on doped  $\text{Li}_7\text{La}_3\text{Zr}_2\text{O}_{12}$  (LLZO) [219, 220]. A cubic polymorph of  $\text{Li}_7\text{La}_3\text{Zr}_2\text{O}_{12}$  shows fast Li-ion conductivity of up to  $1 \times 10^{-3} \text{ S/cm}$  at room temperature, which is comparable to that with liquid-based electrolytes. The cubic phase of  $\text{Li}_7\text{La}_3\text{Zr}_2\text{O}_{12}$  needs to be stabilized by Li vacancy generation, which can be achieved by doping with supervalent cations, that is, doping with  $\text{Al}^{3+}$  on  $\text{Li}^+$  sites leads to a high lithium conductivity of  $\sim 3 \times 10^{-4} \text{ S/cm}$  at 25°C.

$\text{Li}_7\text{La}_3\text{Zr}_2\text{O}_{12}$  owes such high lithium ion conductivity to its unique crystal structure with 3D ion conduction channels within a rigid framework of  $\text{La}_3\text{Zr}_2\text{O}_{12}$ . The cubic  $\text{Li}_7\text{La}_3\text{Zr}_2\text{O}_{12}$  crystal structure, shown in Fig. 3.13, is described with a space group of

$Ia\bar{3}d$  (#230) [221] or  $I\bar{4}3d$  [222] with La cations in 8 coordinated 24c-sites and Zr cations in 6 coordinated 16a octahedral sites. The framework contains interstitial space consisting of the chain of tetragonal 24d-sites occupied by Li cations, which are bridged and partially occupied by Li cation distorted octahedral 96h-sites. The Li-ion transport occurs along chains in a sequence of consecutive jumps from 24d through 96h to another tetrahedral site, as is schematically shown in Fig. 3.13. High-resolution nuclear magnetic resonance and high-temperature neutron diffraction investigations have revealed that the mobility of Li ions at the 24d site is the rate-determining step and the ionic mobility is highly related to the Li-ion concentration [223, 224].

The Li-vacancy concentration is not only responsible for high lithium conductivity but also essential for stabilization of the cubic phase, and 1.5 Li vacancy per formula unit is required to stabilize the cubic phase. For this reason, an extensive study on the doping strategy in  $\text{Li}_7\text{La}_3\text{Zr}_2\text{O}_{12}$  has been done to understand the role of the dopant on the defect structure and the Li conduction mechanism, for example,  $\text{Ta}^{5+}$  [225],  $\text{Nb}^{5+}$  [226],  $\text{W}^{6+}$  [227],  $\text{Ti}^{4+}$  [228],  $\text{Fe}^{3+}$  [229],  $\text{Al}^{3+}$  [230–232], and  $\text{Ga}^{3+}$  [233, 234]. The highest Li conductivities have been reported in  $\text{Al}^{3+}$ - and  $\text{Ga}^{3+}$ -doped systems, being close to  $1 \times 10^{-3}$  S/cm at room temperature with an activation energy of 0.25–0.3 eV.

The properties of  $\text{Li}_7\text{La}_3\text{Zr}_2\text{O}_{12}$  strongly depend on the material's microstructure. The processing conditions, such as the choice of the synthesis route, the sintering temperature and sintering helpers, the processing atmosphere, and storage conditions, can highly affect the ionic conductivity, long-term stability, and susceptibility to Li dendrite growth or crystalline fracturing [235]. In general, a microstructure rich in smaller grains (20–40  $\mu\text{m}$ ) and with a large concentration of grain boundaries is beneficial for ionic transport as well as material stability. Increased area and tortuosity of grain boundaries leads to lower impurity segregation on the grain boundaries and dissipates current, preventing dendrite formation [236]. On the other hand, high contribution of the grain boundaries can lower the overall ionic conductivity, as the grain boundaries' conductivity is usually 2–5 times lower than that of the grains [237].

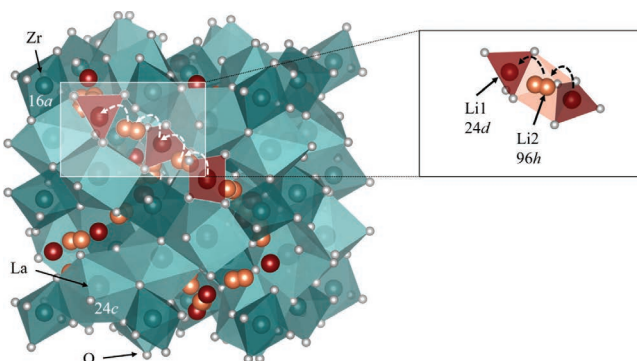


**Figure 3.13** Schematic projection of the unit cell of cubic  $\text{Li}_7\text{La}_3\text{Zr}_2\text{O}_{12}$ , showing possible migration pathways for Li-ion diffusion. Li ions make a sequence of jumps from the highly occupied Li1 tetrahedral 24d-site to the partially occupied 96h octahedral Li2 site (based on Ref. [222]).

Electrical properties of  $\text{Li}_7\text{La}_3\text{Zr}_2\text{O}_{12}$  are also strongly dependent on the processing route and conditions. The conventional solid-state synthesis reaction requires exposure of the material to high temperatures, usually above  $800^\circ\text{C}$ , for thermally activated synthesis of the material and above  $1100^\circ\text{C}$  for sintering for an extended time, usually above 12 h. Exposure to such high temperatures usually leads to lithium loss from the starting powder mixture and results in the formation of highly resistive pyrochlore phase  $\text{La}_2\text{Zr}_2\text{O}_7$ . One could shorten the exposure time or lower the sintering temperature to prevent Li loss, however, this usually leads to a multiphase system, being a mixture of cubic and tetragonal phases. As the temperature and lithium content determine which phase is stabilized, local nonequilibria of these will lead to phase segregation in a volumetric sample. Samples prepared by solid-state reaction usually show conductivities in the range of  $6.1 \times 10^{-4} \text{ S/cm}$  [238]. Alternative synthesis routes, such as the sol-gel combustion method, help lower the synthesis temperature to  $\sim 600^\circ\text{C}$ , reducing the lithium loss and resulting in conductivity values as high as  $3 \times 10^{-4} \text{ S/cm}$  [239]. Powders obtained via wet chemistry methods usually require shorter sintering time but often suffer from low density and phase instability due to lithium loss upon sintering. As the exposure time to a high temperature

seems to be essential for obtaining dense and highly conductive pellet samples, alternative sintering methods have been utilized, such as field-assisted sintering or spark plasma sintering, resulting in samples with bulk conductivity in the range of  $10^{-3}$  S/cm [240, 241]. An efficient and industrial-ready densification technique has not yet been established.

Like other solid electrolytes,  $\text{Li}_7\text{La}_3\text{Zr}_2\text{O}_{12}$  also suffers from instability at the interface. Experimental and computational methods indicate that the surface of Li garnets is not stable and in contact with ambient air, a highly resistive interfacial layer of  $\text{Li}_2\text{CO}_3$  is formed [242–245] as a result of the reaction with  $\text{H}_2\text{O}$  and  $\text{CO}_2$ . The formation of  $\text{Li}_2\text{CO}_3$  leads to increased interfacial resistance and results in lowered cell performance. It has been however shown that with proper fabrication, use of sintering agents [246], microstructure modifications [247], and proper sample handling, that is, surface polishing and storage in protective atmospheres, the surface stability issue can be overcome on a laboratory scale.

When we compare cubic  $\text{Li}_7\text{La}_3\text{Zr}_2\text{O}_{12}$  with other ceramic electrolytes, it's not its high ionic conductivity or possibility of direct application in solid-state batteries that makes this material unique. The most unique feature of Li garnets is the very wide electrochemical stability window, which allows the use of different sets of electrodes and cell designs with performance and properties tailored for specific applications. As per first principles calculation results, Li garnets show a very low reduction potential of  $\sim 0.05$  V and small decomposition energy (Fig. 3.14).

This suggests that unlike other solid electrolyte materials,  $\text{Li}_7\text{La}_3\text{Zr}_2\text{O}_{12}$  could be stable against metallic Li under certain conditions, which makes it a unique candidate for application in high-capacity lithium-air batteries and allows the use of lithium foil as the anode. Developing a good Li/ $\text{Li}_7\text{La}_3\text{Zr}_2\text{O}_{12}$  interface is, however, not an easy task, mainly due to high interfacial resistance [248], growth of Li dendrites [249], and poor adhesion of Li metal to the LLZO surface [250]. It has been demonstrated that interfacial resistance and Li wettability can be significantly improved by engineering the surface of the electrolyte by appliance of a thin layer of  $\text{Al}_2\text{O}_3$  [225], Au [251], Si [252], or Ge [253].

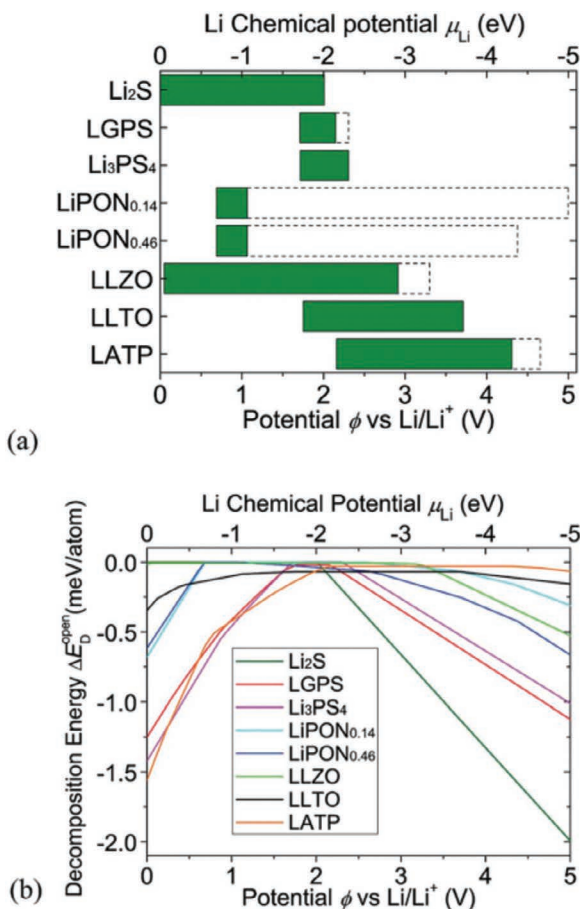


**Figure 3.14** Electrochemical window (a) and decomposition energy (b) of SE materials. Reprinted with permission from Ref. [211].

As mentioned in the introduction to this chapter, replacing liquid electrolytes with their ceramic counterparts promises increased gravimetric and volumetric energy densities of the cell. It has been estimated that in order to compete with conventional liquid electrolytes, the thickness of the solid-state electrolyte in the cell should not exceed  $\sim 50 \mu\text{m}$ . Therefore, advancement of efficient deposition techniques for homogeneous and dense layers of solid-state electrolytes seems to be essential for the development

of all solid-state lithium-ion batteries, as well as for low-scale microbatteries that can be integrated directly with the electronic circuits to minimize energy transmission losses and improve their overall energy efficiency.

Transfer of bulk properties of cubic  $\text{Li}_7\text{La}_3\text{Zr}_2\text{O}_{12}$ , with its wide electrochemical stability window and fast Li transport, to thin films has been attempted using different techniques, such as radio frequency sputtering [254–256], chemical vapor deposition [257], sol-gel methods [258, 259], and pulsed laser deposition (PLD) [260–262]. The majority of reported Li garnet films show, however, conductivity in a range of  $10^{-8}$ – $10^{-6}$  S/cm at room temperature, which is at least 2 orders of magnitude lower than in bulk samples. The reasons for low conductivity should be sought in the high-temperature processing (above  $1000^\circ\text{C}$ ) necessary to obtain a high layer density. Sintering at such high temperatures leads to the loss of lithium ions from the surface and thus to reduced lithium stoichiometry, which hinders not only ionic transport but also cubic phase stabilization. Therefore, to benefit from high conductivity of the  $\text{Li}_7\text{La}_3\text{Zr}_2\text{O}_{12}$  thin films, it is essential to understand the mechanism of cubic phase formation in the beginning. Garbayo et al. analyzed the phase evolution in the pulsed laser-deposited thin films of  $\text{Li}_7\text{La}_3\text{Zr}_2\text{O}_{12}$  co-doped with (Al, Ta) [263]. Films deposited in a wide temperature range of  $50^\circ\text{C}$ – $750^\circ\text{C}$  were compared in terms of morphology, crystal structure, and electrical properties. It has been found that films deposited below  $300^\circ\text{C}$  do not show long-distance ordering and are amorphous, with low total conductivity (in the range of  $10^{-9}$  S/cm at ambient). The maximum conductivity, of around  $10^{-6}$  S/cm at ambient, has been observed for films deposited at  $300^\circ\text{C}$ , showing developed short-distance ordering of Li tetrahedrons. For films deposited above  $500^\circ\text{C}$ , a significant increase in activation energy and drop in conductivity has been observed and related to Li evaporation from the system. As a result of strong Li deficiency, irreversible crystallization of  $\text{La}_2\text{Zr}_2\text{O}_7$  occurs. This first insight into the mechanism of cubic phase stabilization in thin films has led to a new approach to stabilize Li garnet films. As the main challenge seems to be related to the high-temperature processing leading to lithium-ion evaporation from the film surface, an efficient method for fixing the Li stoichiometry

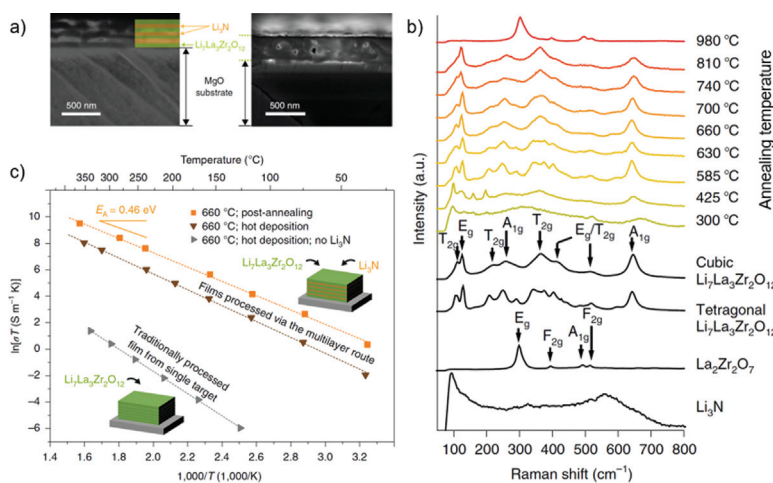


**Figure 3.15** Schematic of the experimental approach for the employment of a multilayer structure to deposit cubic  $\text{Li}_7\text{La}_3\text{Zr}_2\text{O}_{12}$  via PLD. Thin layers of  $\text{Li}_3\text{N}$  were incorporated to compensate for Li loss at elevated temperatures. (a) SEM image of the multilayer structure as deposited at  $300^\circ\text{C}$  and after annealing at  $660^\circ\text{C}$ , showing a dense and uniform film of  $\text{Li}_7\text{La}_3\text{Zr}_2\text{O}_{12}$ , (b) Raman spectra of the multilayer structure after annealing at selected temperatures, and (c) the temperature dependence of the in-plane total conductivity of selected thin films. Reprinted with permission from Ref. [264].

during the processing seems to be essential. Recently, Pfenninger et al. [264] demonstrated a new method for Li loss compensation by using  $\text{Li}_3\text{N}$  interlayers between alternating  $\text{Li}_7\text{La}_3\text{Zr}_2\text{O}_{12}$  layers, as shown in Fig. 3.15.

These  $\text{Li}_3\text{N}$  interlayers act as an internal Li reservoir, which compensates for Li losses during high-temperature densification of the film. Moreover, this approach helped not only enhance Li-ion conduction by 2 orders of magnitude using processing temperatures  $\sim 400^\circ\text{C}$  lower than what is used conventionally but also investigate the full mechanism of the cubic phase formation from amorphous through tetragonal to cubic. It also shed light on the thermal degradation mechanism leading to the formation of  $\text{La}_2\text{Zr}_2\text{O}_7$ .

This processing strategy, offering Li loss compensation, allows one to control lithium stoichiometry in any oxide material. Therefore, it might be adopted for other classes of Li oxides, such

as other solid-state electrolytes as well as high-voltage electrode materials. The ability to control the initial stoichiometry of the Li-containing layers is essential for the fabrication of solid-state energy storage devices offering high energy densities. Moreover, thin film techniques such as PLD enable good physical contact between the electrolyte and the electrode layers, which together with the possibility of engineering the properties of the interface, for example, by developing the active area for charge exchange, may result in enhanced long-term stability and high coulombic efficiencies. These, however, still need to be demonstrated on a semi-industrial scale to have a significant impact on the commercialization of all solid-state batteries.

## References

1. D. E. Fenton, J. M. Parker, P. V. Wright, *Polymer*, **14** (1973) 589.
2. M. Armand, M. Duclot, French patent 7832976, 1978.
3. W. Wieczorek, Z. Florjańczyk, J. R. Stevens, *Electrochim. Acta*, **40** (1995) 2251–2258.
4. W. Liu, N. Liu, J. Sun, P.-C. Hsu, Y. Li, H.-W. Lee, Y. Cui, *Nano Lett.*, **15** (2015) 2740–2745.
5. M. Castriota, D. Teeters, *Ionics*, **11** (2005) 220–225.
6. A. Friesen, X. Monnighoff, M. Borner, J. Haetge, F. M. Schappacher, M. Winter, *J. Power Sources*, **342** (2017) 88–97.
7. E. Quartarone, P. Mustarelli, Polyelectrolytes for batteries, in: S. Kobayashi, K. Müllen, eds. *Encyclopedia of Polymeric Nanomaterials*. Springer, Berlin, Heidelberg, 2014.
8. C. H. Porter, R. H. Boyd, *Macromolecules*, **4** (1971) 589.
9. T. D. Huan, S. Boggs, G. Teyssed, C. Laurent, M. Cakmak, S. Kumare, R. Ramprasad, *Prog. Mater Sci.*, **83** (2016) 236–269.
10. D. F. Shriver, in *Solid State Electrochemistry*, ed. P. G. Bruce, Cambridge University Press, 1985, pp. 95–118.
11. M. Marzantowicz, F. Krok, J. R. Dygas, Z. Florjańczyk, E. Zygałdó-Monikowska, *Solid State Ionics*, **179** (2008) 1670–1678.
12. G. B Appeteccchi, F. Croce, J. Hassoun, B. Scrosati, M. Salomon, F. Cassel, *J. Power Sources*, **114** (2003) 105–112.
13. A. Chandra, *Indian J. Pure Appl. Phys.*, **54** (2016) 583–588.

14. W. Wieczorek, R. Stevens, Z. Florjańczyk, *Solid State Ionics*, **85** (1996) 67–72.
15. F. Croce, L. Persi, B. Scrosati, F. Serraino-Fiory, E. Plichta, M. A. Hendrikson, *Electrochim. Acta*, **46** (2001) 2457–2461.
16. A. Dey, T. Ghoshal, S. Karan, S. K. De, *J. Appl. Phys.*, **110** (2011) 043707.
17. M. Malathi, K. Tamilarasan, V. Ganesan, *Polym. Compos.*, **36** (2015) 42–46.
18. H. Y. Sun, Y. Takeda, N. Imanishi, O. Yamamoto, H.-J. Sohn, *J. Electrochem. Soc.*, **147** (2000) 2462–2467.
19. J.-L. Souquet, M. Lévy, M. Duclot, *Solid State Ionics*, **70/71** (1994) 337–345.
20. J.-L. Souquet, M. Duclot, M. Levy, *Solid State Ionics*, **85** (1996) 149–157.
21. C. Bethier, W. Gorecki, M. Minier, M. B. Armand, J. M. Chabagno, P. Rigaud, *Solid State Ionics*, **11** (1983) 91–95.
22. M. Marzantowicz, J. R. Dygas, F. Krok, A. Łasińska, Z. Florjańczyk, E. ZygałdoMonikowska, A. Affek, *Electrochim. Acta*, **50** (2005) 3969–3977.
23. Z. Gadjourova, Y. G. Andreev, D. P. Tunstall, P. G. Bruce, *Nature*, **412** (2001) 520–523.
24. D. Golodnitsky, E. Strauss, E. Peled, S. Greenbaum, *J. Electrochem. Soc.*, **162** (2015) A2551–A2566.
25. G. Jo, H. Jeon, M. J. Park, *ACS Macro Lett.*, **4** (2015) 225–230.
26. A. K. Łasińska, M. Marzantowicz, J. R. Dygas, F. Krok, Z. Florjańczyk, A. Tomaszewska, E. Zygałdo-Monikowska, Z. Żukowska, U. Lafont, *Electrochim. Acta*, **169** (2015) 61–72.
27. A. M. Stephan, *Eur. Polym. J.*, **42** (2006) 21–42.
28. S. Thomas, G. E. Zaikov, S. V. Valsaraj, *Recent Advances in Polymer Nanocomposites*, CRC Press, 2009.
29. S. Vorrey, D. Teeters, *Electrochim. Acta*, **48** (2003) 2137–2141.
30. W. Liu, S. W. Lee, D. Lin, F. Shi, S. Wang, A. D. Sendek, Y. Cui, *Nat. Energy*, **2** (2017) 17035.
31. P. Jeevanandam, S. Vasudevan, *J. Phys. Chem. B*, **102** (1998) 4753–4758.
32. X. Zhang, J. Xie, F. Shi, D. Lin, Y. Liu, W. Liu, A. Pei, Y. Gong, H. Wang, K. Liu, Y. Xiang, Y. Cui, *Nano Lett.*, **18** (2018) 3829–3838.
33. D. Golodnitsky, E. Peled, *Electrochim. Acta*, **45** (2000) 1431–1436.
34. S. W. Martin, C. A. Angell, *J. Non-Cryst. Solids*, **83** (1986) 185–207.
35. O. Borodin, G. D. Smith, *Macromolecules*, **39** (2006) 1620–1629.

36. R. Zallen, *The Physics of Amorphous Solids*, Wiley, 2007.
37. C. A. Angell, *Electrochim. Acta*, **250** (2017) 368–375.
38. A. Kisliuk, V. Bocharova, I. Popov, C. Gainaru, A. P. Sokolov, *Electrochim. Acta*, **299** (2019) 191–196.
39. J. C. Dyre, *Rev. Mod. Phys.*, **78** (2006) 953.
40. M. G. McLin, C. A. Angell, *Polymer*, **37** (1996) 4713–4721.
41. A. L. L. Videira, L. D. Carlos, *J. Chem. Phys.*, **105** (1996) 8878–8884.
42. M. Marzantowicz, J. R. Dygas, F. Krok, Z. Florjańczyk, E. Zygałdó-Monikowska, *J. Non-Cryst. Solids*, **353** (2007) 4467–4473.
43. M. A. Ratner, A. Nitzan, *Faraday Discuss. Chem. Soc.*, **88** (1989) 19–42.
44. J. N Roberts, L. M. Schwartz, *Phys. Rev. B*, **31** (1985) 5990–5997.
45. I. Alig, S. M. Dudkin, W. Jenninger, M. Marzantowicz, *Polymer*, **47** (2006) 1722–1731.
46. H. X. Wang, Z. X. Wang, H. Li, Q. B. Meng, L. Q. Chen, *Electrochim. Acta*, **52** (2007) 2039–2044.
47. F. Croce, G. B. Appetecchi, L. Persi, B. Scrosati, *Nature*, **394** (1998) 456–458.
48. P. Divan, A. Chandra, *Polym. Compos.*, **33** (2012) 1750–1754.
49. H. J. Gores, J. Barthel, S. Zugmann, D. Moosbauer, M. Amerell, R. Hartl, A. Maurer, in: C. J. Daniel, J. O. Besenhard, eds. *Handbook of Battery Materials*, 2nd Ed., Wiley, 2011, p. 598.
50. K. E. Thomas, S. E. Sloop, J. B. Kerr, J. Newman, *J. Power Sources*, **89** (2000) 132–138.
51. K. Pożyczka, M. Marzantowicz, J. R. Dygas, F. Krok, *Electrochim. Acta*, **227** (2017) 127–135.
52. B. Sun, J. Mindemark, E. V. Morozov, L. T. Costa, M. Bergman, P. Johansson, Y. Fang, I. Furó, D. Brandell, *Phys. Chem. Chem. Phys.*, **18** (2016) 9504–9513.
53. J. Mindemark, B. Sun, E. Törmä, D. Brandell, *J. Power Sources*, **298** (2015) 166–170.
54. O. Borodin, G. D. Smith, W. Henderson, *J. Phys. Chem. B*, **110** (2006) 16879–16886.
55. W. Xu, X.-G. Sun A. Angell, *Electrochim. Acta*, **48** (2003) 2255–2266.
56. T. Mizumo, K. Sakamoto, N. Matsumi, H. Ohno, *Electrochim. Acta*, **50** (2005) 3928–3933.
57. H. Mazor, D. Golodnitsky, E. Peled, W. Wieczorek, B. Scrosati, *J. Power Sources*, **178** (2008) 736–743.

58. H. H. Sumathipala, J. Hassoun, S. Panero, B. Scrosati, *Ionics*, **13** (2007) 281–286.
59. J. Popovic, G. Hasegawa, I. Moudrakovski, J. Maier, *J. Mater. Chem. A*, **4** (2016) 7135–7140.
60. J. Shim, D. G. Kim, H. J. Kim, J. H. Lee, J.-C. Lee, *ACS Appl. Mater. Interfaces*, **7** (2015) 7690–7701.
61. C. Chauvin, F. Alloin, C. Iojoiu, J.-Y. Sanchez, *Electrochim. Acta*, **51** (2006) 5954–5960.
62. F. C. Grozema, A. S. Best, L. van Eijck, J. Stride, G. J. Kearley, S. W. de Leeuw, S. J. Picken, *J. Phys. Chem. B*, **109** (2005) 7705–7712.
63. S. Zugmann, M. Fleischmann, M. Amereller, R. M. Gschwind, H. D. Wiemhöfer, H. J. Gores, *Electrochim. Acta*, **56** (2011) 3926–3933.
64. H. P. Fritz, A. Kuhn, *J. Power Sources*, **41** (1993) 253–261.
65. L. Edman, *J. Phys. Chem. B*, **104** (2000) 7254–7258.
66. A. Plewa, F. Chyliński, M. Kalita, M. Bukat, P. Parzuchowski, R. Borkowska, M. Siekierski, G. Z. Żukowska, W. Wieczorek, *J. Power Sources*, **159** (2006) 431–437.
67. Y. Ding, D. Mua, B. Wu, R. Wang, Z. Zhao, F. Wu, *Appl. Energy*, **195** (2017) 586–599.
68. T. K. Pietrzak, M. Wasiucionek, P. P. Michalski, A. Kaleta, J. E. Garbarczyk, *Mater. Sci. Eng. B*, **213** (2016) 140–147.
69. X. Zuo, J. Zhu, P. Müller-Buschbaum, Y.-J. Cheng, *Nano Energy*, **31** (2017) 113–143.
70. M. Marzantowicz, J. R. Dygas, F. Krok, *Electrochim. Acta*, **53** (2008) 7417–7425.
71. W. Wieczorek, K. Such, J. Przyłuski, Z. Floriańczyk, *Synth. Met.*, **45** (1991) 373–383.
72. A. M. Stephan, R. Thirunakaran, N. G. Renganathan, V. Sundarama, S. Pitchumani, N. Muniyandi, R. Gangadharan, P. Ramamoorthy, *J. Power Sources*, **81–82** (1999) 752–758.
73. C.-W. Kuo, C.-W. Huang, B.-K. Chen, W.-B. Li, P.-R. Chen, T.-H. Ho, C.-G. Tseng, T.-Y. Wu, *Int. J. Electrochem. Sci.*, **8** (2013) 3834–3850.
74. K. Kiran, M. Ravi, Y. Pavani, S. Bhavani, A. K. Sharma, V. V. R. Narashima Rao, *J. Membr. Sci.*, **454** (2014) 200–211.
75. R. L. Lavall, S. Ferrari, C. Tomasi, M. Marzantowicz, E. Quartarone, A. Magistris, P. Mustarelli, S. Lazzaroni, M. Fagnoni, *J. Power Sources*, **195** (2010) 5761–5767.

76. M. Gopinadhan, P. W. Majewski, C. O. Osuji, *Macromolecules*, **43** (2010) 3286–3293.
77. M. Watanabe, M. L. Thomas, S. Zhang, K. Ueno, T. Yasuda, K. Dokko, *Chem. Rev.*, **117** (2017) 7190–7239.
78. A. Wang, S. Kadam, H. Li, S. Shi, Y. Qi, *npj Comput. Mater.*, **15** (2018) 1–26.
79. J. J. An, J. Li, C. Daniel, D. Mohanty, S. Nagpure, D. L. Wood, *Carbon*, **105** (2016) 52–76.
80. F. A. Soto, Y. Ma, J. M. Martinez de la Hoz, J. M. Seminario, P. B. Balbuena, *Chem. Mater.*, **27** (2015) 7990–8000.
81. E. Peled, *J. Electrochem. Soc.*, **126** (1979) 2047.
82. J. B. Goodenough, Y. Kim, *Chem. Mater.*, **22** (2010) 587–603.
83. E. Peled, S. Menkin, *J. Electrochem. Soc.*, **164** (2017) A1703–A1719.
84. A. Friesen, X. Monnighoff, M. Borner, J. Haetge, F. M. Schappacher, M. Winter, *J. Power Sources*, **342** (2017) 88–97.
85. C. Xu, B. Sun, T. Gustafsson, K. Edström, D. Brandell, M. Hahlin, *J. Mater. Chem. A*, **2** (2014) 7256.
86. J. B. Kerr, Y. B. Han, G. Liu, C. Reeder, J. Xie, X. Sun, *Electrochim. Acta*, **50** (2004) 235–242.
87. E. Peled, S. Menkin, *J. Electrochem. Soc.*, **164** (2017) A1703–A1719.
88. K. Fu, Y. Gong, J. Dai, A. Gong, X. Han, Y. Yao, C. Wang, Y. Wang, Y. Chen, C. Yan, Y. Li, E. D. Wachsman, L. Hu, *Proc. Natl. Acad. Sci. U.S.A.*, **113** (2016) 7094–7099.
89. J. J. An, J. Li, C. Daniel, D. Mohanty, S. Nagpure, D. L. Wood, *Carbon*, **105** (2016) 52–76.
90. X. Feng, M. Ouyang, X. Liu, L. Lu, Y. Xia, X. He, *Energy Storage Mater.*, **10** (2018) 246–267.
91. J. W. Fergus, *J. Power Sources*, **195** (2010) 4554–4569.
92. M. Armand, W. Gorecki, R. Andreani, in *Second International Symposium on Polymer Electrolytes*, ed. B. Scrosati, Elsevier Applied Science, New York, 1989, p. 91.
93. G. B. Appetecchi, W. Henderson, P. Villano, M. Berrettoni, S. Passerini, *Electrochim. Soc.*, **148** (2001) A1171–A1178.
94. S. Lascaud, M. Perrier, A. Vallée, S. Besner, J. Prud'homme, M. Armand, *Macromolecules*, **27** (1994) 7469–7477.
95. L. Edman, A. Ferry, M. M. Doeff, *J. Mater. Res.*, **15** (2000) 1950–1954.
96. P. Y. Pennarun, P. Jannasch, *Solid State Ionics*, **176** (2005) 1103–1112.

97. M. Marzantowicz, J. R. Dygas, F. Krok, A. Tomaszewska, Z. Florjańczyk, E. Zygałdo-Monikowska, G. Lapienis, *J. Power Sources*, **194** (2009) 51–57.
98. M. Marzantowicz, J. R. Dygas, F. Krok, Z. Florjańczyk, E. Zygałdo-Monikowska, G. Lapienis, *Solid State Ionics*, **192** (2011) 137–142.
99. Y. Kato, K. Hasumi, S. Yokoyama, T. Yabe, H. Ikuta, Y. Uchimoto, M. Wakihara, *Solid State Ionics*, **150** (2002) 355–361.
100. T. Itoh, Y. Ichikawa, T. Uno, M. Kubo, O. Yamamoto, *Solid State Ionics*, **156** (2003) 393–399.
101. M. Watanabe, T. Endo, A. Nishimoto, K. Miura, M. Yanagida, *J. Power Sources*, **81** (1999) 786.
102. A. T. Lipton, M. C. Lonergan, M. A. Ratner, D. F. Shriver, T. Wong, K. Han, *J. Phys. Chem.*, **98** (1994) 4148–4154.
103. J. L. Acosta, E. Morales, *Solid State Ionics*, **85** (1996) 85–90.
104. Z. Wen, T. Itoh, T. Uno, M. Kubo, T. Wen, O. Yamamoto, *Solid State Ionics*, **175** (2004) 739–742.
105. H.-M. Kao, S.-W. Chao, P.-C. Chang, *Macromolecules*, **39** (2006) 1029–1040.
106. M. Mohammadi, H. Fazli, M. Karevan, J. Davoodi, *Eur. Polym. J.*, **91** (2017) 121–133.
107. Y. F. Zhou, S. Xie, X. W. Ge, C. H. Chen, K. Amine, *J. Appl. Electrochem.*, **34** (2004) 1119–1125.
108. N. Shukla, A. K. Thakur, *Ionics*, **15** (2009) 357–367.
109. S. Ramesh, L. C. Wen, *Ionics*, **16** (2010) 255–262.
110. G. B. Appetecchi, F. Croce, B. Scrosati, *Electrochim. Acta*, **40** (1995) 991–997.
111. J. Vondrák, M. Sedlaríková, J. Velicka, B. Klapste, V. Novák, J. Reuter, *Electrochim. Acta*, **46** (2001) 2047–2048.
112. P. Pal, A. Ghosh, *Electrochim. Acta*, **260** (2018) 157–167.
113. Z. Jiang, B. Carroll, K. M. Abraham, *Electrochim. Acta*, **42** (1997) 2667–2677.
114. A. I. Gopalan, P. Santhosh, K. M. Manesh, J. H. Nho, S. H. Kim, C. G. Hwang, K. P. Lee, *Membr. Sci.*, **325** (2008) 683–690.
115. C. Agrawal, G. P. Pandey, *J. Phys. D: Appl. Phys.*, **41** (2008) 223001.
116. E. Tsuchida, H. Ohno, K. Tsunemi, *Electrochim. Acta*, **28** (1983) 591–595.

117. K. Tsunemi, H. Ohno, E. Tsuchida, *Electrochim. Acta*, **28** (1983) 833–837.
118. H. S. Choe, J. Giaccai, M. Alamgir, K. M. Abraham, *Electrochim. Acta*, **40** (1995) 2289–2293.
119. D. Saikia, Y. W. Chen-Yang, Y. T. Chen, Y. K. Li, S. I. Lin, *Desalination*, **234** (2008) 24–32.
120. S. Ramesh, S. C. Lu, *J. Appl. Polym. Sci.*, **126** (2012) 484–492.
121. Z. X. Wang, B. Y. Huang, H. Huang, L. Q. Chen, R. J. Xue, F. S. Wang, *Electrochim. Acta*, **41** (1996) 1443–1446.
122. N. Voigt, L. van Wüllen, *Solid State Ionics*, **208** (2012) 8–16.
123. H. Hong, C. Liquan, H. Xuejie, X. Rongjian, *Electrochim. Acta*, **37** (1992) 1671–1673.
124. Y. W. Chen-Yang, H. C. Che, F. J. Lin, C. C. Chen, *Solid State Ionics*, **150** (2002) 327–335.
125. A. Ferry, L. Edman, M. Forsyth, D. R. MacFarlane, J. Z. Sun, *J. Appl. Phys.*, **86** (1999) 2346–2348.
126. J. E. Weston, C. H. Steele, *Solid State Ionics*, **7** (1982) 75–79.
127. K. Park, J. H. Cho, K. Shanmuganathan, J. Song, J. Peng, M. Gobet, S. Greenbaum, J. Ellison, J. B. Goodenough, *J. Power Sources*, **263** (2014) 52–58.
128. W. Wieczorek, A. Zalewska, D. Raducha, Z. Florjańczyk, J. R. Stevens, *J. Phys. Chem. B*, **102** (1998) 352–360.
129. W. Wieczorek, A. Zalewska, D. Raducha, Z. Florjańczyk, J. R. Stevens, A. Ferry, *Macromolecules*, **29** (1996) 143–155.
130. Y. W. Chen-Yang, H. C. Chen, F. C. Lin, C. C. Chen, *Solid State Ionics*, **150** (2002) 327–335.
131. C. Y. Chiang, M. J. Reddy, P. P. Chu, *Solid State Ionics*, **175** (2004) 631–635.
132. H. Y. Sun, H. J. Sohn, O. Yamamoto, Y. Takeda, N. Imanishi, *J. Electrochem. Soc.*, **148** (1999) 1672–1676.
133. F. Chen, D. Yang, W. Zha, B. Zhu, Y. Zhang, J. Lia, Y. Gu, Q. Shen, L. Zhang, D. R. Sadoway, *Electrochim. Acta*, **258** (2017) 1106–1114.
134. C.-Z. Zhao, X.-Q. Zhang, X.-B. Cheng, R. Zhang, R. Xu, P.-Y. Chen, H.-J. Peng, J.-Q. Huang, Q. Zhang, *PNAS*, **114** (2017) 11069–11074.
135. J. Płocharski, W. Wieczorek, *Solid State Ionics*, **28–30** (1988) 979–982.
136. S. Kitajima, M. Matsuda, M. Yamato, Y. Tominaga, *Polym. J.*, **45** (2013) 738–743.

137. W. Liu, D. Lin, J. Sun, G. Zhou, Y. Cui, *ACS Nano*, **10** (2016) 11407–11413.
138. L. Chen, Y. Li, S.-P. Li, L.-Z. Fan, C.-W. Nan, J. B. Goodenough, *Nano Energy*, **46** (2018) 176–184.
139. A. S. Pandian, X. C. Chen, J. Chen, B. Bradley, S. Lokitz, R. E. Ruther, G. Yang, K. Lou, J. Nanda, F. M. Delnick, N. J. Dudney, *J. Power Sources*, **390** (2018) 153–164.
140. R. Blanga, L. Burstein, M. Berman, S. G. Greenbaum, D. Golodnitsky, *J. Electrochem. Soc.*, **162** (2015) D3084–D3089.
141. Y. Gong, K. Fu, S. Xu, J. Dai, T. R. Hamann, L. Zhang, G. T. Hitz, Z. Fu, Z. Ma, D. W. McOwen, X. Han, L. Hu, E. D. Wachsman, *Mater. Today*, **21** (2018) 594–601.
142. X. Liu, S. Peng, S. Gao, Y. Cao, Q. You, L. Zhou, Y. Jin, Z. Liu, J. Liu, *ACS Appl. Mater. Interfaces*, **10** (2018) 15691–15696.
143. K. Fu, Y. Gong, J. Dai, A. Gong, X. Han, Y. Yao, C. Wang, Y. Wang, Y. Chen, C. Yan, Y. Li, E. D. Wachsman, L. Hu, *Proc. Natl. Acad. Sci.U.S.A.*, **113** (2016) 7094–7099.
144. J. Bae, Y. Li, F. Zhao, X. Zhou, Y. Ding, G. Yu, *Energy Storage Mater.*, **15** (2018) 46–52.
145. P. Jeevanandam, S. Vasudevan, *J. Phys. Chem. B*, **102** (1998) 4753–4758.
146. J. Syzdek, M. Armand, M. Gizowska, M. Marcinek, E. Sasima, M. Szafran, W. Wieczorek, *J. Power Sources*, **194** (2009) 66–72.
147. C. A. Angell, C. Liu, E. Sanchez, *Nature*, **362** (1993) 137–139.
148. J. Fan, C. A. Angell, *Electrochim. Acta*, **40** (1995) 2397–2400.
149. O. V. Bushkova, S. E. Popov, T. V. Yaroslavtseva, V. M. Zhukovsky, A. E. Nikiforov, *Solid State Ionics*, **178** (2008) 1817–1830.
150. M. Forsyth, J. Sun, D. R. MacFarlane, A. J. Hill, *J. Polym. Sci. Part B: Polym. Phys.*, **38** (2000) 341–350.
151. M. M. Hiller, A.-C. Gentschev, M. Amereller, H. J. Gores, M. Winter, H.-D. Wiemhöfer, *ECS Trans.*, **33** (2011) 3–15.
152. A. Ferry, L. Edman, M. Forsyth, D. R. MacFarlane, J. Sun, *Electrochim. Acta*, **45** (2000) 1237–1242.
153. S. B. Aziz, O. G. Abdullah, M. A. Rasheed, H. M. Ahmed, *Polymers*, **9** (2017) 187.
154. Y.-J. Lim, Y.-H. An, N.-J. Jo, *Nanoscale Res. Lett.*, **7** (2012) 19.
155. D. R. MacFarlane, N. Tachikawa, M. Forsyth, J. M. Pringle, P. C. Howlet, G. D. Elliott, J. H. Davis, M. Watanabe, P. Simon, C. A. Angell, *Energy Environ. Sci.*, **7** (2014) 232–250.

156. K. Tsunashima, F. Yonekawa, M. Sugiya, *Chem. Lett.*, **37** (2008) 314–315.
157. A. Balducci, *Top. Curr. Chem. (Z)*, **375** (2017) 20.
158. Y.-S. Ye, J. Rick, B.-J. Hwang, *J. Mater. Chem. A*, **1** (2013) 2719.
159. A. R. Polu, H.-W. Rhee, *Int. J. Hydrogen Energy*, **42** (2017) 7212–7219.
160. A. Yongxin, C. Xinqun, Z. Pengjian, L. Lixia, Y. Geping, *J. Solid State Electrochem.*, **16** (2011) 383–389.
161. J.-H. Shin, W. A. Henderson, S. Passerini, *J. Electrochem. Soc.*, **152** (2005) A978–A983.
162. E. Simonetti, M. Carewska, G. Maresca, M. De Francesco, G. B. Appeteccchi, *J. Electrochem. Soc.*, **164** (2017) A6213–A6219.
163. J. Fuller, A. C. Breda, R. T. Carlin, *J. Electroanal. Chem.*, **459** (1998) 29.
164. T. E. Sutto, *J. Electrochem. Soc.*, **154** (2007) P101–P107.
165. T. E. Sutto, *J. Electrochem. Soc.*, **154** (2007) P130–P135.
166. Y. He, P. G. Boswell, P. Bühlmann, T. P. Lodge, *J. Phys. Chem. B*, **111** (2007) 4645–4652.
167. G. Polizos, A. Kyritsis, P. Pissis, V. V. Shilov, V. V. Shevchenko, *Solid State Ionics*, **136/137** (2000) 1139–1146.
168. S. Zhang, S. Dou, R. H. Colby, J. Runt, *J. Non-Cryst. Solids*, **351** (2005) 2825–2830.
169. C. Chauvin, F. Alloin, C. Iojoiu, J.-Y. Sanchez, *Electrochim. Acta*, **51** (2006) 5954–5960.
170. M. Marzantowicz, K. Pożyczka, M. Brzozowski, J. R. Dygas, F. Krok, Z. Florjańczyk, G. Lapienis, *Electrochim. Acta*, **115** (2014) 612–620.
171. R. Meziane, J.-P. Bonnet, M. Courty, K. Djellab, M. Armand, *Electrochim. Acta*, **57** (2011) 14–19.
172. J. Sun, D. R. MacFarlane, M. Forsyth, *Solid State Ionics*, **147** (2002) 333–339.
173. N. Byrne D. R. MacFarlane, M. Forsyth, *Electrochim. Acta*, **50** (2005) 3917–3921.
174. N. Shubha, H. Zhu, M. Forsyth, M. Srinivasan, *Polymer*, **99** (2016) 748–755.
175. H. Ohno. K. Ito, *Polymer*, **36** (1995) 891–893.
176. K. Ito, N. Nishina, H. Ohno, *J. Mater. Chem.*, **7** (1997) 1357–1362.
177. K. Ito, Y. Tominaga, H. Ohno, *Electrochim. Acta*, **42** (1997) 1561–1570.
178. M. B. Herath, S. E. Creager, R. V. Rajagopal, O. E. Geiculescu, D. D. DesMarteau, *Electrochim. Acta*, **54** (2009) 5877–5883.

179. T. Fujinami, Y. Buzoujima, *J. Power Sources*, **119–121** (2003) 438–441.
180. O. E. Geiculescu, B. B. Hallac, R. V. Rajagopal, S. E. Creager, D. D. DesMarteau, O. Borodin, G. D. Smith, *J. Phys. Chem. B*, **118** (2014) 5135–5140.
181. L. O. Hagman, P. Kierkegaard, *Acta Chem. Scand.*, **22** (1968) 1822–1832.
182. F. Sudreau, D. Petit, J. P. Boilot, *J. Solid State Chem.*, **83** (1989) 78–90.
183. Y. Kobayashi, T. Takeuchi, M. Tabuchi, K. Ado, H. Kageyama, *J. Power Sources*, **81–82** (1999) 853.
184. H. Aono, E. Sugimoto, Y. Sadaoka, N. Imanaka, G. Adachi, *J. Electrochem. Soc.*, **136** (1989) 590.
185. H. Aono, E. Sugimoto, Y. Sadaoka, N. Imanaka, G.-y. Adachi, *Solid State Ionics*, **40** (1990) 38–42.
186. H. Aono, E. Sugimoto, Y. Sadaoka, N. Imanaka, G.-y. Adachi, *J. Electrochem. Soc.*, **137** (1990) 1023–1027.
187. H. Aono, N. Imanaka, G.-y. Adachi, *Acc. Chem. Res.*, **27** (1994) 265–270.
188. L. Sebastian, J. Gopalakrishnan, *J. Mater. Chem.*, **13** (2003) 433–441.
189. J. Fu, *J. Am. Ceram. Soc.*, **80** (1997) 1901–1903.
190. Y. Zhu, X. He, Y. Mo, *ACS Appl. Mater. Interfaces*, **7** (2015) 23685–23693.
191. A. Aatiq, M. Ménétrier, L. Croguennec, E. Suard, C. Delmas, *J. Mater. Chem.*, **12** (2002) 2971–2978.
192. Y. Ren, K. Chen, R. Chen, T. Liu, Y. Zhang, C. W. Nan, *J. Am. Ceram. Soc.*, **98** (2015) 3603–3623.
193. H.-C. Cho, S. Kuramoto, S. Takase, J.-H. Song, Y. Shimizu, *Sens. Mater.*, **24**(1) (2011) 31–41.
194. X. Xu, Z. Wen, X. Wu, X. Yang, Z. Gu, *J. Am. Ceram. Soc.*, **90** (2007) 2802–2806.
195. J. K. Feng, L. Lu, M. O. Lai, *J. Alloys Compd.*, **501** (2010) 255–258.
196. A. G. Belous, G. N. Novitskaya, S. V. Polyanetskaya, Yu. I. Gornikov, *Inorg. Mater.*, **23** (1987) 412.
197. Y. Inaguma, C. Liquan, M. Itoh, T. Nakamura, T. Uchida, H. Ikuta, M. Wakihara, *Solid State Commun.*, **86** (1993) 689–693.
198. A. I. Ruiz, M. L. Lopez, M. L. Veiga, C. Pico, *Solid State Ionics*, **112** (1998) 291.
199. J. Ibarra, A. Várez, C. León, J. Santamaría, L. M. Torres-Martinez, J. Sanz, *Solid State Ionics*, **134** (2000) 219.
200. C. Chen, K. Amine, *Solid State Ionics*, **144** (2001) 51–57.

201. H.-T. Chung, J.-G. Kim, H.-G. Kim, *Solid State Ionics*, **107** (1998) 153–160.
202. V. Thangadurai, A. Shukla, J. Gopalakrishnan, *Chem. Mater.*, **11** (1999) 835–839.
203. R. Inada, K. Kimura, K. Kusakabe, T. Tojo, Y. Sakurai, *Solid State Ionics*, **261** (2014) 95–99.
204. K. Kimura, K. Wagatsuma, T. Tojo, R. Inada, Y. Sakurai, *Ceram. Int.*, **42** (2016) 5546–5552.
205. B. Huang, B. Xu, Y. Li, W. Zhou, Y. You, S. Zhong, C. A. Wang, J. B. Goodenough, *ACS Appl. Mater. Interfaces*, **8** (2016) 14552–14557.
206. Y. Li, W. Zhou, X. Chen, X. Lü, Z. Cui, S. Xin, L. Xue, Q. Jia, J. B. Goodenough, *Proc. Natl. Acad. Sci.U.S.A.*, **113** (2016) 13313–13317.
207. N. Kamaya, K. Homma, Y. Yamakawa, M. Hirayama, R. Kanno, M. Yonemura, T. Kamiyama, Y. Kato, S. Hama, K. Kawamoto, A. Mitsui, *Nat. Mater.*, **10** (2011) 682–686.
208. Y. Wang, W. D. Richards, S. P. Ong, L. J. Miara, J. C. Kim, Y. Mo, G. Ceder, *Nat. Mater.*, **14** (2015) 1026–1031.
209. Y. S. Jung, D. Y. Oh, Y. J. Nam, K. H. Park, *Isr. J. Chem.*, **55** (2015) 472.
210. Y. Mo, S. P. Ong, G. Ceder, *Chem. Mater.*, **24** (2012) 15–17.
211. Y. Zhu, X. He, Y. Mo, *ACS Appl. Mater. Interfaces*, **7** (2015) 23685–23693.
212. S. P. Ong, Y. Mo, W. D. Richards, L. Miara, H. S. Lee, G. Ceder, *Energy Environ. Sci.*, **6** (2013) 148–156.
213. Y. Sun, K. Suzuki, K. Hara, S. Hori, T. Yano, M. Hara, M. Hirayama, R. Kanno, *J. Power Sources*, **324** (2016) 798–803.
214. Y. Kato, S. Hori, T. Saito, K. Suzuki, M. Hirayama, A. Mitsui, M. Yonemura, H. Iba, R. Kanno, *Nat. Energy*, **1** (2016) 16030.
215. H. Muramatsu, A. Hayashi, T. Ohtomo, S. Hama, M. Tatsumisago, *Solid State Ionics*, **182** (2011) 116–119.
216. V. Thangadurai, H. Kaack, W. J. Weppner, *J. Am. Ceram. Soc.*, **86** (2003) 437–440.
217. V. Thangadurai, S. Narayanan, D. Pinzarlu, *Chem. Soc. Rev.*, **43** (2014) 4714.
218. V. Thangadurai, W. Weppner, *Adv. Funct. Mater.*, **15** (2005) 107–112.
219. R. Murugan, V. Thangadurai, W. Weppner, *Angew. Chem. Int. Ed.*, **46** (2007) 7778–7781.
220. J. Awaka, N. Kijima, H. Hayakawa, J. Akimoto, *J. Solid State Chem.*, **182** (2009) 2046–2052.

221. J. Awaka, A. Takashima, K. Kataoka, N. Kijima, Y. Idemoto, J. Akimoto, *Chem. Lett.*, **40** (2011) 60–62.
222. R. Wagner, G. J. Redhammer, D. Rettenwander, A. Senyshyn, W. Schmidt, M. Wilkening, G. Amthauer, *Chem. Mater.*, **28**(6) (2016) 1861–1871.
223. D. Wang, G. Zhong, W. K. Pang, Z. Guo, Y. Li, M. J. McDonald, R. Fu, J.-X. Mi, Y. Yang, *Chem. Mater.*, **27** (2015) 6650–6659.
224. J. Han, J. Zhu, Y. Li, X. Yu, S. Wang, G. Wu, H. Xie, S. C. Vogel, F. Izumi, K. Momma, Y. Kawamura, Y. Huang, J. B. Goodenough, Y. Zhao, *Chem. Commun.*, **48** (2012) 9840–9842.
225. J. L. Allen, J. Wolfenstine, E. Rangasamy, J. Sakamoto, *J. Power Sources*, **206** (2012) 315–319.
226. S. Mukhopadhyay, T. Thompson, J. Sakamoto, A. Huq, J. Wolfenstine, J. L. Allen, N. Bernstein, D. A. Stewart, M. D. Johannes, *Chem. Mater.*, **27** (2015) 3658–3665.
227. L. Dhivya, N. Janani, B. Palanivel, R. Murugan, *AIP Adv.*, **3** (2013) 082115.
228. C. Shao, Z. Yu, H. Liu, Z. Zheng, N. Sun, C. Diao, *Electrochim. Acta*, **225** (2017) 345–349.
229. D. Rettenwander, C. A. Geiger, M. Tribus, P. Tropper, R. Wagner, G. Tippelt, W. Lottermoser, G. Amthauer, *J. Solid State Chem.*, **230** (2015) 266–271.
230. Y.-T. Chen, A. Jena, W. K. Pang, V. K. Peterson, H.-S. Sheu, H. Chang, R.-S. Liu, *J. Phys. Chem. C*, **121** (2017) 15565–15573.
231. D. O. Shin, K. Oh, K. M. Kim, K. Y. Park, B. Lee, Y. G. Lee, K. Kang, *Sci. Rep.*, **5** (2015) 18053.
232. E. Rangasamy, J. Wolfenstine, J. Sakamoto, *Solid State Ionics*, **206** (2012) 28–32.
233. C. Li, Y. Liu, J. He, K. S. Brinkman, *J. Alloys Compd.*, **695** (2017) 3744–3752.
234. S. Afyon, F. Krumeich, J. L. M. Rupp, *J. Mater. Chem. A*, **3** (2015) 18636–18648.
235. L. Cheng, W. Chen, M. Kunz, K. Persson, N. Tamura, G. Chen, M. Doeff, *ACS Appl. Mater. Interfaces*, **7** (2015) 2073–2081.
236. Y. Ren, Y. Shen, Y. Lin, C.-W. Nan, *ACS Appl. Mater. Interfaces*, **11** (2019) 5928–5937.
237. S. Yu, D. J. Siegel, *Chem. Mater.*, **29** (2017) 9639–9647.
238. D. O. Shin, K. Oh, K. M. Kim, K. Y. Park, B. Lee, Y. G. Lee, K. Kang, *Sci. Rep.*, **5** (2015) 18053.

239. H. El-Shinawi, G. W. Paterson, D. A. MacLaren, E. J. Cussen, S. A. Corr, *J. Mater. Chem.*, **5** (2017) 319–329.
240. M. Botros, R. Djenadic, O. Clemens, M. Möller, H. Hahn, *J. Power Sources*, **309** (2016) 108–115.
241. S.-W. Baek, J.-M. Lee, T. Y. Kim, M.-S. Song, Y. Park, *J. Power Sources*, **249** (2014) 197–206.
242. L. Cheng, E. J. Crumlin, W. Chen, R. Qiao, H. Hou, S. F. Lux, V. Zorba, R. Russo, R. Kostecki, Z. Liu, K. Persson, W. Yang, J. Cabana, T. Richardson, G. Chena, M. Doeff, *Phys. Chem. Chem. Phys.*, **16** (2014) 18294.
243. C. Ma, E. Rangasamy, C. Liang, J. Sakamoto, K. L. More, M. Chi, *Angew. Chem. Int. Ed. Engl.*, **54** (2015) 129.
244. W. Xia, B. Xu, H. Duan, X. Tang, Y. Guo, H. Kang, H. Li, H. Liu, *J. Am. Ceram. Soc.*, **100** (2017) 2832–2839.
245. S. G. Kang, D. S. Sholl, *J. Phys. Chem. C*, **118** (2014) 17402–17406.
246. J. Gai, E. Zhao, F. Ma, D. Sun, X. Ma, Y. Jin, Q. Wu, Y. Cui, *J. Eur. Ceram. Soc.*, **38** (2018) 1673–1678.
247. L. Cheng, W. Chen, M. Kunz, K. Persson, N. Tamura, G. Chen, M. Doeff, *ACS Appl. Mater. Interfaces*, **7** (2015) 2073–2081.
248. B. Wu, S. Wang, W. J. Evans Iv, D. Z. Deng, J. Yang, J. Xiao, *J. Mater. Chem.*, **4** (2016) 15266–15280.
249. Y. Ren, Y. Shen, Y. Lin, C.-W. Nan, *Electrochim. Commun.*, **57** (2015) 27–30.
250. R. Sudo, Y. Nakata, K. Ishiguro, M. Matsui, A. Hirano, Y. Takeda, O. Yamamoto, N. Imanishi, *Solid State Ionics*, **262** (2014) 151–154.
251. C. L. Tsai, V. Roddatis, C. V. Chandran, Q. Ma, S. Uhlenbruck, M. Bram, P. Heitjans, O. Guillon, *ACS Appl. Mater. Interfaces*, **8** (2016) 10617–10626.
252. W. Luo, Y. Gong, Y. Zhu, K. K. Fu, J. Dai, S. D. Lacey, C. Wang, B. Liu, X. Han, Y. Mo, E. D. Wachsman, L. Hu, *J. Am. Chem. Soc.*, **138** (2016) 12258–12262.
253. W. Luo, Y. Gong, Y. Zhu, Y. Li, Y. Yao, Y. Zhang, K. K. Fu, G. Pastel, C. F. Lin, Y. Mo, E. D. Wachsman, L. Hu, *Adv. Mater.*, **29** (2017) 1606042.
254. M. Rawlence, et al., *ACS Appl. Mater. Interfaces*, **10** (2018) 13720–13728.
255. D. J. Kalita, S. H. Lee, K. S. Lee, D. H. Ko, Y. S. Yoon, *Solid State Ionics*, **229** (2012) 14–19.
256. J. Nong, H. Xu, Z. Yu, G. Zhu, A. Yu, *Mater. Lett.*, **154** (2015) 167–169.
257. H. Katsui, T. Goto, *Thin Solid Films*, **584** (2015) 130–134.

258. K. Tadanaga, et al., *J. Power Sources*, **273** (2015) 844–847.
259. M. Bitzer, T. Van Gestel, S. Uhlenbruck, H.-P. Buchkremer, *Thin Solid Films*, **615** (2016) 128–134.
260. J. Tan, A. Tiwari, *ECS Solid State Lett.*, **1** (2012) Q57–Q60.
261. S. Kim, M. Hirayama, S. Taminato, R. Kanno, *Dalton Trans.*, **42** (2013) 13112–13117.
262. J. S. Park, et al., *Thin Solid Films*, **576** (2015) 55–60.
263. I. Garbayo, et al., *Adv. Energy Mater.*, **8** (2018) 1702265.
264. R. Pfenninger, M. Struzik, I. Garbayo, E. Stilip, J. L. M. Rupp, *Nat. Energy*, **4** (2019) 475–483.

## **PART II**

# **ELECTROLYTES FOR POST-LITHIUM-ION SYSTEMS**



Taylor & Francis

Taylor & Francis Group

<http://taylorandfrancis.com>

## Chapter 4

# Electrolytes for Sodium and Sodium-Ion Batteries

Marek Marcinek,<sup>a,b</sup> Anna Bitner-Michalska,<sup>a</sup>  
Anna Szczęsna-Chrzan,<sup>a</sup> and Tomasz Trzeciak<sup>a,b</sup>

<sup>a</sup>*Faculty of Chemistry Technology, Warsaw University of Technology,  
ul. Noakowskiego 3, 00-664 Warszawa, Poland*

<sup>b</sup>*Centre for Advanced Materials and Technologies (CEZAMAT), ul. Poleczki 19,  
02-822 Warszawa, Poland  
marekmar@ch.pw.edu.pl*

### 4.1 Introduction

The total size of the global rechargeable battery market is estimated to have grown from about 10 billion dollars in 2010 to over 30 billion dollars in 2020, with significant growth of electromobility and energy storage systems [1]. Currently, the technology of chemical power sources for small portable devices is based mainly on Li-ion batteries (LIBs). The sources of lithium are not sufficient to meet all needs. This situation leads to research for new materials and solutions. A natural candidate to replace lithium appears to be sodium. Sodium resources (2.83%) significantly exceed lithium resources (0.01%) and are more evenly distributed in the earth's

---

*Designing Electrolytes for Lithium-Ion and Post-Lithium Batteries*

Edited by Włodzisław Wieczorek and Janusz Płocharski

Copyright © 2021 Jenny Stanford Publishing Pte. Ltd.

ISBN 978-981-4877-16-9 (Hardcover), 978-1-003-05093-3 (eBook)

[www.jennystanford.com](http://www.jennystanford.com)

crust [2], which is a strategic factor for the development of new battery systems, especially considering the increasing prices of lithium resources (US\$5000/t Li) (but also cobalt used in cathodic materials) in recent years.

Undergoing the same reaction mechanisms as lithium-ion cells, sodium ones are beginning to be seen as attractive energy storage systems. Ionic sodium cells do not reach such densities of energy as lithium, but for large stationary applications, the availability of sodium and its low price (so far US\$150/t Na) [3] can compensate for these inconveniences. However, resources in both cases should not be identified with supply, which can be controlled, for example, by means of pricing, political, and market strategies, and use of a closed circuit.

The development of sodium-ion batteries (SIBs) began simultaneously with Li-ion batteries (LiBs) in the early 1970s and 1980s, but the success of Li-ion battery chemistry dominated research in Na-ion batteries, which became almost unnoticeable. However, the promising results obtained in recent works indicate, that there is significant potential for materials, design and development in low-temperature Na-ion battery chemistries (Fig. 4.1).

On the other hand, lithium-ion cells passed the test. Starting from its commercialization, the density of energy has increased from 7 to almost 250 Wh/kg and the cost has reduced by 5 times. However, this progress has its limitations estimated somewhere in lithium-ion cells at 300 Wh/kg. Of course, the limit is debatable on the side of resources of lithium (and other materials for the production of lithium-ion cells) and its distribution on the globe. The exchange of lithium for sodium in cells seemed simple at first, but not always in practice. However, today we have a great return to research on sodium materials, crowned with the emergence of several commercialization solutions, such as RS2E, Faradion Limited, Tiamat, Aquion Energy, Novasis Energies, HiNa Battery Technology, and Natron Energy. There has been a huge increase in the last five years in the search of new electrode materials for SIBs [5], that has led to larger capacities and higher voltages. In order to address the shortcomings of existing Li-ion technology, a battery based on sodium as an abundant and cheap element will be developed.

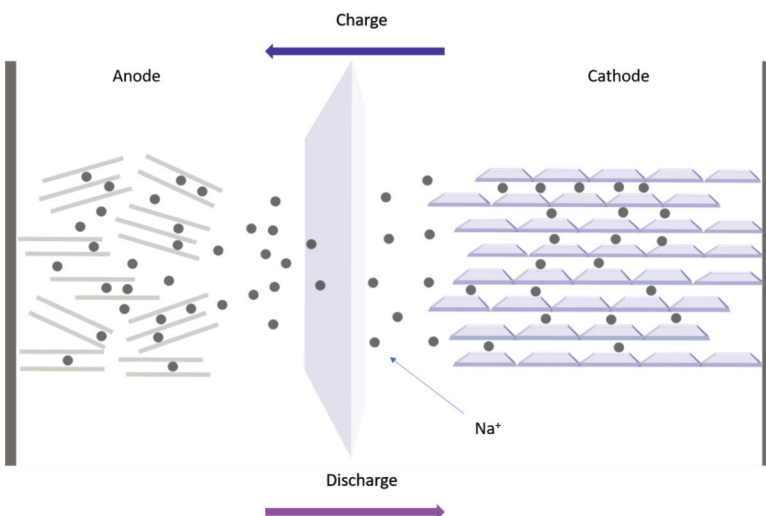


**Figure 4.1** A scheme showing the working principle of sodium-ion battery.  $\text{Na}^+$  ions migrate between a positive electrode (cathode) and a negative electrode (anode) through an  $\text{Na}^+$ -ion electrolyte in between. To prevent a circuit, separator is placed between electrodes.

It is not difficult to guess that the key to the selection of materials is their analogy to lithium cells. However, the comparison of the sodium-ion radius ( $1.02 \text{ \AA}$ ) to lithium ( $0.76 \text{ \AA}$ ), as well as its lower polarity, leads to significant differences in the transport properties of both ions. The above differences have other consequences as well, in terms of coordination, crystal structures, and lattice constants. These differences will have an impact on the charge transfer at the electrode-electrolyte interface. It has been proven, that the desolvation energy is about 30% less for sodium than for lithium [6] and should have a positive effect on the kinetics of electrode reactions.

Many differences between lithium and sodium cells are recognizable when examining their electrodes [7]. For example, on the anode side, an interesting phenomenon is the lack of sodium intercalation into graphite and the resulting need to search for other anode materials.

On the cathodic side an example of a difference is the  $\text{LiCrO}_2$  material and its  $\text{NaCrO}_2$  analogue. Despite both having a similar

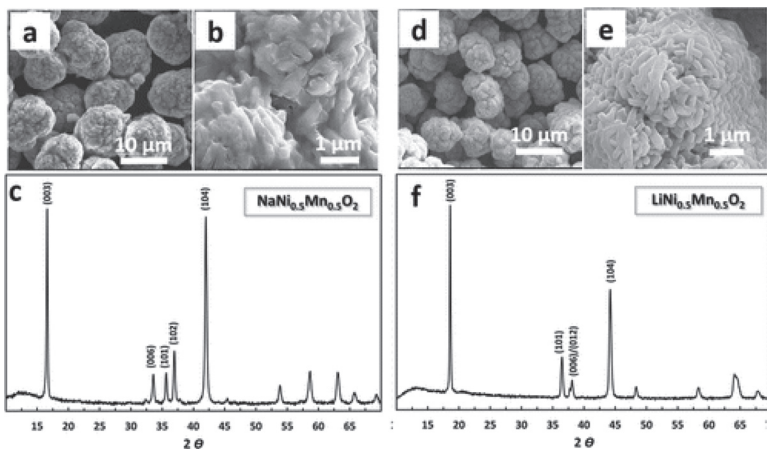


**Figure 4.2** E-SEM images of (a, b)  $\text{NaNi}_{0.5}\text{Mn}_{0.5}\text{O}_2$  and (d, e)  $\text{LiNi}_{0.5}\text{Mn}_{0.5}\text{O}_2$  powders. (c, f) Powder XRD patterns for  $\text{NaNi}_{0.5}\text{Mn}_{0.5}\text{O}_2$  and  $\text{LiNi}_{0.5}\text{Mn}_{0.5}\text{O}_2$ , respectively [9].

crystalline structure,  $\text{LiCrO}_4$  is inactive in lithium-ion cells while  $\text{NaCrO}_2$  is active [8]. Another possibility is the use of the same cathodic material  $\text{MNi}_{0.5}\text{Mn}_{0.5}\text{O}_2$  (with almost identical morphology and structure) in both lithium and sodium cells, only that they achieve different operating parameters (Figs. 4.2 and 4.3).

It has been shown that  $\text{Na}^+$  migration barriers can be even lower than the corresponding  $\text{Li}^+$  migration barriers in both solid and liquid electrolytes, leading to improved battery kinetics [10].

While Na ions' insertion kinetics in transition metal oxides may be relatively fast, the transport of the relatively big Na ions seems to induce irreversible changes in the structure of  $\text{Na}_x[\text{MnNi}] \text{O}_2$  cathodes. Since Na-ion battery technology has been developed in connection with load leveling applications, the stability of sodium insertion in cathode materials upon cycling is a serious concern [9].

Also, sodium does not form aluminum alloys. This phenomenon is beneficial because it allows elimination of the more expensive copper used as a current collector.

A critical review on the progress of electrode materials, binders, additives, and solid electrolyte interface formation for SIBs has recently been published by Sawicki et al. [11].

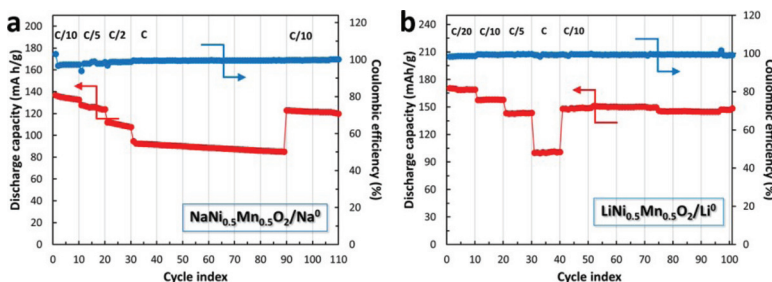


**Figure 4.3** Electrochemical performance of cathodes in half cells. Rate capability and coulombic efficiency of  $\text{NaNi}_{0.5}\text{Mn}_{0.5}\text{O}_2$  electrodes in a 0.5 M  $\text{NaPF}_6/\text{PC:FEC}$  98:2 solution (a) and  $\text{LiNi}_{0.5}\text{Mn}_{0.5}\text{O}_2$  electrodes in a 0.5 M  $\text{LiPF}_6/\text{PC:FEC}$  98:2 solution (b). The experiments were carried out at 30°C [9].

Interestingly, many studies are limited to the description of the difference between sodium and ionic cells only at the electrode level, ignoring the electrolytes [12].

This is partially understandable since the higher voltage of Na compounds ( $-2.73$  V for Na vs.  $-3.04$  V for Li) gives the possibility of better intercalation anodes for Na batteries or Na cathodes that could operate and ensure high working voltages of SIBs within the stability window of current organic electrolyte solutions [13].

Also the theoretical energy density of the whole cell depends mainly on the electrodes. Recently, a lot of attention has been paid to the real working parameters of cells, for example, their actual capacity related to the current loads of charging and discharging. There are significant issues of safety. The importance of the formation and properties of passive layers on the phase boundary of (both negative and positive) electrodes has also been in focus. It is common to make decisions about the possibility of cell operation during the whole period of its life. All these aspects are indirectly dependent on the electrolyte.

Here are the following statistics. The “web of science” after entering the topic “sodium-ion batteries” shows 581 records in 2015 and over 1500 in 2018. Similarly, in 2015, the topic “sodium-ion electrolytes” was displayed in 149 publications and in 2018 almost 300 records. In both cases, this is a threefold increase in the number

of batteries and a twofold increase in the number of electrolytes. This is, of course, an example, but each of the statistics clearly indicates that the subject of sodium-ion cells (and the so-called post-lithium cells) is progressing.

## 4.2 Electrolyte

An electrolyte in an oversimplified “old school” approach is responsible for the charge and mass transfer between electrodes. Similar properties are needed for sodium-ion electrolytes and for lithium ones.

However, in recent times its role has changed from a “passive” provider of solvent-soluble salt ions. Rather, the role has remained the same, but the understanding of the phenomenon has changed. One of the main themes of this book is the introduction of low-coordinating “tailored” anions, that in a targeted way model the mechanism of ion conduction. Another example can be ionic liquid (IL) electrolytes, which significantly reduce the flammability and improve safety of the cell. Finally, additives reduce the possibility of overcharging, or by means of appropriate physicochemical properties, influence the ionic diffusion within the electrodes [14].

However, general composition of a typical electrolyte for nonaqueous-ion batteries is based on solutions of one or more salts in mixtures of two or more solvents. Of course, the use of more than one solvent is due to the fact, that one electrolyte solvent does not reach the expected operating parameters. The formulation of lithium-cell electrolytes was proposed by Tarascon and Guyomard, in 1994, using linear carbonates (dimethyl carbonate [DMC]), as a cosolvent with a cyclic carbonate (ethylene carbonate [EC]) [15]. Due to the similar chemistries of sodium- and lithium-ion batteries, the principles of the latter technology can be used as a basis for the development of the previous one.

In the case of sodium-ion electrolytes, there are no reports that they are fundamentally different from the typical electrolytes used in lithium-ion cells. The problem of nonconductive layers of the SEI and the need to select significantly different electrolytes (see Chapter 5, devoted to magnesium-ion electrolytes) does not exist

here. For sodium-ion cell electrolytes,  $\text{NaPF}_6$  is the predominant salt and the solvents are usually a combination of linear and cyclic alkyl carbonates (such as DMC and EC) [16, 17].

### 4.2.1 Solvents and Systematics

Sodium systems do not differ significantly from lithium systems. The simplest approach is just to focus on liquid and solid systems. More detailed studies usually separate classes of electrolyte: nonaqueous, aqueous, ionic, gel polymer, solid polymers and glass ceramic electrolytes (two last are not described here). The recent research trend shows development of gel polymer electrolyte (GPE) and hybrid materials [8] due to additional advantage of significant thermal safety for sodium-ion batteries operating at room temperature.

#### 4.2.1.1 Liquid electrolytes

Generally, as was mentioned earlier, not many studies of electrolytes have been reported for Na-ion cells. Those, which exist, focus on analogues of the lithium ones, such as based on the propylene carbonate (PC). Due to its high dielectric constant and large liquid range, PC was among the first solvents investigated for both lithium- and sodium-ion technologies. However, researchers found problems; such as PC exfoliation of graphite at the electrolyte/anode interface in lithium-ion systems [19]. That is why the main difference with lithium-ion electrolyte is the wider use of PC as a solvent, which is not used in LIB, because it interacts with the graphite.

The vital primary paper was presented by Palacin et al. in 2012 [20]. Researches refer the changes of conductivity of electrolyte based on  $\text{NaClO}_4$  depending on different types of solvents. The main conclusion is that electrolytes based on single solvent have lower conductivity than those, which contain cosolvent. Depending on its nature, cosolvent may enhance the ionic conductivity by decreasing the viscosity of primary solvent, which is typically higher, and also by improving the dissociation of the salt. The best cosolvent is EC, because it improves conductivity of the electrolyte significantly. For example, 1 M  $\text{NaClO}_4$  in EC:DME shows the best conductivity

results ( $12.55 \text{ mS cm}^{-1}$ ), similar to LP30, which is the most common electrolyte in Li-ion batteries nowadays [17].

As mentioned earlier, due to the many analogies between sodium and lithium systems, it is not surprising that most of the liquid electrolytes are still based on solutions of appropriate salts in single organic solvents or compounds of organic solvents such as PC, EC, DMC, diethyl carbonate (DEC), dimethoxyethane (DME), tetrahydrofuran (THF), and triethylene glycol dimethyl ether (triglyme), which have been intensively studied in the recent past.

Since electrolytes are essential for the proper performance of any battery chemistry, it is the focus on battery research to identify the most appropriate formulation to minimize interface reactions and enhance performance, safety, economy, and environmental aspects. Ponrouch et al. presented a comparative study on diverse electrolyte formulations with different sodium salts ( $\text{NaClO}_4$ ,  $\text{NaPF}_6$ , and  $\text{NaTFSI}$ ), solvents (PC, EC, DMC, DME, DEC, THF, and triglyme) or solvent mixtures (EC:DMC, EC:DME, EC:PC, and EC:triglyme). Detailed studies of viscosity, ionic conductivity, and electrochemical and thermal stability helped establish some intrinsic trends that allowed identifying specific electrolyte formulations with wider ranges of applicability. Studies clearly demonstrated, that the selection of the electrolyte may play a key role in prospective research when looking for new electrode materials and further allowed to establish, that  $\text{NaPF}_6$  in EC:PC fulfills at present all the necessary conditions to be adapted as a standard electrolyte in SIBs [20].

Later works showed that a composition of even three solvents ( $\text{EC}_{0.45}:\text{PC}_{0.45}:\text{DMC}_{0.1}$  with 1 M of Na salt) can be an optimal electrolyte formulation for SIBs. The successful combination of macroscopic properties of these electrolytes, being the result of a set of interrelated factors originating at the molecular level, is exemplified by high ionic conductivity and a low degree of ion pairing, low viscosity, and not the least formation of a suitable SEI layer on negative electrode materials. This electrolyte formulation was used for benchmarking negative (i.e., hard carbon) and positive (i.e.,  $\text{Na}_3\text{V}_2(\text{PO}_4)_2\text{F}_3$  [NVPF]) electrode materials in half cells, enabling the achievement of impressive rate capability and very good capacity retention. Full Na-ion cells were thus assembled

that display an operation voltage of 3.65 V, very low polarization, and excellent capacity retention upon cycling with *ca.* 97 mA h g<sup>-1</sup> of NVPF being recorded after more than 120 cycles with high coulombic efficiency (>98.5%). Good power performance was also observed with 70 mA h g<sup>-1</sup> of NVPF retained at a 5 C rate [21].

#### 4.2.1.1.1 Solid-electrolyte interphase

The so-called SEI formed during the first charge/discharge cycle due to the instability of the electrolyte determines the overall performance (electrochemical, mechanical, and thermal) of the battery system.

There are only a few reports addressing the fundamental aspects of the SEI formed in SIBs, and there is still a big debate on the SEI understanding in lithium-ion systems. However, differences in the general properties of sodium and lithium ions make this knowledge only partially transferrable and it always needs to be verified.

The higher redox potential of Na<sup>+</sup> versus Li<sup>+</sup> (~0.33 V), the lower Lewis acidity of Na<sup>+</sup> resulting in a higher solubility of Na-based SEI compounds (e.g., Na<sub>2</sub>CO<sub>3</sub> vs. Li<sub>2</sub>CO<sub>3</sub>), the lower desolvation energy of Na<sup>+</sup> (by ~25%–30%), the larger ionic radius of Na<sup>+</sup> (>30% larger than Li<sup>+</sup>), the larger coordination shell of Na<sup>+</sup> versus Li<sup>+</sup>, the higher water reactivity of Na<sup>+</sup>, and the lower equivalent volume of Na-based SEI compounds may all affect the SEI behavior. It is plausible to assume that the higher value of the Na/Na<sup>+</sup> potential compared to Li/Li<sup>+</sup> can reduce the electrolyte degradation at the surface of the (de-)sodiated electrode material. This was experimentally examined and confirmed recently. The organic content of the SEI on sodiated hard carbon is strongly dependent on the anion and decreases in the order: NaPF<sub>6</sub> > NaClO<sub>4</sub> > NaTFSI > NaFTFSI > NaFSI [22].

It should also be noted, that SEI-forming electrolyte additives have also been studied *per analogiam* to the lithium systems such as fluoroethylene carbonate (FEC), vinylene carbonate (VC) and t-difluoroethylene carbonate (DFEC) alone or as a mixture. A good example is a publication where the functional electrolyte was composed of 1 M NaPF<sub>6</sub> dissolved in a 1:1 (v/v) mixed solvent of PC and ethyl methyl carbonate (EMC) with 3–4 wt.% of two or three additives, including FEC, prop-1-ene-1,3-sultone (PST), and

1,3,2-dioxathiolane-2,2-dioxide (DTD). It is shown that the capacity retentions of the cells increase to 84.4% and 92.2% after 1000 cycles for electrolytes containing FEC-PST bi-additive and FEC-PST-DTD tri-additive, respectively, as compared with that containing FEC single additive [23].

Also some authors [24] demonstrated, that adiponitrile (ADN) effectively improves the electrochemical performance at high and low temperatures and cycling stability of  $\text{Na}_{0.76}\text{Ni}_{0.3}\text{Fe}_{0.4}\text{Mn}_{0.3}\text{O}_2$  as the cathode material of sodium-ion batteries. Addition of ADN to an electrolyte results in the formation of a more effective SEI film. In particular, the battery using the electrolyte with 3% ADN exhibits the most obvious improvement, which owe to the formation of the most compact, stable and effective SEI film after adding 3% ADN into the electrolyte. At the operating temperature of 45°C, -10°C, and -20°C, the discharge capacity increases by 10.5%, 8%, and 13%, respectively. For the life cycle, the capacity retention of the battery without the addition of ADN drops rapidly to 75% after 40 cycles, while the capacity retention of the battery with 3% ADN still remains 78% after 220 cycles.

#### 4.2.1.2 Ionic liquid-based electrolytes

Sodium-ion as well as lithium-ion systems find weakness in the electrolyte as it contains hazardous, volatile organic solvents. In this scenario, ILs, salts molten at room temperature or below, represent interesting substitutes for the organic electrolyte solvents for enhancing the safety of the electrochemical devices. ILs are considered as strong flame retardants and display almost no vapor pressure in combination with relatively effective ion transport properties and wide chemical, electrochemical, and thermal stability [25].

For sodium-ion batteries the following ILs have been introduced:

- Diethyl methoxyethyl ammonium tetrafluoroborate [DEME]  $[\text{BF}_4^-]$  [26]
- 1-Ethyl-3-methyl imidazolium tetrafluoroborate [EMI] $[\text{BF}_4^-]$  [27, 31]
- 1-Ethyl-3-methylimidazolium bis(fluorosulfonyl)amide  $[\text{C}_2\text{C}_1\text{im}]$  [FSA] [28]

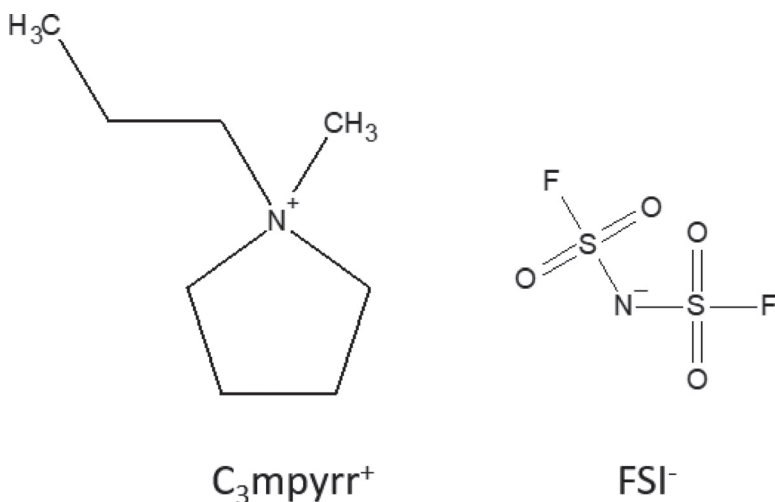


**Figure 4.4** Chemical structure of *N*-ethyl-*N*-methylpyrrolidinium bis(fluorosulfonyl)imide (in the literature FSI anion is also named fluorosulfonamide [32]).

- *N*-methyl-*N*-propylpyrrolidinium bis(fluorosulfonyl)amide [ $\text{C}_3\text{C}_1\text{pyrr}$ ] [FSA] [29, 30]
- Butylmethylpyrrolidinium-bis-(trifluoromethylsulfonyl)-imide [BMP][TFSI] [31]
- Methylpropylpyrrolidinium fluorosulfonamide [ $\text{C}_3\text{mpyr}$ ][FSI] [32]

So far, the room-temperature performance of IL-based electrolytes is often less encouraging than that of (organic) liquid electrolytes [14]. However, if the demands would significantly expand, for example, by the mass production of large-scale power storage battery, the cost would decrease.

An example of IL, FSA does not need an electrolytic fluorination process for synthesis unlike the case of TFSAs, cost reduction for the production being envisaged. Recent binary systems of sodium and quaternary ammonium salts, such as [ $\text{C}_2\text{C}_1\text{im}$ ][FSA] and [ $\text{C}_3\text{mpyr}$ ][FSI], were employed as electrolytes for SIBs.

For these ionic liquids used in sodium-ion batteries, the rise of the temperature effects on the decrease of viscosity and the increase of ionic conductivity. Ionic liquid used in electrolyte may allow the

cell to perform in higher range of temperatures with satisfying ionic conductivity performance. For example, for  $[C_3C_1\text{pyrr}][\text{FSA}]$ , the ionic conductivity increases from 1.9 to 16 mS cm<sup>-1</sup>, when the temperature rises from 25 to 90°C [36]. Such developments can lead to the application of ionic liquids as gel polymer electrolytes for sodium secondary batteries.

An interesting trend is the combined approach optimizing increased performance with increased safety features.

An example is an electrolyte consisting of an organic solvent mixture (EC:PC) and different ILs—EMIImTFSI, BMImTFSI, and Pyr<sub>13</sub>TFSI—and with the NaTFSI salt providing the Na<sup>+</sup> charge carriers [35].

The main disadvantage of ILs is their relatively high viscosity. Adding a suitable amount of organic “thinning” solvents could be a potential solution for this problem: while the electrolyte viscosity is greatly reduced, the electrochemical properties and thermal stability remain almost as good as those of pure IL. Electrolyte mixtures based on 1-ethyl-3-methylimidazolium bis(trifluoromethanesulfonyl) (EMI-TFSI) with carbonate solvents (EC-PC) were published recently [36].

#### 4.2.1.3 Gel systems

Combining the low ionic conductivity and limited mechanical stability of the solid electrolytes and GPEs seemed to be a good compromise between polymer and liquid electrolyte. Their mechanical properties of solids and diffusive properties of liquids, have received increasing attention [37].

GPEs composed of triethylene glycol diacetate-2-propenoic acid butyl ester copolymer and commercial used liquid organic electrolyte were prepared via in situ polymerization. The ionic conductivity of the as-prepared GPE can reach  $5.5 \times 10^{-3}$  S cm<sup>-1</sup> with 6 wt.% monomers and 94 wt.% of liquid electrolyte at 25°C. Additionally, the temperature dependence of the ionic conductivity is consistent with an Arrhenius temperature behavior in a temperature range of 20°C–90°C [38].

Frequently poly(vinylidene difluoride) (PVDF) is used as a gel matrix in electrolytes. It is highly electrochemically stable due to

the presence of a strong electron-withdrawing functional group ( $-C-F$ ). However, PVDF is a semicrystalline polymer and therefore it is usually present as a copolymer with hexafluoropropylene (HFP) with a significantly reduced degree of crystallinity of the system. Also, the well-known PMMA was studied in the sodium area of the research [39].

Generally, the composite systems became very popular due to the improved properties and application in the novel battery chemistries like Na-S [40].

Some concepts of combining gel electrolytes with ILs [41] and combinations of solvents and ceramic additives [39] were also published. Even if such systems are scientifically interesting and of great safety value, the economic aspects of such complex electrolytes can be a very strong limiting factor.

#### 4.2.1.4 Polymer electrolytes

There has been considerably less research focused on solid-polymer electrolytes due to their substandard ionic conductivity at room temperature and reduced interfacial surface area between the electrolyte and the electrode. However, continued interest in such technologies originates from their processing ability and flexibility, higher safety due to the absence of flammable organic solvents and high dimensional stability [42–51]. Despite not being liquid in a wide temperature range, polyethers were first shown to dissolve inorganic salts and conduct resulting ions at room temperature, in the 1970s [52]. Of these, poly(ethylene oxide) (PEO) took center stage in lithium electrolyte research in the 1990s.

For PEO-based, solid-polymer electrolytes in SIB applications, systems were reported on sodium trifluoromethane sulfonate ( $NaCF_3SO_3$ ) [53–56] sodium thiocyanate ( $NaSCN$ ), sodium tetrafluoroborate ( $NaBF_4$ ) [57], sodium bis(trifluoromethanesulfonyl)imide ( $NaTFSI$ ) [58–60], sodium perchlorate ( $NaClO_4$ ) [61], and sodium hexafluorophosphate ( $NaPF_6$ ) [62] salts. Generally, membranes and their lithium analogues show ionic conductivities on the order of  $10^{-5} \text{ S cm}^{-1}$  (room temperature), which is not enough for rechargeable batteries [63, 64]. Only  $NaTFSI$  displays higher ionic conductivities in PEO-based, solid-polymer electrolytes

at room temperature ( $0.1 \text{ mS cm}^{-1}$ ) and about  $1 \text{ mS cm}^{-1}$  above  $80^\circ\text{C}$ .

### 4.2.2 Salts

For SIBs, electrolytes are mainly the same in scope as have been applied in the field of LIB electrolytes for many years. The most frequently studied salt is  $\text{NaClO}_4$ , likely due to a combination of historical and cost reasons. Comparative studies of different Na-salts are still rare. Bhide et al. [65] compared  $\text{NaPF}_6$ ,  $\text{NaClO}_4$ ,  $\text{NaTf}$ , and  $\text{NaTFSI}$  using a common EC:DMC matrix and measured the ionic conductivity as a function of the salt concentration. The concentration is approximately the same as for LIB: 1 M.

In an earlier chapter of this book synthesis, production, and structural and electrochemical properties of pentafluorinated anions-based lithium salts, which showed superior properties to the presently used lithium salts in electrolytes are described [66]. The synthesis and application of “tailor-made” anions in sodium electrolytes is presented in the work by Plewa-Marczewska [67]. It confirmed the high thermal stability of  $300^\circ\text{C}$  salt (through the thermo-gravimetric analyzer technique). Electrolytes based on TDI and PDI anions in PC showed high conductivity with values of about  $4 \text{ mS/cm}$  at  $20^\circ\text{C}$  and this already for 0.5 and 1 M salt concentration for both salts.

It is extremely interesting, that high conductivity values are achieved at low salt concentrations, which is a huge advantage when saving of materials is taken into account. Interesting properties have also been confirmed by the Raman spectroscopy, used to estimate the amount of ionic associations. Raman spectroscopy showed excellent salt dissociation and virtually no ion vapor at concentrations up to 0.5 M. Long-distance ordering of the anionic subnetworks TDI and PDI was also observed by means of X-ray structural studies. In accordance with previous computational simulations, such supramolecular structures are responsible for playing a key role in sodium coordination and thus for significantly facilitating the transport capacity of cations. The combination of this with thermal stability and increased electrochemical stability above 4.5 V for NaTDI and 4.2 V NaPDI versus  $\text{Na}/\text{Na}^+$  makes these salts

interesting as a candidate for sodium electrolyte carrier. Specific interactions between electrolyte components in low-coordinated salt systems have been thoroughly analyzed by X-ray analysis and described in the Chapter 1 of this book.

An electrolyte based on salts of the general anion formula  $\text{YF}_{x-}$ , such as  $\text{PF}_6^-$  [7, 68, 69],  $\text{BF}_4^-$  [70],  $\text{AsF}_6^-$  [71], is unstable in contact with water; during this kind of reaction the toxic hydrogen fluoride is formed. Elimination or reduction of fluorine content in salts should lead to limiting production and emissions of toxic compounds into the environment. Use of a salt that doesn't contain fluorine or fluoro-organic compounds (which doesn't create the same problems as  $\text{YF}_{x-}$ ) also has significant advantages, such as stability of the electrode/electrolyte interface in batteries. In that case, the formation of a fluoride layer at the electrode/electrolyte interface (SEI) is less possible. Secondly, the use of anions with a large amount of nitrogen causes the formation of an electrode-electrolyte passive layer, which has a relatively high conductivity. Components containing nitrogen are known from the literature as stabilizers of the SEI layer. The organofluorine or nonfluorine salts may exhibit significantly improved properties, including greater stability, during the process of charge and discharge and more durability. However, according to the literature, the best conductivities have been measured for fluorinated salts. Electrolyte safety, stability, and cost can be negatively associated with fluorinated salts, encouraging some researchers to looking for nonfluorine options [72].

Furthermore, calculations helped hypothesize that employing anions with a diffuse negative charge and having lower cation-anion interaction energy will dissociate more easily in solvents [7]. In the same research, specific anions were indicated as candidates for practical application in sodium-ion electrolytes. Jónnson and Johannsson dispute that anions with diffuse negative charge will have lower cation-anion interaction energies. As a consequence, these salts will dissociate better in solvents, which will lead to an increase in the number of effective charge carriers. In particular, it has been estimated, that Hückel-type anions have lower interaction energies with  $\text{Na}^+$  than  $\text{Li}^+$  cations. These anions are depicted by a  $\pi$ -coupled system covering the entire anion (including cyanide end groups).

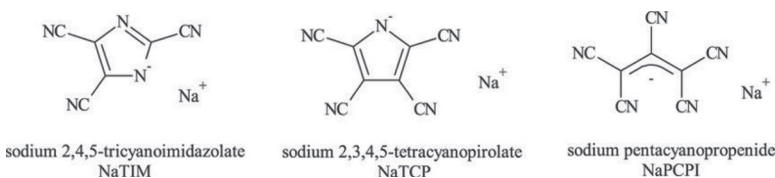


**Figure 4.5** Fluorine-free electrolytes for all-solid sodium-ion batteries based on percyano-substituted organic salts [69].

It has been shown in preceding chapters, that the electron-withdrawing cyanosubstituents introduced in a highly delocalized electron system reduce the basicity of the anion, inhibiting electron donation toward alkali metal cations [74]. Moreover, introducing additional cyanosubstituents decreases the basicity of the anion even more. For example, the  $pK_b$  of sodium 2,3,4,5-tetracyanopirolateanion is quite high, 11.29 to be exact, but it is expected to have low interaction with  $\text{Na}^+$  [75].

In a study by Bitner-Michalska et al. [76], sodium pentacyanopropenide (NaPCPI), sodium 2,3,4,5-tetracyanopirolate (NaTCP), and sodium 2,4,5-tricyanoimidazolate (NaTIM) were dissolved in liquid and solid-polymer electrolytes. Of course these candidates were selected on the basis of their combined properties of fluorine-free composition plus diffused negative charges.

Due to the unique structure of anions, improved ionic conductivities were measured in these systems. As an example, high conductivities ( $>1$  mS/cm) were obtained above  $70^\circ\text{C}$  for solid-polymer electrolyte with a PEO:NaTCP molar ratio of 16:1. Values such as these are obtained in liquid systems. Salts showed high thermal stability and electrochemical stability even up to 5 V. Their performance as electrolytes were benchmarked versus NaPF<sub>6</sub>. This new family of anions can be considered as compounds of a new quality for sodium-ion cell electrolytes.

## 4.3 Summary

There is no doubt sodium batteries have become the focus in the last decade. Recent progress, practical issues, and future prospects

of SIBs clearly indicate that they should be considered as a promising alternative. However, analogical chemistries of lithium and sodium should not be thought to be identical [77].

Theory, principle, material synthesis, and experimental methods for research and development of SIBs should be further established and understood taking into consideration both similarities to and differences from LIBs.

Scientifically, it is interesting to compare how the size of the ions affects the electrode reaction for a given host structure [78]. These differences are specially affecting all elements of the cell and become crucial in the electrode-electrolyte compatibility design. That is however critical, why typical materials used in lithium systems are not usually useful in sodium cells.

On the other hand, that research on SIBs should not be considered as “antilithium” since it deals with the same challenges as lithium systems, for instance, electrolyte decomposition at high voltage, capacity fading after some cycles, dendrite formation (metal electrode), SEI properties, and corrosion. Thus, the overall strategy for the future requires parallel development of all materials for Na-ion batteries with those of LIBs.

Cost-efficient batteries based on abundant elements could become relevant in the future in case resource supply and supply chains become important. More favorable economy of sodium also indicates that sodium cells might be more applicable even in large stationary power plants.

Debating specifically about electrolytes, it should be stated that an electrolyte is no longer “just the third element” of the cell.

An electrolyte is an active player in the overall system and thus should be “tailored” for specific anode and cathode materials—plus aimed for specific applications. It is, therefore, important to understand the mechanisms of the processes of charge transportation within the electrolyte area in order to control the design of electrolyte effectively. It is helpful to know and quantify not only parameters such as ionic conductivity but also parameters such as transference numbers and ion associations.

Many concepts have been tested, including polymer electrolytes, but the future will most likely be based on organic liquid electrolytes. The use of cosolvents (e.g., ILs) to enhance safety has been

considered [79]. Also nonfluorinated salts will be promoted, but this will most likely also happen for LIBs [80].

According to the author, it will also be difficult to universally indicate one electrolyte (and also the composition of a cell) for all applications. Rather, due to the price, performance, safety, and environmental guidelines, it is expected that unique compositions will be designed for each cell operating condition. This remark does not apply only to sodium cells. SIBs are only one strategy of the search for the “Holy Grail” of energy storage devices.

## References

1. J. W. Choi, D. Aurbach, Promise and reality of post-lithium-ion batteries with high energy densities. *Nat. Rev. Mater.*, **1** (2016) 16013.
2. H. Pan, Y.-S. Hu, L. Chen, Room-temperature stationary sodium-ion batteries for large-scale electric energy storage. *Energy Environ. Sci.*, **6** (2013) 2338–2360.
3. F. Li, Z. Wei, A. Manthiram, Y. Feng, J. Ma, L. Mai, Sodium-based batteries: from critical materials to battery systems. *J. Mater. Chem. A*, **7** (2019) 9406–9431.
4. Y. You, A. Manthiram, Progress in high-voltage cathode materials for rechargeable sodium-ion batteries. *Adv. Energy Mater.*, **8** (2017) 1701785.
5. V. Palomares, M. Casas-Cabanas, E. Castillo-Martinez, M. Han, T. Rojo, Update on Na-based battery materials. A growing research path. *Energy Environ. Sci.*, **6** (2013) 2312–2337.
6. M. Okoshi, Y. Yamada, A. Yamada, H. Nakai, Theoretical analysis on de-solvation of lithium, sodium, and magnesium cations to organic electrolyte solvents. *J. Electrochem. Soc.*, **160** (2013) A2160–A2165.
7. J. W. Choi, D. Aurbach, Promise and reality of post-lithium-ion batteries with high energy densities. *Nat. Rev. Mater.*, **1** (2016) 16013.
8. S. Komaba, C. Takei, T. Nakayama, A. Ogata, N. Yabuuchi, Electrochemical intercalation activity of layered  $\text{NaCrO}_2$  vs.  $\text{LiCrO}_2$ . *Electrochim. Commun.*, **12** (2010) 355–358.
9. D. Aurbach, et al., Comparison between Na-ion and Li-ion cells: understanding the critical role of the cathodes stability and the anodes pretreatment on the cells behavior. *ACS Appl. Mater. Interfaces*, **8**(3) (2016) 1867–1875.

10. Y. F. Y. Yao, J. T. Kummer, Ion exchange properties of and rates of ionic diffusion in beta-alumina. *J. Inorg. Nucl. Chem.*, **29**(9) (1967) 2453–2466.
11. M. Sawicki, L. Shaw, Advances and challenges of sodium ion batteries as post lithium ion batteries. *RSC Adv.*, **5** (2015) 53129–53154.
12. Y. Fang, L. Xiao, Z. Chen, X. Ai, Y. Cao, H. Yang, Recent advances in sodiumion battery materials. *Electrochem. Energy Rev.*, **1**(3) (2018) 294–323.
13. S. P. Ong, V. L. Chevrier, G. Hautier, A. Jain, C. Moore, S. Kim, X. H. Ma, G. Ceder, Voltage, stability and diffusion barrier differences between sodium-ion and lithium-ion intercalation materials. *Energy Environ. Sci.*, **4**(9) (2011) 3680–3688.
14. A. Ponrouch, D. Monti, A. Boschin, B. Steen, P. Johansson, M. R. Palacín, Non-aqueous electrolytes for sodium-ion batteries. *J. Mater. Chem. A*, **3** (2015) 22–42.
15. J. M. Tarascon, D. Guyomard, New electrolyte compositions stable over the 0 to 5 V voltage range and compatible with the  $\text{Li}_{1+x}\text{Mn}_2\text{O}_4$ /carbon Li-ion cells. *Solid State Ionics*, **69** (1994) 293–305.
16. A. Ponrouch, R. Dedryvere, D. Monti, A. E. Demet, J. M. Ateba Mba, L. Croguennec, C. Masquelier, P. Johansson, M. R. Palacín, Towards high energy density sodium ion batteries through electrolyte optimization. *Energy Environ. Sci.*, **6** (2013) 2361–2369.
17. A. Ponrouch, E. Marchante, M. Courty, J. M. Tarascon, M. R. Palacín, In search of an optimized electrolyte for Na-ion batteries. *Energy Environ. Sci.*, **5** (2012) 8572–8583.
18. D. Monti, A. Ponrouch, M. Rosa Palacín, P. Johansson, Towards safer sodium-ion batteries via organic solvent/ionic liquid based hybrid electrolytes. *J. Power Sources*, **324** (2016) 712–721.
19. R. Fong, U. von Sacken, J. R. Dahn, Studies of lithium intercalation into carbons using nonaqueous electrochemical cells. *J. Electrochem. Soc.*, **137** (1990) 2009–2013.
20. A. Ponrouch, E. Marchante, M. Courty, J.-M. Tarascon, M. R. Palacín, In search of an optimized electrolyte for Na-ion batteries. *Energy Environ. Sci.*, **5** (2012) 8572–8583.
21. A. Ponrouch, et al., Towards high energy density sodium ion batteries through electrolyte optimization. *Energy Environ. Sci.*, **6** (2013) 2361–2369.
22. G. Eshetu, T. Diemant, M. Hekmatfar, S. Grugeon, R. J. Behm, S. Laurelle, M. Armand, S. Passerini, Impact of the electrolyte salt anion on the solid

- electrolyte interphase formation in sodium ion batteries. *Nano Energy*, **55** (2019) 327–340.
- 23. H. Che, X. Yang, H. Wang, X.-Z. Liao, S. Zhang, C. Wang, Z.-F. Ma, Long cycle life of sodium-ion pouch cell achieved by using multiple electrolyte additives. *J. Power Sources*, **407** (2018) 173–179.
  - 24. X. Song, T. Maeng, Y. Deng, A. Gao, J. Nan, S. Shu, F. Yi, The effects of the functional electrolyte additive on the cathode material  $\text{Na}_{0.76}\text{Ni}_{0.3}\text{Fe}_{0.4}\text{Mn}_{0.3}\text{O}_2$  for sodium-ion batteries. *Electrochim. Acta*, **281** (2018) 370–377.
  - 25. S. Bruttì, M. A. Navarra, G. Maresca, S. Panero, J. Manzi, E. Simonetti, G. B. Appetechi, Ionic liquid electrolytes for room temperature sodium battery systems. *Electrochim. Acta*, **306** (2019) 317–326.
  - 26. M. Egashira, T. Asai, N. Yoshimoto, M. Morita, Ionic conductivity of ternary electrolyte containing sodium salt and ionic liquid. *Electrochim. Acta*, **58** (2011) 95–98.
  - 27. L. S. Plashnitsa, E. Kobayashi, Y. Noguchi, S. Okada, J.-i. Yamaki, *J. Electrochem. Soc.*, **157** (2010) A536–A543.
  - 28. C.-Y. Chen, T. Kiko, T. Hosokawa, K. Matsumoto, T. Nohira, R. Hagiwara, *J. Power Sources*, **332** (2016) 51–59.
  - 29. C. Ding, T. Nohira, K. Kuroda, R. Hagiwara, A. Fukunaga, S. Sakai, K. Nitta, S. Inazawa, *J. Power Sources*, **238** (2013) 296–300.
  - 30. C. Ding, T. Nohira, R. Hagiwara, K. Matsumoto, Y. Okamoto, A. Fukunaga, S. Sakai, K. Nitta, S. Inazawa, *J. Power Sources*, **269** (2014) 124–128.
  - 31. N. Wongittharom, T. C. Lee, C. H. Wang, Y. C. Wang, J. K. Chang, *J. Mater. Chem. A*, **2** (2014) 5655–5661.
  - 32. M. Forsyth, H. Yoon, F. Chen, H. Zhu, D. R. MacFarlane, M. Armand, P. C. Howlett, *J. Phys. Chem. C*, **120** (2016) 4276–4286.
  - 33. (a) K. Matsumoto, Y. Okamoto, T. Nohira, R. Hagiwara, *J. Phys. Chem. C*, **119** (2015) 7648; (b) K. Matsumoto, T. Hosokawa, T. Nohira, R. Hagiwara, A. Fukunaga, K. Numata, E. Itani, S. Sakai, K. Nitta, S. Inazawa, *J. Power Sources*, **265** (2014) 36; (c) K. Matsumoto, R. Taniki, T. Nohira, R. Hagiwara, *J. Electrochem. Soc.*, **162** (2015) A1409.
  - 34. R. Hagiwara, K. Matsumoto, J. Hwang, T. Nohira, Sodium ion batteries using ionic liquids as electrolytes. *Chem. Rec.*, **19** (2019) 758–770 and reference therein.
  - 35. D. Monti, A. Ponrouch, M. R. Palacín, P. Johansson, Towards safer sodiumion batteries via organic solvent/ionic liquid based hybrid electrolytes. *J. Power Sources*, **324** (2016) 712–721.

36. T. D. Vo, H. V. Nguyen, Q. D. Nguyen, Q. Phung, V. M. Tran, P. L. M. Le, Carbonate solvents and ionic liquid mixtures as an electrolyte to improve cell safety in sodium-ion batteries. *J. Chem.*, **2019** (2019) 7980204.
37. Y.Q. Yang, Z. Chang, M. X. Li, X. W. Wang, Y.P. Wa, A sodium ion conducting gel polymer electrolyte. *Solid State Ionics*, **269** (2015) 1–7.
38. H. Fan, H. Li, L.-Z. Fan, Q. Shi, Preparation and electrochemical properties of gel polymer electrolytes using triethylene glycol diacetate-2-propenoic acid butyl ester copolymer for high energy density lithiumion batteries. *J. Power Sources*, **249** (2014) 392.
39. D. Kumar, S. A. Hashmi, Ion transport and ion–filler-polymer interaction in poly(methyl methacrylate)-based, sodium ion conducting, gel polymer electrolytes dispersed with silica nanoparticles. *J. Power Sources*, **195** (2010) 5101–5108.
40. D. Kumar, M. Suleman, S. A. Hashmi, Studies on poly(vinylidenefluoride-co hexafluoropropylene) based gel electrolyte nanocomposite for sodium–sulfur batteries, *Solid State Ionics*, **202** (2011) 45–53.
41. D. Kumar, S. A. Hashmi, Ionic liquid based sodium ion conducting gel polymer electrolytes, *Solid State Ionics*, **181** (2010) 416–423.
42. A. Basile, H., Yoon, D. R. MacFarlane, M. Forsyth, P. C. Howlett, Investigating non-fluorinated anions for sodium battery electrolytes based on ionic liquids. *Electrochim. Commun.*, **71** (2016) 48–51.
43. S. Song, H. M. Duong, A. M. Korsunsky, N. Hu, L. Lu, A  $\text{Na}^+$  superionic conductor for room-temperature sodium batteries song. *Sci. Rep.*, **6** (2016) 32330.
44. D. Larcher, J. M. Tarascon, Towards greener and more sustainable batteries for electrical energy storage. *Nat. Chem.*, **7** (2015) 19–29.
45. S. Wei, A stable room-temperature sodium–sulfur battery. *Nat. Commun.*, **7** (2016) 11722.
46. Y. Q. Yang, Z. Chang, M. X. Li, X. W. Wang, Y. P. Wu, A sodium ion conducting gel polymer electrolyte. *Solid State Ionics*, **269** (2015) 1–7.
47. A. Boschin, P. Johansson, Characterization of  $\text{NaX}$  (X: TFSI, FSI) – PEO based solid polymer electrolytes for sodium batteries. *Electrochim. Acta*, **175** (2015) 124–133.
48. J. Li, Synthesis of sodium poly[4-styrenesulfonyl(trifluoro-methylsulfonyl)imide]-co-ethylacrylate] solid polymer electrolytes. *Electrochim. Acta*, **175** (2015) 232–239.

49. F. Colò, F. Bella, J. R. Nair, M. Destro, C. Gerbaldi, Cellulose-based novel hybrid polymer electrolytes for green and efficient Na-ion batteries. *Electrochim. Acta*, **174** (2015) 185–190.
50. A. Chandra, K. Thakur, Synthesis and ion conduction mechanism on hot-pressed sodium ion conducting nano composite polymer electrolytes. *Arabian J. Chem.*, **9** (2016) 400–407.
51. C. S. Martinez-Cisneros, B. Levenfeld, A. Varez, J. Y. Sanchez, Development of sodium-conducting polymer electrolytes: comparison between filmcasting and films obtained via green processes. *Electrochim. Acta*, **192** (2016) 456–466.
52. D. E. Fenton, J. M. Parker, P. V. Wright, Complexes of alkali metal ions with poly(ethylene oxide). *Polymer*, **14** (1973) 589.
53. B. L. Papke, M. A. Ratner, D. F. Shriver, Vibrational Spectroscopy and structure of polymer electrolytes, poly(ethylene oxide) complexes of alkali metal salts. *J. Phys. Chem. Solids*, **42** (1981) 493–500.
54. C. P. Rhodes, R. Frech, Cation-anion and cation-polymer interactions in  $(\text{PEO})_n\text{NaCF}_3\text{SO}_3$  ( $n = 1\text{--}80$ ). *Solid State Ionics*, **121** (1999) 91–99.
55. R. Frech, Symmetry-based vibrational analysis of polyatomic ionic species in polymer electrolytes: applications to the compounds  $\text{poly}(\text{ethylene oxide})_3\text{LiCF}_3\text{SO}_3$  and  $\text{poly}(\text{ethylene oxide})\text{NaCF}_3\text{SO}_3$ . *Macromolecules*, **33** (2000) 9432–9436.
56. A. Brodin, P. Jacobsson, On the structure of archetypal polymer electrolyte  $\text{PEO}:\text{LiCF}_3\text{SO}_3$ . *Ukr. J. Phys.*, **54** (2009) 259–265.
57. R. Dupon, B. L., Papke, M. A. Ratner, D. H. Whitmore, D. F. Shriver, Influence of ion pairing on cation transport in the polymer electrolytes formed by poly(ethylene oxide)with sodium tetrafluoroborate and sodium tetrahydroborate. *J. Am. Chem. Soc.*, **104** (1982) 6247–6251.
58. M. M., Doeuff, A., Ferry, Y., Ma, L. Ding, L. C. De Jonghe, Effect of electrolyte composition on the performance of sodium/polymer cells. *J. Electrochem. Soc.*, **144** (1997) L20–L22.
59. J. Serra Moreno, et al., Composite  $\text{PEO}_n\text{-NaTFSI}$  polymer electrolyte: preparation, thermal and electrochemical characterization. *J. Power Source*, **248** (2014) 695–702.
60. A. Ferry, M. M. Doeuff, L. C. De Jonghe, Transport property and raman spectroscopic studies of the polymer electrolyte system  $\text{P}(\text{EO})_n\text{-NaTFSI}$ . *J. Electrochem. Soc.*, **145** (1998) 1586–1592.
61. A. Dey, K. Das, S. Karan, S. K. De, Vibrational spectroscopy and ionic conductivity of polyethylene oxide- $\text{NaClO}_4\text{-CuO}$  nanocomposite. *Spectrochim. Acta Part A: Mol. Biomol. Spectr.*, **83** (2011) 384–391.

62. S. A. Hashmi, S. Chandra, Experimental investigations on a sodium-ionconducting polymer electrolyte based on poly(ethylene oxide) complexed with NaPF<sub>6</sub>. *Mater. Sci. Eng.*, **B34** (1995) 18–26.
63. K. Xu, Nonaqueous liquid electrolytes for lithium-based rechargeable batteries. *Chem. Rev.*, **104** (2004) 4303–4417.
64. E. Staunton, Y. G. Andreev, P. G. Bruce, Structure and conductivity of the crystalline polymer electrolyte  $\beta$ -EO6:LiAsF6. *J. Am. Chem. Soc.*, **127** (2005) 12176–12177.
65. A. Bhide, J. Hofmann, A. K. Durr, J. Janek, P. Adelhelm, *Phys. Chem. Chem. Phys.*, **16** (2014) 1987.
66. L. Niedzicki, M. Kasprzyk, K. Kuziak, G. Z. Zukowska, M. Armand, M. Bukowska, M. Marcinek, P. Szczecinski, W. Wieczorek, *J. Power Sources*, **192** (2009) 612.
67. A. Plewa-Marczewska, T. Trzeciak, A. Bitner, L. Niedzicki, M. Dranka, G. Z. Zukowska, M. Marcinek, W. Wieczorek, New tailored sodium salts for battery applications. *Chem. Mater.*, **26**(17) (2014) 4908–4914.
68. M. Fouzi Ghorab, J. M. Winfield, *J. Fluorine Chem.*, **49** (1990) 367–383.
69. T. Hazama, et al., *J. Power Sources*, **54** (1995) 306–309.
70. F. Alloin, J. Y. Sanchez, M. B. Armand, *Electrochim. Acta*, **37** (1992) 1729–1731.
71. V. G. Shteinberg, B. A. Shumm, A. F. Zueva, O. N. Efimov, L. N. Erofeev, *Synth. Met.*, **29** (1989) 7–12.
72. J. Scheers, et al., *J. Power Sources*, **251** (2014) 451–458.
73. E. Jönsson, P. Johansson, *Phys. Chem. Chem. Phys.*, **14** (2012) 10774–10779.
74. M. Dranka, An insight into coordination ability of dicyanoimidazolato anions toward lithium in presence of acetonitrile. Crystal structures of novel lithium battery electrolyte salts. *Polyhedron*, **51** (2013) 111–116.
75. E. S. Howard Jr., Reaction products of aromatic amines with polycyano heterocyclic compounds. United States patent US 3,221,024, 1959.
76. A. Bitner-Michalska, G. M. Nolis, G. Żukowska, A. Zalewska, M. Poterała, T. Trzeciak, M. Dranka, M. Kalita, P. Jankowski, L. Niedzicki, J. Zachara, M. Marcinek, W. Wieczorek, Fluorine-free electrolytes for all-solid sodiumion batteries based on percyano-substituted organic salts. *Sci. Rep.*, **7** (2017) 40036.
77. P. Johansson, R. Pallacin, ERI Alistore White paper 2013.

78. P. K. Nayak, W. Brehm, L. Yang, P. Adelheim, From lithium-ion to sodium-ion batteries: advantages, challenges, and surprises. *Angew. Chem. Int. Ed. Engl.*, **57**(1) (2018) 102–120.
79. D. Monti, A. Ponrouch, M. R. Palacín, P. Johansson, Towards safer sodium-ion batteries via organic solvent/ionic liquid based hybrid electrolytes. *J. Power Sources*, **324** (2016) 712–721.
80. A. Ponrouch, M. Rosa Palacín, Post-Li batteries: promises and challenges, *Philos. Trans. R. Soc. A*, **377** (2019) 20180297.

## Chapter 5

# Multivalent Cation Systems: Electrolytes for Magnesium Batteries

**Janusz Płocharski**

*Faculty of Chemistry, Warsaw University of Technology, Noakowskiego 3,  
00-664 Warszawa, Poland  
janusz.plocharSKI@pw.edu.pl*

Today's market of efficient electrochemical sources of electricity is dominated by lithium-ion systems, which are inevitably approaching their performance limits. The growing demands related to the increasing popularity of electric vehicles, mobile electronics, and energy storage devices for renewable energy sources can be hardly fulfilled by the existing systems, and this awareness propels the run for new solutions. Reversible batteries with magnesium metal anodes seem to be a reasonable alternative. Magnesium has a higher volumetric capacity than lithium, is relatively cheap due to its high abundance, and, what is very important, in contrast to lithium does not form the detrimental dendrites in conducive conditions. In fact, the last point is not so clear at the moment and will be addressed at the end of this chapter. Magnesium has not found wider applications in technology related to electrochemical sources of electricity yet. It is as of now used only in specialized primary cells activated by seawater. These cells with aqueous electrolytes have low operation voltages, moderate capacity, and high self-discharge

---

*Designing Electrolytes for Lithium-Ion and Post-Lithium Batteries*

Edited by Władysław Wieczorek and Janusz Płocharski

Copyright © 2021 Jenny Stanford Publishing Pte. Ltd.

ISBN 978-981-4877-16-9 (Hardcover), 978-1-003-05093-3 (eBook)

[www.jennystanford.com](http://www.jennystanford.com)

rates [1]. Magnesium batteries with nonaqueous electrolytes do not have or at least should not have these deficiencies.

There is extensive scientific literature dedicated to electroplating of metallic magnesium onto various substrates or studies of electrolyte solutions suitable for reversible magnesium deposition in electrochemical cells. Many systems were investigated, and only some of them revealed promising properties. It is not possible to give a full report on these efforts in this chapter. Therefore, only the systems proved to be somehow successful and/or studied by more research groups and/or subjectively believed to be promising are included in this review. Any reader interested in other reviews presenting sometimes different points of view can refer, for example, to Refs. [2–8].

The electrolyte for a magnesium battery should offer high chemical stability, sufficient ionic conductivity, high coulombic efficiency of the deposition/dissolution process, high exchange current density, low overpotential of Mg dissolution/deposition, and Mg deposits of suitable morphology and purity. Elaboration of such an electrolyte is not a small task. In particular, a simple transfer of the huge expertise collected during research on lithium-ion systems is not possible. Application of organic carbonates with magnesium salts of  $\text{BF}_4^-$ ,  $\text{ClO}_4^-$ , or  $\text{PF}_6^-$  anions leads to the irreversible formation of insulating passive layers on magnesium anodes [9, 10]. In fact, the small size and high electric charge of the  $\text{Mg}^{2+}$  cation result in very low ionic mobility, practically all the passive layers formed on magnesium (solid-electrolyte interphases) are insulating, and it is commonly assumed that the Mg metal anode must work in a naked state. Therefore, the significant difference between electrolytes for lithium-ion systems and the ones for magnesium metal batteries is that the latter must not contain organic components prone to reduction at the metallic anode. As a consequence, ethereal solvents like tetrahydrofuran (THF) and glymes are typically used since they offer sufficient chemical stability in the presence of metallic magnesium. A new approach, however, has been recently presented [11] that shows that it may be possible to produce a  $\text{Mg}^{2+}$  conducting layer on a metallic magnesium anode in order to prevent the reduction of the propylene carbonate solvent. At the moment, more research in this direction is required.

## 5.1 Electrolytes Evolved from Grignard Compounds

The earliest reports on magnesium electrodeposition from organic solutions are almost 100 years old [12], but the first practically successful procedures were described in the trailblazing works of Brenner and Sligh [13], who proposed a solution of methyl magnesium chloride and triethylborane in THF as a bath for the deposition of metallic magnesium on various substrates with practically 100% coulombic efficiency. As the authors wrote, the deposits were “white, ductile and contained at least 99% of Mg.” Brenner also reported the deposition of metallic magnesium from THF solutions of magnesium ethyl chloride and decaborane [14]. The Grignard reagents used in these experiments were, however, not suitable for battery applications because of their highly reductive nature.

Progress was achieved when Gregory et al. proposed THF solutions of Mg organic borate compounds, like  $Mg(BBu_2Ph_2)_2$  [15], showing reversible deposition of magnesium but again with too-low oxidative stability (below 2 V vs.  $Mg/Mg^{2+}$ ). Following this idea, the group of Aurbach elaborated more stable electrolytes synthesized by an *in situ* reaction of  $AlCl_{3-n}R_n$  Lewis acids with  $R_2Mg$  Lewis bases in THF or glymes. These systems offered anodic stability above 2.1 V versus  $Mg/Mg^{2+}$  and 100% deposition reversibility. Electrolytes of this type have been applied in the first successful reversible magnesium battery [17] and due to the application of a magnesium **dichloro-complex**, became known as DCC electrolytes. These electrolytes were subjected to very extended investigations, led mostly by the Aurbach group. Structural analytical methods like multinuclear and solid-state nuclear magnetic resonance, Raman spectroscopy, X-ray diffraction on single crystals, Fourier transform infrared, inductively coupled plasma, X-ray photoelectron spectroscopy, and energy-dispersive X-ray spectroscopy measurements were applied, all in parallel with electrochemical experiments. The authors also did quantum-mechanical density-functional theory calculations in order to support and clarify their experimental observations. The results of these detailed studies were included

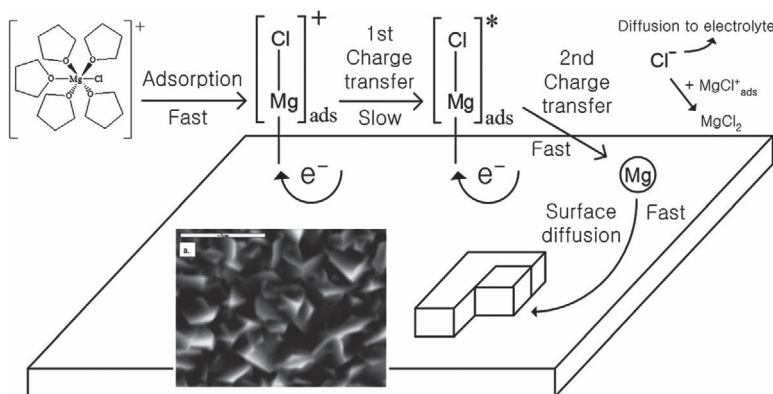


**Figure 5.1** Possible Mg electrodeposition mechanism from complex ether-real electrolyte solutions. Reproduced from Ref. [18], Copyright (2013), with permission of the Royal Society of Chemistry.

in a series of publications and concisely concluded in Ref. [18]. As one of the results of the investigations a probable magnesium deposition mechanism was revealed. The scheme is shown in Fig. 5.1.

Further development of the DCC electrolytes relied on the application of only phenyl groups as ligands and resulted in the so-called all-phenyl complex (APC) electrolyte.  $AlCl_3$  and  $PhMgCl$  precursors dissolved in THF were used in the synthesis [19]. As a result, considerable improvement in the electrolyte's oxidative stability, exceeding 3 V versus  $Mg/Mg^{2+}$ , was achieved, allowing for the application of high-voltage magnesium intercalation cathodes (provided they are elaborated). On top of that, the ionic conductivity was up to 3 times higher in comparison to that in the DCC system, leading to increased magnesium deposition rates. A comparison of the two systems is shown in Fig. 5.2.

## 5.2 Electrolytes with Boron Compounds

The above-mentioned halogen-containing electrolytes have been successfully implemented, thanks to their high oxidation stability as well as almost 100% coulombic efficiency. Practical use of these

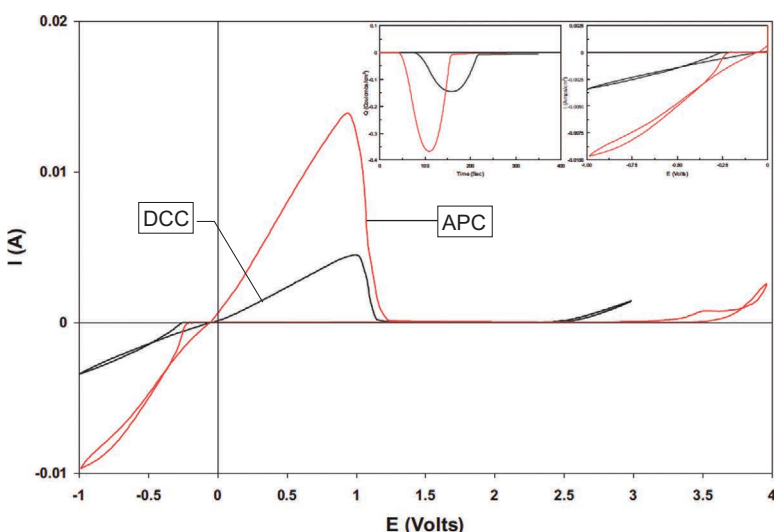


**Figure 5.2** Comparison between the voltammetric behavior of THF solutions containing 0.25 M of the product of the reaction between 1:2  $MgBu_2$  and  $AlCl_2Et$  (ethyl-butyl complex, standard solutions—DCC) and 0.4 M of the product of the reaction between 1:2  $AlCl_3$  and  $PhMgCl$  (all-phenyl complex [APC] solution), as indicated. 25 mV/s, 25°C. Insert on the right: Enlargement of the cyclic voltammograms near 0 V versus  $Mg/Mg^{2+}$ . Insert on the left: The charge balance upon typical Mg deposition-dissolution cycles in these solutions (100% cycling efficiency of Mg deposition). Reprinted with permission from Ref. [19]. Copyright © 2007 WILEY-VCH Verlag GmbH & Co. KGaA, Weinheim.

systems seems, however, to be doubtful because chloride anions induce corrosion of various nonactive but indispensable metallic components of a full battery design. To circumvent this problem, the search for new electrolytes was continued and a promising remedy was offered by selected boron compounds. Mohtadi et al. [21] reported the reversible deposition and stripping of magnesium on a platinum electrode. They used solutions of  $Mg(BH_4)_2$  in THF or dimethoxyethane, with the latter solvent showing a better performance (Fig. 5.3). To prove this concept, complete batteries with magnesium anodes and Chevrel-phase ( $Mo_6S_8$ ) cathodes were assembled and tested. Borohydrides easily undergo oxidation, so the stability of the electrolyte was limited to 1.7 V versus  $Mg/Mg^{2+}$ .

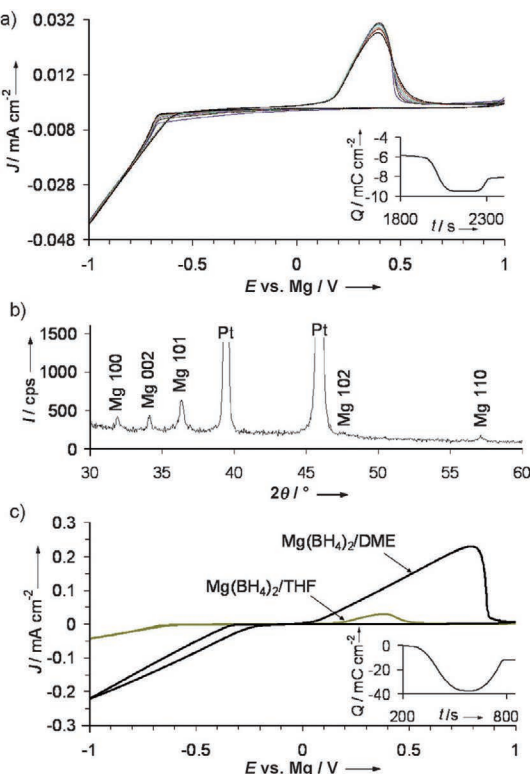


**Figure 5.3** 0.5 M Mg(BH<sub>4</sub>)<sub>2</sub> in THF: (a) Cyclic voltammogram (8 cycles); the inset shows deposition/stripping charge balance (third cycle). (b) XRD results following galvanostatic deposition of Mg on a Pt working electrode. (c) Cyclic voltammogram for 0.1 M Mg(BH<sub>4</sub>)<sub>2</sub>/DME compared to 0.5 M Mg(BH<sub>4</sub>)<sub>2</sub> in THF. The inset shows the deposition/stripping charge balance for Mg(BH<sub>4</sub>)<sub>2</sub>/DME. A Pt working electrode and a Mg reference/counter electrode are used. Reprinted with permission from Ref. [21]. Copyright © 2012 WILEY-VCH Verlag GmbH & Co. KGaA, Weinheim.

and only the low-voltage cathodes like the Mo<sub>6</sub>S<sub>8</sub> could be used. Replacement of Mg(BH<sub>4</sub>)<sub>2</sub> by Mg(BBu<sub>4</sub>)<sub>2</sub> increased the electrolyte oxidative stability to 1.9 V versus Mg/Mg<sup>2+</sup> [24].

Mg(BH<sub>4</sub>)<sub>2</sub> has found another application. Ma et al. [25] studied magnesium bis(trifluoromethane sulfonyl) imide (Mg[TFSI]<sub>2</sub>)/tetraglyme electrolytes and encountered problems because of the

presence of residual water. They added magnesium borohydride as a water scavenger and solved the problem.

The electrolytes described above were based on anions comprising a central atom of Lewis acidity and ligands strongly bound to it or eventually contained electron-withdrawing groups capable of delocalizing the negative charge over the whole anionic molecule (as in the case of the  $\text{TFSI}^-$  anion). Therefore, these species fulfill the requirements of the so-called weakly coordinating anions (WCAs) [26]. An alternative could be the application of a chemically stable polyhedral structure of, for example, *closo*-carborane ions— $\text{CB}_{11}\text{H}_{12}^-$ —[27] whose exohedral boron-carbon bonds are stable and the whole anion is exceptionally weakly coordinating. In addition, the monocarborane ions offer unique properties due to their low nucleophilicity. Tutasaus et al. [28] studied the behavior of new electrolytes comprising magnesium salt of *closo*-carborane  $\text{CB}_{11}\text{H}_{12}^-$  anion dissolved in a triglyme or a tetraglyme. This anion, one of the most weakly coordinating known, has been selected after critical analysis of a series of boron cluster compounds. The electrolytes had sufficient conductivity of 1.8–2.9 mS/cm and reversible deposition/dissolution of magnesium, with coulombic efficiency reaching 99% (in the tetraglyme) as well as overpotentials below 250 mV (Fig. 5.4). Many other operational parameters, like oxidation stability (about 3.8 V versus  $\text{Mg}/\text{Mg}^{2+}$  in a tetraglyme), no corrosion of stainless steel and aluminum, and inertness against redox active molecules, were thoroughly studied and confirmed. Finally, good performance of the carborane electrolyte was verified in a full battery configuration with  $\text{Mo}_6\text{S}_8$  and  $\alpha\text{-MnO}_2$  cathodes. It seems now that this electrolyte fulfills all the requirements of an efficient electrolyte for a magnesium metal battery except the price—carboranes are very expensive compounds at the moment.

In addition to the above-described experimental studies resulting in the elaboration of, say, an ultimate magnesium electrolyte, it is worth mentioning the theoretical study by Zhao et al. [29]. The results of their meticulously performed quantum-mechanical calculations suggested that cyanic group-substituted boron clusters  $\text{B}_{12}(\text{CN})_{12}^{2-}$  will probably offer even better performance than the mentioned carborane anions. The authors calculated that the binding energy of the second electron would be +5.3 eV, probably the highest value for any known molecule.

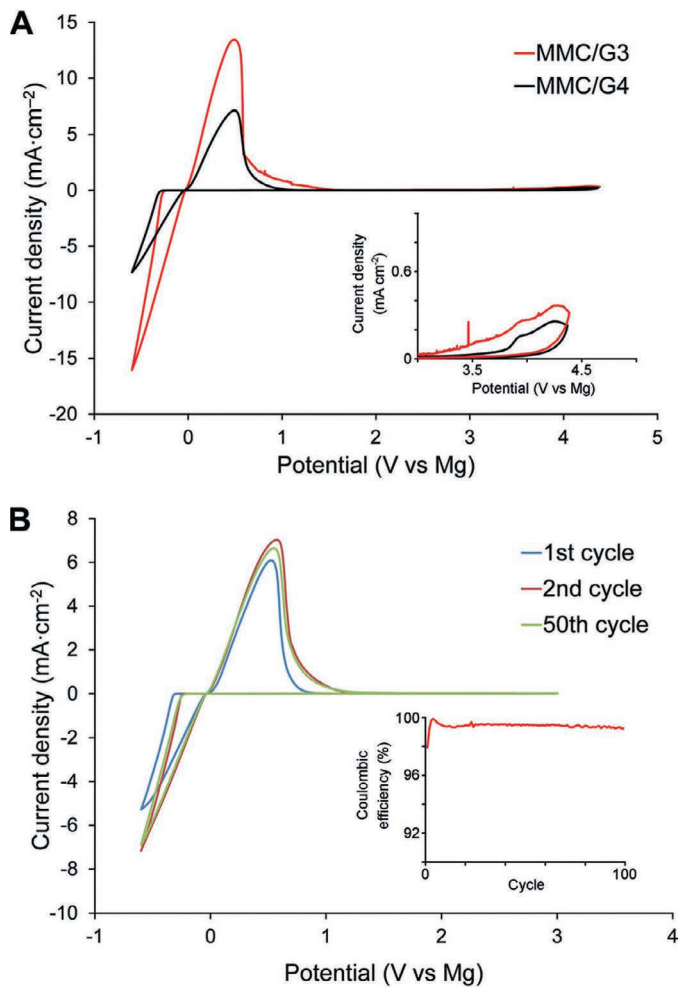


**Figure 5.4** (A) The first scan of a cyclic voltammetry test of 0.75 M  $\text{Mg}(\text{CB}_{11}\text{H}_{12})_2$ /triglyme and 0.75 M  $\text{Mg}(\text{CB}_{11}\text{H}_{12})_2$ /tetraglyme on a Pt electrode collected at 5 mV/s (inset: enlargement of the 3–5 V region). (B) Selected cyclic voltammograms of the 0.75 M  $\text{Mg}(\text{CB}_{11}\text{H}_{12})_2$ /tetraglyme electrolyte on a Pt electrode collected within the potential range of –0.6–3 V (vs.  $\text{Mg}/\text{Mg}^{2+}$ ) at 5 mV/s (inset: cycling efficiencies of Mg deposition and dissolution). Reprinted with permission from Ref. [28]. Copyright © 2015 WILEY-VCH Verlag GmbH & Co. KGaA, Weinheim.

### 5.3 Electrolytes with Hexamethyldisilazide Ions

As mentioned before, the practical implementation of magnesium batteries requires solving several problems, among which those related to a cathode seem to be the most serious. Intercalation cathodic materials of the type used in present lithium-ion systems are problematic for Mg batteries due to very low diffusion rates of the small divalent cations. Conversion cathodes also showed promise, and elemental sulfur was the first choice. Elemental sulfur, however, is electrophilic and requires electrolytes devoid of nucleophilic components in order to prevent any direct reaction between cathode material and electrolyte. This was one of the reasons to study electrolytes described by Kim et al. [30] as well as Zhao-Karger et al. [31], who followed some earlier works (e.g., see Ref. [32]). The authors studied the potentially promising compound hexamethyldisilazide magnesium chloride (abbreviated as HMDSMgCl) and concluded that in order to obtain a well-performing electrolyte, the HMDSMgCl solution should be modified by adding a Lewis acid—for example, AlCl<sub>3</sub>. Both research groups conducted meticulous studies of a reaction product of HMDSMgCl with AlCl<sub>3</sub> identified as [Mg<sub>2</sub>(μ-Cl)<sub>3</sub> · 6THF][HMDSAlCl<sub>3</sub>], which was crystallized, separated, and redissolved in THF. Finally, an electrolyte of sufficient conductivity and electrochemical stability above 3 V versus Mg/Mg<sup>2+</sup> was prepared. In addition, the total chemical inertness of the electrolyte was confirmed, proving the non-nucleophilic character of the mentioned compound as well as the products of its dissociation. A simple Mg/S battery [30] did not, however, work properly due to the too high solubility of sulfur in THF. This failure indicates that THF and similar compounds should be replaced by other solvents of lower sulfur solubility. It is worth noticing that a better performing Mg/S battery but with more complex electrodes and utilizing the hexamethyldisilazide (HMDS) electrolyte dissolved in a tetraglyme was built by Vinayan et al. [33].

A considerably easier way to prepare the HMDS electrolyte was reported by Liao et al. [34], who observed surprisingly high solubility of MgCl<sub>2</sub> in THF solutions of Mg(HMDS)<sub>2</sub>, attributing this effect

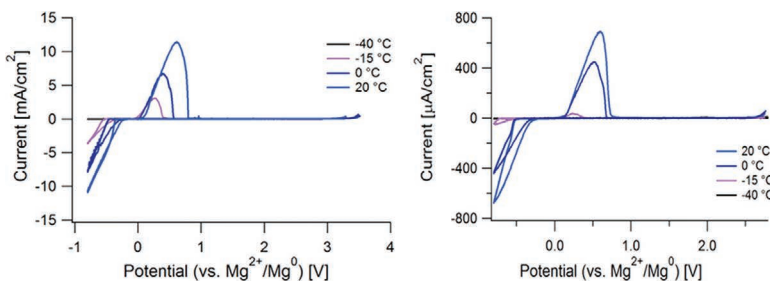


**Figure 5.5** Cyclic voltammograms of (a)  $\text{Mg}(\text{HMDS})_2\text{-}2\text{AlCl}_3$  and (b)  $\text{Mg}(\text{HMDS})_2\text{-}4\text{MgCl}_2$  at 0.5 M Mg THF electrolytes at varying temperatures. Reprinted with permission from Ref. [35]. Copyright (2017) American Chemical Society.

to the reversed Schlenk equilibrium. The resulting electrolyte—the optimal composition was 0.5 M  $\text{Mg}(\text{HMDS})_2\text{:}4\text{MgCl}_2$  in THF—was easy to prepare from commercially available components, did not require preconditioning, and offered acceptable conductivity as well as low deposition overpotential. The electrolyte was tested in a full  $\text{Mg}-\text{Mo}_6\text{S}_8$  coin cell, showing reasonable performance, but seems as though the electrochemical properties of this electrolyte are not superior to the one with the  $\text{AlCl}_3$  additive.

More recently, HMDS electrolytes were investigated by Merrill and Schaefer [35], who compared the two above-mentioned HMDS systems in THF, diglyme and tetraglyme solvents applying an impressive number of analytical methods. They concluded that their  $\text{AlCl}_3$ -containing electrolytes, despite the observed codeposition of aluminum, performed better than those with  $\text{MgCl}_2$ . The comparison is shown in Fig. 5.5, proving considerably higher currents for the  $\text{AlCl}_3$ -containing system. The authors also reported that glyme-based electrolytes revealed worse electrochemical reversibility than those based on THF. On the other hand, the high volatility of THF could be a concern for practical applications.

## 5.4 Simple Inorganic Electrolyte

All the electrolyte systems described above utilize organometallic compounds dissolved in ethereal solutions. Most of these

compounds are highly flammable or even pyrophoric. Therefore, any contact with air or moisture should be strictly avoided, which becomes particularly awkward when magnesium batteries are to be introduced into a consumer market. With this in view, a research group from Pellion Technologies elaborated on a simple electrolyte containing exclusively inorganic salts [36]. Their magnesium aluminum chloride complex (MACC) electrolyte consisted of products of the reactions between  $MgCl_2$  and  $AlCl_3$  dissolved in ethereal solvents like THF, 1,2-dimethoxyethane, and tetraglyme. These compounds react in the solution according to the scheme  $mMgCl_2 + nAlCl_3 \leftrightarrow Mg_mAl_nCl_{[(2*m)+(3*n)]}$ , which explains the necessity of electrolyte conditioning prior to the electrodeposition of Mg. The active magnesium cations in the electrolyte solution were  $MgCl^{+}$  and  $Mg_2Cl_3^{+} \cdot MgCl_2$ :  $AlCl_3$  in the ratio of 1:2 to 3:1 and Mg in concentrations of 0.1 M to 0.5 M, depending on the solvent, were used. The problem of this relatively simple electrolyte

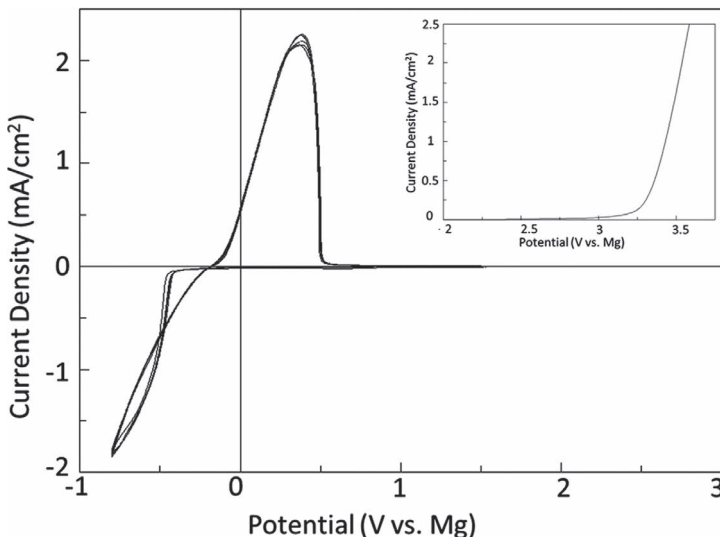


**Figure 5.6** Cyclic voltammogram and linear sweep voltammetry (insert) of 0.25 M MACC 2:1 solution in DME; Pt working electrode; Mg counter and reference electrodes. Measurements at 25 mV/s and ambient conditions. Reproduced from Ref. [36], Copyright (2014), with permission of the Royal Society of Chemistry.

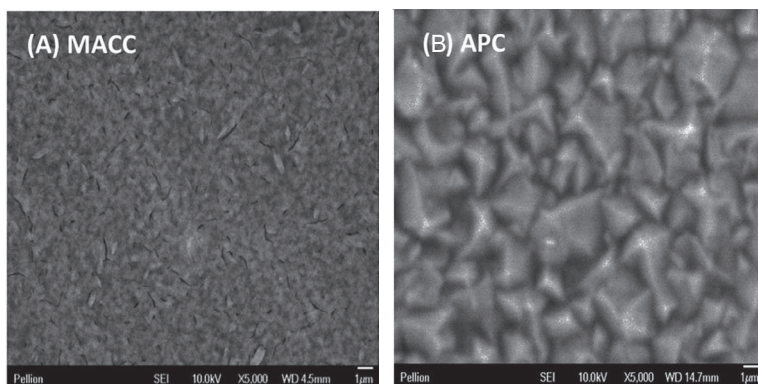


**Figure 5.7** SEM micrographs of about 5 mm thick Mg resulting from galvanostatic plating of Mg onto a Pt working electrode at  $1 \text{ mA}/\text{cm}^2$ ; (A) 0.25 M MACC 2:1 solution in DME and (B) 0.25 M APC 2:1 under the same conditions. Reproduced from Ref. [36], Copyright (2014), with permission of the Royal Society of Chemistry.

is that an anodic magnesium deposit also contains aluminum and chlorine (about 13 and 9 at.%, respectively). It seems, however, that these contaminations do not disturb the correct functioning of a battery system—tests with  $\text{Mo}_6\text{S}_8$  cathodes were successfully performed. Figures 5.6 and 5.7 show cyclic voltammograms for the MACC solution as well as a comparison of the magnesium deposit morphologies for the MACC and APC systems. The apparent size of Mg crystallites was smaller in the case of the MACC electrolyte.

## 5.5 Electrolytes with TFSI Anion

Interesting and very promising results were obtained with application of  $\text{Mg}(\text{TFSI})_2$ . The  $\text{TFSI}^-$  anion is extensively investigated as a component of lithium electrolytes and ionic liquids. It belongs to the group of WCAs, whose properties are beneficial for the ionic dissociation of related salts and lowering of the melting temperatures of ionic liquids. From this point of view, it is similar to the earlier mentioned *closo*-monocarborane anion. Some of the

very first attempts to use  $\text{Mg}(\text{TFSI})_2$  were made by Tran et al. [38], but reduction of acetonitrile rather than magnesium plating was observed in their experiments. Later on, a very comprehensive work on  $\text{Mg}(\text{TFSI})_2$ -based electrolytes was published by Ha et al. [39], who replaced acetonitrile by mixtures of glymes. The reported properties of the  $\text{Mg}(\text{TFSI})_2$  solutions were superior to those of many other systems in terms of corrosive nature, anodic limit, volatility, and solvating power for  $\text{Mg}^{2+}$  cations. In addition, what is important is that the salt is commercially available. The crucial parameters of these TFSI electrolytes are included in Table 5.1. The TFSI electrolytes were then further studied by the Aurbach group [40], [41] who revealed a critical flaw in the TFSI/glyme system. According to their studies, the overpotential related to the magnesium striping/plating process was very high and exceeded 1 V—the related cyclic voltammetry plot is shown in Fig. 5.8a. In fact, this effect would prevent any application of the TFSI/glyme electrolyte in a Mg battery. The authors attributed this high overpotential to the particular nature of a highly stable magnesium-bearing cation:  $[\text{Mg}(\text{DME})_3]^{2+}$  [42]. Introduction of  $\text{MgCl}_2$  into the  $\text{Mg}[\text{TFSI}]_2$ /glyme solution considerably changed its properties, as shown in Fig. 5.8b. The authors claimed that the observed reduction of the overpotential to acceptable values resulted from the ensuing  $[\text{Mg}_2(\mu\text{-Cl})_2(\text{DME})_4]^{2+}$  cation, which was less stable and more prone to liberate magnesium at the electrode. Therefore, chlorides despite their corrosive nature could be irreplaceable in a magnesium battery electrolyte.

The argument of the Aurbach group seems to be reasonable since most of the useful magnesium electrolytes do contain chlorides. There is, however, at least one significant exception. The studies on a carborane-based electrolyte [28] revealed the presence of  $[\text{Mg}(\text{tetraglyme})_2(\text{H}_2\text{O})]^{2+}$  cations, without any chloride content and with a low overpotential. The final elucidation of this controversy needs further investigations. A problem of TFSI as electrolyte, which was also observed by our group, is its high sensitivity to the purity of the salt, with a particularly detrimental role of moisture. The water content must be carefully controlled, and when it is too high, no magnesium deposition occurs.

**Table 5.1** Selected examples of electrolytes for magnesium batteries

Abbreviated name/Composition	Properties/ <i>comments</i>	Year of publication/ <i>References</i>
<b>Grignard compounds</b> $C_6H_5MgBr$ or $C_6H_5CH_2MgCl$ in diethyl ether	<b>Grignard compounds and related systems</b> <ul style="list-style-type: none"><li>Deposit of metallic Mg on a Pt electrode</li></ul>	1927/[12]
<b>Grignard compounds</b> 3MCH <sub>3</sub> MgCl + 1 M $(C_2H_5)_2B$ in THF	<ul style="list-style-type: none"><li>White and ductile deposit of Mg</li><li>Oxidation above 1.5 V vs. Mg/Mg<sup>2+</sup></li><li>Current densities of 2–10 mA/cm<sup>2</sup></li></ul>	1971/[13]
Dichlorocomplex (DCC) $(C_4H_9)_2Mg + C_2H_5AlCl_2$ (1:2) in THF (in situ reaction)	<ul style="list-style-type: none"><li>Oxidative stability at about 2.2 V vs. Mg/Mg<sup>2+</sup></li><li>100% coulombic efficiency (but lower for initial cycles)</li><li>Evidence of decomposition in recent reports</li></ul>	1990/[15] 2014/[16]
All-phenyl complex (APC) $C_6H_5MgCl + AlCl_3$ (2:1) in THF	<ul style="list-style-type: none"><li>Oxidative stability at about 3.2 V vs. Mg/Mg<sup>2+</sup> on Pt</li><li>100% coulombic efficiency (not confirmed by all researchers)</li><li>Active product of general formula <math>(Mg_2(\mu\text{-Cl})_3 \bullet 6\text{THF})(Ph_nAlCl_{4-n})</math>, where <math>n = 1, 2, 3, 4</math></li></ul>	2007/[19] 2011/[20]
<b>Electrolytes with boron compounds</b>		
<b>Mg(BH<sub>4</sub>)<sub>2</sub></b> 0.18 M $Mg(BH_4)_2 + 0.6\text{ M}$ $LiBH_4$ in dimethoxyethane	<ul style="list-style-type: none"><li>Low oxidative stability: 1.7 V vs. Mg/Mg<sup>2+</sup> on Pt</li><li>94% coulombic efficiency</li><li>Noncorrosive electrolyte (no chlorides present)</li><li>Tested in Mg/Chevrel-phase coin battery</li></ul>	2012/[21]

<b>Organic borane magnesium complexes</b>	<ul style="list-style-type: none"> <li>Oxidative stability up to 3.5 V vs. Mg/Mg<sup>2+</sup></li> <li>100% coulombic efficiency (92% initially)</li> </ul>	2012/ [22, 23]
<b>0.5 M tri(3,5-dimethylphenyl)borane + PhMgCl in THF</b>	<ul style="list-style-type: none"> <li>Oxidative stability at about 1.9 V vs. Mg/Mg<sup>2+</sup> on Pt</li> <li>96% coulombic efficiency</li> <li>Current density of about 6 mA/cm<sup>2</sup> at RT</li> <li>Noncorrosive electrolyte</li> </ul>	2013/[24]
<b>Butylborates</b>	<ul style="list-style-type: none"> <li>Oxidative stability at about 1.9 V vs. Mg/Mg<sup>2+</sup> on Pt</li> <li>96% coulombic efficiency</li> <li>Current density of about 6 mA/cm<sup>2</sup> at RT</li> <li>Noncorrosive electrolyte</li> </ul>	2013/[24]
<b>0.2 M Mg(BPh<sub>3</sub>Bu)<sub>2</sub> in THF</b>	<ul style="list-style-type: none"> <li>Oxidation stability at about 3.8 V vs. Mg/Mg<sup>2+</sup> in a tetraglyme</li> <li>99% coulombic efficiency in a tetraglyme</li> <li>Overpotentials below 250 mV</li> <li>Conductivity of 1.8–2.9 mS/cm</li> <li>Current density of about 10 mA/cm<sup>2</sup></li> <li>No corrosion of stainless steel and aluminum</li> <li>Inertness against redox active molecules</li> <li>Tested in Mg/Chevrel and Mg/α-MnO<sub>2</sub> batteries</li> </ul>	2015/[28] 2016/[47]
<b>Carborane</b>	<ul style="list-style-type: none"> <li>Oxidation stability at about 3.8 V vs. Mg/Mg<sup>2+</sup> in a tetraglyme</li> <li>99% coulombic efficiency in a tetraglyme</li> <li>Overpotentials below 250 mV</li> <li>Conductivity of 1.8–2.9 mS/cm</li> <li>Current density of about 10 mA/cm<sup>2</sup></li> <li>No corrosion of stainless steel and aluminum</li> <li>Inertness against redox active molecules</li> <li>Tested in Mg/Chevrel and Mg/α-MnO<sub>2</sub> batteries</li> </ul>	2015/[28] 2016/[47]
<b>HMDSS + AlCl<sub>3</sub></b>	<b>Hexamethyldisilazide electrolytes</b>	
AlCl <sub>3</sub> (0.5 M in THF) + HMDSSMgCl (1.44 M in THF) 1:3, then conditioned, then recrystallized, then redissolved Possible other solvents: di- and tetraglymes and THF/tetraglyme mixtures	<ul style="list-style-type: none"> <li>Identification of the crystallized product as [Mg<sub>2</sub>(μ-Cl)<sub>3</sub> • 6THF][HMDSSAlCl<sub>3</sub>]</li> <li>Oxidative stability at about 3.2 V in THF and 3.9 V vs. Mg/Mg<sup>2+</sup> in a diglyme</li> <li>Conductivities of 0.7–1.7 mS/cm at RT</li> <li>Current density of up to 20 mA/cm<sup>2</sup></li> <li>No reaction with elemental sulfur</li> <li>98% coulombic efficiency in THF; lower reversibility in glymes</li> </ul>	2011/[30] 2013/[31]
		(Contd.)

**Table 5.1** (*Continued*)

Abbreviated name/ Composition	Properties/comments	Year of publication/ References
<b>HMDS + MgCl<sub>2</sub></b> MgCl <sub>2</sub> directly added to $\text{Mg}(\text{HMDS})_2$ in THF to obtain $\text{Mg}(\text{HMDS})_2\text{-}4\text{MgCl}_2$	<ul style="list-style-type: none"> <li>• 88% coulombic efficiency</li> <li>• 230 mV overpotential</li> <li>• Low conductivity (about 0.25 mS/cm at RT for 0.5 M in THF)</li> <li>• No conditioning or crystallization required</li> </ul>	2015/[34] 2017/[35]
<b>Magnesium aluminum chloride complex (MACC)</b> $\text{MgCl}_2\text{+AlCl}_3$ (2:1) in THF or glyme	<ul style="list-style-type: none"> <li>• Oxidative stability of 3.1 V vs. Mg/Mg<sup>2+</sup></li> <li>• Requirement of conditioning</li> <li>• Conductivity of about 2 mS/cm</li> <li>• Codeposition of aluminum</li> <li>• Compatibility with electrophilic cathodes (e.g., sulfur)</li> <li>• Poor results on testing in a Mg/O<sub>2</sub> battery</li> </ul>	2014/[36] 2016/[37]

<b>TFSI electrolytes</b>	
<b>TFSI</b>	<p>0.3–1 M <math>\text{Mg}(\text{TFSI})_2</math> in THF or glymes 0.25 M <math>\text{MgTFSI}_2 + 0.5 \text{ M MgCl}_2</math> in DME</p> <ul style="list-style-type: none"> <li>Oxidative stability above 4 V vs. <math>\text{Mg}/\text{Mg}^{2+}</math> with an Al current collector</li> <li>Conductivity of up to 4.3 mS/cm (1 M in a glyme/diglyme 1:1 mixture)</li> <li>Compatibility with <math>\text{Mo}_6\text{S}_8</math>, PTMA (with a TEMPO moiety), and complex sulfur cathodes</li> <li>Sensitivity to moisture content in terms of performance</li> <li>Removal of detrimental water by traces (in the millimolar range) of <math>\text{Mg}(\text{BH}_4)_2</math></li> <li>High hysteresis of the deposition/stripping process (overpotential up to 1 V) in electrolytes with pure <math>\text{Mg}(\text{TFSI})_2</math></li> <li>Low and acceptable overpotential in electrolytes with <math>\text{MgCl}_2</math></li> </ul>
<b>Miscellaneous electrolytes</b>	<p>2012/[43]</p> <ul style="list-style-type: none"> <li>Air-stable electrolyte</li> <li>Conductivity of 2.6 mS/cm at RT for a 0.5 M solution</li> <li>Coulombic efficiency of about 99% (after 50 cycles)</li> <li>Oxidative stability of 2.6 V vs. <math>\text{Mg}/\text{Mg}^{2+}</math></li> <li>Compatible with a <math>\text{Mo}_6\text{S}_8</math> cathode</li> </ul>
<b>Miscellaneous electrolytes</b>	
<b>Phenolates (<math>\text{ROMgCl}</math> salts)</b>	<p>2-<i>tert</i>-butyl-4-methylphenolate magnesium chloride + EtMgCl + <math>\text{AlCl}_3</math> in THF</p> <ul style="list-style-type: none"> <li>Preliminary results</li> <li>Confirmation of reversible Mg electrodeposition</li> <li>Low current densities at RT</li> <li>Anodic stability <math>&gt; 3</math> V vs. <math>\text{Mg}/\text{Mg}^{2+}</math></li> <li>Requirement of treatment with <math>\text{Mg}(\text{BH}_4)_2</math> for hybrid systems</li> </ul>
<b>Ionic liquids</b>	<p>2016/[45]</p> <p>2019/[44, 46]</p> <ul style="list-style-type: none"> <li><math>\text{Mg}^{2+}</math> and other complex cations combined with TFSI<sup>−</sup> or <math>[\text{CB}_{11}\text{H}_{12}]^−</math> (<i>closo</i>-monocarborane) anions</li> <li>Hybrid systems: <math>\text{Mg}(\text{TFSI})_2 + [\text{C4mpyr}][\text{TFSI}]</math> in a tetraglyme</li> </ul>

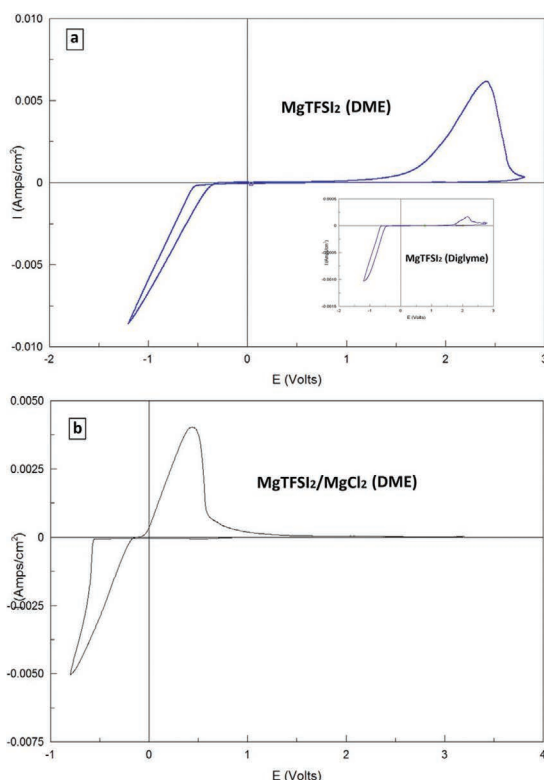


**Figure 5.8** A typical cyclic voltammetry (CV) of Pt working electrodes in (a)  $\text{Mg}[\text{TFSI}]_2$  0.5 M in a DME solution, scanned at 25 mV/s. The inset shows a CV of a Pt electrode in a  $\text{Mg}[\text{TFSI}]_2$  0.5 M solution in a diglyme. (b) 0.25 M  $\text{Mg}[\text{TFSI}]_2$  with  $\text{MgCl}_2$  0.5 M in DME. Mg foils served as reference and counter electrodes, scanned at 25 mV/s. Addition of  $\text{MgCl}_2$  significantly reduces the overpotential for both deposition and dissolution processes. Reproduced with permission from Ref. [40], Copyright (2015) ECS (Creative Commons Attribution 4.0 License).

## 5.6 Miscellaneous Electrolytes

In addition to the above-presented systems, it is necessary to mention some other electrolytes that either do not belong to the described groups or are relatively new. Some of them are, say,

fickle since difficulties in reproducibility of published results are encountered.

An example of a rather exotic system has been presented by Wang et al. [43], who reported the application of magnesium phenolates—salts of the  $\text{ROMgCl}$  type. The electrolytes were prepared by reaction of the phenolate with the alkyl Grignard compound and a Lewis acid. The ready electrolytes did not contain Grignard compounds, so they were “air stable” and offered reasonable electrochemical parameters, but the electrolyte’s synthesis was quite laborious.

It is also necessary to recall attempts to apply ionic liquids as magnesium electrolytes [44, 46]. So far, reversible magnesium electrodeposition was observed, but the results were not promising—oxidative stability was sufficient but current densities were too low due to the low conductivity of the ionic liquids applied.

## 5.7 Comparison of Various Electrolyte Systems

As presented above, many very different systems capable of the reversible electrodeposition of magnesium were investigated and have been reported in literature. A selection of most of the useful systems is included in Table 5.1. An extensive and trustable comparison of these systems is, however, lacking due to obvious reasons. An exception worth acknowledging is an informative work by Lipson et al. [47], who compared six different compositions representing practically most of existing usable concepts of magnesium electrolytes (APC, TFSI/diglyme, TFSI+ $\text{MgCl}_2$ /dimethoxyethane, HMDS+ $\text{MgCl}_2$ /THF, MACC/THF, and monocarborane/tetraglyme). The authors observed considerably lower oxidative stability of all the studied systems when porous electrodes were applied, carbon on stainless steel, for example. The measured potentials were 0.5–1.2 V below the values recorded for a polished platinum electrode (Fig. 5.9). The highest stability was found for the monocarborane electrolyte, and this system also revealed the best performance in a reversibility test.

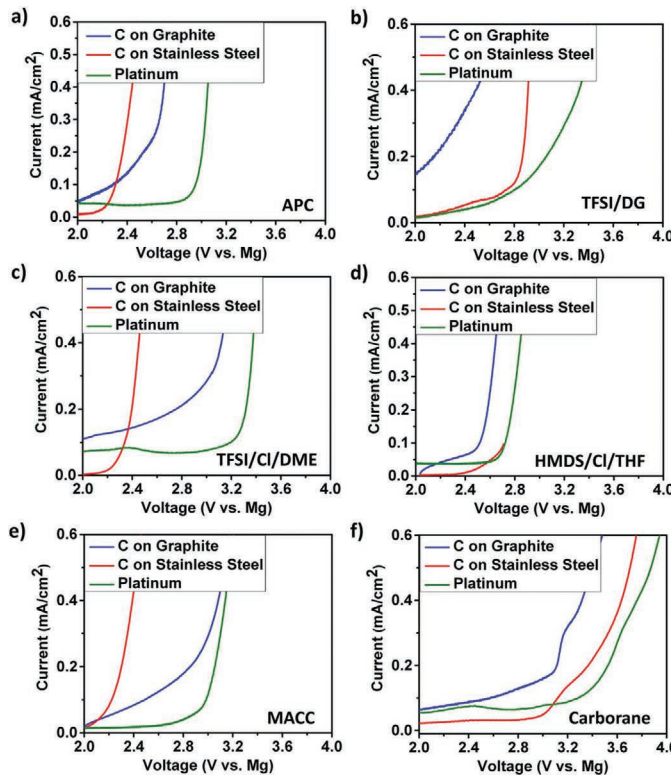


**Figure 5.9** Linear sweep voltammograms for a variety of electrolytes using Pt, carbon black on graphite foil, or carbon black on stainless steel as the working electrode, with Mg metal as the reference and counter electrodes. The electrolytes are (a) 0.4 M APC in THF, (b) 0.5 M Mg[TFSI]<sub>2</sub> in diglyme, (c) 0.5 M Mg[TFSI]<sub>2</sub> plus 1 M MgCl<sub>2</sub> in DME, (d) 0.3 M Mg[HMDS]<sub>2</sub> plus 1.2 M MgCl<sub>2</sub> in THF, (e) 0.04 M MgCl<sub>2</sub> plus 0.08 M AlCl<sub>3</sub> in THF, and (f) 0.5 M Mg[CB<sub>11</sub>H<sub>12</sub>]<sub>2</sub> in tetraglyme. Pt LSVs were measured at 100 mV/s, and the coated electrodes were measured at 5 mV/s. From Ref. [47]. Reproduced by permission of ECS—The Electrochemical Society.

## 5.8 Problem of Dendrites

As indicated in the early studies on magnesium deposition, the metallic layers obtained were solid and smooth—different from lithium metal, which suffers from ubiquitous growth of dendrites—see, for example, Ref. [48]. This strong belief in the dendrite-free

electrodeposition of magnesium should be at least partially revised and verified for any particular electrolyte used. For example, Ding et al. [49] studied magnesium growth from electrolytes comprising  $Mg[TFSI]_2$  dissolved in a mono-, di-, tri-, or tetraglyme. Symmetric coin-type cells with two magnesium electrodes were used. The authors observed the growth of spherical deposits with diameters of about 6–8  $\mu m$  and lamellar substructures. The growth of these globular dendrites damaged the polypropylene separators and led to the short-circuiting of the electrodes. It is also worth mentioning the theoretical study by Lautar et al. [50]. The authors analyzed the surface energies, work functions, adsorption energies, etc., in order to investigate the dependence of morphology evolution on surface orientation. Their conclusion was that dendrite growth during magnesium deposition could not be excluded and it depended on the particular electrolyte's composition and conditions of Mg growth.

## 5.9 Summary

The international search for reliable electrolytes for various types of magnesium batteries has not finished yet. Therefore, the presented descriptions of the electrolytes intentionally include both older concepts as well as new useful or promising systems. In fact, at least a few systems offer acceptable properties but there is still room for improvements in terms of not only deposition/stripping kinetics but also economy and safety issues. In addition, any electrolyte should be compatible with the electrodes in terms of composition and since the problem of high-capacity cathodes, both intercalation or conversion ones, has not been solved yet, electrolytes should be tested in combination with these electrode materials.

The simplest system is obviously the MACC electrolyte. It seems to be optimal for preliminary investigations of new anode/cathode systems but because of its corrosive nature and low ionic conductivity, it will perhaps not be implemented in a practical battery.  $Mg[TFSI]_2$  in ethereal solvents has good electrochemical stability, is noncorrosive, and is commercially available but ap-

parently suffers from too-high overpotentials. This deficiency can be removed by the addition of chlorides but at the expense of other problems. Magnesium *closو-carborane* in a triglyme or a tetraglyme, probably the most promising system, seems at the moment to fulfill the highest number of technical criteria but is expensive. And finally, dendrite growth of magnesium deposits is not excluded—a close inspection of any deposit morphology is necessary.

## References

1. R. F. Koontz, R. D. Lucero, Magnesium water-activated batteries, in *Handbook of Batteries*, eds. D. Linden, T. B. Reddy, McGraw-Hill, 2002, pp. 17.1–17.27.
2. H. D. Yoo, I. Shterenberg, Y. Gofer, G. Gershinsky, N. Pour, D. Aurbach, Mg rechargeable batteries: an on-going challenge. *Energy Environ. Sci.*, **6** (2013) 2265]; [R. Mohtadi, F. Mizuno, Magnesium batteries: current state of the art, issues and future perspectives. *Beilstein J. Nanotechnol.*, **5** (2014) 1291–1311].
3. P. Saha, M. K. Datta, O. I. Velikokhatnyi, A. Manivannan, D. Alman, P. N. Kumta, Rechargeable magnesium battery: current status and key challenges for the future, *Prog. Mater. Sci.*, **66** (2014) 1–86.
4. J. Muldoon, C. B. Bucur, T. Gregory, Quest for nonaqueous multivalent secondary batteries: magnesium and beyond. *Chem. Rev.*, **114** (2014) 11683–11720.
5. C. B. Bucur, T. Gregory, A. G. Oliver, J. Muldoon, Confession of a magnesium battery. *J. Phys. Chem. Lett.*, **6** (2015) 3578–3591.
6. J. Muldoon, C. B. Bucur, T. Gregory, Fervent hype behind magnesium batteries: an open call to synthetic chemists—electrolytes and cathodes needed. *Angew. Chem. Int. Ed.*, **56** (2017) 12064–12084.
7. R. Attias, M. Salama, B. Hirsch, Y. Goffer, D. Aurbach, Anode-electrolyte interfaces in secondary magnesium batteries. *Joule*, **3** (2019) 27–52.
8. D. Sharon, M. Salama, R. Attias, D. Aurbach, Electrolyte solutions for “beyond Li-ion batteries”: Li-S, Li-O<sub>2</sub>, and Mg batteries. *Electrochim. Soc. Interface*, **28** (2019) 71–77.
9. D. Aurbach, I. Weissman, Y. Gofer, E. Levi, Nonaqueous magnesium electrochemistry and its application in secondary batteries. *Chem. Rec.*, **3** (2003) 61.

10. Z. Lu, A. Schechter, M. Moshkovich, D. Aurbach, On the electrochemical behavior of magnesium electrodes in polar aprotic electrolyte solutions. *J. Electroanal. Chem.*, **466** (1999) 203.
11. S.-B. Son, T. Gao, S. P. Harvey, K. X. Steirer, A. Stokes, A. Norman, C. Wang, A. Cresce, K. Xu, C. Ban, An artificial interphase enables reversible magnesium chemistry in carbonate electrolytes. *Nat. Chem.*, **10** (2018) 532–539.
12. L. W. Gaddum, H. E. French, The electrolysis of Grignard solutions. *J. Am. Chem. Soc.*, **49** (1927) 1295–1299.
13. A. Brenner, J. L. Sligh, Electrodeposition of magnesium and beryllium from organic baths. NASA report CR-111850 (1971).
14. A. Brenner, Note on the electrodeposition of magnesium from an organic solution of a magnesium-boron complex. *J. Electrochem. Soc.*, **118** (1971) 99–100.
15. T. D. Gregory, R. J. Hoffman, R. C. Winterton, Nonaqueous electrochemistry of magnesium – applications to energy storage. *J. Electrochem. Soc.*, **137** (1990) 775–780.
16. C. J. Barile, R. Spatney, K. R. Zavadil, A. A. Gewirth, Investigating the reversibility of in situ generated magnesium organohaloaluminates for magnesium deposition and dissolution. *J. Phys. Chem. C*, **118** (2014) 10694–10699.
17. D. Aurbach, Z. Lu, A. Schechter, Y. Gofer, H. Gizbar, R. Turgeman, Y. Cohen, M. Moshkovich, E. Levi, Prototype systems for rechargeable magnesium batteries. *Nature*, **407** (2000) 724–727.
18. H. D. Yoo, I. Shterenberg, Y. Gofer, G. Gershinsky, N. Pour, D. Aurbach, Mg rechargeable batteries: an on-going challenge. *Energy Environ. Sci.*, **6** (2013) 2265–2279.
19. D. Aurbach, G. S. Suresh, E. Levi, A. Mitelman, O. Mizrahi, O. Chusid, M. Brunelli, Progress in rechargeable magnesium battery technology. *Adv. Mater.*, **19** (2007) 4260–4267.
20. N. Pour, Y. Gofer, D. T. Major, D. Aurbach, Structural analysis of electrolyte solutions for rechargeable Mg batteries by stereoscopic means and DFT calculations. *J. Am. Chem. Soc.*, **133** (2011) 6270–6278.
21. R. Mohtadi, M. Matsui, T. S. Arthur, S.-J. Hwang, Magnesium borohydride: from hydrogen storage to magnesium battery. *Angew. Chem. Int. Ed.*, **51** (2012) 9780.
22. Y.-s. Guo, F. Zhang, J. Yang, F. Wang, Electrochemical performance of novel electrolyte solutions based on organoboron magnesium salts. *Electrochim. Commun.*, **18** (2012) 24–27.

23. Y.-s. Guo, F. Zhang, J. Yang, F.-f. Wang, Y. NuLi, S.-i. Hirano, Boron-based electrolyte solutions with wide electrochemical windows for rechargeable magnesium batteries. *Energy Environ. Sci.*, **5** (2012) 9100–9106.
24. J. Muldoon, C. B. Bucur, A. G. Oliver, J. Zajicek, G. D. Allred, W. C. Boggess, Corrosion of magnesium electrolytes: chlorides – the culprit. *Energy Environ. Sci.*, **6** (2013) 482–487.
25. Z. Ma, M. Kar, C. Xiao, M. Forsyth, D. R. MacFarlane, Electrochemical cycling of Mg in Mg[TFSI]2/tetraglyme electrolytes. *Electrochim. Commun.*, **78** (2017) 29–32.
26. I. Krossing, I. Raabe, Noncoordinating anions—fact or fiction? a survey of likely candidates. *Angew. Chem. Int. Ed.*, **43** (2004) 2066.
27. R. N. Grimes, *Carboranes*, 3rd edition, Academic Press, 2016.
28. O. Tütusaus, R. Mohtadi, T. S. Arthur, F. Mizuno, E. G. Nelson, Y. V. Sevryugina, An efficient halogen-free electrolyte for use in rechargeable magnesium batteries. *Angew. Chem. Int. Ed.*, **54** (2015) 7900–7904.
29. H. Zhao, J. Zhou, P. Jena, Stability of  $\text{B}_{12}(\text{CN})_{12}^{2-}$ : implications for lithium and magnesium ion batteries. *Angew. Chem. Int. Ed.*, **55** (2016) 3704–3708.
30. H. S. Kim, T. S. Arthur, G. D. Allred, J. Zajicek, J. G. Newman, A. E. Rodnyansky, A. G. Oliver, W. C. Boggess, J. Muldoon, Structure and compatibility of a magnesium electrolyte with a sulphur cathode. *Nat. Commun.*, **2** (2011) 427.
31. Z. Zhao-Karger, X. Zhao, O. Fuhrer, M. Fichtner, Bisamide based non-nucleophilic electrolytes for rechargeable magnesium batteries. *RSC Adv.*, **3** (2013) 16330.
32. C. Liebenow, Z. Yang, P. Lobitz, The electrodeposition of magnesium using solutions of organomagnesium halides, amidomagnesium halides and magnesium organoborates. *Electrochim. Commun.*, **2** (2000) 641–645.
33. B. P. Vinayan, Z. Zhao-Karger, T. Diemant, V. S. K. Chakravadhanula, N. I. Schwarzburger, M. A. Cambaz, R. J. Behm, C. Kübel, M. Fichtner, Performance study of magnesium–sulfur battery using a graphene based sulfur composite cathode electrode and a non-nucleophilic Mg electrolyte. *Nanoscale*, **8** (2016) 3296.
34. C. Liao, N. Sa, B. Key, A. K. Burrell, L. Cheng, L. A. Curtiss, J. T. Vaughey, J. J. Woo, L. Hu, B. Pan, Z. Zhang, The unexpected discovery of the  $\text{Mg}(\text{HMDS})_2/\text{MgCl}_2$  complex as a magnesium electrolyte for

- rechargeable magnesium batteries. *J. Mater. Chem. A*, **3** (2015) 6082–6087.
35. L. C. Merrill, J. L. Schaefer, Electrochemical properties and speciation in Mg(HMDS)<sub>2</sub>based electrolytes for magnesium batteries as a function of ethereal solvent type and temperature. *Langmuir*, **33** (2017) 9426–9433.
  36. R. E. Doe, R. Han, J. Hwang, A. J. Gmitter, I. Shterenberg, H. D. Yoo, N. Pour, D. Aurbach, Novel, electrolyte solutions comprising fully inorganic salts with high anodic stability for rechargeable magnesium batteries. *Chem. Commun.*, **50** (2014) 243–245.
  37. G. Vardar, J. G. Smith, T. Thompson, K. Inagaki, J. Naruse, H. Hiramatsu, A. E. S. Sleightholme, J. Sakamoto, D. J. Siegel, C. W. Monroe, Mg/O<sub>2</sub> battery based on the magnesium–aluminum chloride complex (MACC) electrolyte. *Chem. Mater.*, **28** (2016) 7629–7637.
  38. T. T. Tran, W. M. Lamanna, M. N. Obrovac, Evaluation of Mg[N(SO<sub>2</sub>CF<sub>3</sub>)<sub>2</sub>]<sub>2</sub>/acetonitrile electrolyte for use in Mg-Ion cells. *J. Electrochem. Soc.*, **159**(12) (2012) A2005–A2009.
  39. S.-Y. Ha, Y.-W. Lee, S. W. Woo, B. Koo, J.-S. Kim, J. Cho, K. T. Lee, N.-S. Choi, Magnesium(II) bis(trifluoromethane sulfonyl) imide-based electrolytes with wide electrochemical windows for rechargeable magnesium batteries. *ACS Appl. Mater. Interfaces*, **6** (2014) 4063–4073.
  40. I. Shterenberg, M. Salama, H. D. Yoo, Y. Gofer, J.-B. Park, Y.-K. Sun, D. Aurbach, Evaluation of (CF<sub>3</sub>SO<sub>2</sub>)<sub>2</sub>N–(TFSI) based electrolyte solutions for Mg batteries. *J. Electrochem. Soc.*, **162**(13) (2015) A7118–A7128.
  41. M. Salama, I. Shterenberg, L. J. W. Shimon, K. Keinan-Adamsky, M. Afri, Y. Gofer, D. Aurbach, Structural analysis of magnesium chloride complexes in dimethoxyethane solutions in the context of Mg batteries research. *J. Phys. Chem. C*, **121** (2017) 24909–24918.
  42. M. Salama, I. Shterenberg, H. Gizbar, N. N. Eliaz, M. Kosa, K. Keinan-Adamsky, M. Afri, L. J. W. Shimon, H. E. Gottlieb, D. T. Major, Y. Gofer, D. Aurbach, Unique behavior of dimethoxyethane (DME)/Mg(N(SO<sub>2</sub>CF<sub>3</sub>)<sub>2</sub>)<sub>2</sub> solutions. *J. Phys. Chem. C*, **120** (2016) 19586–19594.
  43. F.-f. Wang, Y.-s. Guo, J. Yang, Y. Nuli, S.-i. Hirano, A novel electrolyte system without a Grignard reagent for rechargeable magnesium batteries. *Chem. Commun.*, **48** (2012) 10763–10765.
  44. Z. Ma, M. Forsyth, D. R. MacFarlane, M. Kar, Ionic liquid/tetraglyme hybrid Mg[TFSI]2 electrolytes for rechargeable Mg batteries. *Green Energy Environ.*, **4** (2019) 146–153.

45. G. A. Giffin, Ionic liquid-based electrolytes for “beyond lithium” battery technologies. *J. Mater. Chem. A*, **4** (2016) 13378.
46. M. Kar, O. Tütusaus, D. R. MacFarlane, R. Mohtadi, Novel and versatile room temperature ionic liquids for energy storage. *Energy Environ. Sci.*, **12** (2019) 566–571.
47. A. L. Lipson, S.-D. Han, B. Pan, K. A. See, A. A. Gewirth, C. Liao, J. T. Vaughey, B. J. Ingram, Practical stability limits of magnesium electrolytes. *J. Electrochem. Soc.*, **163**(10) (2016) A2253–A2257.
48. D. Aurbach, Y. Cohen, M. Moshkovich, The study of reversible magnesium deposition by in situ scanning tunneling microscopy. *Electrochem. Solid-State Lett.*, **4** (2001) A113–A116.
49. M. S. Ding, T. Diemant, J. Behm, S. Passerini, G. A. Giffin, Dendrite growth in Mg metal cells containing Mg(TFSI)<sub>2</sub>/glyme electrolytes. *J. Electrochem. Soc.*, **165**(10) (2018) A1983–A1990.
50. A. Kopac Lautar, D. Kopac, T. Rejec, T. Bancic, R. Dominko, Morphology evolution of magnesium facets: DFT and KMC simulations. *Phys. Chem. Chem. Phys.*, **21** (2019) 2434.

## Chapter 6

# Multivalent Cation Systems: Toward Aluminum, Zinc, and Calcium Batteries

**Michał Piszcza and Maciej Siekierski**

*Faculty of Chemistry, Warsaw University of Technology, Noakowskiego 3,  
00-664 Warszawa, Poland  
alex@ch.pw.edu.pl*

### 6.1 Introduction

The supremacy of sodium and potassium over lithium is not related to their electrochemical properties but to their critically higher abundance in the earth's crust and, therefore, significantly easier availability and lower price. On the other hand, electrolytes with multivalent charge carriers, together with the use of appropriate anodes, are natural candidates for high-energy-density batteries due to their properties, which lead to chemical stability and operational safety with a relatively low equivalent molar weight (12 for magnesium and 9 for aluminum), comparable to this characteristic of lithium. The driving force behind research on post-lithium multivalent materials is, therefore, related to surpassing the properties of these metals in terms of the achievable energy

---

*Designing Electrolytes for Lithium-Ion and Post-Lithium Batteries*

Edited by Włodzisław Wieczorek and Janusz Płocharski

Copyright © 2021 Jenny Stanford Publishing Pte. Ltd.

ISBN 978-981-4877-16-9 (Hardcover), 978-1-003-05093-3 (eBook)

[www.jennystanford.com](http://www.jennystanford.com)

density. The gain of electrochemical properties like volumetric and gravimetric capacity, together with economical aspects, makes them much more attractive than the currently used Li-based materials. An additional advantage of the proposed materials is related to their much easier handling than lithium or sodium, where strict conditions and the risk of spontaneous decomposition and/or ignition is a serious problem. To fulfill the expectation of metallic anodes based on multivalent metals the electrolyte is the only limitation. The serious bottleneck in electrolytes with multivalent cations is related to their complex electrochemistry, including electrolyte properties and electrode reactions, and the not-transferable know-how from Li-ion technology. However, even in the case of lithium in its early stages of investigation, its practical application was not easy. It was only after many years of intensive research that the problems with Li batteries were overcome. In fact, the appropriate electrode and an understanding of the fundamental electrode/electrolyte behavior were the key points. Successful application of a metal is mostly limited by the development of the appropriate electrolyte, one that makes reversible reactions on the electrodes possible. Apart from the widely investigated application of magnesium, the other metals are really attractive and have to be tested as candidates for future battery chemistries.

Figure 6.1 gives basic information about the possible anode metallic materials (naturally transferred to cations in the electrolytes) that can be applied in batteries [1]. The significant difference can be found in the first two graphs of Fig. 6.1, showing data regarding their abundance and what is natural if commercialization is targeted—the price. In terms of volumetric capacity, Al reaches the highest value because of a three-electron redox reaction and low density ( $8056 \text{ mA g cm}^{-3}$ ). Considering the standard potential of multivalent metals, calcium reaches the lowest value of  $-2.86 \text{ V}$  versus standard hydrogen electrode (SHE). The combined values of these parameters can be, ion consequence, directly transferred to the high-energy-density value of the relevant batteries. Apart from magnesium, high gravimetric capacity and low potential make Al and calcium the best candidates for high-power batteries. Though it does not look too attractive in the list, zinc appears in it because of another reason. Higher potential, in this

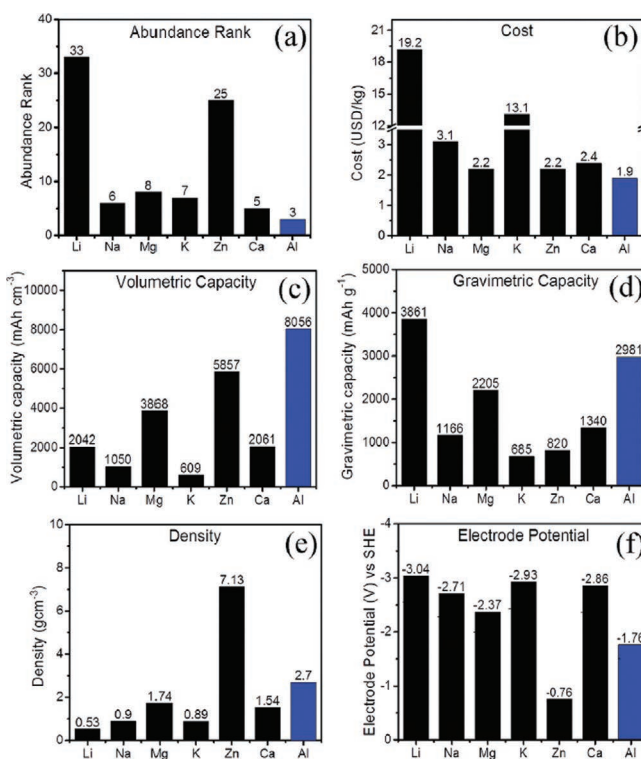


**Figure 6.1** Comparison of basic properties of different metals as anode candidates [26].

case, leads to milder operating conditions and, as a consequence, use of “totally safe” components, that is, water with appropriate additives. This makes zinc a good candidate for modern batteries not only limited to alkaline type. The scientific society needs to put in huge effort to identify the best electrolyte solutions not interfering with the anode structures of numerous, metal anodes exhibiting attractive properties.

As mentioned earlier in the book, the electrolyte and the electrode together give a two-phase system with special interfacial properties. The oxidized stage of metals in the electrolytes is one major factor essential for proper operation. Multivalent cations have much stronger coulombic interaction with anion and solvent

because of their high charge and low ionic radii. For example, the radii of  $Zn^{2+}$ ,  $Li^+$ , and  $Mg^{2+}$  are above 0.7 Å and of  $Na^+$  and  $Ca^{2+}$  are close to 1 Å and extreme values are represented by  $K^+$  ( $r = 1.38$  Å) and  $Al^{3+}$  ( $r = 0.53$  Å). This entails a series of potential problems with multivalent ions: (i) there is salt dissociation, where strong coulombic interactions have to be broken by high-dielectric-constant ( $\epsilon$ ) solvents, (ii) after salt dissociation, the interaction with solvent molecules is much stronger, restricting electrochemical reactions, and (iii) solvent interactions with anions result in ion pairing and creation of electrochemically inactive ion pairs. The higher charge and/or smaller ionic radius leads to an ion with a higher surface charge density.

A high-dielectric-constant solvent may dissolve salts to sufficient concentration, but later, strong interactions between solvent molecules and ions will make them more resistant to electrochemical reactions. Additionally, the solvation shell can be much bigger than in the case of single-valence ions, decreasing ion mobility. At the same time, the electrolyte has to guarantee high ionic conductivity, reached by the low-viscosity solvent. Even when the electrolyte operates at ambient temperature, its electrochemical stability must not be overlooked. A compromise between all the properties is key for the successful operation of all types of electrolytes. As an electrolyte is a unique medium in contact with all cell components and governs the battery electrochemistry, it is essential to achieve a long cycle life. The selection of electrolyte components is, therefore, crucial for a commercially viable and successful battery. The evolution of the selected electrolyte types is, hence, described below.

The discussion in this chapter does not cover issues like cathode electrode materials, which are much more complex for multivalent ions, and corrosion in full cell conditions, which has a significant impact on overall battery operation, especially in the case of highly corrosive electrolytes. However, it has to be clear that at least in terms of the metallic anode, one of the important challenges is related to the electrolyte/electrode interface, where a highly resistive passivation layer can be formed (i.e., a metal oxide layer). The passivation layer affects the overall battery power performance. The reversibility of the electrode reactions, such as dendrite growth and efficiency, is tuned by the changes in the electrolyte composition.

In addition, differences exist between various electrode materials in terms of their stiffness. For example, Young's modulus values of Li, Mg, Ca, and Al are 4.9 GPa, 45 GPa, 20 GPa, and 69 GPa, respectively. The high values cause significant trouble in anode thin film production in the whole design of the cell.

## 6.2 Aluminum

As mentioned earlier, an aluminum cation has a triple charge (three-electron reaction) and the gravimetric capacity of aluminum is equal to  $2981 \text{ mA h g}^{-1}$ , with a potential versus SHE equal to  $-1.76 \text{ V}$ . Together with the relatively low density of aluminum ( $d = 2.7 \text{ g cm}^{-3}$ ), it has a 4 times higher volumetric capacity than Li metal. In addition, Al is first in terms of abundance among all metals, making it extremely attractive. Moreover, the price of aluminum (10 times lower than lithium) reduces the cost of kilowatt-hours of potential Al battery. Assuming all of the above, aluminum is an attractive candidate for multivalent electrolytes for batteries. Nonetheless the aluminum cation, with a high charge and a small radius ( $0.56 \text{ \AA}$ ), has the highest surface charge density among all the ions presented above. Because this property owes its existence to the presence of strong coulombic forces, dissociated ions have strong and large-in-volume solvation shells. This results in low diffusion of ions inside the liquid electrolyte. Moreover, when one focuses on the properties of the electrolyte/metallic electrode interface, pristine aluminum is passivated by a protective aluminum oxide ( $\text{Al}_2\text{O}_3$ ) layer. Unfortunately, even when exhibiting thickness of only a few nanometers ( $\sim 5 \text{ nm}$ ) in an ambient atmosphere/conditions, it is a good electronic and ionic insulator. This oxide layer reduces the plating reaction potential to a value below the theoretical value, causing a delay in or complete ceasing of the electrochemical activity of aluminum. Therefore, it focuses the natural trend in electrolyte development on the improvement of ion transport by, for example, appropriate solvent composition selection, resulting in reduced viscosity of the solution. Electrolytes have to reduce the negative effect of interfacial reactions on the metallic electrode. In addition, batteries based on aluminum (due to relatively high thermal stability

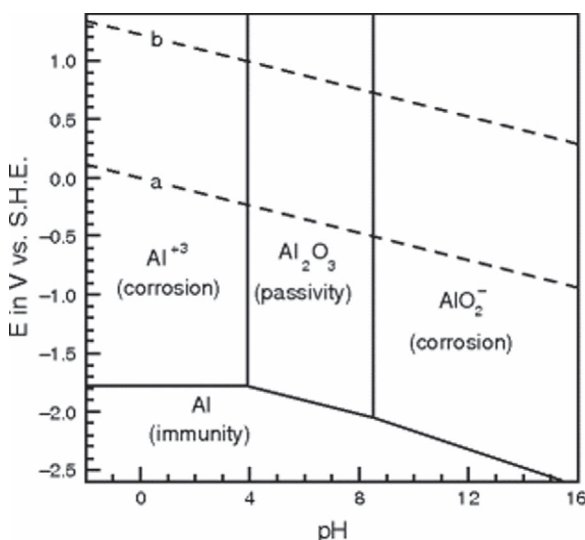


**Figure 6.2** Pourbaix diagram of Al [2].

of the interfacial layer and possibility of different solvent choice) are declared as ones exhibiting a much wider operational temperature window ( $-30^{\circ}\text{C}$  to  $+80^{\circ}\text{C}$ ) in comparison with the commercially available lithium-ion cells and supercapacitors [2].

### 6.2.1 Water-Based Electrolytes

The application of water-based electrolytes has many advantages, like low cost, simple operation, and favorable environmental factor. However, aluminum reduction in an aqueous solution at thermodynamic potential ( $E_o = -1.66$  V versus SHE) is hindered by the hydrogen evolution reaction that takes place at a more positive potential value (Fig. 6.2) [2]. The acidic medium is completely excluded from practical applications as the spontaneous oxidation of aluminum anode destroys the cell. The high pH value can be an attractive feature for an electrolyte in terms of Al oxidation, mostly in systems based on alloyed anodes.

The first attempt to create Al-based batteries was made using aqueous media with simple basic solutions. In the nineteenth

century, the Buff cell [3], based on Al anode and carbon cathode, was investigated. One century later, in 1950, the dry Leclanche cell was presented [2, 4]. In the following years, several primary aluminum systems were proposed, such as Al/MnO<sub>2</sub>, Al/Ag<sub>2</sub>O, Al/H<sub>2</sub>O<sub>2</sub>, Al/S, Al/Fe(CN)<sub>6</sub><sup>3-</sup>, and Al/NiOOH [5], all working in aqueous media. However, the presented batteries are of the primary type, without even the possibility of charging. Moreover, the effective electrochemistries of the relevant cells are plagued by the formation of an oxide layer. This passive film on the aluminum metal anode decreases the battery voltage and efficiency. According to the Pourbaix plot, alkali media can act here as potent corrosive agents, needed to dissolve the aluminum oxide passivation film (Fig. 6.2). The basicity of the electrolyte has to be sufficiently high to overcome the solubility of Al(OH)<sub>3</sub> and form favorable Al(OH)<sub>4</sub><sup>-</sup>. The potential of the anode cleansed by the alkali media is, therefore, close to its thermodynamic value. However, the alkali media result in an accelerated rate of wasteful corrosion, limiting the battery shelf life [6]. On the other hand, reversal of the reaction of aluminum plating in terms of hypothetical battery charging is also problematic at least for two reasons. The limited surface diffusion of ions before charge transfer upon the electrode reaction is responsible for dendrite formation, which makes smooth aluminum plating impossible. Moreover, the thermodynamic reduction potential of nonpassivated aluminum is much below the hydrogen evolution of protonic solvents and, hence, deposition of aluminum is impossible in aqueous electrolytes. This was the main driving force behind the development of the alloyed Al-air batteries. Therefore, a separate description should be provided for the cases of the 'classical' pure Al anode, as well as, for the Al alloys based ones. A few solutions related to primary Al batteries working with aqueous electrolytes are presented below.

Manganese compounds were utilized as cathode and Al alloys as anode. The electrolytes used were mostly AlCl<sub>3</sub>\*6H<sub>2</sub>O and CrCl<sub>3</sub>\*6H<sub>2</sub>O as potent corrosive agents and later alkaline solutions KOH and NaOH. Moreover, additives like 0.3 M KMnO<sub>4</sub> and 0.006 MNa<sub>2</sub>SnO<sub>3</sub> were utilized [7]. The electrolyte composition with Mn and Sn compounds maximizes aluminum columbic efficiency and enhances cell voltage, increasing the operational voltage and, in consequence, permitting high aluminum discharge currents [8].

Alternatives to Mn-based cathodes are batteries with silver oxide active material [9]. Relatively high power and energy efficiency are attractive characteristics, but these batteries have found application mostly in underwater and military applications. An electrolyte dedicated for silver oxide cathodes is a concentrated alkaline solution (38%–40%). By changing the concentration of the metal hydroxide, the ionic conductivity can be tuned. However, such a high base concentration may accelerate oxidation of cell elements and enhance the polarization phenomena appearing at very high discharge rates. In some particular cell constructions, the cathode application determines the electrolyte composition. While focusing on the application of Al batteries in underwater applications, seawater can be applied as an electrolyte, with the addition of  $\text{H}_2\text{O}_2$  as an oxidizing agent [10].

Al-sulfur batteries are based on alkaline electrolytes with  $\text{K}_2\text{S}$  as the additive, where apart from  $\text{OH}^-$ -based compounds, various poly(sulfides) are present, like  $\text{S}^{2-}$ ,  $\text{S}_2^{2-}$ ,  $\text{S}_3^{2-}$ , ...,  $\text{S}_8^{2-}$ . An important fact is that these batteries, despite a potential of around 1.7 V, have a very high faradic capacity of  $361.7 \text{ Ah kg}^{-1}$ . There are another types of Al-water-based batteries, with either ferricyanide or nickel oxide hydroxide counter electrodes but both these combinations are also based on an alkaline solution.

Summarizing water-based electrolytes, the alkaline solution is needed to dissolve the passivation layer but restricts the battery application only to primary cells with Al metal electrode. The main effort for electrochemical improvement is focused on proper electrodes modification. So far, three electrode materials have shown success in terms of a reversible reaction with  $\text{Al}^{3+}$  in aqueous electrolytes: anatase  $\text{TiO}_2$ , copper-hexacyanoferrate ( $\text{CuHCF}$ ), and aerogel  $\text{V}_2\text{O}_5$  [11–16]. As the designs do not contain Al metal anodes, agents to passivate the strong corrosive characteristic of an “extreme” alkaline solution are in these cases not needed. Of course, the replacement of the metallic electrode results in a much lower cell capacity. Most of the electrolytes are based on  $\text{Al}(\text{NO}_3)_3$  or  $\text{Al}_2(\text{SO}_4)_3$ , both of which are highly water soluble. However, the full Al-ion cell was assembled utilizing  $\text{TiO}_2$  as an anode material and  $\text{CuHCF}$  as a cathode one [17], with the aqueous  $\text{AlCl}_3$  solution as an electrolyte. The water-based electrolyte is characterized by a

low pH value, resulting from cationic hydrolysis. The 1 M solution of  $\text{AlCl}_3$  as an electrolyte is sufficiently stable against hydrogen evolution even at 1.5 V versus saturated calomel electrode (SCE). The addition of HCl decreases the pH value and increases the cathodic peak current by hydrogen evolution on the anatase anode but without dominant intercalation/adsorption of hydrogen ion over the  $\text{Al}^{3+}$  ones. The anode was stabilized by the presence of the  $\text{Al}^{3+}$  ions. The oxidation of the  $\text{TiO}_2$  electrode was slightly affected by the addition of hydrochloric acid. While the cathodic oxygen evolution appears on the cathode surface above 1.3 V versus SCE, its operational potential has to be limited to 1 V versus SCE. Moreover, the application of an electrolyte containing 1 mol  $\text{dm}^{-3}$  KCl results in no rise in the redox activity of the anode. Therefore, the redox phenomena were related to the presence of the  $\text{Al}^{3+}$  ions in the electrolytic solution. The cathode side exhibits more facile insertion of  $\text{K}^+$  in comparison with the  $\text{Al}^{3+}$  ones. The use of a mixed  $\text{Al}^{3+}/\text{K}^+$  electrolyte in the cell based on  $\text{TiO}_2$  and CuHCF makes the design, in fact, the aluminum-potassium battery.

### 6.2.2 Nonaqueous Systems

The main features related to the application of a nonaqueous electrolyte in aluminum electrochemistry are high conductivity of the system, improved electrode kinetics, and the electrolyte's wide stability potential window. The group of the said electrolytes comprises three major families: chloroaluminate salts, room temperature molten salts/ionic liquids, and organic solvent-based systems [2, 18].

The  $\text{NaCl}-\text{AlCl}_3$  system was invented way back in the 1970s [19]. In these systems,  $\text{Na}^+$  can be substituted by  $\text{K}^+$  and the molar ratio of  $\text{MCl}:\text{AlCl}_3$  can be tuned. The higher the aluminum salt content, the higher is the system acidity, and the predominant type of charge carrier is, therefore, shifted from  $\text{AlCl}_4^-$  toward  $\text{Al}_2\text{Cl}_7^-$  anions. Importantly, both complexes can discharge on the cathode, allowing for cathodic deposition of aluminum. The dependence of the electrode exchange current density on the composition of the melt (mole fraction of  $\text{AlCl}_3$ ) for the aluminum ion charge transfer process, an important feature, was proved. Therefore, a multistep

electrode reaction mechanism was proposed [20, 21]. Moreover, investigations have proven a dominant effect of the aluminum chloride ( $\text{AlCl}_3$ ) content on the appearance of aluminum deposits obtained. Therefore, the dendritic growth of the deposited layer can be controlled and overridden. To obtain this expected feature, the current density must be strictly controlled or the addition of an organic suppressor, such as tetraethyl ammonium chloride or urea [22], must be considered. Inorganic additives, such as  $\text{PbCl}_2$ ,  $\text{SnCl}_2$ , and  $\text{MnCl}_2$ , are on the other hand, of lesser importance. Many attempts with various cathodes, such as chlorine, sulfur, and sulfides, were made.  $\text{FeS}_2$  and  $\text{FeS}$  are the most common cathode materials due to their wide availability. For example, at  $175^\circ\text{C}$ , an  $\text{Al}/\text{NaCl}-\text{AlCl}_3/\text{MeS}_2$  battery system [23] was found to exhibit a high discharge capacity, unfortunately along with a significant capacity loss upon cycling. The latter was attributed to the solubility of metal sulfides in the melted electrolyte. In further works [24, 25], the operational temperature of the cell was decreased to  $100^\circ\text{C}$  by means of electrolyte composition optimization. A detailed overview of numerous chloride-based electrolytic systems applicable in the secondary aluminum cells, together with the juxtaposition of appropriate cathode materials, is given in Ref. [26] by Das et al. Moreover, the authors identify the elevated operational temperature of the said systems as their predominant drawback and suggest the addition of room temperature ionic liquids (RTILs) to them as a partial solution to this problem.

Further decrease of the operational temperature can be achieved by the sole use of organic chlorides, such as *n*-butyl-pyridinium-chloride, 1-methyl-3-ethylimidazolium-chloride, and 2-dimethyl-3-propylimidazolium-chloride [27–30]. An electrolyte is obtained through the dissolution of the aluminum chloride in these RTILs. Therefore, a molten mixture of 1,4-dimethyl-1,2,4-triazolium chloride and  $\text{AlCl}_3$  has been proposed for use in the secondary battery [31]. Another ionic liquid widely used as an aluminum secondary cell electrolyte consists of aluminum chloride and 1-butyl-3-methylimidazolium chloride [32]. It is proved that by controlling the  $\text{Al}_2\text{Cl}_7^-$  concentration and thus the molar ratio of the constituents, one can significantly influence the electrochemical performance of these chlorides. Wang et al. [33] performed a thorough study of

the same cation-based ionic liquid– $\text{AlCl}_3$  electrolytes containing  $\text{Cl}^-$ ,  $\text{Br}^-$ , and  $\text{I}^-$  counter ions as their organic part. The widest stability window was observed for the chlorides (4.7 V), while it was 3.9 V for the bromides and only 2 V for the iodides. The ionic conductivities of the electrolytes followed the same pattern. Moreover, the stability was found to be composition dependent. For example, for Al: BMI molar ratios in the 1:1 to 2:1 range, the anode limiting potential was found to be equal to 2.6 V versus  $\text{Al}/\text{Al}^{3+}$ , while for the ratio equal to 0.8, it was limited to 1.75 V. In another study, delivered by Wang et al. [34], a high-quality natural graphite cathode was successfully tested in a cell containing the currently known electrolyte  $\text{AlCl}_3$ /[EMIm]Cl. The molar ratio of  $\text{AlCl}_3$  to 1-ethyl-3-methylimidazolium chloride ([EMIm]Cl) was fixed at about 1:3, and simple mixing was used as the method of electrolyte synthesis. The same electrolyte was tested against CMK-3 mesoporous carbon-based cathode by Zafar and coworkers [35], obtaining a design that was called “a super-long-life” one. The stability of the battery was determined to be higher than 36,000 reversible cycles, with 97% coulombic efficiency. In addition, to modify the performance of the ionic liquid-based aluminum electrolytes with  $\text{AlCl}_3/\text{Et}_3\text{NHCl}$ , organic solvents such as toluene, benzene, dichloromethane (DCM), and 1,2-dichlorethane (DCE) were applied. Compositions with solvent:electrolyte molar ratios in the 0.1 to 1 range were investigated by Xia et al. [36]. DCM and DCE were found to be superior to the two aromatic compounds, while the optimized volume ratio was determined to be equal to 0.2. It was found that the performance of the aluminum secondary battery can be greatly improved by these means. It is worth noticing that the deposition and dissolution of aluminum in quaternary ammonium chloroaluminate-based ionic liquids has a current efficiency ranging from 85% to 100% [37]. Haloaluminate-based ionic liquids, unfortunately, suffer from certain drawbacks, enlisted by Das et al. in Ref. [26]. They are found to be corrosive, viscous, and hygroscopic. Therefore, the halogen-free variants of the RTIL electrolyte bases are investigated. Many of them have found application in aluminum deposition. On the other hand, only a few reports of their use in batteries have been delivered till now. For example, Wang et al. [38] developed a noncorrosive and water-stable electrolyte from aluminum tri-fluoromethansulfonate

( $\text{Al}[\text{TfO}]_3$ ) and 1-butyl-3-methylimidazolium trifluoromethanesulfonate. The solution was tested in an Al-V<sub>2</sub>O<sub>5</sub> cell. Though 1-butyl-1-methylpyrrolidinium bis(trifluorome-thanesulfonyl)imide and 1-ethyl-3-methylimidazolium bis(trifluoromethanesulfonyl)imide were proposed as Al-cell electrolytes, no results of their successful battery testing were delivered by Elia and coworkers in the same research paper [39]. Finally, it is worth stressing that RTIL electrolyte immobilization into a polymer gel leads to an unfavorable complexing of the chloroaluminate anions with the polymeric chains. This unwanted phenomenon is observed for PEO, PAN, PMMA, and PFdF [39]. On the other hand, PAAM was successfully used for this purpose by Sun et al. [40] for an [EMIM]Cl-AlCl<sub>3</sub> system.

When it comes to the third and last of the above-mentioned electrolyte families—the ones utilizing organic solvents—Kitada et al. presented the first evidence of the reversible electrodeposition of Al from an AlCl<sub>3</sub> solution in a diglyme (1:5 molar ratio) [41]. Their investigation was extended to other ether-based electrolytes, such as triglymes, tetraglymes, and butyldiglyme [42]. According to the authors, the glyme-based systems can be considered as ionic liquids as well, which seems to be a slightly curious claim. The electrolyte investigated by Reed et al. [43] was composed of a diglyme solution of  $\text{Al}[\text{TfO}]_3$ . The results presented for the latter case are partially similarly to the former ones mentioned above as the reversible Al deposition was confirmed here as well but for only a few initial electrochemical cycles. Later, severe passivation of the Al electrode was observed hindering the process of interest. A new Al(ClO<sub>4</sub>)<sub>3</sub>-based electrolyte reported by Zhang et al. [44] was obtained by the dissolution of a carefully dehydrated salt in a propylene carbonate (PC)-fluoroethylene carbonate mixture. The battery prepared from this exhibited high discharge voltage plateaus (about 1 V) together with high rate capacity and long cycle life (more than 400 cycles). The said battery is claimed by the authors to be a member of a novel “dual ion” design class due to the fact that aluminum plating on the anode is parallel to the intercalation of the ClO<sub>4</sub><sup>-</sup> anions into the specially prepared 3D graphene-based cathode.

### 6.3 Calcium

While most of the attention in multivalent ion battery development has focused on Mg-ion batteries, works of Gummow et al. [45] have focused on calcium. This at-the-first-glance exotic point of interest can be easily explained if one takes into consideration not only its electrochemical properties but also its availability and price and the lack of environmental hazards related to its use. However, its reactivity draws security risks that are high in comparison with those of magnesium and aluminum but fairly acceptable in comparison with those of lithium, sodium, and first of all potassium. In contrast to many other multivalent metal systems, research in the field of Ca-based ones is still in its infancy since the reversible deposition and stripping of calcium in conventional electrolytes was first demonstrated in 2016 by Ponrouch and coworkers [46]. The reported process is limited to the elevated temperature range, affecting the operational conditions of the resulting cells. A wide range of solvent-salt combinations was tested against calcium electrodes in a 1991 study by Aurbach [47]. Butyrolactone (BL), PC, acetonitrile, and tetrahydrofuran (THF) were used as solvents while  $\text{Ca}(\text{ClO}_4)_2$  was used as a salt in the first stage of the investigation. Due to the inapplicably low solubility of the chosen salt in THF, in the second stage, THF was investigated in combination with  $\text{LiClO}_4$  and  $((\text{CH}_3)_3\text{C})_4\text{NClO}_4$ . The third stage covered the electrolytes comprising of  $\text{LiClO}_4$  and  $((\text{CH}_3)_3\text{C})_4\text{NClO}_4$  salts and BL as a solvent. In all cases, the first cycle voltammograms were quite different from the steady-state ones. Therefore, the irreversible character of the calcium deposition and stripping processes was confirmed for all the systems studied. Additional confirmation of this conclusion can be drawn from spectroscopic studies presented herein. Obtained Fourier transform infrared spectra were typical for solvent reduction but not calcium deposition products.

Similarly defined problems related to the limited reversibility of the plating/stripping reaction concern the relatively new research in the field of calcium anode-based batteries utilizing “classical” cathode materials. For example, modified Prussian blue-based cathode material was tested in calcium coin cells by Tojo et al. [48].

A 0.5 M  $\text{Ca}(\text{TFSi})_2$  solution in acetonitrile  $\text{CH}_3\text{CN}$  was used as an electrolyte. The cell worked in ambient temperature and showed reversible capacities of 40 mA h g<sup>-1</sup> even at 12 cycles without destruction of the open framework structure of the cathode material under investigation. One of the major limitations in the development of calcium cells found by Ponrouch and Palacin [49] was related to the limited availability of the appropriate salts. Therefore, the synthesis of  $\text{Ca}(\text{PF}_6)_2$  salt, a direct analog of the most commonly used lithium salt, has been reported recently by Ingram et al. [50] and by the group headed by Grey [51]. According to Ingram, the in-house obtained salt was applicable in a cell as an ethylene carbonate (EC) solution despite the significant decomposition of the anion.

In consequence of the above drawback, an aqueous electrolyte based on a 1 M  $\text{Ca}(\text{NO}_3)_2$  solution was tested as an interaction media for calcium ions into a potassium birnessite  $\text{K}_{0.31}\text{MnO}_2 \cdot 0.25\text{H}_2\text{O}$  anode material. The authors stipulate that the successful intercalation demonstrated by Hyoung et al. in Ref. [52] is indicative of a successful aqueous calcium cell design. No suggestions toward a compatible cathode were provided in the paper, which limits somehow the value of the provided prediction. In addition, Staniewicz investigated a primary  $\text{Ca}-\text{SOCl}_2$  cell, an analog of the well-known “liquid cathode” lithium-based commercial solution, as early as in 1980 [53]. The electrolyte here was made of  $\text{SOCl}_2$  with one of the three in-house developed calcium salts,  $\text{Ca}(\text{AlCl}_4)_2$ ,  $\text{Ca}(\text{FeCl}_4)_2$ , and  $\text{Ca}(\text{SbCl}_6)_2$ , being dissolved in it.

A research study claimed as a breakthrough was recently reported by researchers from the Karlsruhe Institute of Technology [54]. A newly developed salt calcium tetrakis(hexafluoroisopropoxy)borate forms a stoichiometric 1:4 complex with dimethoxyethane (DME), melting in 57°C and remaining stable up to 97°C, when partial decomposition related to DME release is observed. The solid complex can be dissolved in an appropriate solvent—which in the simplest case will be DME. The so-obtained electrolyte allows for reversible plating and striping of calcium in an ambient temperature, characterized by conductivity of about 8 mS/cm and exhibiting oxidative electrochemical stability up to 4.5 V. On the basis of the presented preliminary electrochemical results, this achievement is stipulated by its authors to be a key

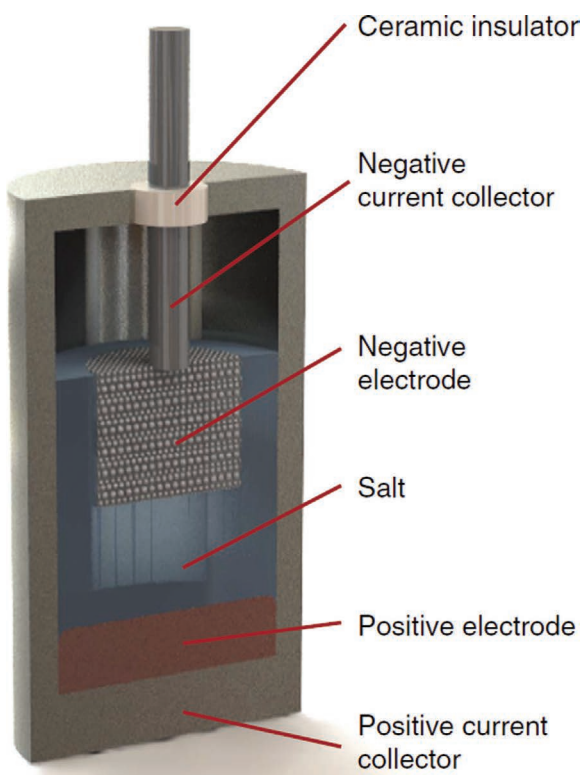


**Figure 6.3** Schematic diagram of the liquid metal battery [55].

opening to the commercialization of calcium batteries. Another promising and potentially fruitful concept of a calcium liquid metal battery was developed by Sadoway [55] (Fig. 6.3). In general, it consists entirely of liquid active components: a low-density liquid metal negative electrode, an intermediate-density molten salt electrolyte, and a high-density liquid metal positive electrode. Due to their mutual immiscibility, these active components further self-segregate into three distinct layers according to their densities. Here, a number of combinations based on elementary calcium and Ca-Mg alloys and various molten salt electrolytes were investigated against the Bi-based cathode. The electrolyte compositions as well as the obtained current densities are listed in Table 6.1.

**Table 6.1** Self-discharge current density of cells with a Bi positive electrode at 1.25 V

Negative electrode	Salt	Temperature (°C)	$J_{\text{self}}$ (mA cm <sup>-2</sup> )
Ca	CaCl <sub>2</sub>	800	>1000
Ca	CaCl <sub>2</sub> –CaI (51.4 and 48.6 mol%, resp.)	650	>300
Ca	LiCl–CaCl <sub>2</sub> (65 and 35 mol%, resp.)	650	~10
Ca–Mg (20 and 80 mol%, resp.)	LiCl–CaCl <sub>2</sub> (65 and 35 mol%, resp.)	650	~1
Ca–Mg (20 and 80 mol%, resp.)	LiCl–KCl–CaCl <sub>2</sub> (37, 28, and 35 mol%, resp.)	650	~4
Ca–Mg (20 and 80 mol%, resp.)	KCl–CaCl <sub>2</sub> (74 and 26 mol%, resp.)	650	~10
Ca–Mg (20 and 80 mol%, resp.)	LiCl–NaCl–CaCl <sub>2</sub> (37, 28, and 35 mol%, resp.)	650	~12
Ca–Mg (90 and 10 mol%, resp.)	LiCl–CaCl <sub>2</sub> (65 and 35 mol%, resp.)	650	~4

Source: [55]

## 6.4 Zinc

Zn is thermodynamically unstable in water and in various aqueous solutions, and it tends to dissolve in them, with the evolution of hydrogen over the whole pH range [56]. According to Li et al. [57], the majority of studies devoted to Zn electrochemistry focus on Zn-air batteries. Moreover, his report claims that selecting the proper electrolyte system is in this case critical in achieving a better-performing cell. The electrolytes most used in Zn-based batteries (e.g., rechargeable alkaline manganese dioxide, Ni-Zn, and Zn-Air) have been alkaline aqueous solutions containing potassium hydroxide (KOH) [58–60], sodium hydroxide (NaOH) [61–63],

and lithium hydroxide [64]. Particularly Zn anode-based batteries usually operate with the use of alkaline aqueous solutions of KOH and NaOH. According to Li and Dai [65], the former is more popular due to its good low-temperature performance, originating from faster electrode kinetics and higher conductivity of the solutions. The maximum electric conductivity of the solution is reached at 7 M or 30 wt.% of KOH dissolved. For example, 1 M KOH with the addition of 20 mM Zn(Ac)<sub>2</sub> was applied by Zhang et al. [66] in a novel cell design based on a zinc nanosheet anode material and a NiCo<sub>2</sub>O<sub>4</sub> nanosheets cathode. The major disadvantages correlated with the use of aqueous alkaline electrolytes are (i) the dissolution of zinc, (ii) precipitation of insoluble carbonates, (iii) electrolyte evaporation, (iv) ambient moisture uptake, and (v) hydrogen evolution. A more extensive description of these problems is given by Mainar et al. [67]. The incorporation of additives, inorganic [68–70] or organic [71], allows for overriding the major drawbacks of the alkaline electrolyte described by Xu and coworkers [72], such as dendritic growth, passivation, and self-discharge.

In addition, polymer-immobilized hydrogels were tested in these systems as a remedy for water loss being their crucial degradation factor. The said systems are not true solid polymeric electrolytes as the zinc ion mobility is related to the immobilized liquid phase and not to the polymeric one. KOH was immobilized in a polymeric system by Othman [73, 74]. According to Mohamad [75] hydrogelled 6 M KOH was found to improve the specific capacity of the battery while polyvinyl alcohol (PVA)-based hydrogel was claimed by Fu et al. [76] to improve the cyclability of the cell to more than 120 cycles. Moreover, poly(ethylene glycol) (average molecular weight [AMW] = 500 and 1000) with PVA (AMW = 5000) and m-PVA (AMW = 13,000) was tested by Kakeya and coworkers [77] as water activity controlling additives to 4 M KOH aqueous electrolyte, leading to enhanced zinc electrode rechargeability.

## 6.5 Conclusions

Whereas each of the above-described types of cell exhibits its own specific features, drawbacks, and problems, some common points

can be found despite these differences. First of all, in parallel to the great expectations, there is no evident commercial success of the “modern design” rechargeable cell utilizing multivalent metals. The main problems hindering such success are the chemical instability of the metallic anode toward the aqueous electrolytic solutions, its corrosion, and, in consequence, the need of application of corrosion inhibitors in the case of aluminum and zinc and sole use of a nonaqueous aprotic solvents in the case of the most reactive calcium. The application of nonaqueous designs is in this case as well as in the other two limited by the low reversibility of the metal striping/plating reaction related to the presence of insoluble reaction products. Solid polymeric electrolytes being a great expectation of the metallic lithium and sodium-based systems are here not applicable as the multivalent cations are strongly coordinated by the polymeric chains and, therefore, totally immobilized. In consequence, various aqueous and nonaqueous gel polymeric electrolytes are considered as an important alternative to the said. Therefore, due to the limited applicability of the classical cell designs, some novel highly specific ones, such as above-mentioned liquid metal battery [54], have been developed and reached the commercial stage. On the other hand, many problems and solutions concerning these cells are shared, with their air-cathode based counterparts described elsewhere in this book.

## References

1. G. Girishkumar, B. McCloskey, A. C. Luntz, S. Swanson, W. Wilcke, Lithium-air battery: promise and challenges. *J. Phys. Chem. Lett.*, **1** (2010) 2193–2203, doi: 10.1021/jz1005384.
2. Y. Hu, D. Sun, B. Luo, L. Wang, Recent progress and future trends of aluminum batteries. *Energy Technol.*, **7** (2019) 86–106.
3. H. F. Bauman, G. B. Adams, Lithium-water-air battery automotive propulsion. Final report, October 28, 1976–September 28, 1977. [360 mW/cm<sup>2</sup>]. United States: N. p., 1977. Web.
4. Unites States Patent #US3000997A, Leclanche type dry cells of high storageability.

5. J. L. Schaefer, Y. Lu, S. S. Moganty, P. Agarwal, N. Jayaprakash, L. A. Archer, Electrolytes for high-energy lithium batteries. *Appl. Nanosci.*, **2** (2012) 91–109, doi: 10.1007/s13204-011-0044-x.
6. G. Girishkumar, B. McCloskey, S. C. Luntz, S. Swanson, W. Wicke, Lithium-air battery: promise and challenges. *J. Phys. Chem. Lett.*, **1**(14) (2010) 2193–2203.
7. H. Zhou, Y. Wang, H. Li, P. He, The development of a new type of rechargeable batteries based on hybrid electrolytes. *ChemSusChem*, **3**(9) (2010) 1009–1019.
8. S. Licht, A novel aqueous aluminumpermanganate fuel cell. *Electrochim. Commun.*, **1**(1) (1999) 33–36, [https://doi.org/10.1016/S1388-2481\(98\)00010-1](https://doi.org/10.1016/S1388-2481(98)00010-1).
9. D. S. Keir, M. J. Pryor, P. R. Sperry, The influence of ternary alloying additions on the galvanic behavior of aluminum-tin alloys. *J. Electrochem. Soc.*, **116**(3) (2007) 319, <https://doi.org/10.1149/1.2411837>.
10. A. P. Karpinski, S. J. Russell, J. R. Serenyi, J. P. Murphy, Silver based batteries for high power applications. *J. Power Sources*, **91**(1) (2000) 77–82, [https://doi.org/10.1016/S0378-7753\(00\)00489-4](https://doi.org/10.1016/S0378-7753(00)00489-4).
11. Ø. Hasvold, K. H. Johansen, O. Mollestad, S. Forseth, N. Størkersen, The alkaline aluminium/hydrogen peroxide power source in the Hugin II unmanned underwater vehicle. *J. Power Sources*, **80** (1999) 254–260.
12. Y. J. He, J. F. Peng, W. Chu, Y. Z. Li, D. G. Tong, Black mesoporous anatase TiO<sub>2</sub> nanoleaves: a high capacity and high rate anode for aqueous Al-ion batteries. *J. Mater. Chem. A*, **2** (2014) 1721–1731.
13. S. Liu, G. L. Pan, G. R. Li, X. P. Gao, Copper hexacyanoferrate nanoparticles as cathode material for aqueous Al-ion batteries. *J. Mater. Chem.*, **3** (2015) 959–962.
14. L. D. Reed, S. N. Ortiz, M. Xiong, E. J. Menke, A rechargeable aluminum-ion battery utilizing a copper hexacyanoferrate cathode in an organic electrolyte. *Chem. Commun.*, **51** (2015) 14397–14400.
15. M. Pasta, C. D. Wessells, N. Liu, J. Nelson, M. T. McDowell, R. A. Huggins, M. F. Toney, Y. Cui, Full open-framework batteries for stationary energy storage. *Nat Commun.*, **5** (2014) 307, <https://doi.org/10.1038/ncomms4007>.
16. D. R. Trócoli, D. F. La Mantia, An aqueous zinc-ion battery based on copper hexacyanoferrate. *ChemSusChem*, **8** (2015) 481–485.
17. Z. Jia, B. Wang, Y. Wang, Copper hexacyanoferrate with a well-defined open framework as a positive electrode for aqueous zinc ion batteries. *Mater. Chem. Phys.*, **149–150** (2015) 601–606.

18. A. Holland, R. D. McKerracher, A. Cruden, R. G. A. Wills, An aluminium battery operating with an aqueous electrolyte. *J. Appl. Electrochem.*, **48**(3) (2018) 243–250, <http://doi.org/10.1007/s10800-018-1154-x>.
19. Q. Li, N. J. Bjerrum, Aluminum as anode for energy storage and conversion: a review. *J. Power Sources*, **110** (2002) 1–10.
20. B. R. Boston, in J. Braunstein, G. Mamantov, G. P. Smith (eds.), *Advances in Molten Salt Chemistry*, Vol. 1, Plenum Press, New York, 1971, p. 129.
21. K. Schultz, H. Hoff, Electrode kinetics of aluminium in chloride melts with respect to electrocrystallization. *Electrochim. Acta*, **17** (1972) 119–133.
22. K. Schultz, H. Hoff, Austauschstromdichte und komplexbildung von aluminium in alkalitetrachloroaluminaten. *Electrochim. Acta*, **17** (1972) 1783–1788.
23. K. Grjotheim, K. Matiasovsky, Some problems concerning aluminium electro-plating in molten salts. *Acta Chem. Scand. A*, **34** (1980) 666–670.
24. N. Takami, N. Koura, Improvement of the positive electrode for the Al/FeS<sub>2</sub> secondary cell with a basic AlCl<sub>3</sub>-NaCl melt. *Denki Kagaku*, **56** (1988) 28.
25. H. A. Hjuler, S. von Winbush, R. W. Berg, N. J. Bjerrum, A novel inorganic low melting electrolyte for secondary aluminum-nickel sulfide batteries. *J. Electrochem. Soc.*, **136** (1989) 901.
26. N. Takami, N. Koura, *J. Electrochem. Soc.*, **136** (1989) 730.
27. S. K. Das, S. Mahapatrab, H. Lahan, Aluminium-ion batteries: developments and challenges. *J. Mater. Chem. A*, **5** (2017) 6347–6367.
28. R. Gale, R. Osteryoung, Potentiometric investigation of dialuminum heptachloride formation in aluminum chloride-1-butylpyridinium chloride mixtures. *Inorg. Chem.*, **18** (1979) 1603–1605.
29. J. S. Wilkes, J. A. Levisky, R. A. Wilson, C. L. Hussey, Dialkylimidazolium chloroaluminate melts: a new class of room-temperature ionic liquids for electrochemistry, spectroscopy and synthesis. *Inorg. Chem.*, **21** (1982) 1263–1264.
30. G. F. Reynolds, C. J. Dymek, Primary and secondary room temperature molten salt electrochemical cells. *J. Power Sources*, **15** (1985) 109–118.
31. J. Dymek, G. F. Reynolds, J. S. Wilkes, *J. Power Sources*, **17** (1987) 134.
32. B. Vestergaard, N. J. Bjerrum, I. Petrushina, H. A. Hjuler, R. W. Berg, M. Begtrup, Molten triazolium chloride systems as new aluminum battery electrolytes. *J. Electrochem. Soc.*, **140** (1993) 3108.

33. F. Wu, N. Zhu, Y. Bai, Y. Gao, C. Wu, An interface-reconstruction effect for rechargeable aluminum battery in ionic liquid electrolyte to enhance cycling performances. *Green Energy Environ.*, **3** (2018) 71–77.
34. H. Wang, S. Gu, Y. Bai, S. Chen, N. Zhu, C. Wu, F. Wu, Anion-effects on electrochemical properties of ionic liquid electrolytes for rechargeable aluminum batteries. *J. Mater. Chem. A*, **3** (2015) 22677–22686.
35. D.-Y. Wang, C.-Y. Wei, M.-C. Lin, C.-J. Pan, H.-L. Chou, H.-A. Chen, M. Gong, Y. Wu, C. Yuan, M. Angell, Y.-J. Hsieh, Y.-H. Chen, C.-Y. Wen, C.-W. Chen, B.-J. Hwang, C.-C. Chen, H. Dai, Advanced rechargeable aluminium ion battery with a high-quality natural graphite cathode. *Nat. Commun.*, **8** (2017) 14283.
36. Z. A. Zafar, S. Imtiaz, R. Li, J. Zhang, R. Razaq, Y. Xin, Q. Lia, Z. Zhang, Y. Huang, A super-long life rechargeable aluminum battery. *Solid State Ionics*, **320** (2018) 70–75.
37. S. Xia, X.-M. Zhang, K. Huang, Y.-L. Chen, Y.-T. Wu, Ionic liquid electrolytes for aluminium secondary battery: influence of organic solvents. *J. Electroanal. Chem.*, **757** (2015) 167–175.
38. T. Schoetz, C. Ponce de Leon, M. Ueda, A. Bund, State of the art of rechargeable aluminum batteries in non-aqueous systems. *J. Electrochem. Soc.*, **164**(14) (2017) A3499–A3502.
39. H. Wang, S. Gu, Y. Bai, S. Chen, F. Wu, C. Wu, High-voltage and noncorrosive ionic liquid electrolyte used in rechargeable aluminum battery. *ACS Appl. Mater. Interfaces*, **8** (2016) 27444–27448.
40. G. A. Elia, K. Marquardt, K. Hoeppner, S. Fantini, R. Lin, E. Knipping, W. Peters, J.-F. Drillet, S. Passerini, R. Hahn, An overview and future perspectives of aluminum batteries, *Adv. Mater.*, **28**(35) (2016) 7564–7579.
41. X.-G. Sun, Y. Fang, X. Jiang, K. Yoshii, T. Tsuda, S. Dai, Polymer gel electrolytes for application in aluminum deposition and rechargeable aluminum ion batteries. *Chem. Commun.*, **52** (2016) 292–295.
42. A. Kitada, K. Nakamura, K. Fukami, K. Murase, *Electrochemistry*, **82** (2014) 946–948.
43. A. Kitada, K. Nakamura, K. Fukami, K. Murase, Electrochemically active species in aluminum electrodeposition baths of AlCl<sub>3</sub>/glyme solutions. *Electrochim. Acta*, **211** (2016) 561–567.
44. L. D. Reed, A. Arteaga, E. J. Menke, A combined experimental and computational study of an aluminum triflate/diglyme electrolyte. *J. Phys. Chem. B*, **119** (2015) 12677–12681.

45. E. Zhang, W. Cao, B. Wang, X. Yua, L. Wang, Z. Xu, B. Lu, A novel aluminum dual-ion battery. *Energy Storage Mater.*, **11** (2018) 91–99.
46. R. J. Gummow, G. Vamvounis, M. B. Kannan, Y. He, Calcium-ion batteries: current state-of-the-art and future perspectives. *Adv. Mater.*, **30** (2018) 1801702.
47. A. Ponrouch, C. Frontera, F. Barde, M. R. Palacin, Towards a calcium-based rechargeable battery. *Nat. Mater.*, **15** (2016) 169–172.
48. D. Aurbach, R. Skaletsky, Y. Gofer, The electrochemical behavior of calcium electrodes in a few organic electrolytes. *J. Electrochem. Soc.*, **138**(12) (1991) 3536–3545.
49. T. Tojo, Y. Sugiura, R. Inada, Y. Sakurai, Reversible calcium ion batteries using a dehydrated prussian blue analogue cathode. *Electrochim. Acta*, **207** (2016) 22–27.
50. A. Ponrouch, M. R. Palacin, On the road toward calcium-based batteries. *Curr. Opin. Electrochem.*, **9** (2018) 1–7.
51. A. L. Lipson, B. Pan, S. H. Lapidus, C. Liao, J. T. Vaughey, B. J. Ingram, Rechargeable Ca-ion batteries: a new energy storage system. *Chem. Mater.*, **27** (2015) 8442–8447.
52. E. N. Keyzer, P. D. Matthews, Z. Li, A. D. Bond, C. P. Grey, D. S. Wright, Synthesis of  $\text{Ca}(\text{PF}_6)_2$ , formed via nitrosonium oxidation of calcium. *Chem. Commun.*, **53** (2017) 573–4576.
53. J. Hyoung, J. W. Heo, S.-T. Hong, Investigation of electrochemical calcium-ion energy storage mechanism in potassium birnessite. *J. Power Sources*, **390** (2018) 127–133.
54. R. J. Staniewicz, A study of the calcium-thionyl chloride electrochemical system. *J. Electrochem. Soc.*, **127**(4) (1980) 782–789.
55. Z. Li, O. Fuhr, M. Fichtner, Z. Zhao-Karger, Towards stable and efficient electrolytes for room-temperature rechargeable calcium batteries. *Energy Environ. Sci.*, **12** (2019) 3496–3501.
56. T. Ouchi, H. Kim, B. L. Spatocco, D. R. Sadoway, Calcium-based multi-element chemistry for grid-scale electrochemical energy storage. *Nat. Commun.*, **7** (2016) 10999.
57. X. G. Zhang, *Corrosion and Electrochemistry of Zinc*, Plenum Press, New York, 1996.
58. Q. Li, J. Chen, L. Fan, X. Kong, Yi. Lu, Progress in electrolytes for rechargeable Li-based batteries and beyond. *Green Energy Environ.*, **1** (2016) 18–42.
59. W. J. Wruck, et al., Rechargeable  $\text{Zn}-\text{MnO}_2$  alkaline batteries *J. Electrochem. Soc.*, **138** (1991) 3560–3567.

60. T. Shoji, T. Yamamoto, Charging and discharging behavior of zinc-manganese dioxide galvanic cells using zinc sulfate as electrolyte. *J. Electroanal. Chem.*, **362** (1993) 153–157.
61. R. Patrice, et al., Understanding the second electron discharge plateau in MnO<sub>2</sub>-based alkaline cells. *J. Electrochem. Soc.*, **148** (2001) A448–A455.
62. P. Sapkota, H. Kim, Zinc-air fuel cell, a potential candidate for alternative energy. *J. Ind. Eng. Chem.*, **15** (2009) 445–450.
63. A. Iarochenko, A. Shteman, Electrochemical air breathing voltage supply and power source having in-situ neutral-pH electrolyte. US 2010/0119919A1 (2010).
64. M. Mokaddem, P. Volovitch, K. Ogle, The anodic dissolution of zinc and zinc alloys in alkaline solution. I. Oxide formation on electrogalvanized steel. *Electrochim. Acta*, **55** (2010) 7867–7875.
65. J. J. Xu, et al., Novel zinc ion conducting polymer gel electrolytes based on ionic liquids. *Electrochim. Commun.*, **7** (2005) 1309–1317.
66. Y. Li, H. Dai, Recent advances in zinc-air batteries. *Chem. Soc. Rev.*, **43** (2014) 5257–5275.
67. H. Zhang, X. Zhang, H. Li, Y. Zhang, Y. Tong, P. Zhang, X. Lu, Flexible rechargeable Ni/Zn battery based on self-supported NiCo<sub>2</sub>O<sub>4</sub> nanosheets with high power density and good cycling stability. *Green Energy Environ.*, **3** (2018) 56–62.
68. A. R. Mainar, et al., Alkaline aqueous electrolytes for secondary zinc-air batteries: an overview. *Int. J. Energy Res.*, **40** (2016) 1032–1049.
69. R. F. Thornton, E. J. Carlson, Properties of alternate electrolytes for secondary zinc batteries. *J. Electrochem. Soc.*, **127** (1980) 1448–1452.
70. Y. Sato, M. Kanda, H. Niki, M. Ueno, K. Murata, T. Shiogami, T. Takamura, Long life sealed nickel-zinc cell using a new separator. *J. Power Sources*, **9** (1983) 147–159.
71. J. McBreen, E. Gannon, Bismuth oxide as an additive in pasted zinc electrodes. *J. Power Sources*, **15** (1985) 169–177.
72. Y. Sharma, M. Aziz, J. Yusof, K. Kordesch, Triethanolamine as an additive to the anode to improve the rechargeability of alkaline manganese dioxide batteries. *J. Power Sources*, **94** (2001) 129–131.
73. M. Xu, D. G. Ivey, Z. Xie, W. Qu, Rechargeable Zn-air batteries: progress in electrolyte development and cell configuration advancement. *J. Power Sources*, **283** (2015) 358–371.

74. R. Othman, W. J. Basirun, A. H. Yahaya, A. K. Arof, Hydroponics gel as a new electrolyte gelling agent for alkaline zinc-air cells. *J. Power Sources*, **2** (2001) 34–41.
75. R. Othman, A. H. Yahaya, A. K. Arof, Zinc-air cell with KOH-treated agar layer between electrode and electrolyte containing hydroponics gel. *J. New Mater. Electrochem. Syst.*, **5** (2002) 177–182.
76. A. A. Mohamad, Zn/gelled 6M KOH/O<sub>2</sub> zinc-air battery. *J. Power Sources*, **159** (2006) 752–757.
77. J. Fu, U. L. Dong, F. M. Hassan, L. Yang, Z. Bai, M. G. Park, Z. Chen, Flexible high-energy polymer-electrolyte-based rechargeable zinc-air batteries. *Adv. Mater.*, **27** (2015) 5617–5622.
78. T. Kakeya, A. Nakata, H. Arai, Z. Ogumi, Enhanced zinc electrode rechargeability in alkaline electrolytes containing hydrophilic organic materials with positive electrode compatibility. *J. Power Sources*, **407** (2018) 180–184.

## Chapter 7

# Electrolytes for Metal-Air Batteries

**Maciej Siekierski, Michał Piszcza, and Grażyna Żukowska**

*Faculty of Chemistry, Warsaw University of Technology, Noakowskiego 3,  
00-664 Warszawa, Poland*

*alex@ch.pw.edu.pl, mpiszcza@ch.pw.edu.pl, zosia@ch.pw.edu.pl*

### 7.1 Introduction

Jung and coworkers in 2012 [1, 2] demonstrated that only when a stable electrolyte is chosen can an appropriately designed Li-air cell reach application-expected operational parameters, including cycle number, capacity, and charge/discharge rates. An ideal electrolyte for a Li-air battery should exhibit numerous and often contradictive features. Whereas they seem to adhere to the general expectations from electrolytes, at least some of them must be addressed in terms of this specific type of application: (i) Reduced volatility and low vapor pressure are extremely important because the cell is air breathing. (ii) Decreased flammability must be expected as oxygen is present in the cell along with the catalytic cathode. (iii) A wide electrochemical stability window and enhanced stability against chemical reduction and oxidation are needed since both lithium metal and lithium peroxide are in contact with the electrolyte.

---

*Designing Electrolytes for Lithium-Ion and Post-Lithium Batteries*

Edited by Władysław Wieczorek and Janusz Płocharski

Copyright © 2021 Jenny Stanford Publishing Pte. Ltd.

ISBN 978-981-4877-16-9 (Hardcover), 978-1-003-05093-3 (eBook)

[www.jennystanford.com](http://www.jennystanford.com)

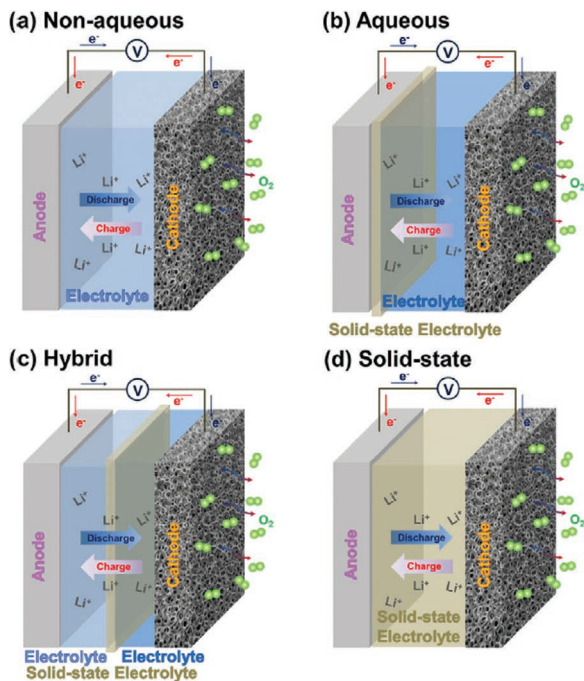


**Figure 7.1** Schematic configuration of metal-air batteries (Refs. [3, 4]).

(iv) Appropriate lithium cation transport properties (conductivity, dissociation, and cationic transference number) are even more important as the ion transport path is relatively long. (v) Adequate physicochemical properties (viscosity, polarity, and salt solubility) must be tailored to a specific cell design different from the typical Li-ion commercial one. (vi) Stability in contact with water vapor and “moisture tolerance” are a must as the system remains open to atmosphere. This list does not address issues extremely important for an open system: (i) toxicity of the electrolyte and its (in first-order volatile) deterioration and decomposition products, (ii) their environmental friendliness, and (iii) recyclability of the electrolyte itself, a whole cell being much more complicated in its design. The points listed above aside, four major design variants of the Li-air (and to some extent other Me-air ones) cell must be distinguished (see Fig. 7.1 [3, 4]). These are:

- Aprotic: Incorporating an organic electrolyte
- Aqueous: Incorporating a water-based electrolyte (and often a lithium conductive anode protection layer)
- Hybrid: With the organic anolyte and the aqueous catholyte separated by a lithium conductive membrane
- Solid state: Incorporating a polymer electrolyte, a glass-ceramic electrolyte, or a combination of them

## 7.2 Lithium-Air Systems

### 7.2.1 Organic and Polymeric Electrolytes

Li-air batteries are considered as a promising alternative to ion cells due to their high energy density. However, using them is still challenging. In the past decade, many strategies (including electrolyte modification) have been explored, promoting the development of metal-air batteries.

Interest in the Li-air system started growing in the late 1990s, when Abraham and Jiang first showed the working principle of a nonaqueous Li-air cell [5]. The demonstrated ability of the reversible formation of  $\text{Li}_2\text{O}_2$  was of particular importance for its application in energy storage devices. One of the main problems in anhydrous systems is the high polarization during charge-discharge processes, resulting in the reaction of  $\text{Li}_2\text{O}_2$  subsequently with water and with  $\text{CO}_2$ , with  $\text{Li}_2\text{CO}_3$  as the final product. As a result, a high energy loss is noticed between discharge and charge. Therefore, one of the main problems to solve is to develop an electrolyte stable in a highly oxidizing environment [6].

In such an environment, a solvent may degrade in several ways, such as via a nucleophilic attack, auto-oxidation, acid-base reactions, proton-mediated reactions, and chemical reduction by elementary Li. The first type of solvent decomposition scheme is found in solvents having strongly polarized functional groups and an electron-deficit atom, such as carbon in esters or amides or sulfur in sulfoxides, serving as acceptors for  $\text{O}_2^-$ . Acid-base reactions are responsible for the degradation of the solvent molecules with the hydrogen atom located at the  $\alpha$  or  $\beta$  position. This mechanism

is found in acetonitrile and dimethyl sulfoxide (DMSO)-based solutions. A typical lithium-air battery with an anhydrous solvent consists of a metal lithium electrode and a porous air electrode with active materials separated by the solution of lithium salt in an aprotic solvent.  $\text{Li}_2\text{O}_2$  is insoluble in an anhydrous solution, which leads to the deposition of the insulating layer on the electrode material and to the filling of the pores on the air side, resulting in the shortening of the discharging period. The first nonaqueous electrolytes applied in such systems were typical carbonate-based liquid electrolytes doped with  $\text{LiPF}_6$ . For example, in the battery proposed by Abraham and Jiang, the electrolyte used was a  $\text{LiPF}_6$ -propylene carbonate (PC)-ethylene carbonate (EC)-polyacrylonitrile (PAN) gel and the air electrode was Chevron carbon modified with *co*-phthalocyanine. The capacity of this system was equal 600 mA h g<sup>-1</sup> after two cycles [5]. It was found, however, that carbonates undergo decomposition in a highly oxidizing environment. During the oxidation, superoxides are formed, reacting further with carbonate solvents. The decomposition path leads to the formation of unwanted  $\text{Li}_2\text{CO}_3$  and alkylcarbonates instead of  $\text{Li}_2\text{O}_2$ , which results in the irreversible degradation of the solvent and poor cyclability of the carbonate-based solvents in air conditions [3, 7–9]. Attempts to improve the stability of the cell include the use of additives, such as calyx[6]arene, and result in the improvement of the charge capacity of the PAN-EC-PC-lithium bis(oxalato)borate ( $\text{LiBOB}$ )-C[6]A of ~20% [10].

Several other types of aprotic organic solvents were tested, such as ethers, esters (mostly lactones), nitriles, amides, and sulfoxides [11]. A separate, widely studied group is based on ionic liquids (ILs). Ethers, mostly ethylene oxide oligomers, with 4–10 repeat units in a chain, exhibit low volatility and are considered as more stable against oxidation [12]. Freunberger et al. found that oxidation products were similar for both linear and cyclic ethers, such as glymes (1–4), 1,3-dioxolane, and 2-methyltetrahydrofuran [13]. Bryantsev showed that glyme-based electrolytes are stable against  $\text{O}_2^-$  [14]. Systematic research by Schwenke et al. on the dependence of the compound stability on the chain length of the ethylene oxide oligomers revealed that short-chain glymes ( $n = 1 – 4$ ) of high purity were resistant against superoxides [15]. Horwitz et al. studied

highly concentrated lithium bis(trifluoromethanesulfonyl)imide (LiTFSI) and lithium trifluoromethanesulfonate solutions in mono- and diglyme (DG). Some differences between  $\text{Li}_2\text{O}_2$  formation in monoglyme and DG solutions observed herein resulted from different ionic association equilibria in the studied systems [16]. The electrochemical stability can be as high as 4.5 V versus  $\text{Li}/\text{Li}^+$ , which makes these systems particularly interesting in order to achieve batteries with long cyclability. Typically, ether-based electrolytes are obtained in the form of polymer gels, which give additional advantages, such as enhanced mechanical and thermal stability. There are several types of polymer matrixes used in these gels. The most common is a porous membrane consisting of fluorinated polymers, such as poly(vinylidene fluoride-*co*-hexafluoropropene) (PVdF-HFP), soaked in the electrolyte solution [17–19]. The other type is obtained by *in situ* polymerization and cross-linking of acrylic or epoxy monomers in the electrolyte [20–22]. In both cases, the matrix only weakly interacts with the lithium salt and the mechanism of conductivity is the same as the one observed in liquid electrolytes. Another way of gel formation is cross-linking of a tetruglyme (TG) by mixing it with lithium ethylenediamine. The reaction product forms a protective layer on the surface of the lithium electrode. A separate class is formed by ternary mixtures of glymes, lithium salts, and ILs [23].

Sulfoxide-based electrolytes offer many advantages in comparison with carbonate-containing electrolytes, such as low volatility, low viscosity, high  $\text{O}_2$  diffusion, and resistance against oxidation [24–26]. It has been shown, however, that DMSO undergoes decomposition during the charging process [27, 28]. A study on complex  $\text{LiI}/\text{H}_2\text{O}/\text{LiTFSI}/\text{Pyr}_{14}\text{TFSI}/\text{DMSO}$  conducted by Kim et al. has shown the formation of a  $\text{LiOH}$  and  $\text{Li}_2\text{O}_2$  mixture during cell discharge. The presence of sulfolane slightly increased the  $\text{LiOH}$  deposition, as well as improved the decomposition of both  $\text{LiOH}$  and  $\text{Li}_2\text{O}_2$  during charging [25].

The effect of salt concentration on  $\text{LiO}_2$  solubility was studied by Watanabe's group [29]. In a highly concentrated LiTFSI-DMSO solution (above 3 M), the solubility of  $\text{LiO}_2$  and the formation of  $\text{LiOH}$  are largely suppressed while the deposition rate of  $\text{Li}_2\text{O}_2$  increases. The inhibition of solvent decomposition was observed in

other superconcentrated systems, for example, (3–5 M) LiNO<sub>3</sub>/N,N-dimethylacetamide (DMA) electrolytes [30]. In both cases, the main reason for the enhanced stability was the much higher auto-oxidative stability of the solvent-Li<sup>+</sup> complex than that of the noncomplexed solvent molecules.

A majority of the efforts concerning nitriles are focused on acetonitrile-based electrolytes, despite their relatively high volatility. Properties of other nitriles are much less known. Recently, there is growing focus on nitriles with higher molecular weights, for example, trimethylacetonitrile (TMA) or compounds with two cyano groups, such as adiponitrile [31] and sebaconitrile [32]. Bryantsev et al. checked the stability of a family of nitriles and dinitriles against oxidation [31] using theoretical calculations coupled with electrochemical and gas chromatography–mass spectrometry experiments. TMA and ortho- and para-substituted derivatives of benzonitrile appeared to be the most stable here. In the last case, the presence of electron-donating groups at ortho and para position with respect to the nitrile group decreases the oxidative capability of the latter.

Amides are considered as stable against nucleophilic substitution by peroxides, for example, the stability window of a 1 M LiTFSI/DMA electrolyte reaches 4.2 V [31]. The main problem is the relatively high volatility of alkyl substituted amides and their high reactivity toward a lithium electrode, resulting in the fast decomposition of the solvent due to the lack of a stable solvent-electrolyte interphase (SEI). A possible way to prevent solvent degradation and stabilize SEI formation is related to the use of LiNO<sub>3</sub> salt [6, 30]. The group of Balaish [6] tested a 1 M LiNO<sub>3</sub>/DMA electrolyte, which retained over 95% of the cell's initial capacity after 80 operational cycles performed at 0.1 mA cm<sup>-2</sup>.

A new concept is represented by the use of double organic hybrid electrolytes, consisting of two different electrolytic solutions separated by a porous membrane. For example, one can find an electrolyte based on a TG solution on the anode (Si) side, separated by the lithiated Nafion/polytetrafluoroethylene (PTFE) microporous membrane from the carbonate-based solution on the carbon black cathode side [33]. The obtained system is characterized by a high

reversible capacity of  $\sim 18,000 \text{ mA h g}^{-1}$  of the cathode material and long-term cycling stability.

Room-temperature ionic liquids (RTILs) offer some advantages over typical electrolytes, such as thermal stability and a wide electrochemical stability window. The possibility to modify the cation by adding substituents (e.g., ether side chains) helps obtain ILs characterized by properties precisely tuned to the expectations of the particular applications [34]. The properties of the anion, on the other hand, strongly affect the viscosity of the resulting electrolyte and its ability to form an SEI. For example, replacing the commonly known  $\text{TFSI}^-$  anions by  $\text{B}(\text{CN})_4^-$  anions results in lowering of the viscosity, whereas the use of bis(fluorosulfonyl)imide ( $\text{FSI}^-$ ) leads to the stabilization of the protective layer formed on the electrode surface and so on. RTILs can be used either as lone solvents or in the above-mentioned mixtures with glymes or other solvents.

Polymer electrolytes utilizing RTILs as solvents or plasticizers consist of polymer gels with a PVdF-HFP matrix and solid PEO-based membranes plasticized with ILs [35–38].

Solid polymer electrolytes appear to be particularly attractive for use in lithium batteries. The most widely used matrix for anhydrous ones is poly(ethylene oxide) (PEO), which is, however, not sufficiently stable against oxidization [39, 40]. It was shown by Harding et al. [40] that polymers containing oligoether chains in their structure are sensitive to auto-oxidation. Therefore, the application of any electrolytes with ether units would require the addition of oxidation inhibitors or the development of insulating layers separating the polymer from the oxidizing neighborhood. Low-molecular-weight polyether carbonate may be used as an alternative polymer matrix. Including the carbonate units in the PEO backbone plasticizes the systems and allows for better mobility of the polymer chains. The lithium-air battery developed by Lu and coworkers [41], which is based on the solid polycarbonate-LiBF<sub>4</sub> electrolyte, exhibited electrochemical stability similar to that exhibited by batteries based on typical liquid electrolytes.

Further stabilization of the electrolyte can be achieved by the addition of compounds counteracting oxidation and/or stabilizing the electrolyte/lithium electrode interface. It was shown by Kumara

et al. [42] that the doping of PEO-lithium bis((pentafluoroethyl)sulfonyl)imide (LiBETI) membranes with boron nitride (BN) and Li<sub>2</sub>O leads to improved cell stability, most likely due to the formation of an SEI on the lithium surface. Another possibility relates to the application of redox mediators, enabling the decomposition of the discharge products. Guo et al. [43] successfully used LiI in LiTFSI-tetraethylene glycol dimethyl ether (TEGDME) electrolytes, achieving improvement in thermal stability and elongated cyclability compared with the nonmodified electrolyte.

Several classes of compounds, such as viologens, phthalocyanines, and quinones, act as catalysts, accelerating the oxidation of the Li<sub>2</sub>O<sub>2</sub> layer. Shen et al. [44] proved that the addition of 2,5-di-*tert*-butyl-1,4-benzoquinone catalyst improves the oxygen reduction reaction (ORR) and oxygen evolution reduction, resulting in a higher oxidation rate of Li<sub>2</sub>O<sub>2</sub> in a LiTFSI/DMSO electrolyte. Finally, it is worth going through the review of Kim et al. [45] addressing many theoretical issues concerning electrolytes, including their mechanisms of degradation. To conclude this section, one should state that most of the presented organic solvents were, finally, found to be practically inapplicable due to their limited oxidative stability against lithium peroxide present at the cathodic side in the cell. Even the most promising classes of molecules—namely nitrile- and sulfur-containing ones—are far below the industry-oriented expectations.

## 7.2.2 Aqueous

Describing the solutions applied in aqueous lithium-air systems, it is worth seeing how the retrospective view delivered by Girishkumar et al. [46] is developed in further research works. It must be first stated that their initial claim “the lithium-air systems captured worldwide attention in 2009 as a possible battery for electric vehicle propulsion applications” is not fully correct because the Department of Energy’s report of 1977 [47] claims that “cell and battery tests were made to evaluate the technology involved in the operation of a Li-H<sub>2</sub>O-air battery.” In these very initial investigations power densities of 44 mW/cm<sup>2</sup> (2.2 V, 200 mA/cm<sup>2</sup>) were obtained in cells with cathodes catalyzed by platinum black.

The quasi-primary systems (involved in the assumptions of external reprocessing of 50,000 tons of lithium per year) were found to be potentially viable for automotive applications, while the major field of development was then identified as “operation of a larger size battery with automatic control of electrolyte dilution and power optimization.” The final conclusion concerning reversibility of the system claimed in a later paper [46] sounds quite similar: “[T]here is no evidence that the electrochemical reaction is reversible, except by mechanically removing the reaction products and replacing them with fresh reactants.” Similar conclusions were reached at the same time by Lockheed Co. after testing the Li-air systems with a lithium metal anode immersed in a concentrated LiOH aqueous solution for military applications [48, 49]. On the other hand, a great advantage of aqueous systems is stated to be related to the solubility of the lithium oxidation products in water, resulting in the lack of cathode clogging and its volume expansion, as well as improved round-trip efficiency [50]. All the features mentioned above seem to be important enough to focus on for further development of these solutions. One of the major advantages of the approach provided is related to the elimination of the expensive Li salts from the electrolyte formulation. Even without their use, the so-created systems exhibit improved dissociation, salt solubility, and solution conductivity. Another advantage here is related to the use of non-noble ORR catalysts, which allow for four-electron transfer at the cathode [50].

This leads to the separate task of developing good Li-ion-conducting membranes that protect the anode from reacting vigorously with H<sub>2</sub>O. This issue is separately addressed in the following sections of the chapter. Similar benefits of aqueous electrolytes are also claimed in Refs. [51–53]. An aqueous cell is described by Zhang and coworkers in Ref. [54] as one incorporating a “three-phase reaction zone”: a liquid (electrolyte) phase, a solid (catalyst/carbon) phase, and a gas (O<sub>2</sub>) phase. In this case, the air electrode is dry. Moreover, according to Ref. [3], in aqueous (and hybrid, addressed separately) lithium-air batteries, the aqueous solvent, H<sub>2</sub>O, contrary to the nonaqueous one, participates in the electrode reaction as a reactant. Therefore, the additional amount of electrolyte can inevitably decrease the specific energy density of

the cell. In addition, according to Tarasevich et al. [55], the limit of solubility for LiOH at ambient temperature is reached at 12.5 g of hydroxide per 100 g of water and an additional amount of solvent is needed to prevent its deposition, resulting in further decrease in the theoretical energy density of the battery.

In terms of their composition, aqueous electrolytes are limited to weak or strong acidic or basic solutions. The typical aqueous solution is, according to reports by groups led by Zhang [56] and He [57], the LiOH-LiCl-H<sub>2</sub>O mixture in which, as declared by Shimonishi et al. [58, 59], the LiCl concentration and/or pH can vary. In other words, the addition of LiCl to a saturated aqueous solution of 5.12 M LiOH significantly decreases its pH value to 8.14. On the other hand, according to Zheng and coworkers [60], many other solutions, such as diluted LiOH, chloric acid/LiClO<sub>4</sub>, and HNO<sub>3</sub>/LiNO<sub>3</sub>, can be used instead. Therefore, a solution based on plain aqueous LiOH electrolyte was patented in France in 2014 [61] by Stevens et al. In general the addition of supporting salts such as LiClO<sub>4</sub>, LiCl, and LiNO<sub>3</sub> [58] is necessary to provide a high concentration of Li<sup>+</sup> while maintaining a low pH value. However, LiCl and LiNO<sub>3</sub> are hygroscopic. Therefore, they can scavenge water from the atmospheric moisture during battery operation, alleviating, in consequence, the need for quantitative addition of water for the battery reactions. But, according to Lai et al. [62], alkaline electrolytes with a high concentration of LiCl suffer from several important drawbacks. Not only the solubility of LiOH is significantly decreased in comparison with pristine water solutions, but also issues such as low practical energy density and gaseous Cl<sub>2</sub> evolution must be considered during the battery operation. Summarizing the biggest problem facing cells incorporating alkaline electrolytes is the discharge-related precipitation of LiOH in the form of its monohydrate (LiOH · H<sub>2</sub>O). The material is characterized by low solubility and an insulating character and exhibits the ability to clog the pores of the cathode. Another problem is related to the formation of insoluble Li<sub>2</sub>CO<sub>3</sub>, originating from the reaction of the alkaline electrolyte with the CO<sub>2</sub> present in the air. This deposit can block the active surface of the catalyst particles as well. On the other hand, as stated by Le et al. [63], 1 M LiNO<sub>3</sub> solutions with pH 12 and pH 14 were successfully used as the aqueous

**Table 7.1** Summary of specific capacities and energy densities of lithium-air batteries with some aqueous electrolytes

Aqueous solution	Minimum amount H <sub>2</sub> O for 1 M of product (mol)	Specific capacity (mA h g <sup>-1</sup> )	Energy density at OCV <sup>a</sup> = 3.69 V (Wh/kg)
LiOH	11.14	129.19	476.70
CH <sub>3</sub> COOH	8.15	130.97	483.28
HClO <sub>3</sub>	1.09	262.51	968.68
HClO <sub>4</sub>	10.07	95.83	353.63
HCOOH	7.35	152.10	561.24
HNO <sub>3</sub>	3.76	208.49	769.33
H <sub>2</sub> SO <sub>4</sub>	17.86	72.73	268.37
HBr	2.67	211.31	779.74
HCl	2.79	316.88	1169.29

Source: [3, 65]

<sup>a</sup>Open-circuit voltage

electrolyte in the cells of interest. The pH of the solution was in this case, as well, adjusted by the addition of LiOH. According to research by Matsui and coworkers [64], the addition of 0.1% of H<sub>2</sub>O<sub>2</sub> to an electrolyte solution saturated with LiOH seems not only to prevent the hydrolysis of Li<sub>2</sub>O<sub>2</sub> but also to significantly increase the operational current of the cell and improve its rechargeability.

On the other hand, one can observe (see Table 7.1) that the highest energy density could be reached by using strongly acidic solutions, such as HCl and HClO<sub>3</sub>, due to the high solubility of the discharge products in them. In addition, it was reported by Li et al. that aqueous Li-air batteries with H<sub>2</sub>SO<sub>4</sub>-based [66] and H<sub>3</sub>PO<sub>4</sub>-based [67, 68] electrolytes can also be designed. The role of the PTFE-based interlayer between the aqueous 1 M H<sub>2</sub>SO<sub>4</sub> electrolyte and a cathode was investigated by the group led by Li [69]. It was found that the use of PTFE can effectively mitigate the water loss from the electrolyte solution, which is one of the most important problems limiting the lifetime of the cell. Increase in the PTFE amount improved the battery performance, with the limit at 30 wt.%. Higher concentrations were destructive toward oxygen diffusion within the cathode. Other polyprotic organic acids, such as malonic acid and citric acid, have also been incorporated into aqueous electrolytes by Lai et al. [62]. This resulted in an increase in

the discharge capacity to values even higher than those observed for hydrochloric acid. In addition, a delay in the generation of insoluble discharge products was observed. An aqueous Li-air battery with a malonic acid electrolyte was reported by Visco et al. in their patent application [70] as operational for 77 cycles.

Further improvement can be achieved by the use of one from the set of active compounds for acidic aqueous electrolytes, as claimed by the same authors in their paper [71]. The invention here is based on the fact that in various embodiments, the active compound dissolved in the catholyte is an active proton generator that dissociates over the course of discharge, thus yielding active protons in the catholyte that take part in the cell reaction as the discharge proceeds. The ingredients include (i) mono- and polyprotic organic acids and their acid salts, (ii) functionally substituted carboxylic acids, (iii) carboxylic acid derivatives, including acyl halides, anhydrides, esters, amides, and nitriles, (iv) lactones, (v) esters of inorganic acids, (vi) sulfur-containing organic acids, such as sulfonic acids, or their derivatives, such as sulfonamides, (vii) phenols, (viii) inorganic neutral and acid salts, including mixtures of said salts, (ix) amphoteric hydroxides, (x) onium salts formed with organic acids, and finally (xi) onium salts formed with inorganic acids. The declared advantage of the so-obtained cells is related to their increased cathode capacity per unit weight and their improved energy density.

Recently, the application of “water-in-salt” and hydrate-melt electrolytes has become a hot topic [72]. These novel electrolyte compositions with nonflammable and green advantages show immense potential as substitutes for the highly volatile, flammable, and toxic nonaqueous electrolytes. According to Yamada et al. [73], the hydrate-melt electrolyte is preferred because of its extended wide electrochemical window. For example, the hydrate-melt electrolyte ( $\text{Li}(\text{TFSI})_{0.7}(\text{BETI})_{0.3} \cdot 2\text{H}_2\text{O}$ , HMEL) with an  $\text{H}_2\text{O}$  content of only  $\sim 10$  wt.% was introduced and applied in a Li-air battery by Wu et al. [72]. In this case the  $\text{H}_2\text{O}$  is coordinated with  $\text{Li}^+$ ,  $\text{TFSI}^-$ , and  $\text{BETI}^-$ . In consequence, no “free”  $\text{H}_2\text{O}$  molecules exist in the electrolyte. Compared with the TEGDME (tetraglyme)-based electrolyte, the hydrate-melt one shows no decomposition while the former one involves severe side reactions. Moreover, in this case,

there is no need to apply a protective layer on the surface of the lithium electrode.

In all other cases reported in Refs. [46, 51–53], due to obvious incompatibility of water with metallic lithium, one must consider that all-aqueous Li-air batteries must be equipped with an inert (but sufficient to facilitate the shuttling reaction conductive for the  $\text{Li}^+$  ions) ceramic solid-state electrolyte deposited on the anode, protecting it from deterioration. Therefore, some other problems will arise when using these electrolytes, such as the instability of the said materials toward them. Whereas these issues will be addressed in detail in the following section, their overview can be found in a paper delivered by the group of Yamamoto [74].

### 7.2.3 Ceramic and Glassy

As claimed by Zhang and Foster [54] an ideal solid-state electrolyte should exhibit a high value of lithium-ion conductivity together with a very low diffusion coefficient for the other “parasitic” species, such as  $\text{O}_2$  and  $\text{H}_2\text{O}$ . If it is considered as a part of a layered multielectrolyte system, there is need for high stability in the aqueous and nonaqueous electrolytes. Contrarily, in an all-solid design, high resistance toward direct reaction with lithium metal is expected. According to Kitaura and Zhou [75], the first solid-state Li-air battery dates back to 1987; its structure was similar to a solid-state fuel cell, utilizing stabilized  $\text{ZrO}_2$  as a solid-state electrolyte; therefore, it worked in the  $600^\circ\text{C}$ – $850^\circ\text{C}$  operational temperature range. The design of the said electrolyte is described by Semkow and Sammells in Ref. [76]. According to Yang et al. [77], in this device, an alloyed anode  $\text{FeSi}_2\text{Li}_x$  was immersed in the anolyte of a ternary molten salt, like  $\text{LiF}$ ,  $\text{LiCl}$ , and  $\text{Li}_2\text{O}$ , where  $\text{Li}_2\text{O}$  played the role of not only the electrolyte constituent but also the reaction product. Despite the promising electrochemical performance of the cell, its further development was hindered by the high operating temperature and the complex battery configuration.

On the other hand, the prospective analysis delivered by Kim et al. [45] claims that the best results to date use thin films of Li-ion-conducting ceramics (lithium superionic conductor [LISICON]-type materials) to encase lithium metal in a manner described in

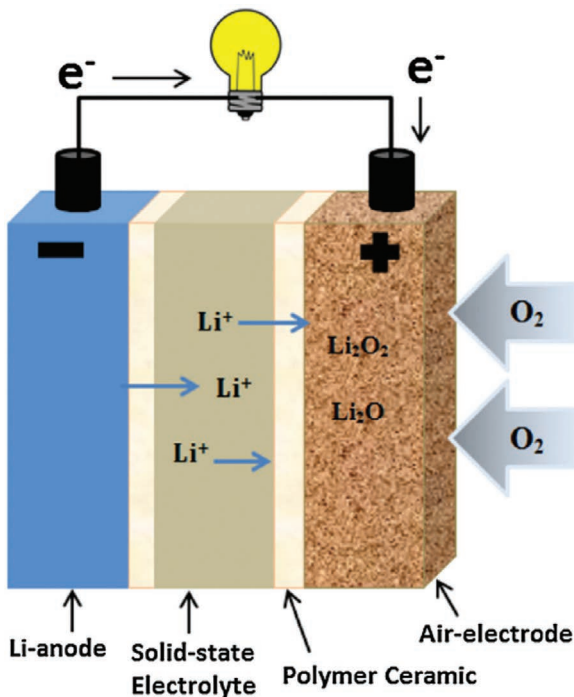


**Figure 7.2** Solid state Li-air cell design incorporating anode and cathode protective interlayers (Ref. [1]).

the patent claim of Visco et al. [78]. The ceramic-based artificial SEI protects lithium metal from atmospheric contamination and with its strong barrier properties is essential for both the all-solid and hybrid systems. The ceramic is claimed here to be reduced by the Li-metal anode, forming compounds such as  $\text{Li}_3\text{P}$  and  $\text{Li}_3\text{N}$ . Therefore, a three-layer lithium anode is formed that is stable in both acidic and basic aqueous media. On the other hand, a protection layer can be intentionally inserted in between (see Fig. 7.2) to prevent any undesirable reaction between lithium and the conductive layer. This so-called buffer layer has to possess high ionic conductivity and must be stable in contact with Li. Capsoni et al. [79] delivered an overall description of various interfacial materials under investigation. A more detailed study of systems containing lithium phosphorous oxy-nitride (LiPON) was delivered

by Chung et al. [80], while LiPON combined with a  $\text{Li}_4\text{Ti}_5\text{O}_{12}$  intercalated anode was investigated by Lu and coworkers [81, 82]. Zhang et al. applied  $\text{Li}_3\text{N}$  [83], while  $\text{Cu}_3\text{N}$  was tested by Visco et al. [78]. In another study conducted by Li et al. [84], in situ reaction between a rhombohedral sodium superionic conductor (NASICON)-type electrolyte  $\text{LiZr}_2(\text{PO}_4)_3$  and Li metal was applied to construct an intermediate layer containing  $\text{Li}_3\text{P}$  and  $\text{Li}_8\text{ZrO}_6$ . This was achieved in a preheating stage conducted at  $350^\circ\text{C}$  for 30 min. The problem of interlayers for ceramic materials was studied extensively with the application of materials such as amorphous Si and Al by Luo and coworkers [85], Ge by Fu et al. [86], Au once again by the group of Luo [87],  $\text{ZnO}$  by Wang et al. [88], and  $\text{Al}_2\text{O}_3$  by the groups of Tsai [89] and Han [90]. The group of Han [90] presented the results obtained when the added oxide reacts with molten metallic Li, forming a Li-ion-conductive layer comprising  $\text{Li}_2\text{Al}_4\text{O}_7$ . Therefore, a significant improvement in material interface properties is achieved both in terms of ceramic material wetting and its chemical interfacial stability. These two if achieved together result in an effective decrease in the interfacial impedance by more than 3 orders of magnitude. In another study by Liu et al. [91], the results of which were reported by Lai et al. [62] as well, an amorphous  $\text{Ge}^0$  thin film is deposited on an lithium aluminum germanium phosphate (LAGP) surface by sputtering. The film is found to effectively suppress the reduction reaction of  $\text{Ge}^{4+}$ , as well as to facilitate “intimate” interfacial contact between the Li metal anode and the LAGP electrolyte. A problem of stabilization of the electrolyte-facing side of the LATP ( $\text{Li}_{1+x+y}\text{Al}_x\text{Ti}_{2-x}\text{Si}_y\text{P}_{3-y}\text{O}_{12}$ ) and LAGP slabs is addressed by Yang et al. in Ref. [92]. Here, a layer of lithium titanate was deposited on the ceramic plates by radio frequency magnetron sputtering from a  $\text{Li}_4\text{Ti}_5\text{O}_{12}$  target. The said modification was, finally, found to decrease the interfacial resistivity in the 20% to 50% range, corresponding with the discharge current increase in the 70% to 80% range.

On the other hand, ceramic layers are claimed to be brittle, too thick, and hardly reproducible in sizes larger than tens of centimeter square. Therefore, Kumar and coworkers [93–96] declared polymer-ceramic composites as potentially valuable solutions. The key component of the solid-state lithium-air battery is the high-

Li-ion-conducting glass ceramic, for example, LAGP exhibiting a  $18.5\text{Li}_2\text{O}:6.07\text{Al}_2\text{O}_3:37.05\text{GeO}_2:37.05\text{P}_2\text{O}_5$  molar composition. It is sandwiched between two polymer-ceramic composite layers containing  $\text{Li}_2\text{O}$  and BN as the inorganic constituents, PEO as the organic one, and  $\text{LiN}(\text{SO}_2\text{CF}_2\text{CF}_3)_2$  (LiBETI) as a source of  $\text{Li}^+$  ions. As reported by Hong et al. and Li et al. [75, 97], LAGP has a nonstoichiometric composition of  $\text{Li}_{1+x}\text{Al}_x\text{Ge}_{2-x}(\text{PO}_4)_3$ , being a derivative of  $\text{LiGe}_2(\text{PO}_4)_3$ . Its crystals possess a rhombohedral type of lattice with a space group of R3c. Within it, an open 3D framework of  $\text{GeO}_6$  octahedral sites shares all their corners with  $\text{PO}_4$  tetrahedral sublattice units. In consequence, a rigid  $[\text{Ge}_2(\text{PO}_4)_3]^-$  skeleton is formed, allowing  $\text{Li}^+$  ions to freely migrate through the 3D tunnels in its structure. It can be applied not only in the form of composites but also as sandwiched structures where a polymeric buffer layer formed from PEO [98] or PEO(BN) [99–101] can effectively reduce the charge transfer resistance between the Li foil and the solid-state electrolyte LAGP, but unfortunately, Li dendrites are formed. In another work [102], Kitaura and Zhou investigated the possibility of the use of an interlayer composed of PEO-LiTFSI between a Li foil anode and a  $\text{Li}_{1+x+y}\text{Al}_x(\text{Ti},\text{Ge})_{2-x}\text{Si}_y\text{P}_{3-y}\text{O}_{12}$  solid electrolyte membrane; the Li-air battery can be discharged at varied current densities. In this case, the formation of dendrites is observed only for charging subcycles and they appear in about an hour of cell operation. In other studies, a polymer protective layer was used to increase the overall conductivity of the LATP separator at room temperature. In this case ILs were added to the polymer by Zhang et al. [103], resulting in an order of magnitude increase in conductivity. A variant of the modification was obtained by the same authors by the introduction of dispersed  $\text{BaTiO}_3$  [83] or by Koizumi and coworkers [104], who used a combination of LATP and  $\text{BaTiO}_3$ , introducing their mixture into the polymer layer. LATP materials of various preparation methods described in Refs. [105–109] and, therefore, varying in their conductivity values were also investigated by Aleshin et al. [107] toward minimization of the interfacial resistivity. According to the report of Zhang et al. [110], a typical LATP plate has a thickness of around 260  $\mu\text{m}$  and ionic conductivity of  $3.5 \times 10^{-4}$  S/cm at 25°C and  $1.4 \times 10^{-3}$  S/cm at 60°C and is provided by the Japanese company Ohara owning a US

patent [106]. On the other hand, Puech et al. in Ref. [111] introduced an ultrathin 50  $\mu\text{m}$  LATP separator working with both organic and LiOH-saturated aqueous electrolytes. According to Li et al. [112] the initial concept of material introduced by Visco et al. [78] can be generalized toward the application of various ceramic materials of the formula  $\text{Li}_{1+x}\text{A}_x\text{M}_{2-x}(\text{PO}_4)_3$  ( $\text{A} = \text{Al, Sc, Y}$ ;  $\text{M} = \text{Ti, Ge}$ ). A slightly different definition of LATP originating materials is given in Ref. [55], where the “A” list is extended by the addition of lanthanum and M is fixed as Ti. An even wider definition of NASICON-type materials is given by Nemoria et al. in Ref. [113]. A niobium-containing variation  $\text{Li}_{1.3}\text{Al}_{0.5}\text{Nb}_{0.2}\text{Ti}_{1.3}(\text{PO}_4)_3$  (LANTP) was tested here.

In addition to the stabilization of LATP/LAGP against a lithium anode, polymeric protective layers are also claimed by Kitaura et al. [114] to be able to stop lithium dendrite formation, as described by Zhang and coworkers in Ref. [83], where they were countered with the aqueous catholyte. For example, PEO doped with LiTFSI has been tested by groups of Zhang [83], Liu [115], and Wang [116] in a Li/PEO<sub>18</sub>-LiTFSI/LATP ( $\text{Li}_{1+x+y}\text{Ti}_{2-x}\text{Al}_x\text{P}_{3-y}\text{Si}_y\text{O}_{12}$  ceramic electrolyte)/1 M LiCl/Pt cell. The same polymer-ceramic sandwich and catalyst were tested once again by Zhang et al. [117] in a CH<sub>3</sub>COOLi-saturated CH<sub>3</sub>COOH-H<sub>2</sub>O solution. A novel, advanced design of the Li-air battery utilizing LATP material has been described by Zhu et al. in Ref. [118]. In this case, a multilayered ceramic separator was paired with an organic carbonate-based electrolyte acting as an interlayer for the lithium anode. To obtain this, a glass microfiber filter immersed in a commercial EC:dimethyl carbonate (DMC) electrolyte = 1:3, vol.%) was sealed with glue between Li metal and LATP electrolyte. In this case, the electrolyte was integrated with the air cathode. In the first step (LATP), powders of composition  $\text{Li}_{1.3}\text{Al}_{0.3}\text{Ti}_{1.7}(\text{PO}_4)_3$  were prepared by either solid-phase reaction or a sol-gel process. Next, the ceramic grains were mixed, with starch playing here the role of a pore former, pressed into the form of pellets and finally sintered at 850°C for 15 h to form a structure called by Yang and coworkers [77] as an “LATP scaffold.” Subsequently, the integrated structure was obtained by spin-coating an LATP electrolyte premembrane dispersion onto the top surface of the previously obtained LATP scaffold, which was once again sintered at 1000°C for 5 h.

To counter these—at first glance very promising results—it must be stressed that both LATP and LAGT plates were found by Li et al. [112] to be unstable in acid and alkaline (1 M LiOH) aqueous solutions. It was discovered by Shimonishi and coworkers that LATP remains more stable in lithium-ion-saturated solutions, such as  $\text{CH}_3\text{COOLi}$ -saturated  $\text{CH}_3\text{COOH}-\text{H}_2\text{O}$  solution [58] and LiOH-saturated solution [119]. The latter research report suggests that there is a possibility of developing an aqueous alkaline lithium-air battery as the electrolyte is saturated with LiOH at deep discharge. Once again, the report of Shimonishi et al. [120] claims a three-week stability of LATP immersed in the  $\text{CH}_3\text{COOH}$  (HAc)- $\text{H}_2\text{O}$ -saturated  $\text{CH}_3\text{COOLi}$  (LiAc) and  $\text{HCOOH}$  (HFc)- $\text{H}_2\text{O}$ -saturated  $\text{LiCOOH}$  (LiFc) solutions, confirmed with X-ray diffraction (XRD) experiments. Another solution to the instability problem was delivered by Imanishi and coworkers [58, 59, 121], who addressed this issue by effectively lowering the pH by adding LiCl to the electrolytic solution (see the section above). The stability of LAGP was, as well, tested in various acid and alkaline aqueous electrolytes by He et al. [122]. It was found that LAGP would decompose toward impurity phase  $\text{Li}_3\text{PO}_4$  after being immersed in an alkaline aqueous LiOH solution. However, similarly to LATP it exhibited excellent stability in saturated  $\text{LiCl}-\text{CH}_3\text{COOH}-\text{H}_2\text{O}$  and  $\text{LiCl}-\text{LiOH}-\text{H}_2\text{O}$  solutions. LANTP was, on the other hand, found by the group of Nemoria [113] to be stable against a 10 M LiCl aqueous solution with 1.5 M LiOH immobilized with a conventional alkyl amide-type superabsorbent polymer. These findings suggest some candidate aqueous electrolytes for long-term operation of lithium-air batteries. Zhou et al. [123] have also investigated the stabilization of the ceramic separator in a cell designed with a Li/ceramic electrolyte/LAGP@carbon nanotube configuration.

It is worth stressing that the focus on LATP-/LAGP-type materials results from the drawbacks of the other ceramic separators investigated. Not only are LISICON-type materials found to decrease the high load operational voltage of the cell, as claimed by Wang et al. [124], but also the LIPON/LISICON interface during cycling [125] was demonstrated by Stevens et al. to exhibit a decrease in the interface layer uniformity and also its deformation and rupture due to mechanical constraints. LISICON corrosion in alkaline solutions

is also claimed as a severe drawback [79] needing modifications in the cell design. In addition, it was found that LISICON-type materials suffer from proton exchange in water [126–128], which makes them unstable in aqueous catholyte solutions. In systems separated by a ceramic LISICON or NASICON film, as described by Wang et al. in Ref. [129], the aqueous compartment solution may also be made of acetic acid (90 vol.%)–H<sub>2</sub>O–CH<sub>3</sub>COOLi (10 vol.%), 1 M KOH, or a phosphate buffer catholyte like 0.1 M H<sub>3</sub>PO<sub>4</sub>/1 M LiH<sub>2</sub>PO<sub>4</sub>. Finally, it was reported by Li et al. [130] that the same buffer solution characterized in this case by the net pH value of 3.14 is at room temperature able to hinder the corrosion of the LATP ceramic membrane.

Contrary to the above, a new garnet-type lithium-ion-conducting solid electrolyte of Li<sub>7</sub>La<sub>3</sub>Zr<sub>2</sub>O<sub>12</sub> was reported by Weppner et al. [131], exhibiting a high ionic conductivity of  $2.4 \times 10^{-4}$  S/cm at 25°C. In its nonstoichiometric form Li<sub>7-x</sub>La<sub>3</sub>Zr<sub>2</sub>O<sub>12-1/2x</sub> was found to be stable in the saturated aqueous solution by Shimonishi et al. [132], while it was found to exhibit application disadvantages similar to the ones mentioned above for the LISICON-based systems and related to severe interfacial polarization even at moderate current densities. In 2017, a solid-state Li-air battery was designed by Sharafi et al. [133] omitting the application of the polymeric interlayer coating. The electrolyte was based on a similar zirconate electrolyte (Li<sub>7</sub>La<sub>3</sub>Zr<sub>2</sub>O<sub>12</sub> [LLZO]). To decrease the interfacial resistivity, multistage mechanical processing, including dry polishing, wet polishing, and heat treatments, was applied to remove the surface layer of the LLZO plate. Other papers investigating these structures include those in Refs. [134–138]. Xu et al. [139] improved interfacial compatibility and suppressed Li dendrite formation by the synthesis of the two-phase Li<sub>3</sub>PO<sub>4</sub>-added garnet-type Li<sub>6.5</sub>La<sub>3</sub>Zr<sub>1.5</sub>Ta<sub>0.5</sub>O<sub>12</sub> (LLZTO) electrolyte. In this case, Li<sub>3</sub>PO<sub>4</sub> addition not only influences Li<sup>+</sup> transport across grain boundaries but also improves interfacial stability at the time when Li metal plating/stripping reactions are occurring at the interface. These benefits are achieved as a self-limiting and ion-conducting interface, Li<sub>3</sub>P, is formed *in situ* when Li flux reacts with glassy Li<sub>3</sub>PO<sub>4</sub>. Additionally, the additive may decrease the rate of reaction between garnet and moist air and reduce the thickness of the Li-

ion-insulating  $\text{Li}_2\text{CO}_3$  layer formed in the reaction with atmospheric  $\text{CO}_2$ . An alternative approach was presented by He et al. [140], where a Sn-Al alloy was used as an interlayer for the LLZTO garnet-type electrolyte, reducing the interfacial resistance by about 20 times. In addition, Goodenough et al. [141] used LLZTO as an inorganic part of the polymer ceramic composite electrolyte. LiTFSI was used to introduce lithium charge carriers into the PEO matrix. The PEO-LLZTO composite electrolytes exhibit not only improved conductivity but also enhanced interfacial stability against Li electrodes. Moreover, Li dendrite growth is effectively suppressed. The latter phenomenon can be attributed to the mechanically robust and stable framework provided by PEO while the former one to the stable chemical and electrochemical performance of LLZTO.

According to Akhtar and Akhtar [1], among the various inorganic materials investigated, one can find oxides, sulfides, phosphate compounds [96, 142, 143], and perovskites [63, 144–147]. Other types of inorganic  $\text{Li}^+$ -conducting materials are described in the more general reviews [148, 149]. According to a report by Tarasevich et al. [55], other candidates for ceramic separators include  $\text{LiTi}_2(\text{PO}_4)_3$  and  $\text{Li}_{3x}\text{La}_{2/3-x}\text{TiO}_3$ . In particular, the material of composition  $\text{Li}_{0.33}\text{La}_{0.57}\text{TiO}_3$  is claimed to possess improved stability in contact with deionized water, as well as improved conductivity, when compared to LATP [1]. Independently from these claims, LAGP described in Refs. [150–152] and LATP depicted in Refs. [153, 154] have been identified as fast  $\text{Li}^+$ -ion-conducting electrolytes most suitable for solid-state Li-air batteries, confirmed in numerous works, for example, in Refs. [105, 106, 155, 156]. LATP is claimed by Yang et al. [77] to be thermally and chemically unstable, with  $\text{Ti}^{4+}$  ions reduction occurring at the lithium interface. LAGP seems to be more stable but has also been reported to react with Li metal. Therefore, contrary to the above-stated conclusion, the latter paper is probably based on the research by Ma et al. presented in Ref. [157], which claims that LLZO material is superior to LATP/LAGP ones due to the fact that it is stable against the Li metal anode. While upon using of the LATP/LAGP materials their internal surface of the material became reduced, leading to the implantation of  $\text{Li}^+$  cations into its structure. A tetragonal-like LLZO interface created in such a manner is stable even when extremely

thin (its thickness is around five elementary cells). This effectively hinders further parasitic reactions without compromising the ionic conductivity. On the other hand, according to Lai et al. [62], the drawbacks of garnet-type solid electrolytes fatal for the open Li-air batteries originate from their instability toward moisture and CO<sub>2</sub>, as well as a high interfacial resistance value resulting from their poor adhesion with electrodes. It is further increased [158–160] by the formation of a thick Li<sub>2</sub>CO<sub>3</sub> layer and Li-Al-O glass phase separation. To overcome all the above-mentioned drawbacks, several neoteric technologies are suggested by Yang et al. in Ref. [77]. These are (i) hybrid electrolytes obtained by incorporating oxide-type crystal growth (i.e., LLZO) into molten glass, (ii) the formation of heterojunction-type solid-state electrolyte crystal layer on cathode substrate promoted by the growth of the crystal in the molten flux, and (iii) the development of a non-sintered-type solid-state battery using solid electrolytes.

A totally different approach flows from the well-known phenomenon of high diffusivity of lithium in silicon single crystals. Therefore, single-crystalline silicon membranes were tested as a lithium-ion-conducting material in a lithium-air battery by Zhang et al. [54] and the group of Truong [161]. With thicknesses ranging from 2 to 20 μm, they exhibited lithium-ion conductivities in the range of 10<sup>-6</sup> S/cm, correlated with an extremely low diffusion coefficient of oxygen at room temperature, remaining in the range 10<sup>-44</sup> cm<sup>2</sup>s<sup>-1</sup>. Therefore, efficient protection of the lithium anode from direct chemical oxidation, together with favorable lithium transport, allowed for reasonable current densities. To avoid contact problems between lithium and silicon, an interlayer of organic carbonated-based lithium-conducting electrolyte was applied between them. Therefore, an SEI that is typical for carbonates was formed on the anode surface, increasing the overall cell resistance. According to Lai et al. [62], additional problems arise as Si wafers are unstable in direct contact with Li anodes, which necessitates the introduction of buffer layers and results in further increases in the internal resistance and manufacturing cost and affects safety issues. Consequently, the performance of such silicon membranes should be re-evaluated in stable, nonaqueous electrolytes or aqueous electrolytes. Tan et al. [54] claim that further investigations are

needed to improve lithium transport in a silicon membrane, which, as suggested, can be achieved, for example, by material doping. For this particular design class, one faces mostly problems related to the lithium/ceramic electrolyte interface, which is fragile to contact arising from lithium cycling. Another problem limited to systems utilizing aqueous catholytes is related to the limited stability of the ceramic materials against solution-activated degradation. A more detailed description of the inorganic lithium-conducting materials is given Chapter 3 of this book.

### 7.2.4 Hybrid Systems

The mixed-electrolyte Li-air battery configuration was initially proposed by Zhou et al. [53]. In this design the anode (with its organic electrolytic solution) and the porous cathode (with its aqueous electrolyte) are separated by a water-impermeable, lithium-ion-conductive membrane (e.g., LISICON). This approach, in which an organic liquid electrolyte layer is treated as described by Capsoni et al. [79], is claimed by Visco and coworkers [78] as a separate design, called by Wang et al. [124] as a “hybrid” lithium-air battery. In the relatively early study [4], Visco and coworkers tested a wide range of hybrid three-layer electrolyte combinations comprising dimethyl formamide, DG, TG, ethyl acetate, sulfolane, and tris(pentafluorophenyl)borane as organic solvents; LiTFSI and LiPF<sub>6</sub> as solvent-soluble salts; LAGP and LATP as ceramic separators; and LiCl, NH<sub>4</sub>Cl, LiNO<sub>3</sub>, NH<sub>4</sub>NO<sub>3</sub>, LiOH, malonic acid, citric acid, and imidazole, as well as phosphate buffer building compounds (H<sub>3</sub>PO<sub>4</sub> and Na<sub>2</sub>HPO<sub>4</sub>), as aqueous electrolyte ingredients. The paper demonstrated good cycling at reasonable current densities (C/5 discharge) and high current densities for short bursts (>1C rate for 5 min.). On the other hand, it was also demonstrated that primary Li-Air batteries of the tested design can achieve spectacular specific energies of over 800 Wh/kg.

In this case, a solvent-based electrolyte can be understood as a second protective layer for the LATP ceramic separator. In these works, a dual electrolyte configuration was investigated using an EC/DMC electrolyte as the anolyte, with the aqueous system applied in the cathode compartment. According to Grande et al. [50], an

obvious limitation of the hybrid systems must be clearly stated. It is based on the fact that the more layers are used in the cell design, the higher is the number of the Li<sup>+</sup> mass-transport interfacial limitations. Therefore, there is hinderance to the possibility of using higher current densities in comparison with the pristine nonaqueous systems.

On the other hand, according to the previously cited work of Lai et al. [62], achieving practical application of hybrid and aqueous Li-air batteries should allow for higher system-level energy density even if theoretical energy densities of hybrid and aqueous Li-air batteries are lower than those of nonaqueous ones. In the case of hybrid and aqueous electrolytes reported by Black et al. in Ref. [162], the major challenges include maintaining the long-term stability of the Li anode against H<sub>2</sub>O permeating to its surface through the ceramic separator (and organic electrolyte in the case of the hybrid systems) and avoiding the precipitation of LiOH in the cathode area.

Examples of hybrid systems utilizing a melt quenching–obtained LAGP separator are described by Safanama and coworkers in [163, 164]. The investigations covered both purely aqueous and hybrid designs. In both cases, a 5 M LiOH or a 10 M LiCl solution in water was used as the catholyte. The system with direct contact of the ceramic slab was compared with the one where commercial EC/DMC+LiPF<sub>6</sub> anolyte was used as an interface layer. Initially, preliminary experiments were conducted in which the stability of the LAGP slab was verified by means of XRD examinations. It was found that GeO<sub>2</sub> in its trigonal form being, indeed, the impurity in the LAGP material can be washed away from it as this form of germanium dioxide is water soluble. A hybrid cell was found to exhibit considerably smaller overpotential during charging, which is attributed to the improved contact between Li anode and LAGP provided by the organic electrolyte. A significant increase in the acceptable current density is also reported as an effect of cell hybridization. An LATP separator was used in a design described by the same group in Ref. [165], assembled this time with the use of an unspecified “typical” organic anolyte and an alkaline aqueous catholyte. The obtained results were compared with the symmetric dual-organic design, resulting in an increased capacity of the hybrid proposed. The same separator was tested by Zhao et al. [166] with

EC:DMC 1:1 + 1 M LiPF<sub>6</sub> anolyte and phosphate buffer (0.1 M H<sub>3</sub>PO<sub>4</sub>+ 1 M LiH<sub>2</sub>PO<sub>4</sub>) as the catholyte. While the authors claim optimistically that the cell exhibits very good stability after extended cycles in air, a little earlier they had declared a “mild” degradation after only 20 cycles of cell operation. Therefore, the suggestion that phosphate buffer solution proves to be a promising catholyte seems to be only partially justified by the results presented. In another study delivered by Li et al. [167] 0.1 M H<sub>3</sub>PO<sub>4</sub>+ 1 M Li<sub>2</sub>SO<sub>4</sub> was used as the catholyte to eliminate the influence of protons originating from the previously applied LiH<sub>2</sub>PO<sub>4</sub>. An LATP separator and an unspecified (probably commercial) organic anolyte complete the cell design. It was found that by this catholyte composition the hydrolysis of Li<sub>3</sub>PO<sub>4</sub> by Li<sub>2</sub>SO<sub>4</sub> is suppressed. This leads to the lower pH values observed toward the end of discharge. Therefore, a high capacity along with a high cell voltage can be obtained, making the proposed solution superior to phosphate buffer-based ones. Another interesting example of breakthroughs against limits is a dual-hybrid design (see Fig. 7.3) described by Wang et al. [168]. Similar to the other hybrid Li-air systems, it is based on an organic anolyte (1 M LiClO<sub>4</sub> dissolved in EC:DEC) and an aqueous 1 M KOH based catholyte separated by a LISICON membrane. A second level of hybridization is achieved through the incorporation of the second electrode (based on the activated carbon) into the anode compartment. Therefore, like the commercially available lithium-ion capacitors, it combines the features of a galvanic cell and a supercapacitor in one device. The stability of various ceramic separators applicable in the hybrid Li-air cells versus a set of aqueous catholytes is described in detail by He et al. in Ref. [169]. On the other hand, the same paper practically omits the issue of anolyte selection, declaring “common” aprotic solvents as most applied due to their widest availability.

The paper also claims that due to the separation of the organic solvent from the air cathode (and discharge products such as Li<sub>2</sub>O<sub>2</sub> deposited there), the issue of their oxidative stability here, contrary to the purely aprotic designs, is almost completely unimportant. The influence of the ionic conductivity of the ceramic separator was investigated in another work of Li et al. [170]. A combination of the previously mentioned catholytic (0.1 M H<sub>3</sub>PO<sub>4</sub>+ 1 M LiH<sub>2</sub>PO<sub>4</sub>)

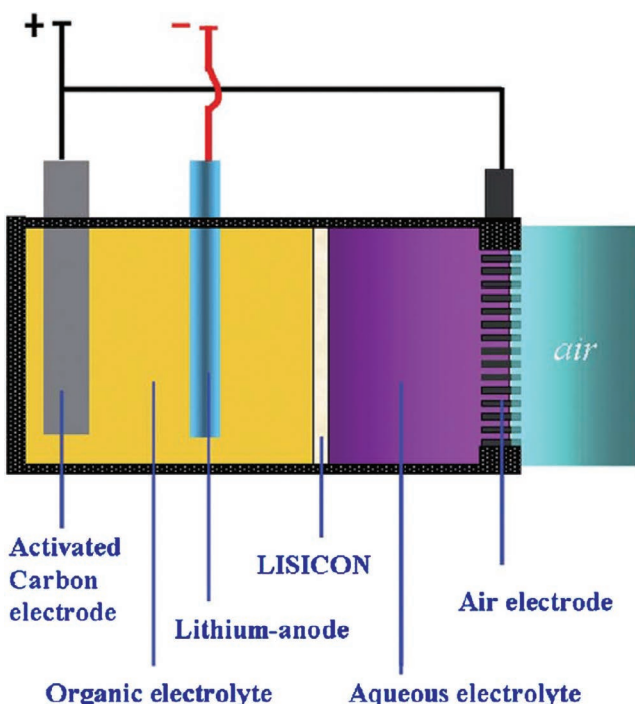


**Figure 7.3** A schematic representation of the lithium-air capacitor battery with a hybrid electrolyte (Ref. [168]).

and anolytic (1 M LiPF<sub>6</sub> dissolved in EC:DEC 1:1) solution was used here. It reports the performance of a cell assembled with two types of LATP membranes of the same thickness (150 µm) but exhibiting different values of ionic conductivity at room temperature ( $1 \times 10^{-4}$  S/cm vs.  $2.5 \times 10^{-4}$  S/cm). In the impedance imaging, the more than twofold reduction in total internal resistivity of the cell (from 250 to 100 Ωcm<sup>2</sup>) observed can be correlated with the improved polarization behavior of the latter cell and a specific power density increase from about 25 to over 40 mW/cm<sup>2</sup>. To solve the LATP stability problem in acidic aqueous electrolytes, a basic organic additive in the form of imidazole was used by Li et al. An equivalent amount of this heterocyclic compound was added to the acid solution to immobilize protons in the form of an imidazole-acid complex by Li et al. [171]. In this case, 1 M LiPF<sub>6</sub> dissolved in EC/DEC

(1:1 v/v) was used as an anolyte. The obtained results proved that the addition of 6.06 M of imidazole to 6 M HCl + 1 M LiCl results in the final solution having a pH value of about 5 and, therefore, alleviates the corrosion of the solid-state electrolyte immersed in it. However, on the other hand, it was found by Lai et al. [62] as well as by Manthiram and Li [172] that imidazole-buffered electrolytes are not stable at high voltages because the imidazole will be oxidized prior to water splitting during the charging process.

A membrane-less structure was obtained by Zhu and coworkers [173] through the integration of an LATP catholyte with a cathodic catalytic layer also based on LATP ceramic material. This bifunctional layer was obtained in a sol-gel process and later sandwiched in a glass microfiber mat immersed in commercial EC:DMC:LiPF<sub>6</sub> anolyte and Li anode. The authors claim that this battery design can solve two major problems—high ohmic losses and limited active interface surface—and, therefore, is recognized to have high potential for applications. Though this cell design is claimed to be “hybrid,” it does not fulfill the strict definition of this construction variant mentioned earlier. A completely different approach is demonstrated by Wu et al. in Ref. [174]. Here an atypical hybrid structure was obtained without the use of a ceramic separator and based on the achievement of stability of the direct interface between two immiscible electrolytes. The liquid catholyte was composed of 0.5 M H<sub>2</sub>SO<sub>4</sub> solution. A 0.5 M LiClO<sub>4</sub> solution in PC was used as the anolyte, with the addition of 0.5 M of TBAPF<sub>6</sub> quaternary ammonium salt. Jellification with poly(methyl methacrylate) (PMMA) enabled the soft solidification of the anolyte, making its interface with aqueous solution stable. PMMA concentrations in the 5%–30% were tested and concentrations of 10%–20% were found to be most suitable in terms of a compromise between the growing-with-polymer-amount interface stability and decreasing ionic conductivity. Finally, an interesting but unsuccessful attempt to create a new inorganic material applicable as a separator in hybrid systems was described by Schroeder et al. [175, 176] and Zhao and coworkers [177]. Li<sub>3</sub>OCl and Li<sub>3</sub>OBr materials characterized by an antiperovskite structure were synthesized previously from LiOH and LiCl/LiBr by the same authors by means of the synthetic procedure described in an earlier work of Zhao et al. [178]. While the Li<sub>3</sub>OBr

material was found to be stable against PC, DEC, DMC, and 1,2-dimethoxyethane (DME), unfortunately both water and commercial second-generation electrolytes (EMC:EC 7:3 + 1.2 M LiPF<sub>6</sub>) tended to dissolve it. Finally, it is worth noting that Mehta et al. [179] delivered a theoretical attempt to hybrid cell optimization based on the mathematical model of the phenomena occurring within it. The provided model assumes that the voltage drops across the electrolyte and the electron conductive material are lower than 1% of the open cell voltage of the battery. One can conclude that while the proposed hybrid design seems to be the most promising one in terms of helping avoid both the oxidative instability problems related to the organic electrolytes and the contact problems exhibited by the lithium anode/ceramic electrolyte interface, the design proposed is not only much more complicated and, therefore, less valuable in terms of commercialization but also suffers from the same issues of the ceramic materials degradation as those caused by the aqueous catholytes in the above-mentioned design variants.

It is worth delivering an abbreviated description of a relatively new concept of a flow lithium-air cell. The idea was introduced by Zhou in his 2010 report [180]. The cell contains two subunits: an energy conversion unit and a product recycling unit (see Fig. 7.4). An organic electrolyte serves as an anolyte and a LISICON ceramic membrane as a separator. While the lithium metal anode, anolyte, and internal catholyte (1 M LiNO<sub>3</sub>) are stationary, an organic membrane separating the second catholyte (1 M LiOH) is recycled through the cell to avoid the accumulation of the reaction products in the cathode compartment. An external separation block is used to eliminate the excessive LiOH from the solution. The same group proposed a flow system utilizing a soluble catalyst dissolved in an aqueous catholyte [181]. Chen et al. [182] presented a design similar in concept but utilizing a Celgard 2400 separator soaked in 1.2 M LiPF<sub>6</sub> in EC/DMC in a ratio of 1:1 by weight in an anodic compartment and 0.85 M CH<sub>3</sub>COOH and CH<sub>3</sub>COOLi dissolved in deionized water as a cyclable catholyte. The subsequent modifications were proposed by the group of Zhu [183], including the use of an organic catholyte able to dissolve the ORR catalyst. On the other hand, Ruggeri et al. [184] proposed the use of a

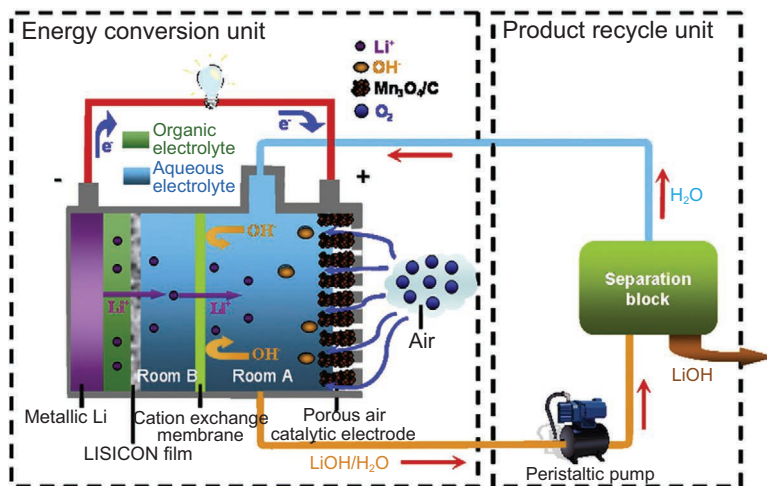


**Figure 7.4** A schematic representation of the developed Li-air fuel cell system with an energy conversion unit and a product recycle unit (Ref. [180]).

TG-based dispersion of Super-P® and Pureblack® catalytically active carbons. In addition, a similar concept but utilizing an IL-based electrolyte was introduced by Monaco and coworkers [185]. A significant improvement in cell performance was achieved by Ruggeri et al. [186] by the development of a semisolid TG-based catholyte formulation allowing for the percolation of the dispersed carbon structures. The theoretical approach to the achievable enhancements was described in Ref. [187], where Huang and Faghri developed a 2D model for an aprotic flow battery.

### 7.3 Sodium

Sodium has reportedly shown promising results as an alternative to metal-air battery. According to Chawla [188], the utilization of sodium in a battery system allows for 3 to 5 times reduction in the costs calculated per unit of stored energy. Kang et al. [189] investigated a hybrid system comprising a sodium metal anode, 1 M NaClO<sub>4</sub> in EC/DMC (1:1) with 1 vol.% fluoroethylene

carbonate (FEC) as an anolyte, a solid conductor of  $\text{Na}_3\text{Zr}_2\text{Si}_2\text{PO}_{12}$  composition and with conductivity equal to  $1.3 \times 10^{-3} \text{ S/cm}$  as a separator, a 1 M aqueous solution of NaOH as the catholyte, and a porous air cathode containing a dual-phase  $\text{MnCo}_2\text{O}_4/\text{N-rGO}$  hybrid as the catalyst. The ceramic material used was prepared in the same way as described by Liang et al. in Ref. [190], where either the same carbonate base mixture or DG with 0.5 M  $\text{dm}^{-3}$  of  $\text{NaCF}_3\text{SO}_3$  dissolved served as an anolyte when the composition of the catholyte remained intact. A hybrid system of similar design is described by Khan and coworkers [191]. A NASICON plater was used as the central separator whereas a 1 M solution of  $\text{NaCF}_3\text{SO}_3$  in TG (TEGDME) and 0.1 M NaOH aqueous solution served as anolyte and catholyte, respectively. It was found that the aqueous-nonaqueous hybrid sodium-air cells described by Kang et al. in Ref. [192] possess a higher theoretical open circuit voltage and theoretical specific capacity as well as lower charge/discharge over potential in comparison to the “pure,” nonaqueous designs described by Liang et al. [193] and Hayashi and coworkers [194]. In addition, the cathode blockage caused by the discharge products in nonaqueous cells is successfully eliminated in the hybrid ones; therefore, their electrochemical performance is significantly improved, as in the case of the lithium-air hybrids described above. Three main drawbacks of alkaline electrolytes were identified by Kang and coworkers [195]: (i) a decrease in the discharge voltage with increment in the concentration of NaOH (resulting from higher solubility of oxygen in lower alkaline concentration), (ii) an increase in the internal resistance when NaOH is utilized during long-term working, leading to a larger cell voltage hysteresis, and (iii) a decrease in the electrochemical performances of cells due to the side reactions caused by carbon dioxide. Therefore, a hybrid sodium-air cell based on acidic electrolytes was proposed and claimed to exhibit superior electrochemical performance when compared to the alkali metal-air one. In this case, 0.1 M HAc + 0.1 M NaAc and 0.1 M  $\text{H}_3\text{PO}_4 + 0.1 \text{ M Na}_2\text{SO}_4$  were utilized as catholyte to improve conductivity and ensure the stability of the battery (otherwise the applied NASICON ceramic separator can be degraded by HCl or  $\text{HNO}_3$  solutions of the first choice). On the organic/anodic side of the cell, the importance of tailoring the aprotic solvent was

featured by Liang et al. in their contribution [193], in which they applied electrolyte compositions similar to those mentioned in the previously reported works of Kang and coworkers [189, 190]. Ether-based organic electrolytes behaved superior to carbonate-based ones in the case of diethylene glycol dimethyl ether (DEGME) (diglyme)- $\text{NaCF}_3\text{SO}_3$ , as reported by Hartmann et al. [196], and according to Kim and coworkers [197] respond well over TEGDME- $\text{Na NaClO}_4$  ones. In both cases, the solutions were compared with the respective carbonate-based electrolytes. Moreover, DEGME was found by groups of Dan et al. [198] and Jian and coworkers [199] to be superior to TEGDME. On the other hand, Guo et al. [200] reported that in  $\text{Na-O}_2$  cells, stabilized superoxide species might abstract hydrogen from polyether-based solvents such as TG, resulting in in situ generation of water molecules in the electrolyte. In addition, the decomposition process of glyme-type solvents was proved to occur even in "dry" electrolytic solutions. Side-products such as carbonate, carboxylate, and esters were identified by means of in situ molecular spectroscopy experiments. In another research, Liu et al. [201] proved by means of Fourier transform infrared spectroscopy and solid-state nuclear magnetic resonance that DME deteriorates, forming sodium salts, such as formate, acetate, and hydroxide. Influence of the type of organic solvent (DEGME, DMSO, MeCN, DMA) in the sodium trifluoromethanesulfonate-based electrolytes on the discharge product type was investigated by means of surface-enhanced Raman spectroscopy by Aldous and Hardwick [202]. Solvents of high donor numbers were found to promote the creation  $\text{NaO}_2$  while the low-donor-number-exhibiting ones tended to yield  $\text{Na}_2\text{O}_2$  instead. These results were obtained for the carefully dried solvents where the water contamination did not exceed 10 ppm. On the other hand, Sharon et al. [203] suggest that the value of DN does not affect the discharge product significantly. This discrepancy can be explained by the presence of water in the latter experiments. In a study conducted by Ortiz-Vitoriano and coworkers [204], intentionally added water (up to 6000 ppm) led to the formation of  $\text{NaO}_2$  in all solvents studied. More generally, the presence of protic solvent in the electrolyte composition leads to the same shift in the occurring reactions that was observed in the work of Sharon et al. [203].

When it comes to salts,  $\text{NaPF}_6$  was claimed by Das et al. [198] and Liu and coworkers [205] to be a better salt than  $\text{NaClO}_4$  when dissolved in DME. In tests conducted by Lutz et al. [206], perchlorates, triflates, hexafluorophosphates, and TFSI-based salt were investigated in DME, DMSO, and MeCN as part of a Na-air cell. For DME solvent the TFSI-based salt was found to be unstable, whereas perchlorates and triflates led to a continuous growth of SEI on the Na anode. Finally, within the same contribution,  $\text{NaPF}_6$  was reconfirmed as a salt allowing for the formation of a stable interface.

Applicability of a 1 M  $\text{NaPF}_6$  solution in a 1:1 mixture of EC and DMC (without the addition of FEC) was confirmed by Sun et al. [207]. An interesting approach toward the improvement of a fully organic Na-air cell is presented by Yin and coworkers in [208]. Here, an unspecified “typical” organic electrolyte is placed, with NaI added to act as a dissolved catalyst. It was found that the cycling performance of the cell is strongly dependent on the concentration of the dissolved NaI. The discharge and charge processes of the Na-air battery in a 0.05 M NaI-containing electrolyte were found to be highly reversible and stable for up to 150 cycles. On the other hand, the impact of the composition of the catholyte was examined by Hayashi et al. [194]. In this case, 0.5 M  $\text{NaPF}_6$  in PC-FEC electrolyte was investigated with a NASICON-type ceramic separator while the concentration of the aqueous NaOH catholytic solution varied in the 0.01 to 0.5  $\text{Mdm}^{-3}$  range. It was found that the cell voltage decreases nearly proportionally to the logarithm of  $c_{\text{NaOH}}$ . The Israeli group led by Peled and Golodnitsky investigated [209] a solid polymer electrolyte obtained by dispersing high-surface-area  $\text{Al}_2\text{O}_3$  nanoparticles in PEO/TEGDME. Another composition of the polymeric electrolyte proposed by them [210] was based on PEO  $M_w = 5 \times 10^6$  with NaTf salt  $\text{Na}:O = 1:20$ , with the addition of 6% w/w of nanoporous  $\text{Al}_2\text{O}_3$  and 10% v/v of methyl methanesulfonate. It was prepared according to an earlier work by the same group [211]. It was compared with the  $\text{PYR}_{14}\text{TFSI}$  ionic liquid based electrolyte containing of 0.5 M NaTf and 0.1 M  $\text{Na}_2\text{SO}_4$  as the additives which was prepared according to Blum et al. [212]. The latter composition (the one with NaTF and  $\text{Na}_2\text{SO}_4$ ) was here found to be superior to the former one. On the other hand, Zha et al. [200] found  $\text{PP}_{13}\text{TFSI}$  to be not stable enough in the cell tests. Das et al.

[213] found the IL-based electrolyte  $\text{NaCF}_3\text{SO}_3/1\text{-ethyl-3-methylimidazolium trifluoromethanesulfonate}$  (EMIM Tf) to be superior to common aprotic solvents. The same conclusion was drawn by Kang and coworkers [192] in the case of  $\text{Na}_x[\text{FSI-C2C1im}] [\text{FSI}]_x$  RTIL comprising the same cation and bis(fluorosulfonyl) amide anion ( $x = 0, 3$ ).

## 7.4 Potassium

From the point of view of the air-cathode-equipped cell, potassium is believed to be a softer cation in comparison with sodium and, especially, lithium. Consequently, according to Sharon and coworkers [203], it generates lower value of the overpotential in the ORR reaction in comparison with the other two alkali metals. Unfortunately, due to significant safety issues, potassium metal is not relevant for any future technological applications. Nevertheless, it is important to focus on some issues resulting from the research on potassium-containing cells. Wu et al. [214] demonstrated a workable  $\text{K-O}_2$  cell containing  $\text{KPF}_6$  salt in DME as an electrolyte.  $\text{KO}_2$  was the sole discharge product. This compound was found by Schwenke and coworkers [215] to degrade the aprotic solvents. It was also found that purified glymes and DMSO solvents are reasonably stable in the presence of  $\text{KO}_2$ . However, the commercialized polyethers, which contain various impurities, undergo reactions with  $\text{KO}_2$ . Similar experiments were performed by the same group on  $\text{Pyr}_{14}\text{TFSI}$  IL-based electrolytes [216]. The reactions of  $\text{O}_2^-$  with the pyrrolidinium cation were much faster in comparison with the glyme solvents. Deceleration of the side reactions leading to the solvent decomposition was obtained by Ren et al. [217] by introducing a  $\text{K}^+$  ion-selective membrane able to prevent the diffusion of the oxygen toward the anode. In consequence, the membrane-based  $\text{KO}_2$  cell exhibited both improved cycling performance and less prominent changes of the overpotential values in comparison with the results presented by Sharon et al. in their review [203]. In another study originating from the same research group potassium bis(trifluoromethanesulfonyl)imide (KTFSI) salt was found to be superior to the previously mentioned  $\text{KPF}_6$ . It was

discovered to improve the stability of the potassium metal. The formation of a stable SEI inhibiting continuous decomposition of the DME solvent and suppressing the reactions with the oxygen species was observed in another work of Ren and coworkers [218]. It was suggested that the mentioned anode protection layer is formed due to reactions occurring between the potassium metal, the TFSI anions, and small amounts of DME. DME was proved by Zha and coworkers [200] and Zhang et al. [219] to be a solvent standard for the electrolyte in K-air batteries, where it exhibits good stability.

When it comes to other cathode types, the cathode material  $\text{KTi}_2(\text{PO}_4)_3$  was found by Leonard et al. [220] to be cyclable in a water-in-salt-type electrolyte based on potassium acetate. The electrolyte, with a stability window of 3.2 V, is claimed to be suitable for use in aqueous potassium cells. Unfortunately, this assumption is not confirmed by any measurements of complete devices. Gao and coworkers [221] reported a polyaniline-based cathode as successfully cyclable against a metallic potassium anode in a cell separated by a gel polymeric electrolyte. The gel matrix was obtained in a similar way to that used for the preparation of its sodium-conducting variant proposed by the same authors in Ref. [222], namely in free radical copolymerization of methyl methacrylate and tetraethylene glycol dimethacrylate. A  $\text{KPF}_6$  solution in a PC:FEC mixture was used to provide the potassium ion-mobile phase of the gel. An organic perylene-3,4,9,10-tetracarboxylic dianhydride cathode was used by Fei et al. [223] in a cell utilizing a polycarbonate-based polymeric electrolyte. KTFSI salt was used to provide room-temperature conductivity exceeding  $10^{-5}$  S/cm, which is 2 orders of magnitude higher than for a PEO-KIO<sub>3</sub> reference system. The membrane polypropylene-*co*-1-butene)-SPE was synthesized by a facile solution-casting method reported in an earlier work of Zhang and coworkers [224]. In the cell, the polymer was prepared in the form of a composite with a cellulose-based nonwoven membrane providing mechanical strength to the film. The liquid organic electrolyte solution of 1 M  $\text{KBF}_4$  in 3:7 EC/EMC (wt.) was applied in a cell with a Prussian blue cathode [225] by Eftekhari. The potassium secondary battery proposed is claimed to bear some valuable advantages, such as

high cyclability, low cost, and simplicity of fabrication, attributed to the excellent intercalation/deintercalation performance of the cathode toward potassium ions. In another study EC+DEC and EC+DEC+FEC solvent mixtures were paired with KPF<sub>6</sub> and potassium bis(fluorosulfonyl)imide salts by Zhang et al. [226] to examine the properties of the potassium-intercalated material GeP<sub>5</sub>. Good reversibility of the electrochemical process with a specific capacity of 500 mA h g<sup>-1</sup> was confirmed. Last but not the least, a leak-tight potassium ion exchange membrane based on the  $\beta''$ -alumina structure was reported by Crosbie et al. [227]. A novel method of ion exchange was invented here and introduced to convert the original sodium-doped material into a potassium-containing one. Vapor ion exchange in the atmosphere of vaporized KCl helped overcome the drawback of the “classical” method based on immersion in molten KNO<sub>3</sub>. The modification was needed as the latter method was found to fracture the modified material.

## 7.5 Magnesium

Despite widely known passivation-related problems, a magnesium anode is, as reported by Sharon et al., believed to be able to maintain its reversible behavior [203]. Furthermore, conjugating the magnesium anode and an oxygen cathode results in one of the highest theoretical values of energy density in battery cells. Despite these attractive properties, the development of a practical Mg-O<sub>2</sub> battery was hindered (since 1970, when the research began), mostly due to the high corrosion rate of metallic magnesium in water. Nevertheless, recent research conducted by Zhang et al. [228] and Jensen with coworkers [229] shows that tuning the pH value to a value above 10, together with the formulation of the electrolyte as a near-saturated aqueous solution of LiCl, MgCl<sub>2</sub>, or a mixture of these two salts, can suppress the hydrogen evolution reaction and promote the corrosion resistance of Mg. Moreover, it was proved that the type of anion also plays an important role. On comparing NaCl, KHCO<sub>3</sub>, NH<sub>4</sub>NO<sub>3</sub>, NaNO<sub>3</sub>, NaNO<sub>3</sub> + HNO<sub>3</sub>, Mg(NO<sub>3</sub>)<sub>2</sub> + NaNO<sub>2</sub>, NaNO<sub>2</sub>, Na<sub>2</sub>SO<sub>4</sub>, MgCl<sub>2</sub>, and MgBr<sub>2</sub>, Sathyaranayana and Munichandraiah [230] found that the

$\text{Mg}(\text{NO}_3)_2 + \text{NaNO}_2$  mixture is superior to other investigated salts. As found by Godard et al. [231] a low concentration of salt is usually necessary to slow down anode corrosion. Further electrolyte modification achieved through the nanodispersion of  $\text{MoS}_2$  in aqueous  $\text{MgCl}_2$  was proposed by Shyma and coworkers in [232]. The resulting “slurry” was used as a “catalytic” electrolyte, resulting in about 20% improvement in the cell capacity in comparison with the basic  $\text{MgCl}_2$  electrolyte.

Among the currently investigated magnesium-based systems most of the applications struggle for biocompatibility of the resulting air-breathing cells. Zhao et al. [233] studied the performance of batteries utilizing  $\text{NaCl}$ -based aqueous electrolytes containing as additives phosphate and vanadate corrosion inhibitors. In the research, the phosphate anion was found to exhibit a stronger inhibiting effect than the vanadate one. The authors concluded that in addition to (or rather in consequence of) the suppression of the corrosion of the anode the respective electrode coulombic efficiency was improved. In addition, the batteries exhibited extremely low anodic efficiency losses in the no-discharging periods. Moreover, phosphates are favored in magnesium-based cells due to their biocompatibility, making them a prospective energy source for biimplants. A much more complicated system is presented by Yu et al. in Ref. [234]—a cytocompatible electrochemical system. It is based on a tricomponent hydrogel matrix obtained by a two-step cross-linking process. A poly(3,4-ethylenedioxythiophene) poly(styrene sulfone) system is ionically cross-linked by means of infiltration by an aqueous solution of  $\text{Mg}(\text{NO}_3)_2$ . Here, the  $\text{Mg}^{2+}$  cations act as an electrostatic cross-linking agent for the negatively charged poly(styrene sulfone) chains. Finally, a layer of polypyrrole (PPy) is electrochemically deposited on the surface of the hydrogel membrane. Another example of a totally different approach toward biodegradable magnesium-conducting membranes is in the work of the group led by Forsyth and MacFarlane [235], where silk fibroin (SF) was used as the polymeric protein backbone of a gel-type electrolyte plasticized with the choline nitrate ( $\text{SF}-[\text{Ch}][\text{NO}_3]$ ) IL as a plasticizing solvent. It was found that IL presence is responsible for the structural transition of the protein. Moreover, C–C–OH moieties belonging to it are found to be responsible for the interactions with

$Mg^{2+}$  cations. In another work by the same research group [236] a biocompound-based (choline nitrate) IL was gelled with chitosan and assembled with a PPy cathode and a Mg anode to create a biocompatible solid-state Mg-air device. The polymer gel was found to function not only as an electrolyte and a separator but also as the glue to hold all of the device components together.

In contrast, relatively few studies have explored the possibility of designing a rechargeable  $Mg-O_2$  cell utilizing a nonaqueous electrolyte. A magnesium-aluminum chloride complex (MACC) electrolyte was reported by Vardar et al. [237]. Nonaqueous  $Mg-O_2$  cells that operate at elevated temperatures were reported in Refs. [238, 239] by Shiga et al. The electrolytes applied included Mg salts such as  $Mg(ClO_4)_2$  and  $Mg(N(SO_2CF_3)_2)_2$  dissolved in both organic solvents and ILs. Due to the formation of impermeable passivation layers, various countermeasures were applied, such as the use of ILs, proposed by MacFarlane et al. [240, 241] (e.g., trihexyl(tetradecyl)phosphonium chloride). Trihexyl(tetradecyl)phosphonium dicyanamide and tributyl(decyl)phosphonium chloride were used by Khoo and coworkers [242]. They claimed that when mixed with water, both are promising solutions. Another type of system was proposed by the group of Aurbach [243] after they synthesized the modified Grignard-type electrolyte. Another Grignard-based electrolyte, 1 M EtMgBr dissolved in tetrahydrofuran (THF), was successfully tested by Cheng et al. [244] against a 3D porous anode. The all-inorganic MACC solution in DME was found to result in a high discharge capacity but poor rechargeability of the final cell. On the other hand, a high-temperature system based on a Mg anode and a Ca-stabilized  $ZrO_2$  oxygen-conducting electrolyte was reported by Inoishi and coworkers [245] as a stable device even at 800°C. The problem found relates to the fact that the calcium-stabilized zirconia electrolyte cannot pump oxygen to a level that leads to  $MgO$  reduction at 1073 K because of the low transport number of oxide ions. Therefore, the performance of this cell in terms of its rechargeability is a failure. The paper states, however, that a rechargeable Mg-air battery could be achieved by using an electrolyte with high stability in a reducing atmosphere or by decreasing the operating temperature.

## 7.6 Calcium

Issues related to the reversibility of the calcium stripping/plating electrochemical reactions [246–248] were found to limit the applicability of this metal in the classical cell designs described in Chapter 6. In contrast to the above-mentioned studies, in one of the lately studied Ca-air cells, 0.5 M  $\text{Ca}(\text{ClO}_4)_2$  in PC and  $\text{Ca}(\text{ClO}_4)_2$ ,  $\text{Ca}(\text{BF}_4)_2$ , or  $\text{Ca}(\text{TFSI})_2$  in EC:PC were used as an nonaqueous electrolyte [249]. At elevated temperatures ( $50^\circ\text{C}$ – $100^\circ\text{C}$ )  $\text{Ca}(\text{ClO}_4)_2$  and  $\text{Ca}(\text{BF}_4)_2$  were proved to establish conditions for reversible plating and stripping, with the latter being superior to the former. Moreover, research provided by Wang et al. utilized 1.5 M  $\text{Ca}(\text{BH}_4)_2$  in THF [250], proving that in this case reversibility can be achieved at ambient temperature. The effect of the salt concentration was investigated by Reinsberg and coworkers [251], where the DMSO solutions of  $\text{Ca}(\text{ClO}_4)_2$  of various concentrations, ranging from 0.1 to 0.4  $\text{Mdm}^{-3}$ , were tested. It was found that THF-based Ca-ion electrolytes with  $\text{Ca}(\text{BF}_4)_2$  offer the best reversible Ca plating and stripping performance among all tested till now. Unfortunately, the plating efficiency is still below the 99.98% threshold claimed by Whittingham [252] as required for practical cell applications. On the one hand, little work has been performed till now on the use of superconcentrated aqueous electrolytes, for example, one containing  $\text{Ca}(\text{NO}_3)_2$  tested by Lee and Jeong [253]. On the other hand, the very early patent claim of Cooper et al. [254] states that the aqueous electrolyte for a calcium-based battery should consist of alkali metal hydroxide and alkali metal chloride added to promote a stable electrode state. In addition, a small amount of corrosion inhibitor, such as sodium stannate, can be added to the solution.

## 7.7 Aluminum

While the original development of the Al-air cell utilizing alkaline electrolytes can be traced back to the works of Zaromb [255] and Trevethan et al. [256], published in the early 1960s, it unfortunately

showed that the alkaline solution can absorb carbon dioxide from air. This harms the cell's performance by crystallization of carbonates. Therefore, Despic et al. [257] were the first to explore the Al-air cell with the saline electrolyte containing 12% of sodium chloride. To improve the cell performance additives such as sodium phosphate, sodium sulfate, sodium fluoride, and sodium bicarbonate were investigated as coagulants to  $\text{Al(OH)}_3$  produced in the cell. According to the review paper of Li and Bjerrum [258], the best results can be obtained for the NaF addition. Flocculating agents to precipitate the discharge product have also been examined by Rao et al. [259]. On the other hand, it has been found that an acidic electrolyte is beneficial to improve the battery performance. This observation was confirmed by the works of Buri et al. [260] and Equy and coworkers [261]. Systems of this type were further investigated by Holzer et al. [262, 263].

Despite the above-mentioned drawbacks the most popular alkaline-based designs are still under investigation. Liquid 4 M NaOH and 7 M KOH solutions were tested by Ilyukhina and coworkers [264], with the addition of  $\text{Na}_2\text{SnO}_3$  trihydrate being recognized on the basis of the work of Kapali et al. [265] as a most powerful corrosion inhibitor of aluminum in alkaline media. The optimal concentration of the additive was found to be around 0.04 M when coupled with the electrolyte based on 4 M NaOH and containing 20% sodium citrate with the addition of 0.4% CaO. The level of inhibition can be further extended by the synergistic effect when 0.01 M  $\text{In(OH)}_3$  is added to the stannate-containing electrolyte, as proved by Egan et al. [266]. The indium compound was found to act as the sole inhibitor, though it was weaker than the tin-based one, while the addition of gallium was found to be unviable. On the other hand, Albert et al. [267] used as additives  $\text{CaCl}_2$  dihydrate (2.5%) and NaCl (0.1%-3%) based on a 4 M NaOH solution containing 20% sodium citrate. Other additives to the electrolyte enlisted in Ref. [266] include cationic surfactants, for example, cetyltrimethylammonium bromide (CTAB), which was found by Al-Rawashdeh et al. [268] and Abdel-Gaber and coworkers [269] to weakly inhibit the corrosion of aluminum. In contrast, cetyltrimethylammonium chloride was found to be inactive. Lupine seed extract was found to inhibit the open-circuit corrosion of the

aluminum anode as well [266]. To immobilize the liquid, gelled systems were tested as an electrolyte in Al-air galvanic cells by Li et al. [112]. Moreover, polymer-based host membranes often used in modern research were the focus for this type of battery. The final form of the electrolyte is in this case a PAA (poly(acrylic acid)), poly(vinyl alcohol), or PEO gel doped with aqueous alkaline solution, which was demonstrated by Zhang et al. [270]. PAA/KOH with the addition of ZnO as the corrosion inhibitor of the anode is claimed to give the highest ionic conductivity value when compared to other polymer host membranes investigated. The resulting cell exhibits valuable electrochemical characteristics while on the other hand, issues related to mechanical and thermal stability of the membrane need to be improved as they affect both overall cell performance and durability. In research by Pino and coworkers [271], a PAA-based gel was cross-linked with *N,N'*-methylene-bisacrylamide and doped with ZnO and ZnCl<sub>2</sub> as a corrosion inhibitor. The behavior of various alloyed anodes containing Ga, In, Sn, or Mg were tested in an alkaline electrolyte based on KOH immobilized in the gel. In research by Mokhtar et al. [272], ecofriendly, easily recyclable chitosan hydrogel-based membranes were found to show superior electrochemical performance in a coin-design Al-air cell. In addition they are claimed to be easily recyclable. Further improvement of the system performance was achieved by Liu and coworkers [273] by the addition of a 10% SiO<sub>2</sub> filler to the biohydro gel electrolyte. The silicon-based filler was found to be superior to ones based on zinc oxide and tin oxide.

A hybrid dual-electrolyte design has been described by Wang et al. in Ref. [274]. The organic anolyte 3 M KOH in anhydrous methanol as a solvent and the aqueous catholyte 3 M KOH in H<sub>2</sub>O were separated by a strong alkali anion exchange membrane AMI7001 based on the quaternary ammonium salts and developed by Membrane International Inc. The hybrid successfully suppressed the parasitic reaction and hence achieved superior anodic capacities compared with a two-sided aqueous Al-air cell equipped with the same membrane. On the other hand, Egan et al. [266] demonstrated that the applicability of a two-sided alcohol-based design is limited due to their lack of oxidative stability in contact with the cathodic catalyst.

A totally different approach was presented by Bogolowski et al. [275], who utilized  $\text{AlCl}_3$  solution in an acetamide-urea deep-eutectic solvent. The properties of the resulting electrolyte were additionally improved by the addition of an EMIMCl-based IL. A more detailed discussion of the limitations hindering the application of ILs in Al-air cells is provided in Ref. [266]. A Sb(V)-doped  $\text{SnP}_2\text{O}_7$   $\text{OH}^-$  solid conductor was investigated by Hibino et al. [276]. They also found that hydroxide ion exchange capability occurring in the bulk of the  $\text{SnP}_2\text{O}_7$  material results from the charge compensation upon the partial substitution of  $\text{Sn}^{4+}$  with  $\text{Sb}^{5+}$  [277]. An optimized composition  $\text{Sn}_{0.92}\text{Sb}_{0.08}\text{P}_2\text{O}_7$  is claimed to exhibit the highest hydroxide ion conductivity. The same research group [278] attributed an additional advantage of the proposed material over the MeOH-based aqueous electrolytes to its high tolerance to the  $\text{CO}_2$  present in ambient air. A ceramic Al-ion conductor was used by Mori in his research [279]. Two separate layers of  $\text{Al}_2(\text{WO}_4)_3$  were placed, one on top of the aluminum anode and the other underneath the air cathode. An anodic film was obtained by printing of the slurry composed of  $\text{Al}_2(\text{WO}_4)_3$  powder and terpineol on the aluminum anode, followed by its annealing at  $600^\circ\text{C}$ . On the other hand, the  $\text{Al}_2(\text{WO}_4)_3$  lid was prepared by mixing the  $\text{Al}_2(\text{WO}_4)_3$  ceramic component with the PVdF polymeric binder and pressing the resulting mixture into the form of a disk.  $\text{NaOH}$  was placed in between, creating a space for the accumulation of the cell discharge products. Unfortunately, the material was found to be unstable in the long term, with the replacement of  $\text{Al}^{3+}$  cations in its structure by  $\text{Na}^+$  ones. How to partially overcome the mentioned drawback was proposed by the same author in his paper a year later [280]. It was achieved by the addition of electroactive carbon to the  $\text{Al}_2(\text{WO}_4)_3$ -PVdF lid substrate, by which a bifunctional electrolyte-electrode composite replaced the two separate layers present in the original design.

## 7.8 Zinc

Recently, the interest of the scientific community [281, 282] turned toward the development of secondary zinc-air batteries based on

aqueous neutral electrolytes. A neutral electrolyte has two principal advantages in comparison to an alkaline electrolyte: (i) it avoids the carbonization of the electrolyte and (ii) it reduces dendrite formation. Both factors might improve the cycle life of the secondary zinc-air batteries due to the “neutral” pH of the electrolyte. A summary of the precursor salts used in the said systems is delivered in Table 7.2. One must notice an important fact related to the ionic equilibria present in many of the electrolytic compositions. The zinc ions present form reducible complexes with the appropriate anionic species. The nonalkaline solutions proposed are, of course, not free from some operational drawbacks. For example, Amendola [283] reported that for aqueous chloride-based electrolytes, the more general problem is related to their strongly corrosive properties, while the rechargeable batteries using them also suffer from the side reaction involving chlorine evolution during cell charging, which discourages oxygen evolution and reduces overall cell charging. Therefore, additives able to mitigate this unwanted process are introduced into the electrolyte formula. Some examples of these compounds are delivered in the last section of Table 7.2. Hassan [284] reports that for perchlorates, problems related to their reduction are observed. He discovered a whole family of possible intermediates formed during zinc perchlorate reduction, including chlorate  $\text{Zn}(\text{ClO}_3)_2$ , chlorite  $\text{Zn}(\text{ClO}_2)_2$ , and hypochlorite  $\text{Zn}(\text{ClO})_2$ , which are all soluble species and do not, fortunately, contribute to the passivating layer. Other aqueous neutral electrolytes have also been reported. As presented in other two works of Amendola et al. [285, 286], they can be based on sulfates, nitrates, carbonates, tetrafluoroborates, methane sulfonates, permanganates, hexafluorophosphates, borates, or phosphates or their mixtures. A modification of the well-known zinc manganese dioxide cell electrochemistry by changing its electrolyte composition is reported by Zhang and coworkers [287]. Aqueous solutions of 3 M  $\text{ZnSO}_4$ , 3 M  $\text{Zn}(\text{CF}_3\text{SO}_3)_2$ , and 3 M  $\text{Zn}(\text{CF}_3\text{SO}_3)_2$  with a 0.1 M  $\text{Mn}(\text{CF}_3\text{SO}_3)_2$  additive were found to be significantly better in comparison with the reference electrolyte composition—45 wt.% KOH solution.

According to a report of Jindra et al. [289] acidic electrolytes have barely been utilized in rechargeable zinc-air batteries because they require a suitable catalyst and support to overcome problems

**Table 7.2** Reported aqueous neutral electrolytes for zinc-based cells

Chloride-based electrolyte	References	Other electrolyte	References
KCl	[289]	$\text{BF}_4^-$	[285, 286]
NaCl	[289]	$\text{BO}_3^{3-}$	[285, 286]
$\text{NH}_4\text{Cl}$	[283, 289, 290]	$\text{CH}_3\text{SO}_3^-$	[285, 286]
$\text{PbCl}_2, \text{PbCl}_4$	[285]	$\text{CO}_3^{2-}$	[285, 286]
$\text{HgCl}_2, \text{Hg}_2\text{Cl}_2$	[285]	$\text{MnO}_4^-$	[285, 286]
$\text{CdCl}_2$	[285]	$\text{NO}_3^-$	[285, 286, 289]
$\text{BiCl}_3$	[285]	$\text{PF}_6^-$	[285, 286]
$\text{SnCl}_2, \text{SnCl}_4$	[285]	$\text{PO}_4^{3-}$	[285, 286]
$\text{LiCl}$	[285]	$\text{SO}_4^{2-}$	[285, 286, 289]
$\text{MgCl}_2$	[289]	$\text{S}_2\text{O}_3^{2-}$	[289]
$\text{ZnCl}_2$	[289, 290]	$\text{ClO}_4^-$	[284, 291, 292]
Additives to minimize chlorine evolution			
$\text{CoCl}_2$			[285]
$\text{IrO}_2$			[285]
$(\text{NH}_2)_2\text{CO}$			[285]
Soluble manganese salts			[285]

Source: [288]

related to the catalytic activity of the air electrode and the low life times of the electrolytes. In addition, Zhang et al. [293] claimed that in acidic media, the passivation of a zinc surface does not occur without the presence of film-forming agents. Despite these problems acidic electrolytes were used in zinc-ceria flow batteries and in zinc-oxygen cells. In the latter case, Blurton et al. [294] patented an aqueous acid electrolyte selected from a group consisting of  $\text{H}_2\text{SO}_4$ ,  $\text{H}_3\text{PO}_4$ , and  $\text{H}_3\text{BO}_3$  and mixtures thereof. The authors claim that the solution hindered dendrite formation and its lack of carbon dioxide adsorption problems are characteristic of alkaline electrolytes. Lewenstein and Terrace [295] reported that quaternary ammonium salts are inhibitors of hydrogen evolution for zinc in acidic solutions. Unfortunately, no direct evidence of their applicability in other-than-Leclanche-type cell-oriented applications was provided as the observation originates from galvanic plating research. On the other hand, inorganic inhibitors such as indium and lead compounds were found to be inferior to the organic ones, such as CTAB, when it comes to zinc-based redox flow electrolytes formulation. Special

attention was paid by Ivey et al. [296] to the application of organic acids in the electrolyte formulation. Methane sulfonic acid, polyvinyl sulfonic acid, and polyvinyl sulfuric acid were also, unfortunately, found to be undesirable for practical application due to the anode instability. It is worth pointing out that according to Kordesch et al. [297], independently of its “neutral” composition, a  $\text{ZnBr}_2$ -based electrolyte applied in a Zn-carbon cell (and found there superior to “classical”  $\text{ZnCl}_2$  one) can be described as an acidic composition as it reveals pH values in the range between 3 and 4.

On the other hand, while extensive work was performed in the field of organic lithium electrolytes, analogic zinc-oriented systems remain strongly underdeveloped. The available reports claim that the performance of the zinc anode in these systems is very promising. For example, Guerfi et al. [298] selected an organic electrolyte based on PC and 0.3 M fluoro-based salt ( $\text{Zn}(\text{TFSI})_2$ ) that reached more than 1700 cycles at 99.8% efficiency at 1C charge/discharge rate with the use of basic emeraldine form of poly(aniline) as a cathode. As an alternative, organic electrolytes based on polymers and RTILs were also tested in these systems. PC, EC, and DMSO have been proposed as aprotic solvents for zinc cells.  $\text{Zn}(\text{CF}_3\text{SO}_3)_2$  solutions in organic solvents were immobilized in PAN and PVdF, reaching attractive conductivity values. Unfortunately, they are, due to their volatility, inapplicable in open designs such as zinc-air ones.

Ye et al. [299] and the group lead by Armand [300] found that liquid olygoethers are characterized by not only reduced volatility but also the capability to dissolve zinc salt such as  $\text{Zn}(\text{TFSI})_2$  tenfold better than organic carbonates. In addition, Abraham and coworkers [301] declare that they are potentially applicable in the form of gels with Kynar® or PMMA. Unfortunately, according to the latter contribution, their use in real applications is still not feasible due to the poor solubility of zinc salts in polymeric gels. Giua et al. [302] and Baril et al. [303] found zinc-conducting solid polymeric electrolytes to be inapplicable due to their limited conductivity.

One of the declared advantages of using aprotic RTILs for Zn-air battery systems is that Zn corrosion from hydrogen evolution can be avoided due to the absence of protons in the electrolyte. The current efficiency for electrodepositing Zn in RTILs is improved

as a consequence, usually exceeding 85% as per Ivey et al. [304]. Many aprotic RTILs [305–311] were used as aprotic solvents. Compositions such as 1-butyl-1-methylpyrrolidinium bis(trifluoromethanesulfonyl)imide, 1-ethyl-3-methylimidazolium bis(trifluoromethanesulfonyl)imide, 1-butyl-1-methylpyrrolidinium dicyanamide, and 1-ethyl-3-methylimidazolium dicyanamide (EMI-DCA) have been proposed and evaluated. Their application is reported to lead to “partial” benefits, such as (i) improvement of current density, (ii) increase in the energetic efficiency of the cell roundtrip, as well as, (iii) the suppression of the zinc deposition overpotential occurring in the case of the latter of the investigated RTILs. Therefore, according to the report of Li et al. [112] the final application-oriented conclusion related to them is rather disappointing as the performance of zinc-air batteries using KOH as the electrolyte could not yet be replicated by any aprotic electrolyte. Detailed analysis of the possibilities related to the application of RTIL as the basis for the electrolytes used in secondary zinc batteries is delivered by Mainar et al. [288]. Here it is worth pointing out two problems arising in this field. The first is related to the presence of zinc cation in form of anionic complexes, with moieties originating from the IL as ligands. This makes RTILs, in general, undesirable for facile electrochemical reduction. The problem can be ameliorated by incorporating the IL cation moieties into the complex structure. The second issue that must be here addressed is the need for a fundamental understanding of the influence of water addition on the physical and electrochemical behavior of electrode reactions occurring in the IL-containing cell. Hence, hydrophobic compounds are according to Xu and coworkers [312] desirable for achieving a stable electrolyte system under open-air conditions.

A cheaper and greener replacement of an RTIL is a deep eutectic solvent (DES). Abbot et al. [313] declared it as being capable of dissolving various metal oxides because the said mixtures are able to donate or accept electrons or protons to form hydrogen bonds, which confer excellent dissolution properties. Their main drawback is related to their significantly higher viscosity in comparison with that of the typical RTIL. An acetamide-based DES has been claimed by Narayanan et al. [314] as an electrolyte to be used in developing zinc-based cells. Binary (acetamide  $\text{Zn}(\text{ClO}_4)_2$ ) and tertiary (with the addition of urea) molten electrolytes were found to be suitable

for secondary zinc batteries. The problem of viscosity was solved by the addition of low-molecular-weight fluorinated compounds by Zhang et al. [315]. Mainar and coworkers [288] delivered an extensive review of the prospective DES chemistries. Other applicable molten salt systems are based on high-temperature melts of alkaline metal carbonates. Liu et al. [316] found the carbonate mixture  $\text{Li}_{0.87}\text{Na}_{0.63}\text{K}_{0.50}\text{CO}_3$  to form eutectics with NaOH. The so-obtained melts are applicable at 550°C as electrolytes in a high-temperature zinc-air cells. A replacement of NaOH to KOH was, on the other hand, found to improve the cell characteristics. Liu and coworkers [317] achieved in this case both higher discharge rates and higher discharge voltages.

Review papers presented by Pei et al. [318] and Martirosyan [319] underline the importance of the application of an additional separator to both prevent the mixing of catholyte and anolyte and retard zinc dendrite growth. Merla et al. [320] claim that the material used for this purpose should meet the basic requirements, including stability, electrical insulation, ionic conductivity, and electrolyte storage. The fulfillment of these requirements was proven by Sapkota and Kim for organic polymer porous membranes [321] and by Dewi et al. [322] for Celgard 4560 and Celgard 5550 separators. Saputra and coworkers [323] achieved promising results for an “inorganic” in-house prepared MCM-41 membrane made from a cationic surfactant, cetyl-trimethyl-ammonium bromide, and a silica-covered organic template. Xu et al. [304] found that hybrid electrolytes, being a combination of aqueous or nonaqueous systems and ILs, garnered attention as potential new generations of electrolytes. The same authors [296] found that the addition of EMI-DCA to aqueous KOH solution prevents dendritic growth, leading to homogenous and porous Zn film deposition. In a study by Liu et al. [324], the addition of DMSO as a cosolvent allowed for a significant decrease in the viscosity of the RTIL-based electrolyte. In addition, a polar solvent such as DMSO was found by Persson [325] to facilitate the solvation of Zn ions and by Trahan and coworkers [326] as capable of stabilizing ORR intermediates (in this case superoxide radicals). Xu et al. [327] observed a synergistic effect of adding both water and DMSO to EMI-DCA, leading to improved reversibility, cyclability, and kinetics of the Zn redox reactions. It should be, however, pointed out that, independently of their

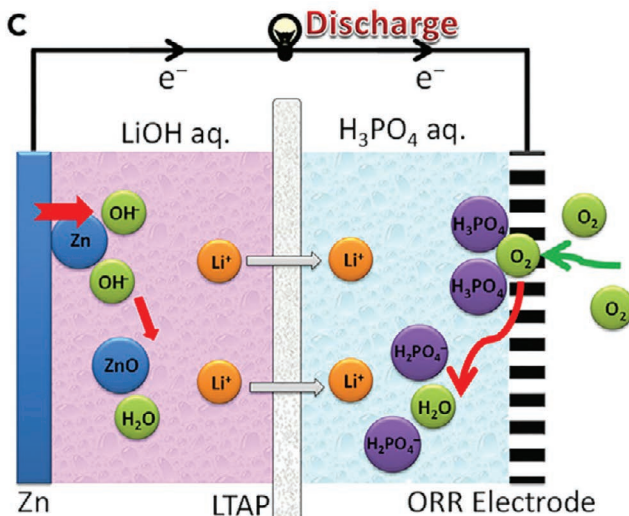


**Figure 7.5** Schematic design of a zinc-air cell utilizing the ion-mediator concept (Ref. [328]).

features, the multicomponent electrolytes significantly increase the complexity of the nature of the cell electrochemical processes. Finally, Yu and Manthiram [328] presented an example of a totally different approach to a zinc electrochemistry-based cell, presenting in the cited paper “a recently proposed and validated” mediator-ion battery concept. It is unique due to the fact that the redox reactions at the anode and cathode are ionically linked by the shuttling of a mediator ion through a solid-state electrolyte (see Fig. 7.5). Therefore, a  $\text{Li}^+$  or  $\text{Na}^+$  transporting membrane acts as a “messenger” to balance the charge transfer at the anode and cathode. The transported ions do not play a direct role in the electrochemical reactions occurring. For example, a  $\text{KOH}/\text{LiOH}$  anolyte, an LATP ( $\text{Li}_{1+x+y}\text{Al}_x\text{Ti}_{2-x}\text{Si}_y\text{P}_{3-y}\text{O}_{12}$ ) ceramic separator, and a  $\text{KMnO}_4/\text{H}_2\text{SO}_4$  catholyte are used with a zinc anode and a current-collective cathode to form a  $\text{Zn-KMnO}_4$  cell with an operational voltage in the range of 2.8 V. Other combinations presented include (i) a  $\text{Zn}(\text{NO}_3)_2$  anolyte and  $\text{LiNO}_3$  catholyte Daniel-type  $\text{Zn-Cu}$  cell, (ii) a  $\text{LiOH}$  anolyte and  $\text{Br}_2/\text{LiBr}$  catholyte  $\text{Zn-Br}_2$  cell, and (iii) a  $\text{LiOH}$  anolyte  $\text{H}_3\text{PO}_4$  and  $\text{LiH}_2\text{POP}_4$  catholyte

Zn-air one. In both cases, the same as previously mentioned LATP-type separator was used.

## 7.9 Miscellaneous

A totally different strategy of the system design was introduced when it comes to an iron-air battery. According to Xu and Manthiram [329], it is possible to assemble a high-voltage battery without using the iron ion conductor, by applying a  $\text{Li}^+$  or  $\text{Na}^+$  conductive solid electrolyte to strategically separate an alkaline anolyte from an acidic catholyte. It is stressed that despite the fact that the electrolytes are prevented from mixing, the ceramic layer serves as an ionic mediator responsible for electrochemical charge transfer. In consequence,  $\text{Li}^+$  or  $\text{Na}^+$  ions are not involved in either anode or cathode reactions. LATP, purchased from Ohara Corporation, Japan, with a  $\text{Li}^+$ -ion conductivity of  $\sim 1 \times 10^{-4}$  S/cm at room temperature, and  $\text{Na}_3\text{Zr}_2\text{Si}_2\text{PO}_{12}$ , purchased from 421 Energy Corporation, South Korea, with a  $\text{Na}^+$ -ion conductivity of  $\sim 1 \times 10^{-3}$  S/cm at room temperature were used as lithium- and sodium-conducting separators, respectively. An expected compatibility with the respective solid-state electrolyte was delivered by the use of  $\text{LiOH}$  and  $\text{NaOH}$  aqueous solutions as the anode electrolytes.  $\text{H}_3\text{PO}_4$  dissolved in water provided the acidic conditions needed for the cathode compartment. To accommodate the mediator ions in the solid electrolytes, different supporting electrolytes— $\text{LiH}_2\text{PO}_4$  and  $\text{NaH}_2\text{PO}_4$ , respectively—were added to the catholytes of the two battery systems. A different approach is demonstrated by Licht et al. in Ref. [330], where molten  $\text{Li}_2\text{CO}_3$  serves not only as an electrolyte but also as a solvent for iron oxide, which is the reaction product of the high-temperature Fe-air cell. An all-solid system based on anionic  $\text{O}^{2-}$  transport in a ceramic membrane was proposed by Trocino and coworkers in Ref. [331] (see Fig. 7.6). In this particular case, either gadolinia-doped ceria ( $\text{Gd}_{0.1}\text{Ce}_{0.9}\text{O}_2$ ) or lanthanum gallate, codoped with strontium and magnesium ( $\text{La}_{0.8}\text{Sr}_{0.2}\text{Ga}_{0.8}\text{Mg}_{0.2}\text{O}_3$  [LSGM]), was utilized as an electrolyte working in the temperature range of  $600^\circ\text{C}$ – $800^\circ\text{C}$ , which was the continuation of previous works provided by Zhao et al.

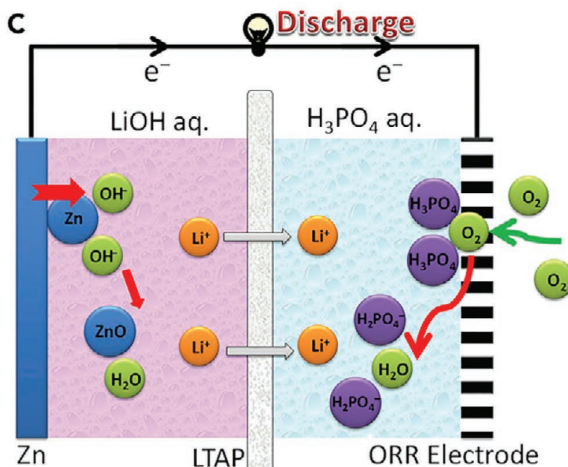


**Figure 7.6** The concept of an iron-air battery utilizing an oxygen-ion-conducting electrolyte (Ref. [331]).

[332], Berger et al. [333], Trocino et al. [334], and Inoishi and coworkers [335, 336], who used an LSGM oxide ion conductor of a slightly different composition:  $\text{La}_{0.9}\text{Sr}_{0.1}\text{Ga}_{0.8}\text{Mg}_{0.2}\text{O}_3$ . Finally, Mckerracher et al. [337] delivered a more complete review of iron-air systems.

Mg- and Fe-based cells described above aside, Chawla [188] has described systems using  $\text{W}/\text{WO}_2$  (more detailed investigations can be found in works of Zhao et al. [338, 339]),  $\text{Mo}/\text{MoO}_2$  (described in detail by Zhao et al. in Ref. [340]), and  $\text{Si}/\text{SiO}_2$  (tested by Inoishi and coworkers [341]). All three “exotic” chemistries utilized a  $\text{ZrO}_2$ -type oxygen-conducting electrolyte. Similarly to the Mg-based electrolyte, their working temperature was always around  $800^\circ\text{C}$ , which kept the anodes solid. In contrast to the above, a liquid anode configuration working in the same temperature range and with the same type of electrolyte was studied by Jayakumar et al. [342, 343], utilizing redox couples based on Sn, Bi, Sb, In, or Pb as an electroactive anode material. Otaegui et al. [344] also found these anode materials to be the most interesting choice. Negligible degradation of the active components after 4500 cycles at  $800^\circ\text{C}$  for more than 6000 h was reported here for the system,

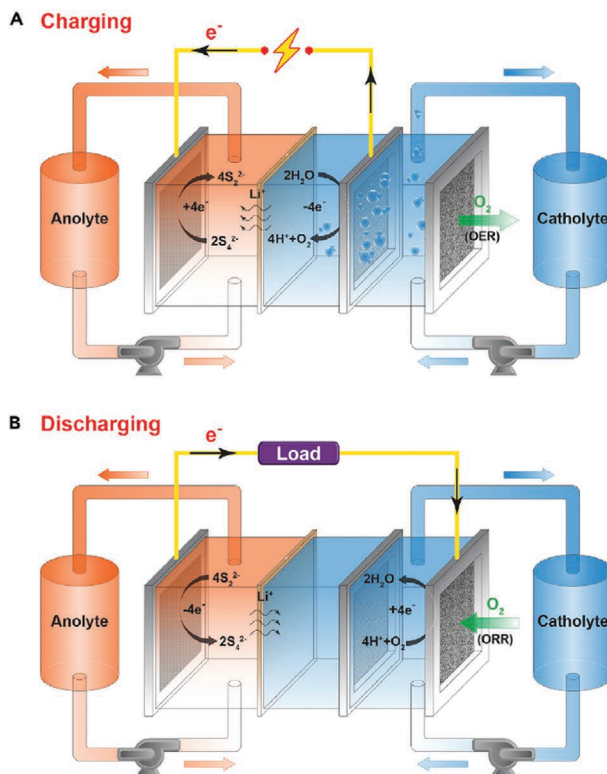


**Figure 7.7** Air-breathing aqueous sulfur flow battery concept (Ref. [351]).

together with coulombic efficiency of more than 99%. A low-temperature variation of the tin-air cell was introduced, as well, by Sumathi et al. [345] based on polymer electrolytes containing a 3 M aqueous methane sulfonic acid solution gelled with polyacrylamide. Cohn et al. described another “exotic” design, namely a silicon-air battery utilizing an  $\text{EMI} \cdot (\text{HF})_{2.3}\text{F}$  RTIL [346, 347] or a composite polymer electrolyte [348]. In the latter case, the same IL was immobilized in a poly-HEMA matrix obtained by free radical *in situ* polymerization. The gel-polymer electrolyte here was prepared according to methods described previously by Tsuda and coworkers in [349], and the IL itself was prepared as described by Hagiwara et al. [350]. An even more exotic sulfur-air battery is intended by

Li et al. [351] for ultralow-cost large-scale long-duration electrical storage (see Fig. 7.7). The catholyte here was prepared by dissolving  $\text{Li}_2\text{SO}_4$  or  $\text{Na}_2\text{SO}_4$  in 0.1 M or 0.5 M  $\text{H}_2\text{SO}_4$ . The option for an alkaline catholyte was also analyzed but rejected due to the lower final cell operational voltage. The anolyte solutions were prepared by the dissolution of elementary sulfur in mixed solutions of either  $\text{Li}_2\text{S}$  and  $\text{LiOH}$  or  $\text{Na}_2\text{S}$  and  $\text{NaOH}$ . Finally, as the starting polysulfide composition, the electrolyte contained a wide range of the polysulfides averaged to the  $\text{Li}_2\text{S}_4$  or  $\text{Na}_2\text{S}_4$ . The anolyte and catholyte compartments were separated by a ceramic  $\text{Li}^+$  or  $\text{Na}^+$  ionic conductor (LISICON or NASICON type), depending on the cation utilized in both of them. In another concept of the air battery, presented by Grosse-Austing et al. [352], with the dissolved anode reactant, the vanadium-air battery anode compartment utilizes a typical vanadium redox flow battery anodic solution containing 1.13 M of  $\text{VOSO}_4$  dissolved in 2 M aqueous  $\text{H}_2\text{SO}_4$ , which in a pure form serves as a catholyte. A double Nafion-type ion exchange membrane is used to separate the half-cells, limiting the vanadium cross-over into the cathodic compartment to a near zero.

## 7.10 Conclusions

The specific demands of the “exotic” designs described above aside, the main points to remember are: (i) the electrolyte is a critical part of alkali metal-air and other metal-air batteries; (ii) its properties are closely related to its performance; (iii) each metal-air system has its own requirements regarding the characteristics of electrolytes; (iv) there are, however, some common features, for example, for oxygen ion conductors; and (v) finding a stable, low-volatility, nontoxic, and high-oxygen-solubility electrolyte with a wide electrochemical window is a common goal for all systems. In general, investigations cover five main types of electrolytes: (i) aqueous, (ii) aprotic organic solvent based, (iii) IL based, (iv) polymeric, and (v) inorganic/ceramic. Combinations of the groups mentioned above are often found in the form of gels, layered structures, and hybrid aqueous-organic designs. In the case of strongly active metals, like sodium, the aqueous solution

**Table 7.3** Properties of some elements that can be used as air battery anodes

Element	Abundance in crust (ppm)	Density (g/cm <sup>3</sup> )	E <sub>0</sub> vs. NHE (volts)	Cell voltage (volts)	Specific capacity (Ah/g)	Energy density (Wh/kg)	Radius M <sup>0</sup> /M <sup>n+</sup> (pm)
Lithium	18	0.53	-3.04	2.96	3.86	3505	157/76
Sodium	28,300	0.97	-2.71	2.33	1.17	1602	191/102
Magnesium	20,900	1.74	-2.37	3.1	2.21	3910	160/72
Aluminum	81,300	2.70	-1.66	1.2–1.6	2.98	2800	143/53
Silicon	277,200	2.33	-0.91	1–1.2	3.85	2143	118/-
Potassium	25,900	0.86	-2.93	2.48	0.69	935	235/138
Calcium	36,300	1.54	-2.87	20	1.34	2500	197/100
Iron	50,000	7.87	-0.89	1–1.28	0.96	764	126/70
Zinc	75	6.51	-0.76	1.65	0.82	1086	137/74

Note: Data gathered from Refs. [198, 203, 247, 258] and supplemented by the authors of the chapter.

must be separated from the anode with usually a Na-conductive ceramic separator. For others, such as magnesium and aluminum, corrosion inhibitors are added to the electrolyte. Finally, Table 7.3 can serve as a comparison of some operational properties of various anodes for air-breathing electrochemical cells. Herein, it is worth noticing that most popular and extensively researched systems, such as those consisting of lithium and zinc anodes, are unaffordable in terms of their globally understood availability. In addition, whereas lithium-, sodium-, potassium-, and surprisingly iron-based cells are generally considered as reversible, most of the presented multivalent anodic element-based solutions suffer from either intrinsic or operational rechargeability limitations. Once again, omitting the problems related to the “exotic” designs, one must, therefore, stress that the struggle, reported here, to achieve reversibility in the plating/stripping reactions of calcium, magnesium, aluminum, and zinc is the major limiting factor in the development of the above-mentioned cell designs utilizing them.

Finally, from a list of six major problems that should be solved in the field of lithium power sources, at least two are related to the electrolyte of the cell: (i) investigation and design of new solvents and lithium salts that are highly stable in an oxygen atmosphere (and in the presence of Li<sub>2</sub>O<sub>2</sub>) and (ii) formulation of the key task represented by the study of the mechanism of degradation

phenomena, determined by the presence of impurities and products of parasitic reactions between the components. In the case of nonaqueous electrolytes, the main focus should be on improving their stability in an oxidation environment. Progress in this field is the key to a reasonable cycling life of the resulting cell. To achieve this target not only should solvents and lithium salts be considered, the functional additives aimed at stabilizing the electrolyte should be developed as well. Another feature that should be taken into consideration in solvent choice is the issue of minimizing oxygen solubility and diffusivity. For aqueous electrolytes [130], due to their participation in the electrochemical reactions, cell energy density optimization is an underestimated issue that must paid great attention when building an industrially applicable battery characterized by a high capacity. Moreover, the stability of the solution against the solid-state electrolyte membranes is equally crucial for the performance, reliability, and safety of the batteries. Therefore, careful assessment of this issue is needed. In addition, when a system is converted from using an oxygen-based cathode to using ambient air, the presence of N<sub>2</sub>, CO<sub>2</sub>, and, in the case of the nonaqueous aprotic systems, H<sub>2</sub>O vapor can lead to a series of side reactions, causing poor reaction reversibility and deterioration of the electrochemical performance of the organic solvent and ceramic separator-based designs.

## References

1. N. Akhtar, W. Akhtar, Prospects, challenges, and latest developments in lithium-air batteries *Int. J. Energy Res.*, **39** (2015) 303–316.
2. H. G. Jung, J. Hassoun, J. B. Park, et al., An improved high-performance lithium-air battery. *Nat. Chem.*, **4**(7) (2012) 579–585.
3. P. Tan, H. R. Jiang, X. B. Zhu, L. An, C. Y. Jung, M. C. Wu, L. Shi, W. Shyy, T. S. Zhao, Advances and challenges in lithium-air batteries. *Appl. Energy*, **204** (2017) 780–806.
4. S. J. Visco, V. Y. Nimon, A. Petrov, K. Pridatko, N. Goncharenko, E. Nimon, L. De Jonghe, Y. M. Volkovich, D. A. Bograchev, Aqueous and nonaqueous lithium-air batteries enabled by water-stable lithium metal electrodes. *J. Solid State Electrochem.*, **18** (2014) 1443–1456.

5. K. M. Abraham, Z. Jiang, A polymer electrolyte-based rechargeable lithium/oxygen battery. *J. Electrochim. Soc.*, **143** (1996) 1–5.
6. M. Balaish, A. Kraytsberg, Y. Ein-Eli, A critical review on lithium-air battery electrolytes. *Phys. Chem. Chem. Phys.*, **16** (2014) 2801.
7. F. Mizuno, S. Nakanishi, Y. Kotani, S. Yokoishi, H. Iba, Rechargeable Li-air batteries with carbonate-based liquid electrolytes. *Electrochemistry*, **78** (2010) 403–405.
8. J. Xiao, J. Hu, D. Wang, D. Hu, W. Xu, G. L. Graff, Z. Nie, J. Liu, J.-G. Zhang, Investigation of the rechargeability of Li-O<sub>2</sub> batteries in non-aqueous electrolyte. *J. Power Sources*, **196** (2011) 5674–5678.
9. S. A. Freunberger, Y. Chen, Z. Peng, J. M. Griffin, L. J. Hardwick, F. Barde, P. Novak, P. G. Bruce, Reactions in the rechargeable lithium-O<sub>2</sub> battery with alkyl carbonate electrolytes. *J. Am. Chem. Soc.*, **133** (2011) 8040–8047.
10. M. Z. Kufian, A. K. Arof, Effect of Calix[6]arene on charge discharge behaviour of lithium air cell based on PAN-LiBOB gel polymer electrolyte. *Mater. Technol.*, **29** (2014) A114–A117.
11. D. G. Kwabi, N. Ortiz-Vitoriano, S. A. Freunberger, Y. Chen, N. Imanishi, P. G. Bruce, Y. Shao-Horn, Materials challenges in rechargeable lithium-air batteries. *MRS Bull.*, **39** (2014) 443–452.
12. N. Garcia-Araez, P. Novák, Critical aspects in the development of lithium-air batteries. *J. Solid State Electrochem.*, **17** (2013) 1793–1807, doi: 10.1007/s10008-013-1999-1.
13. S. A. Freunberger, Y. Chen, N. E. Drewett, L. J. Hardwick, F. Barde, P. G. Bruce, The lithium-oxygen battery with ether-based electrolytes. *Angew. Chem., Int. Ed.*, **50** (2011) 8609–8613.
14. V. S Bryantsev, B. Giordani, W. Wlaker, M. Blanco, S. Zecevic, K. Sasaki, J. Uddin, D. Addison, J. V. Chase, Predicting solvent stability in aprotic electrolyte Li-air batteries: nucleophilic substitution by the superoxide anion radical (O<sub>2</sub><sup>•-</sup>). *J. Phys. Chem. A*, **115** (2011) 12399–12409.
15. K. U. Schwenke, S. Meini, X. Wu, H. A. Gasteiger, M. Piana, Stability of superoxide radicals in glyme solvents for non-aqueous Li-O<sub>2</sub> battery electrolytes. *Phys. Chem. Chem. Phys.*, **15** (2013) 11830–11839.
16. G. Horwitz, M. Factorovich, J. Rodriguez, D. Laria, H. R. Corti, Ionic transport and speciation of lithium salts in glymes: experimental and theoretical results for electrolytes of interest for lithium-air batteries. *ACS Omega*, **3** (2018) 11205–11215.

17. Y. Li, Y. Yin, K. Guo, X. Xue, Z. Zou, X. Li, T. He, H. Yang, Tuning pore structure of the poly(vinylidene difluoride hexafluoropropylene) membrane for improvement in rate performance of Li-oxygen battery. *J. Power Sources*, **241** (2013) 288–294.
18. T. Liu, Z. Chang, Y. Yin, K. Chen, Y. Zhang, X. Zhang, The PVDF-HFP gel polymer electrolyte for Li-O<sub>2</sub> battery. *Solid State Ionics*, **318** (2018) 88–94.
19. J. Yi, S. Guo, P. He, H. Zhou, Status and prospects of polymer electrolytes for solid-state Li-O<sub>2</sub> (air) batteries. *Energy Environ. Sci.*, **10** (2017) 860–884.
20. L. Leng, X. Zeng, P. Chen, T. Shu, H. Song, Z. Fu, H. Wang, S. Liao, A novel stability-enhanced lithium-oxygen battery with cellulose-based composite polymer gel as the electrolyte. *Electrochim. Acta*, **176** (2015) 1108–1115.
21. J. J. Xu, H. Ye, Polymer gel electrolytes based on oligomeric polyether/cross-linked PMMA blends prepared via in situ polymerization. *Electrochim. Commun.*, **7** (2005) 829–835.
22. X. Lei, X. Liu, W. Ma, Z. Cao., Y. Wang, Y. Ding, Flexible lithium-air battery in ambient air with an in situ formed gel electrolyte. *Angew. Chem.*, **130** (2018) 16363–16367.
23. G. A. Elia, R. Bernhard, J. Hassoun, A lithium-ion oxygen battery using a polyethylene glyme electrolyte mixed with an ionic liquid. *RSC Adv.*, **5** (2015) 21360–21365.
24. C. Wang, Z. Xie, Z. Zhou, Lithium-air batteries: challenges coexist with opportunities. *APL Mater.*, **7** (2019) 040701, doi: 10.1063/1.5091444.
25. G. Kim, T. Liu, I. Temprano, E. A. Petrucco, N. Barrow, C. P. Grey, Cycling non-aqueous lithium-air batteries with dimethyl sulfoxide and sulfolane Co-solvent. *Johnson Matthey Technol. Rev.*, **62** (2018) 332–340.
26. M. Asadi, B. Sayahpour, P. Abbasi, A. T. Ngo, K. Karis, J. R. Jokisaari, C. Liu, B. Narayanan, M. Gerard, P. Yasaee, X. Hu, A. Mukherjee, K. Chun Lau, R. S. Assary, F. Khalili-Araghi, R. F. Klie, L. A. Curtiss, A. Salehi-Khojin, A lithium–oxygen battery with a long cycle life in an air-like atmosphere. *Nature*, **555** (2018) 502–506.
27. N. Mozhzhukhina, F. Marchini, W. R. Torres, A. Y. Tesio, L. P. Mendez De Leo, F. J. Williams, E. J. Calvo, Insights into dimethyl sulfoxide decomposition in Li-O<sub>2</sub> battery: understanding carbon dioxide evolution. *Electrochim. Commun.*, **80** (2017) 16–19.

28. D. G. Kwabi, T. P. Batcho, C. V. Amanchukwu, N. Ortiz-Vitoriano, P. Hammond, C. V. Thompson, Y. Shao-Horn, Chemical instability of dimethyl sulfoxide in lithium-air batteries. *J. Phys. Chem. Lett.*, **5** (2014) 2850–2856.
29. R. Tatara, D. G. Kwabi, T. P. Batcho, M. Tulodziecki, K. Watanabe, H.-M. Kwon, M. L. Thomas, K. Ueno, C. V. Thompson, K. Dokko, Y. Shao-Horn, M. Watanabe, Oxygen reduction reaction in highly concentrated electrolyte solutions of lithium bis(trifluoromethanesulfonyl) amide/dimethyl sulfoxide. *J. Phys. Chem. C*, **121** (2017) 9162–9172.
30. V. Giordani, J. Uddin, V. S. Bryantsev, G. V. Chase, D. Addison, High concentration lithium nitrate/dimethylacetamide electrolytes for lithium/oxygen cells. *J. Electrochem. Soc.*, **163**(13) (2016) A2673–A2678.
31. V. S. Bryantsev, J. Uddin, V. Giordani, W. Walker, D. Addison, G. V. Chase, The identification of stable solvents for nonaqueous rechargeable Li-air batteries. *J. Electrochem. Soc.*, **160**(2013) A160–A171.
32. W. Xu, J. Hu, M. H. Engelhard, S. A. Towne, J. S. Hardy, J. Xiao, J. Feng, M. Y. Hu, J. Zhang, F. Ding, M. E. Gross, J.-G. Zhang, The stability of organic solvents and carbon electrode in nonaqueous Li-O<sub>2</sub> Batteries. *J. Power Sources*, **215** (2012) 240–247.
33. H. Deng, Y. Qiao, S. Wu, F. Qiu, N. Zhang, P. He, H. Zhou, Non-aqueous, metal-free, and hybrid electrolyte Li-ion O<sub>2</sub> battery with a single-ion-conducting separator. *ACS Appl. Mater. Interfaces*, **11** (2019) 4908–4914, doi: 10.1021/acsami.8b15747.
34. V. L. Martins, R. M. Torresi, Ionic liquids in electrochemical energy storage. *Curr. Opin. Electrochem.*, **9** (2018) 26–32.
35. N.-S. Choi, B. Koo, J.-T. Yeon, K. Tae Lee, D.-W. Kim, Effect of a novel amphiphilic ionic liquid on lithium deposition in gel polymer electrolytes. *Electrochim. Acta*, **56** (2011) 7249–7255.
36. H. Wang, N. Imanishi, A. Hirano, Y. Takeda, O. Yamamoto, Electrochemical properties of the polyethylene oxide Li(CF<sub>3</sub>SO<sub>2</sub>)<sub>2</sub>N and ionic liquid composite electrolyte. *J. Power Sources*, **219** (2012) 22–28.
37. D. Zhang, R. Li, T. Huang, A. Yu, Novel composite polymer electrolyte for lithium air batteries. *J. Power Sources*, **195** (2010) 1202–1206.
38. S. Liu, H. Wang, N. Imanishi, T. Zhang, A. Hirano, Y. Takeda, O. Yamamoto, J. Yang, Effect of co-doping nano-silica filler and N-methyl-N-propylpiperidinium bis(trifluoromethanesulfonyl)imide into polymer electrolyte on Li dendrite formation in Li/poly(ethylene oxide)-Li(CF<sub>3</sub>SO<sub>2</sub>)<sub>2</sub>N/Li. *J. Power Sources*, **196** (2011) 7681–7686.

39. K. Amine, L. A. Curtiss, J. Lu, K. C. Lau, Z. Zhang, Y.-K. Sun, Lithium air batteries having ether-based electrolytes. US Patent No.: US 9,478,837 B2 (2016).
40. J. R. Harding, C. V. Amanchukwu, P. T. Hammond, Y. Shao-Horn, Instability of poly(ethylene oxide) upon oxidation in lithium-air batteries. *J. Phys. Chem. C*, **119** (2015) 6947–6955.
41. Q. Lu, Y. Gao, Q. Zhao, J. Li, X. Wang, F. Wang, Novel polymer electrolyte from poly(carbonate-ether) and lithium tetrafluoroborate for lithium oxygen battery. *J. Power Sources*, **242** (2013) 677–682.
42. J. Kumara, S. J. Rodrigues, B. Kumara, Interface-mediated electrochemical effects in lithium/polymer-ceramic cells. *J. Power Sources*, **195** (2010) 327–334.
43. Z. Guo, C. Li, J. Liu, Y. Wang, Y. Xia, A long-life lithium-air battery in ambient air with a polymer electrolyte containing a redox mediator. *Angew. Chem. Int. Ed.*, **56** (2017) 7505–7509.
44. Z.-Z. Shen, S.-Y. Lang, Y. Shi, J.-M. Ma, R. Wen, L.-J. Wan, Revealing the surface effect of the soluble catalyst on oxygen reduction/evolution in Li-O<sub>2</sub> batteries. *J. Am. Chem. Soc.*, **141** (2019) 6900–6905.
45. T. Kim, W. Song, D.-Y. Son, L. K. Ono, Y. Qi, Lithium-ion batteries: outlook on present, future, and hybridized technologies. *J. Mater. Chem. A*, **7** (2019) 2942–2964.
46. G. Girishkumar, B. McCloskey, A. C. Luntz, S. Swanson, W. Wilcke, Lithium-air battery: promise and challenges. *J. Phys. Chem. Lett.*, **1** (2010) 2193–2203, doi: 10.1021/jz1005384.
47. H. F. Bauman, G. B. Adams, Lithium-water-air battery automotive propulsion. Final report, October 28, 1976–September 28, 1977. [360 mW/cm<sup>2</sup>/sup 2/J]. United States: N. p., 1977. Web.
48. W. R. Momoyer, J. L. Morris, Lockheed Missiles and Space Co. Report 1979, 1.
49. W. R. Momoyer, E. L. Littauer, Development of a lithium-water-air primary battery, in *Energy to the 21st century; Proceedings of the Fifteenth Intersociety Energy Conversion Engineering Conference*, Seattle, Wash., August 18–22, 1980. Vol. 2 (A80-48165 21-44) New York, American Institute of Aeronautics and Astronautics, Inc., (1980) pp. 1480–1486.
50. L. Grande, E. Paillard, J. Hassoun, J.-B. Park, Y.-J. Lee, Y.-K. Sun, S. Passerini, B. Scrosati, The lithium/air battery: still an emerging system or a practical reality? *Adv. Mater.*, **27** (2015) 784–800.

51. J. L. Schaefer, Y. Lu, S. S. Moganty, P. Agarwal, N. Jayaprakash, L. A. Archer, Electrolytes for high-energy lithium batteries. *Appl. Nanosci.*, **2** (2012) 91–109, doi: 10.1007/s13204-011-0044-x.
52. S. Hasegawa, N. Imanishi, T. Zhang, J. Xie, A. Hirano, Y. Takeda, O. Yamamoto, Study on lithium/air secondary batteries—stability of NASICON-type lithium ion conducting glass-ceramics with water. *J. Power Sources*, **189** (2009) 371–377.
53. H. Zhou, Y. Wang, H. Li, P. He, The development of a new type of rechargeable batteries based on hybrid electrolytes. *ChemSusChem*, **3**(9) (2010) 1009–1019.
54. S. S. Zhang, D. Foster, J. Read, Discharge characteristic of a non-aqueous electrolyte Li/O<sub>2</sub> battery. *J. Power Sources*, **195** (2010) 1235–1240.
55. M. R. Tarasevich, V. N. Andreev, O. V. Korchagin, O. V. Tripachev, Lithium–oxygen (air) batteries (state-of-the-art and perspectives). *Prot. Met. Phys. Chem. Surf.*, **53**(1) (2017) 1–48.
56. J.-G. Zhang, D. Wang, W. Xu, J. Xiao, R. E. Williford, Ambient operation of Li/Air batteries. *J. Power Sources*, **195** (2010) 4332–4337.
57. P. He, Y. Wang, H. Zhou, A Li-air fuel cell with recycle aqueous electrolyte for improved stability. *Electrochim. Commun.*, **12** (2010) 1686–1689.
58. Y. Shimonishi, T. Zhang, N. Imanishi, D. Im, D. J. Lee, A. Hirano, Y. Takeda, O. Yamamoto, N. Sammes, *J. Power Sources*, **196** (2011) 5128–5132.
59. Y. Shimonishi, T. Zhang, P. Johnson, N. Imanishi, A. Hirano, Y. Takeda, O. Yamamoto, N. Sammes, *J. Power Sources*, **195** (2010) 6187.
60. J. P. Zheng, P. Andrei, M. Hendrickson, E. J. Plichta, *J. Electrochem. Soc.*, **158** (2011) A43–A46.
61. P. Stevens G. Toussaint, F. Moureaux, M. Chatenet, Electrolyte aqueux pour batterie lithium-air, EP2777090A1 (2014).
62. J. Lai, Y. Xing, N. Chen, L. Li, F. Wu, R. Chen, *Angew. Chem. Int. Ed.*, (2019), doi: 10.1002/anie.201903459.
63. H. T. T. Le, N. Duc Tung, Y. J. Kim, C. N. Park, C. J. Park, A perovskite-structured aluminium-substituted lithium lanthanum titanate as a potential artificial solid-electrolyte interface for aqueous rechargeable lithium-metal-based batteries. *Electrochim. Acta*, (2017) 248–232.
64. M. Matsui, A. Wada, Y. Matsuda, O. Yamamoto, Y. Takeda, N. Imanishi, A novel aqueous lithium–oxygen cell based on the oxygen-peroxide redox couple. *Chem. Commun.*, **51** (2015) 3189.

65. J. P. Zheng, P. Andrei, M. Hendrickson, E. J. Plichta, The theoretical energy densities of dual-electrolytes rechargeable Li-air and Li-air flow batteries. *J. Electrochem. Soc.*, **158** (2011) A43–A46.
66. Y. F. Li, K. Huang, Y. C. A. Xing, Hybrid Li-air battery with buckypaper air cathode and sulfuric acid electrolyte. *Electrochim. Acta*, **81** (2012) 20–24.
67. L. J. Li, X. S. Zhao, A. Manthiram, A dual-electrolyte rechargeable Li-air battery with phosphate buffer catholyte. *Electrochim. Commun.*, **14** (2012) 78–81.
68. L. J. Li, X. S. Zhao, A. Manthiram, Polyprotic acid catholyte for high capacity dual-electrolyte Li-air batteries. *Phys. Chem. Chem. Phys.*, **14** (2012) 12737–12740.
69. Y. Li, K. Huang, J. D. MacGregor, Y. Xing, The role of PTFE in cathode transition layer in aqueous electrolyte Li-air battery. *Electrochim. Acta*, **191** (2016) 996–1000.
70. S. J. Visco, L. C. De Jonghe, Y. S. Nimon, A. Petrov, K. Pridatko, Catholytes for aqueous lithium/air battery cells. Cathodes and reservoirs for aqueous lithium/air battery cells. US Patent #8323820 (2012).
71. S. J. Visco, Y. S. Nimon, L. C. De Jonghe, A. Petrov, N. Goncharenko, Aqueous lithium air batteries. US Patent 9660311 B2 (2017).
72. S. Wu, Y. Qiao, S. Yang, J. Tang, P. He, H. Zhou, Clean electrocatalysis in a  $\text{Li}_2\text{O}_2$  redox-based Li– $\text{O}_2$  battery built with a hydrate-melt electrolyte. *ACS Catal.*, **8** (2018) 1082–1089.
73. Y. Yamada, K. Usui, K. Sodeyama, S. Ko, Y. Tateyama, A. Yamada, *Nat. Energy*, **1** (2016) 16129.
74. O. Yamamoto, N. Imanishi, Aqueous lithium-air batteries, in Z. Zhang, S. S. Zhang (eds.), *Rechargeable Batteries*, Springer International Publishing Switzerland (2015), pp. 559–585.
75. F. Li, H. Kitaura, H. Zhou, *Energy Environ. Sci.*, **6** (2013) 2302.
76. K. W. Semkow, A. F. Sammells, *J. Electrochem. Soc.*, **134** (1987) 2084.
77. C.-S. Yang, K.-N. Gao, X.-P. Zhang, Z. Sun, T. Zhang, Rechargeable solid-state Li-air batteries: a status report. *Rare Met.*, **37**(6) (2018) 459–472.
78. S. J. Visco, B. D. Katz, Y. S. Nimon, L. C. De Jonghe, Protected active metal electrode and battery cell structures with nonaqueous interlayer architecture. US Patent #7282295 (2007).
79. D. Capsoni, M. Bini, S. Ferrari, E. Quartarone, P. Mustarelli, Recent advances in the development of Li-air batteries. *J. Power Sources*, **220** (2012) 253–263.

80. K. Chung, W.-S. Kim, Y.-K. Choi, *J. Electroanal. Chem.*, **566** (2004) 263–267.
81. Y. Lu, E. Crumlin, T. Carney, *J. Phys. Chem. C*, **117** (2013) 25948.
82. Y. Lu, E. Crumlin, G. Veith, J. R. Harding, *Sci. Rep.*, **2** (2012) 715.
83. T. Zhang, N. Imanishi, S. Hazegawa, A. Hirano, J. Xie, Y. Takeda, O. Yamamoto, N. Sammes, *Electrochim. Solid State Lett.*, **12** (2009) A132–A135.
84. Y. Li, W. Zhou, X. Chen, X. Lu, Z. Cui, S. Xin, L. G. Xue, Q. X. Jia, J. B. Goodenough, Mastering the interface for advanced all-solid-state lithium rechargeable batteries. *Proc. Natl. Acad. Sci. U.S.A.*, **113** (47) (2016) 13313.
85. W. Luo, Y. H. Gong, Y. Z. Zhu, K. K. Fu, J. Q. Dai, S. D. Lacey, C. W. Wang, B. Y. Liu, X. G. Han, Y. F. Mo, Transition from superlithiophobicity to superlithiophilicity of garnet solid-state electrolyte. *J. Am. Chem. Soc.*, **138** (37) (2016) 12258.
86. K. Fu, Y. H. Gong, B. Y. Liu, Y. Z. Zhu, S. M. Xu, Y. G. Yao, W. Luo, C. W. Wang, S. D. Lacey, J. Q. Dai, Toward garnet electrolyte-based Li metal batteries: an ultrathin, highly effective, artificial solid-state electrolyte/metallic Li interface, *Sci. Adv.*, **3** (4) (2017) e1601659.
87. W. Luo, Y. Gong, Y. Zhu, Y. Li, Y. Yao, Y. Zhang, K. Fu, G. Pastel, C. F. Lin, Y. F. Mo, Reducing interfacial resistance between garnet-structured solid-state electrolyte and Li-metal anode by a germanium layer. *Adv. Mater.*, **29** (22) (2017) 1606042.
88. C. W. Wang, Y. H. Gong, B. Y. Liu, K. Fu, Y. G. Yao, E. Hitz, Y. J. Li, J. Q. Dai, S. M. Xu, W. Luo, Conformal, nanoscale ZnO surface modification of garnet-based solid-state electrolyte for lithium metal anodes. *Nano Lett.*, **17** (1) (2016) 565.
89. C. L. Tsai, V. Roddatis, C. V. Chandran, Q. Ma, S. Uhlenbruck, M. Bram, P. Heitjans, O. Guillon,  $\text{Li}_7\text{La}_3\text{Zr}_2\text{O}_{12}$  interface modification for Li dendrite prevention. *ACS Appl. Mater. Interfaces*, **8** (16) (2016) 10617.
90. X. G. Han, Y. H. Gong, K. Fu, X. F. He, G. T. Hitz, J. Q. Dai, A. Pearse, B. Y. Liu, H. Wang, G. Rublo, Y. F. Mo, V. Thangadurai, E. D. Wachsman, L. B. Hu, Negating interfacial impedance in garnet-based solid-state Li metal batteries. *Nat. Mater.*, **16** (5) (2016) 572.
91. Y. Liu, C. Li, B. Li, H. Song, Z. Cheng, M. Chen, P. He, H. Zhou, *Adv. Energy Mater.*, **8** (2018) 1702374.
92. T. Yang, X. Liu, L. Sang, F. Ding, Control of interface of glass-ceramic electrolyte/liquid electrolyte for aqueous lithium batteries. *J. Power Sources*, **244** (2013) 43–49.

93. B. Kumar, J. Kumar, R. Leese, J. P. Fellner, S. J. Rodrigues, K. M. Abraham, A solid-state, rechargeable, long cycle life lithium-air battery. *J. Electrochem. Soc.*, **157** (1) (2010) A50–A54.
94. B. Kumar, J. Kumar, *J. Electrochem. Soc.*, **157** (2010) A611.
95. P. Kichambare, J. Kumar, S. J. Rodrigues, B. Kumar, *J. Power Sources*, **196** (2011) 3310.
96. J. Kumar, B. Kumar, *J. Power Sources*, **194** (2009) 1113.
97. H. Y.-P. Hong, *Mater. Res. Bull.*, **13** (1978) 117.
98. B. Liu, Y. Gong, K. Fu, X. Han, Y. Yao, G. Pastel, C. Yang, H. Xie, E. D. Wachsman, L. Hu, *ACS Appl. Mater. Interfaces*, **9** (2017) 18809–18815.
99. C. Brissot, M. Rosso, J. N. Chazalviel, S. Lascaud, *J. Power Sources*, **81** (1999) 925.
100. C. Brissot, M. Rosso, J. N. Chazalviel, P. Baudry, S. Lascaud, *Electrochim. Acta*, **43** (1998) 1569.
101. M. Rosso, T. Gobron, C. Brissot, J. N. Chazalviel, S. Lascaud, *J. Power Sources*, **97–98** (2001) 804.
102. H. Kitaura, H. Zhou, *Adv. Energy Mater.*, **2** (2012) 889–894.
103. T. Zhang, N. Imanishi, A. Hirano, et al., *Electrochim. Solid-State Lett.*, **14** (2011) A45.
104. Y. Koizumi, D. Mori, S. Taminato, O. Yamamoto, Y. Takeda, N. Imanishi, Lithium-stable NASICON-type lithium-ion conducting solid electrolyte film coated with a polymer electrolyte. *Solid State Ionics*, **337** (2019) 101–106.
105. J. Fu, *Solid State Ionics*, **96** (1997) 195–200.
106. J. Fu, Lithium ion conductive glass-ceramics, US Patent #5702995 (1997).
107. G. Y. Aleshin, D. A. Semenenko, A. I. Belova, T. K. Zakharchenko, D. M. Itkis, E. A. Goodilin, Y. D. Tretyakov, *Solid State Ionics*, **184** (2011) 62–64.
108. T. Zhang, N. Imanishi, S. Hasegawa, A. Hirano, J. Xie, Y. Takeda, O. Yamamoto, N. Sammes, *J. Electrochem. Soc.*, **155** (2008) A965.
109. N. Imanishi, Y. Takeda, O. Yamamoto, *Electrochemistry*, **80** (2012) 706.
110. T. Zhang, N. Imanishi, Lithium-air batteries, in T. Osaka, Z. Ogumi (eds.), *Nanoscale Technology for Advanced Lithium Batteries*, Nanostructure Science and Technology 182, doi: 10.1007/978-1-4614-8675-6\_15, Springer Science+Business Media, New York (2014) pp. 227–241.

111. L. Puech, C. Cantau, P. Vinatier, G. Toussaint, P. Stevens, Elaboration and characterization of a free standing LiSICON membrane for aqueous lithium-air battery, *J. Power Sources*, **214** (2012) 330–336.
112. Q. Li, J. Chen, L. Fan, X. Kong, Y. Lu, *Green Energy Environ.*, **1** (2016) 18–42.
113. H. Nemoria, X. Shang, H. Minami, S. Mitsuoka, M. Nomura, H. Sonoki, Y. Morita, D. Mori, Y. Takeda, O. Yamamoto, N. Imanishi, Aqueous lithium-air batteries with a lithium-ion conducting solid electrolyte  $\text{Li}_{1.3}\text{Al}_{0.5}\text{Nb}_{0.2}\text{Ti}_{1.3}(\text{PO}_4)_3$ . *Solid State Ionics*, **317** (2018) 136–141.
114. H. Kitaura, H. Zhou, *Adv. Energy Mater.*, **2** (2012) 889–894.
115. S. Liu, N. Imanishi, T. Zhang, A. Hirano, Y. Takeda, O. Yamamoto, J. Yang, *J. Electrochem. Soc.*, **157** (2010) A1092–A1098.
116. H. Wang, D. Im, D. J. Lee, M. Matsui, Y. Takeda, O. Yamamoto, N. Imanishi, A composite polymer electrolyte protect layer between lithium and water stable ceramics for aqueous lithium-air batteries. *J. Electrochem. Soc.*, **160** (4) (2013) A728–A733.
117. T. Zhang, N. Imanishi, Y. Shimonishi, et al., *Chem. Commun.*, **46** (2010) 1661.
118. X. B. Zhu, T. S. Zhao, Z. H. Wei, P. Tan, G. Zhao, A novel solid-state  $\text{Li}-\text{O}_2$  battery with an integrated electrolyte and cathode structure. *Energy Environ Sci.*, **8** (9) (2015) 2782.
119. Y. Shimonishi, T. Zhang, P. Johnson, N. Imanishi, A. Hirano, O. Yamamoto, N. Sammes, A study on lithium/air secondary batteries—stability of NASICON-type glass ceramics in acid solutions. *J. Power Sources*, **195** (2010) 6187–6191.
120. Y. Shimonishi, T. Zhang, P. Johnson, N. Imanishi, A. Hirano, Y. Takeda, O. Yamamoto, N. Sammes, A study on lithium/air secondary batteries—stability of NASICON-type glass ceramics in acid solutions. *J. Power Sources*, **195** (2010) 6187–6191.
121. M. Zhang, K. Takahashi, N. Imanishi, Y. Takeda, O. Yamamoto, B. Chi, J. Pu, J. Li, *J. Electrochem. Soc.*, **159** (2012) A1114–A1119.
122. K. He, C. Zu, Y. Wang, B. Han, X. Yin, H. Zhao, et al., Stability of lithium ion conductor NASICON structure glass ceramic in acid and alkaline aqueous solution. *Solid State Ionics*, **254** (2014) 78–81.
123. H. Kitaura, H. Zhou, *Energy Environ. Sci.*, **5** (2012) 9077.
124. Y. Wang, H. Zhou, *J. Power Sources*, **195** (2010) 358–361.
125. P. Stevens, G. Toussaint, G. Caillon, P. Viaud, P. Vinatier, C. Cantau, O. Fichet, C. Sarrazin, M. Mallouki, *ECS Trans.*, **28** (2010) 1–12.

126. M. Nyman, T. M. Alam, S. K. McIntyre, G. C. Bleier, D. Ingersoll, *Chem. Mater.*, **22** (2010) 5401–5410.
127. Z. F. Yow, Y. L. Oh, W. Gu, R. P. Rao, S. Adams, *Solid State Ionics*, **292** (2016) 122–129.
128. L. Truong, V. Thangadurai, *Chem. Mater.*, **23** (2011) 3970–3977.
129. Y. G. Wang, P. He, H. S. Zhou, *Energy Environ. Sci.*, **4** (2011) 4994–4999.
130. L. Li, X. Zhao, A. Manthiram, A dual-electrolyte rechargeable Li-air battery with phosphate buffer catholyte. *Electrochim. Commun.*, **14** (2012) 78–81.
131. R. Murugan, V. Thangadurai, W. Weppner, Fast lithium ion conduction in garnet-type  $\text{Li}_7\text{La}_3\text{Zr}_2\text{O}_{12}$ . *Angew. Chem. Int. Ed.*, **46** (2007) 7778–7781.
132. Y. Shimonishi, A. Toda, T. Zhang, A. Hirano, N. Imanishi, O. Yamamoto, Y. Takeda, Synthesis of garnet-type  $\text{Li}_{7-x}\text{La}_3\text{Zr}_2\text{O}_{12-1/2x}$  and its stability in aqueous solutions. *Solid State Ionics*, **183** (2011) 48–53.
133. A. Sharafi, E. Kazyak, A. L. Davis, S. Y. T. Thompson, D. J. Siegel, N. P. Dasgupta, J. Sakamoto, Surface chemistry mechanism of ultra-low interfacial resistance in the solid-state electrolyte  $\text{Li}_7\text{La}_3\text{Zr}_2\text{O}_{12}$ , *Chem. Mater.*, **29** (18) (2017) 7961.
134. X. Yang, D. Kong, Z. Chen, Y. Sun, Y. Liu, Low-temperature fabrication for transparency Mg doping  $\text{Li}_7\text{La}_3\text{Zr}_2\text{O}_{12}$  solid state electrolyte. *J. Mater. Sci. Mater. Electron.*, **29** (2) (2018) 1523.
135. J. Zheng, Y.-Y. Hu, New insights into the compositional dependence of Li-ion transport in polymer-ceramic composite electrolytes. *ACS Appl. Mater. Interfaces*, **10** (2018) 4113.
136. F. Chen, D. Yang, W. Zha, B. Zhu, Y. Zhang, J. Li, Y. P. Gu, Q. Shen, L. M. Zhang, D. R. Sadoway, Solid polymer electrolytes incorporating cubic  $\text{Li}_7\text{La}_3\text{Zr}_2\text{O}_{12}$  for all-solid-state lithium rechargeable batteries. *Electrochim. Acta*, **258** (2017) 1106.
137. T. T. Yang, Y. Li, W. W. Wu, Z. Z. Cao, W. Y. He, Y. F. Gao, J. R. Liu, G. R. Li, The synergistic effect of dual substitution of Al and Sb on structure and ionic conductivity of  $\text{Li}_7\text{La}_3\text{Zr}_2\text{O}_{12}$  ceramic. *Ceram. Int.*, **44** (2) (2018) 1538.
138. S. H. Yang, M. Y. Kim, D. H. Kim, H. Y. Jung, H. M. Ryu, J. H. Han, M. S. Lee, H. S. Kim, Ionic conductivity of Ga-doped LLZO prepared using Couette-Taylor reactor for all-solid lithium batteries. *J. Ind. Eng. Chem.*, **56** (2017) 422.

139. B. Y. Xu, W. L. Li, H. N. Duan, H. J. Wang, Y. P. Guo, H. Li H. Z. Liu,  $\text{Li}_3\text{PO}_4$ -added garnet-type  $\text{Li}_{6.5}\text{La}_3\text{Zr}_{1.5}\text{Ta}_{0.5}\text{O}_{12}$  for Li-dendrite suppression. *J. Power Sources*, **354** (2017) 68.
140. M. He, Z. Cui, C. Chen, Y. Li, X. Guo, *J. Mater. Chem. A*, **6** (2018) 11463–11470.
141. J. Bae, Y. Li, J. Zhang, X. Zhou, F. Zhao, Y. Shi, J. B. Goodenough, G. Yu, *Angew. Chem. Int. Ed. Engl.*, **57** (2018) 2096–2100.
142. Y. Sun, Lithium ion conducting membranes for lithium air batteries. *Nano Energy*, **2** (5) (2013) 801–816.
143. R. Kanno, M. Murayama, Lithium ionic conductor Thio-LISICON: the  $\text{Li}_2\text{S}-\text{GeS}_2-\text{P}_2\text{S}_5$  system. *J. Electrochem. Soc.*, **148** (7) (2001) A742–A746.
144. B. Shin, S. Choi, Y. Tak, Electrocatalytic activity of Co-based perovskite oxides for oxygen reduction and evolution reactions. *Int. J. Electrochem. Sci.*, **11** (7) (2016) 5900.
145. Y. T. Li, B. Y. Xu, H. H. Xu, H. N. Duan, X. J. Lu, S. Xin, W. D. Zhou, F. G. Xue, G. T. Fu, A. Manthiram, J. B. Goodenough, Hybrid polymer garnet electrolyte with a small interfacial resistance for lithium-ion batteries. *Angew. Chem. Int. Ed.*, **56** (3) (2017) 753.
146. C. Uhlmann, P. Braun, J. Illig, A. Weber, E. Ivers-Tiffée, Interface and grain boundary resistance of a lithium lanthanum titanate ( $\text{Li}_{3x}\text{La}_{2/3-x}\text{TiO}_3$ , LLTO) solid electrolyte. *J. Power Sources*, (307) (2016) 578.
147. B. Huang, B. Y. Xu, Y. T. Li, W. D. Zhou, Y. You, S. W. Zhong, C. A. Wang, J. B. Goodenough, Li-ion conduction and stability of perovskite  $\text{Li}_{3/8}\text{Sr}_{7/16}\text{Hf}_{1/4}\text{Ta}_{3/4}\text{O}_3$ . *ACS Appl. Mater. Interfaces*, **8** (23) (2016) 14552.
148. P. Knauth, *Solid State Ionics*, **180** (2009) 911.
149. M. Armand, *Solid State Ionics*, **69** (1994) 309.
150. P. Kichambare, S. Rodrigues, J. Kumar, Mesoporous nitrogen-doped carbon-glass ceramic cathodes for solid-state lithium-oxygen batteries. *ACS Appl. Mater. Interfaces*, **4** (1) (2012) 49.
151. Y. Liu, B. Li, H. Kitaura, X. Zhang, M. Han, P. He, H. S. Zhou, Fabrication and performance of all-solid-state Li-air battery with SWCNTs/LAGP cathode. *ACS Appl. Mater. Interfaces*, **7** (31) (2015) 17307.
152. H. Kitaura, H. Zhou, All-solid-state lithium-oxygen battery with high safety in wide ambient temperature range. *Sci. Rep.*, **5** (2015) 13271.

153. X. B. Zhu, T. S. Zhao, Z. H. Wei, P. Tan, G. Zhao, A novel solid-state Li-O<sub>2</sub> battery with an integrated electrolyte and cathode structure. *Energy Environ Sci.*, **8** (9) (2015) 2782.
154. Y. Suzuki, K. Kami, K. Watanabe, N. Imanishi, Characteristics of discharge products in all-solid-state Li-air batteries. *Solid State Ionics*, **278** (2015) 222.
155. J. S. Thokchom, B. Kumar, Composite effect in superionically conducting lithium aluminium germanium phosphate based glass-ceramic. *J. Power Sources*, **185** (1) (2008) 480–485.
156. J. S. Thokchom, B. Kumar, The effects of crystallization parameters on the ionic conductivity of a lithium aluminum germanium phosphate glass-ceramic. *J. Power Sources*, **195** (9) (2010) 2870–2876.
157. C. Ma, Y. Cheng, K. Yin, J. Luo, A. Sharafi, J. Sakamoto, J. Li, K. L. More, N. J. Dudney, M. Chi, Interfacial stability of Li metal-solid electrolyte elucidated via in situ electron microscopy. *Nano Lett.*, **16** (11) ((2016) 7030.
158. K. Hofstetter, A. J. Samson, S. Narayanan, V. Thangadurai, *J. Power Sources*, **390** (2018) 297–312.
159. Y. Jin, P. J. McGinn, *J. Power Sources*, **239** (2013) 326–331.
160. C. W. Ahn, J. J. Choi, J. Ryu, B. D. Hahn, J. W. Kim, W. H. Yoon, J. H. Choi, J. S. Lee, D. S. Park, *J. Power Sources*, **272** (2014) 554–558.
161. T. T. Truong, Y. Qin, Y. Ren, Z. Chen, M. K. Chan, J. P. Greeley, et al. Single-crystal silicon membranes with high lithium conductivity and application in lithium-air batteries. *Adv. Mater.*, **23** (2011) 4947–4952.
162. R. Black, B. Adams, L. F. Nazar, *Adv. Energy Mater.*, **2** (2012) 801–815.
163. D. Safanama, S. Adams, High efficiency aqueous and hybrid lithium-air batteries enabled by Li<sub>1.5</sub>Al<sub>0.5</sub>Ge<sub>1.5</sub>(PO<sub>4</sub>)<sub>3</sub> ceramic anode-protecting membranes. *J. Power Sources*, **340** (2017) 294–301.
164. D. Safanama, D. Damianoa, R. P. Rao, S. Adams, Lithium conducting solid electrolyte Li<sub>1+x</sub>Al<sub>0x</sub>Ge<sub>2-x</sub>(PO<sub>4</sub>)<sub>3</sub> membrane for aqueous lithium air battery. *Solid State Ionics*, **262** (2014) 211–215.
165. D. Safanama, S. Adams, High efficiency aqueous and hybrid lithium-air batteries enabled by Li<sub>1.5</sub>Al<sub>0.5</sub>Ge<sub>1.5</sub>(PO<sub>4</sub>)<sub>3</sub> ceramic anode-protecting membranes, *J. Power Sources*, **340** (2017) 294–301.
166. L. Li, X. Zhao, A. Manthiram, dual-electrolyte rechargeable Li-air battery with phosphate buffer catholyte. *Electrochem. Commun.*, **14** (2012) 78–81.

167. L. Li, X. Zhao, Y. Fu, A. Manthiram, Polyprotic acid catholyte for high capacity dual-electrolyte Li-air batteries. *Phys. Chem. Chem. Phys.*, **14** (2012) 12737–12740.
168. Y. Wang, P. He and H. Zhou, A lithium–air capacitor–battery based on a hybrid electrolyte. *Energy Environ. Sci.*, **4** (2011) 4994–4999.
169. P. He, T. Zhang, J. Jiang and H. Zhou, Lithium–air batteries with hybrid electrolytes. *J. Phys. Chem. Lett.*, **7** (2016) 1267–1280.
170. L. Li, A. Manthiram, Dual-electrolyte lithium–air batteries: influence of catalyst, temperature, and solid-electrolyte conductivity on the efficiency and power density. *J. Mater. Chem. A*, **1** (2013) 5121–5127.
171. L. Li, Y. Fu, A. Manthiram, Imidazole-buffered acidic catholytes for hybrid Li-air batteries with high practical energy density. *Electrochim. Commun.*, **47** (2014) 67–70.
172. A. Manthiram, L. Li, *Adv. Energy Mater.*, **5** (2015) 1401302.
173. X. B. Zhu, T. S. Zhao, Z. H. Wei, P. Tan, G. Zhao, A novel solid-state Li–O<sub>2</sub> battery with an integrated electrolyte and cathode structure. *Energy Environ. Sci.*, **8** (2015) 2782–2790.
174. B. Wu, X. Chen, C. Zhang, D. Mu and F. Wu, Lithium–air and lithium–copper batteries based on a polymer stabilized interface between two immiscible electrolytic solutions (ITIES). *New J. Chem.*, **36** (2012) 2140–2145.
175. D. J. Schroeder, A. A. Hubaud, J. T. Vaughey, Stability of the solid electrolyte Li<sub>3</sub>OBr to common battery solvents. *Mater. Res. Bull.*, **49** (2014) 614–617.
176. D. J. Schroeder, A. A. Hubaud, J. T. Vaughey, Stability of the solid electrolyte Li<sub>3</sub>OBr to common battery solvents. *Mater. Res. Bull.*, **49** (2014) 614–617.
177. Y. S. Zhao, L. L. Daemen. *J. Am. Chem. Soc.*, **134** (2012) 15042–15047.
178. Ibid.
179. M. Mehta, V. Bevara, P. Andrei, Maximum theoretical power density of lithium–air batteries with mixed electrolyte. *J. Power Sources*, **286** (2015) 299–308.
180. P. He, Y. Wang, H. Zhou, A Li–air fuel cell with recycle aqueous electrolyte for improved stability. *Electrochim. Commun.*, **12** (12) (2010) 1686–1689.
181. Y. Wang, P. He, H. Zhou, *Adv. Energy Mater.*, **2** (2012) 770–779.
182. X. J. Chen, A. Shellikeri, Q. Wu, J. P. Zheng, M. Hendrickson, E. J. Plichta, A high-rate rechargeable Li–air flow battery. *J. Electrochem. Soc.*, **160** (10) (2013) A1619–A1623.

183. Y. G. Zhu, C. Jia, J. Yang, F. Pan, Q. Huang, Q. Wang, Dual redox catalysts for oxygen reduction and evolution reactions: towards a redox flow Li–O<sub>2</sub> battery. *Chem. Commun.*, **51** (2015) 9451–9454.
184. I. Ruggeri, C. Arbizzani, F. Soavi, Carbonaceous catholyte for high energy density semi-solid Li/O<sub>2</sub> flow battery. *Carbon*, **130** (2018) 749–757.
185. S. Monaco, F. Soavi, M. Mastragostino, Role of oxygen mass transport in rechargeable Li/O<sub>2</sub> batteries operating with ionic liquids. *J. Phys. Chem. Lett.*, **4** (9) (2013) 1379–1382.
186. I. Ruggeri, C. Arbizzani, F. Soavi, A novel concept of Semi-solid, Li redox flow air (O<sub>2</sub>) battery: a breakthrough towards high energy and power batteries. *Electrochim. Acta*, **206** (10) (2016) 291–300.
187. J. Huang, A. Faghri, Capacity enhancement of a lithium oxygen flow battery. *Electrochim. Acta*, **174** (2015) 908–918.
188. N. Chawla, Recent advances in air-battery chemistries. *Mater. Today Chem.*, **12** (2019) 324–331.
189. Y. Kang, D. Zou, J. Zhang, F. Liang, K. Hayashi, H. Wang, D. Xue, K. Chen, K. R. Adair, X. Sun, Dual-phase spinel MnCo<sub>2</sub>O<sub>4</sub> nanocrystals with nitrogen-doped reduced graphene oxide as potential catalyst for hybrid Na–Air batteries. *Electrochim. Acta*, **244** (2017) 222–229.
190. F. Liang, K. Hayashi, A high-energy-density mixed-aprotic-aqueous sodium-air cell with a ceramic separator and a porous carbon electrode. *J. Electrochem. Soc.*, **162** (2015) A1215.
191. Z. Khan, N. Parveen, S. A. Ansari, S. T. Senthilkumar, S. Park, Y. Kim, H. Cho, H. Ko, Three-dimensional SnS<sub>2</sub> nanopetals for hybrid sodium-air batteries. *Electrochim. Acta*, **257** (2017) 328–334.
192. Y. Kang, F. Liang, K. Hayashi, Hybrid sodium-air cell with Na[FSA-C<sub>2</sub>C<sub>1</sub>im][FSA] ionic liquid electrolyte. *Electrochim. Acta*, **218** (2016) 119–124.
193. F. Liang, K. Hayashi, A high-energy-density mixed-aprotic-aqueous sodium-air cell with a ceramic separator and a porous carbon electrode. *J. Electrochem. Soc.*, **162** (2015) A1215.
194. K. Hayashi, K. Shima, F. Sugiyama, A mixed aqueous/aprotic sodium/air cell using a NASICON ceramic separator. *J. Electrochem. Soc.*, **160** (2013) A1467.
195. Y. Kang, F. Su, Q. Zhang, F. Liang, K. R. Adair, K. Chen, D. Xue, K. Hayashi, S. C. Cao, H. Yadegari and X. Sun, Novel high-energy-density rechargeable hybrid sodium–air cell with acidic electrolyte. *Appl. Mater. Interfaces*, **10** (2018) 23748–23756.

196. P. Hartmann, C. L. Bender, M. Vra9car, A. K. Durr, A. Garsuch, J. Janek, P. Adelhelm, A rechargeable room-temperature sodium superoxide ( $\text{NaO}_2$ ) battery. *Nat. Mater.*, **12** (2013) 228.
197. J. Kim, H.-D. Lim, H. Gwon, K. Kang, Sodium–oxygen batteries with alkyl-carbonate and ether based electrolytes. *Phys. Chem. Chem. Phys.*, **15** (2013) 3623.
198. S. K. Das, S. Lau, L. A. Archer, Sodium–oxygen batteries: a new class of metal–air batteries. *J. Mater. Chem. A*, **2** (2014) 12623.
199. Z. Jian, Y. Chen, F. Li, T. Zhang, C. Liu and H. Zhou, *J. Power Sources*, **251** (2014) 466.
200. N. Zha, X. Guo, Cell chemistry of sodium–oxygen batteries with various nonaqueous electrolytes. *J. Phys. Chem. C*, **119** (2015) 25319–25326.
201. T. Liu, G. Kim, M. T. L. Casford, C. P. Grey, Mechanistic insights into the challenges of cycling a nonaqueous  $\text{Na}-\text{O}_2$  battery. *J. Phys. Chem. Lett.*, **7** (2016) 4841–4846.
202. I. M. Aldous, L. J. Hardwick, Solvent-mediated control of the electrochemical discharge products of non-aqueous sodium–oxygen electrochemistry. *Angew. Chem. Int. Ed.*, **55** (2016) 8254–8257.
203. D. Sharon, D. Hirshberg, M. Afri, A. A. Frimer, M. Noked, D. Aurbach, Aprotic metal–oxygen batteries: recent findings and insights. *J. Solid State Electrochem.*, **21** (2017) 1861–1878.
204. N. Ortiz-Vitoriano, T. P. Batcho, D. G. Kwabi, B. Han, N. Pour, K. P. C. Yao, C. V. Thompson, Y. Shao-Horn, Rate-dependent nucleation and growth of  $\text{NaO}_2$  in  $\text{Na}-\text{O}_2$  batteries. *J. Phys. Chem. Lett.*, **6** (2015) 2636–2643.
205. W. Liu, Q. Sun, Y. Yang, J.-Y. Xie, Z.-W. Fu, *Chem. Commun.*, **49** (2013) 1951.
206. L. Lutz, D. A. Dalla Corte, M. Tang, E. Salager, M. Deschamps, A. Grimaud, L. Johnson, P. G. Bruce, J.-M. Tarascon, Role of electrolyte anions in the  $\text{Na}-\text{O}_2$  battery: implications for  $\text{NaO}_2$  solvation and the stability of the sodium solid electrolyte interphase in glyme ethers. *Chem. Mater.*, **29** (2017) 6066–6075.
207. Q. Sun, Y. Yang, Z.-W. Fu, Electrochemical properties of room temperature sodium–air batteries with non-aqueous electrolyte. *Electrochem. Commun.*, **16** (2012) 22–25.
208. W.-W. Yin, Z. Shadike, Y. Yang, F. Ding, L. Sang, H. Li, Z.-W. Fu, A long-life Na–air battery based on a soluble  $\text{NaI}$  catalyst. *Chem. Commun.*, **51** (2015) 2324–2327.

209. E. Peled, D. Golodnitsky, H. Mazor, M. Goor, S. Avshalomov, *J. Power Sources*, **196** (2011) 6835.
210. E. Peled, D. Golodnitsky, R. Hadar, H. Mazor, M. Goor, L. Burstein, Challenges and obstacles in the development of sodium-air batteries. *J. Power Sources*, **244** (2013) 771–776.
211. E. Peled, D. Golodnitsky, H. Mazor, M. Goor, S. Avshalomov, *J. Power Sources*, **196** (2011) 6835–6840.
212. A. Blum, T. Duvdevani, M. Philosoph, N. Rudy, E. Peled, *J. Power Sources*, **5449** (2003) 1–4.
213. S. K. Das, S. Xu, L. A. Archer, *Electrochim. Commun.*, **27** (2013) 59.
214. X. Ren, Y. Wu, A low-overpotential potassium-oxygen battery based on potassium superoxide. *J. Am. Chem. Soc.*, **135** (2013) 2923–2926.
215. K. U. Schwenke, S. Meini, X. Wu, H. A. Gasteiger, M. Piana, Stability of superoxide radicals in glyme solvents for non-aqueous Li-O<sub>2</sub> battery electrolytes. *Phys. Chem. Chem. Phys.*, **15** (2013) 11830–11839.
216. K. U. Schwenke, S. Meini, X. Wu, H. A. Gasteiger, M. Piana, Reactivity of the ionic liquid Pyr14TFSI with superoxide radicals generated from KO<sub>2</sub> or by contact of O<sub>2</sub> with Li<sub>7</sub>Ti<sub>5</sub>O<sub>12</sub>. *J. Electrochem. Soc.*, **162** (2015) A905–A914.
217. X. Ren, K. C. Lau, M. Yu, X. Bi, E. Kreidler, L. A. Curtiss, Y. Wu, Understanding side reactions in K-O<sub>2</sub> batteries for improved cycle life. *ACS Appl. Mater. Interfaces*, **6** (2014) 19299–19307.
218. X. Ren, M. He, N. Xiao, W. D. McCulloch, Y. Wu, Greatly enhanced anode stability in K-oxygen batteries with an in situ formed solvent- and oxygen-impermeable protection layer. *Adv. Energy Mater.*, **7** (2017) 1601080.
219. X. Zhang, X.-G. Wang, Z. Xie, Z. Zhou, Recent progress in rechargeable alkali metal-air batteries. *Green Energy Environ.*, **1** (2016) 4–17.
220. D. P. Leonard, Z. Wei, G. Chen, F. Du, X. Ji, Water-in-salt electrolyte for potassium-ion batteries. *ACS Energy Lett.*, **3** (2018) 373–374.
221. H. Gao, L. Xue, S. Xin, J. B. Goodenough, A high-energy-density potassium battery with a polymer-gel electrolyte and a polyaniline cathode. *Angew. Chem. Int. Ed.*, **57** (2018) 5449–5453.
222. H. Gao, W. Zhou, K. Park, J. B. Goodenough, A sodium-ion battery with a low-cost cross-linked gel-polymer electrolyte. *Adv. Energy Mater.*, (2016) 1600467.
223. H. Fei, Y. Liu, Y. An, X. Xu, G. Zeng, Y. Tian, L. Ci, B. Xi, S. Xiong, J. Feng, Stable all-solid-state potassium battery operating at room

- temperature with a composite polymer electrolyte and a sustainable organic cathode. *J. Power Sources*, **399** (2018) 294–298.
224. J. Zhang, J. Zhao, L. Yue, Q. Wang, J. Chai, Z. Liu, X. Zhou, H. Li, Y. Guo, G. Cui, *Adv. Energy Mater.*, **5** (2016) 1501082.
225. A. Eftekhari, Potassium secondary cell based on Prussian blue cathode. *J. Power Sources*, **126** (2004) 221–228.
226. W. Zhang, Z. Wu, J. Zhang, G. Liu, N.-H. Yang, R.-S. Liu, W. K. Pang, W. Li, Z. Guo, Unraveling the effect of salt chemistry on long-durability high phosphorus- concentration anode for potassium ion batteries. *Nano Energy*, **53** (2018) 967–974.
227. G. M. Crosbie, G. J. Tennenhouse, Potassium beta-alumina membranes. *J. Am. Ceram. Soc.*, **65** (4) (1982) 187–191.
228. T. Zhang, Z. Tao, J. Chen, Magnesium-air batteries: from principle to application. *Mater. Horiz.*, **1** (2014) 196–206
229. B. W. Jensen, M. Gaadingwe, D. R. Macfarlane, M. Forsyth, *Electrochim. Acta*, **53** (2008) 5881–5884.
230. S. Sathyaranayana, N. Munichandraiah, *J. Appl. Electrochem.*, **11** (1981) 33–39.
231. H. P. Godard, W. P. Jepson, M. R. Bothwell, R. L. Lane, *The Corrosion of Light Metals*, John Wiley & Sons, 1967.
232. A. P. Shyma, S. Palanisamy, N. Rajendhran, R. Venkatachalam, Enhanced discharge capacity of Mg-air battery with addition of water dispersible nano MoS<sub>2</sub> sheet in MgCl<sub>2</sub> electrolyte. *Ionics*, **25** (2019) 583–592.
233. Y. Zhao, G. Huang, C. Zhang, C. Peng, F. Pan, Effect of phosphate and vanadate as electrolyte additives on the performance of Mg-air batteries. *Mater. Chem. Phys.*, **218** (2018) 256–261.
234. C. Yu, C. Wang, X. Liu, X. Jia, S. Naficy, K. Shu, M. Forsyth, G. G. Wallace, A cytocompatible robust hybrid conducting polymer hydrogel for use in a magnesium battery. *Adv. Mater.*, **28** (2016).
235. X. Jia, C. Wang, V. Ranganathan, B. Napier, C. Yu, Y. Chao, M. Forsyth, F. G. Omenetto, D. R. MacFarlane, G. G. Wallace, A biodegradable thin-film magnesium primary battery using silk fibroin-ionic liquid polymer electrolyte. *ACS Energy Lett.*, **2** (2017).
236. X. Jia, Y. Yang, C. Wang, C. Zhao, R. Vijayaraghavan, D. R. MacFarlane, M. Forsyth G. G. Wallace, Biocompatible ionic liquid–biopolymer electrolyte-enabled thin and compact magnesium–air batteries. *Appl. Mater. Interfaces*, **6** (2014) 21110–21117.

237. G. Vardar, J. G. Smith, T. Thompson, K. Inagaki, J. Naruse, H. Hiramatsu, A. E. S. Sleightholme, J. Sakamoto, D. J. Siegel, Charles W. Monroe, Mg/O<sub>2</sub> battery based on the magnesium–aluminum chloride complex (MACC) electrolyte. *Chem. Mater.*, **28** (2016) 7629–7637.
238. T. Shiga, Y. Hase, Y. Kato, M. Inoue, K. A. Takechi, Rechargeable non-aqueous Mg-O<sub>2</sub> battery. *Chem. Commun.*, **49** (2013) 9152–9154.
239. T. Shiga, Y. Hase, Y. Yagi, N. Takahashi, K. Takechi, Catalytic cycle employing a TEMPO-anion complex to obtain a secondary Mg-O<sub>2</sub> battery. *J. Phys. Chem. Lett.*, **5** (2014) 1648–1652.
240. P. C. Howlett, T. Khoo, G. Mooketsi, J. Efthimiadis, D. R. MacFarlane, M. Forsyth, *Electrochim. Acta*, **55** (2010) 2377.
241. P. C. Howlett, W. Neil, T. Khoo, J. Z. Sun, M. Forsyth, D. R. MacFarlane, *Isr. J. Chem.*, **48** (2008) 313.
242. T. Khoo, P. C. Howlett, M. Tsagouria, D. R. Mac Farlane, M. Forsyth, The potential for ionic liquid electrolytes to stabilise the magnesium interface for magnesium/air batteries. *Electrochim. Acta*, **58** (2011) 583–588.
243. R. E. Doe, R. Han, J. Hwang, A. J. Gmitter, I. Shterenberg, H. D. Yoo, N. Pour, D. Aurbach, Novel, electrolyte solutions comprising fully inorganic salts with high anodic stability for rechargeable magnesium batteries. *Chem. Commun.*, **50** (2014) 243–245.
244. G. Cheng, Q. Xui, X. Zhao, F. Ding, J. Zhang, X.-J. Liu, D.-X. Cao, Electrochemical discharging performance of 3D porous magnesium electrode in organic electrolyte. *Trans. Nonferrous Met. Soc. China*, **23** (2013) 1367–1374.
245. A. Inoishi, Y.-W. Ju, S. Ida, T. Ishihara, Mg-air oxygen shuttle batteries using a ZrO<sub>2</sub>-based oxide ion-conducting electrolyte. *Chem. Commun.*, **49** (2013) 4691–4693.
246. R. J. Gummow, G. Vamvounis, M. B. Kannan, Y. He, Calcium-ion batteries: current state-of-the-art and future perspectives. *Adv. Mater.*, (2018) 1801702.
247. A. Ponrouch, C. Frontera, F. Barde, M. R. Palacin, *Nat. Mater.*, **15** (2016) 169–172.
248. D. Aurbach, R. Skaletsky and Y. Gofer, The electrochemical behavior of calcium electrodes in a few organic electrolytes. *J. Electrochem. Soc.*, **138** (12) (1991) 3536–3545.
249. G. Amatucci, F. Badway, A. Singhal, B. Beaudoin, G. Skandan, T. Bowmer, I. Plitz, N. Pereira, T. Chapman, R. Jaworski, *J. Electrochem. Soc.*, **148** (2001) A940.

250. D. Wang, X. Gao, Y. Chen, L. Jin, C. Kuss, P. G. Bruce, Plating and stripping calcium in an organic electrolyte. *Nat Mater.*, **17** (1) (2018) 16–20.
251. P. Reinsberg, C. J. Bondue, H. Baltruschat, Oxygen reduction in  $\text{Ca}^{2+}$ -containing electrolytes as a promising alternative to sodium-oxygen batteries. *J. Phys. Chem.C*, **120** (2016) 22179–22185.
252. M. S. Whittingham, *Proc. IEEE*, **100** (2012) 1518.
253. C. Lee, S.-K. Jeong, *Chem. Lett.*, **45** (2016) 1447.
254. J. F. Cooper, P. K. Hosner, B. E. Kelly, Electrochemical cell with calcium anode. US Patent 4154903 (1979).
255. S. Zaromb, *J. Electrochem. Soc.*, **109** (1962) 1125.
256. L. Trevethan, D. Bockstie, S. Zaromb, *J. Electrochem. Soc.*, **110** (1963) 267.
257. A. R. Despic, D. M. Drazic, M. M. Purenovic, N. Cikovic, *J. Appl. Electrocochem.*, **6** (1976) 527.
258. Q. Li, N. J. Bjerrum, Aluminum as anode for energy storage and conversion: a review. *J. Power Sources*, **110** (2002) 1–10.
259. B. M. L. Rao, W. Kobasz, W. H. Hoge, R. P. Hamlen, W. Halliop, N. P. Fitzpatrick, Advances in aluminum—air salt water batteries, in O. J. Murphy, S. Srinivasan, B. E. Conway (eds.), *Electrochemistry in Transition*, Plenum Press, New York (1992) pp. 629–639.
260. G. Buri, Wluedi, O. Haas, *J. Electrochem. Soc.*, **136** (1989) 2167.
261. J. F. Equerry, S. Muller, J. Desilverstro, O. Haas, *J. Electrochem. Soc.*, **139** (1992) 1499.
262. F. Holzer, S. Muller, J. Desilverstro, O. Haas, *J. Appl. Electrochem.*, **23** (1993) 125.
263. S. Muller, F. Holzer, J. Desilverstro, O. Haas, *J. Appl. Electrochem.*, **26** (1996) 1217.
264. A. V. Ilyukhina, B. V. Kleymenov, A. Z. Zhuk, Development and study of aluminum-air electrochemical generator and its main components. *J. Power Sources*, **342** (2017) 741–749.
265. V. Kapali, S. V. Iyer, V. Balaramachandran, K. B. Sarangapani, M. Ganesan, M. A. Kulandainathan, A. S. Mideen, Studies on the best alkaline electrolyte for aluminium/air batteries. *J. Power Sources*, **39** (1992) 263–269.
266. D. R. Egan, C. Ponce de León, R. J. K. Wood, R. L. Jones, K. R. Stokes, F. C. Walsh, Developments in electrode materials and electrolytes for aluminium-air batteries. *J. Power Sources*, **236** (2013) 293–310.

267. I. J. Albert, M. A. Kulandainathan, M. Ganesan, V. Kapali, *J. Appl. Electrochem.*, **19** (1989) 547.
268. N. A. F. Al-Rawashdeh, A. K. Maayta, *Anti-corrosion Meth. Mater.*, **52** (2005) 160.
269. A. M. Abdel-Gaber, E. Khamis, H. Abo-Eldahab, S. Adeel, *Mater. Chem. Phys.*, **124** (2010) 773.
270. Z. Zhang, C. C. Zuo, Z. H. Liu, Y. Yu, Y. X. Zuo, Y. Song, *J. Power Sources*, **251** (2014) 470–475.
271. M. Pino, J. Chacon, E. Fatas, P. Ocon, Performance of commercial aluminium alloys as anodes in gelled electrolyte aluminium-air batteries. *J. Power Sources*, **299** (2015) 195–201.
272. M. Mokhtar, M. Zainal M. Talib, E. Herianto, S. M. Tasirin, W. M. F. W. Ramli, W. R. W. Daud, J. Sahari, Recent developments in materials for aluminum e air batteries: a review. *J. Ind. Eng. Chem.*, **32** (2015) 1–20.
273. Y. Liu, Q. Sun, X. Yang, J. Liang, B. Wang, A. Koo, R. Li, J. Li, X. Sun X, High-performance and recyclable Al-air coin cells based on ecofriendly chitosan hydrogel membranes. *ACS Appl. Mater. Interfaces*, **10** (2018) 19730–19738.
274. L. Wang, F. Liu, W. Wang, G. Yang, D. Zheng, Z. Wu, M. K. H. Leung, A high-capacity dual-electrolyte aluminum/air electrochemical cell. *RSC Adv.*, **4** (2014) 30857.
275. N. Bogolowski, J. Drillet, Activity of different  $\text{AlCl}_3$ -based electrolytes for the electrically rechargeable aluminium-air battery. *Electrochim. Acta*, **274** (2018) 353–358.
276. T. Hibino, K. Kobayashi, M. Nagao, An all-solid-state rechargeable aluminium-air battery with a hydroxide ion-conducting Sb(V)-doped  $\text{SnP}_2\text{O}_7$  electrolyte. *J. Mater. Chem. A*, **1** (2013) 14844.
277. T. Hibino, Y. B. Shen, M. Nishida, M. Nagao, *Angew. Chem., Int. Ed.*, **51** (2012) 10786–10790.
278. T. Hibino, K. Kobayashi, *J. Mater. Chem. A*, **1** (2013) 6934–6941.
279. R. Mori, A new structured aluminium-air secondary battery with a ceramic aluminium ion conductor. *RSC Adv.*, **3** (2013) 11547.
280. R. Mori, A novel aluminium-air secondary battery with long-term stability. *RSC Adv.*, **4** (2014) 1982.
281. W. Thomas Goh, et al., A near-neutral chloride electrolyte for electrically rechargeable zinc-air batteries. *J. Electrochem. Soc.*, **161** (2014) A2080–A2086.

282. A. Sumboja, et al., Durable rechargeable zinc-air batteries with neutral electrolyte and manganese oxide catalysts. *J. Power Sources*, **332** (2016) 330–336.
283. S. Amendola, et al., Bifunctional (rechargeable) air electrodes. WO 2012/021550 A2 (2012).
284. H. H. Hassan, Perchlorate and oxygen reduction during Zn corrosion in a neutral medium. *Electrochim. Acta*, **51** (2006) 5966–5972.
285. S. Amendola, et al., Electrically rechargeable, metal-air battery systems and methods. WO 2012/012558 A3 (2012).
286. S. Amendola, et al., Electrically rechargeable metal-air battery systems and methods. US 2012/0021303 A1 (2012).
287. N. Zhang, F. Cheng, J. Liu, L. Wang, X. Long, X. Liu, F. Li, J. Chen, Rechargeable aqueous zinc-manganese dioxide batteries with high energy and power densities. *Nat. Commun.*, **8** (2017) 405.
288. A. R. Mainar, E. Iruin, L. C. Colmenares, A. Kvasha, I. de Meatza, M. Bengoechea, O. Leonet, I. Boyano, Z. Zhang, J. A. Blazquez, An overview of progress in electrolytes for secondary zinc-air batteries and other storage systems based on zinc. *J. Energy Storage*, **15** (2018) 304–328.
289. J. Jindra, J. Mrha, M. Musilová, Zinc-air cell with neutral electrolyte. *J. Appl. Electrochem.*, **3** (1973) 297–301.
290. M. Abdallah, A. Y. El-Etre, M. F. Moustafa, Amidopoly ethylamines as corrosion inhibitors for zinc dissolution in different acidic electrolytes. *Port. Electrochim. Acta*, **27** (2009) 615–630.
291. H. H. Hassan, et al., Participation of the dissolved O<sub>2</sub> in the passive layer formation on Zn surface in neutral media. *Electrochim. Acta*, **52** (2007) 6929–6937.
292. H. H. Hassan, Corrosion behaviour of zinc in sodium perchlorate solutions. *Appl. Surf. Sci.*, **174** (2001) 201–209.
293. X. G. Zhang, Corrosion and electrochemistry of zinc, in M. Schlesinger, M. Paunovic (eds.), *Modern Electroplating*, 5th edn, Spring Street, New York (2011) p. 1996.
294. K. F. Burton, A. F. Sammells, Secondary zinc/oxygen electrochemical cells using inorganic oxyacid electrolytes. Pat. No. 4,220,690 (1980).
295. H. L. Lewenstein, M. Terrace, Electrolytic cell with minimal water dissipation, US 3,928,066 (1975).
296. M. Xu, D. G. Ivey, W. Qu, Z. Xie, E. Dy, in A. Brooks (ed.), *Ionic Liquids: Synthesis, Characterization and Applications*, Nova Science Publishers, Inc. (2014) pp. 99–123.

297. K. V. Kordesch, C. Fabjan, J. D. Iavad, J. Oliveira, Rechargeable zinc-carbon hybrid cells. *J. Power Sources*, **65** (1997) 77–80.
298. A. Guerfi, J. Trottier, I. Boyano, I. De Meatza, J. A. Blazquez, S. Brewer, K. S. Ryder, A. Vijh, K. Zaghib, High cycling stability of zinc-anode/conducting polymer rechargeable battery with non-aqueous electrolyte. *J. Power Sources*, **248** (2014) 1099–1104.
299. H. Ye, J. J. Xu, Zinc ion conducting polymer electrolytes based on oligomeric polyether/PVDF-HFP blends. *J. Power Sources*, **165** (2007) 500–508.
300. M. B. Armand, J. R. MacCallum, C. A. Vicent, *Polymer Electrolyte Reviews*, Vol. 1, Elsevier Applied Science, New York, 1987.
301. K. M. Abraham, Z. Jiang, B. Carroll, Highly conductive PEO-like polymer electrolytes. *Chem. Mater.*, **9** (1997) 1978–1988.
302. M. Giua, S. Panero, B. Scrosati, X. Cao, S. G. Greenbaum, Investigation of mixed cation effects in  $\text{PEO}_9\text{Zn}_{1-x}\text{Cu}_x(\text{CF}_3\text{SO}_3)_2$  polymer electrolytes. *Solid State Ionics*, **83** (1996) 73–78.
303. D. Baril, Y. Chabre, M. B. Armand, Zinc conducting polymer electrolytes based on a vehicular process. *J. Electrochem. Soc.*, **140** (9) (1993) 2687–2690.
304. M. Xu, D. G. Ivey, Z. Xie, W. Qu, Rechargeable Zn-air batteries: progress in electrolyte development and cell configuration advancement. *J. Power Sources*, **283** (2015) 358–371.
305. M. Xu, D. G. Ivey, Z. Xie, W. Qu, *J. Power Sources*, **283** (2015) 358–371.
306. T. J. Simons, A. A. J. Torriero, P. C. Howlett, D. R. Macfarlane, M. Forsyth, *Electrochem. Commun.*, **18** (2012) 119–122.
307. M. Xu, D. G. Ivey, Z. Xie, W. Qu, *Electrochim. Acta*, **89** (2013) 756–762.
308. C. O. Laoire, S. Mukerjee, K. M. Abraham, E. J. Plichta, M. A. Hendrickson, *J. Phys. Chem. C*, **114** (2010) 9178–9186.
309. G. Girishkumar, B. McCloskey, A. C. Luntz, S. Swanson, W. Wilcke, *J. Phys. Chem. Lett.*, **1** (2010) 2193–2203.
310. M. Kar, T. J. Simons, M. Forsyth, D. R. MacFarlane, *Phys. Chem. Chem. Phys.*, **16** (2014) 18658–18674.
311. M. Kar, B. Winther-Jensen, M. Forsyth, D. R. MacFarlane, *Phys. Chem. Chem. Phys.*, **15** (2013) 7191–7197.
312. M. Xu, et al., The state of water in 1-butyl-1-methyl-pyrrolidinium bis (trifluoromethanesulfonyl)imide and its effect on Zn/Zn(II) redox behavior. *Electrochim. Acta*, **97** (2013) 289–295.

313. A. P. Abbott, et al., Processing of metals and metal oxides using ionic liquids. *Green Chem.*, **13** (2011) 471–481.
314. N. S. Venkata Narayanan, B. V. Ashokraj, S. Sampath, Ambient temperature, zinc ion-conducting, binary molten electrolyte based on acetamide and zinc perchlorate: application in rechargeable zinc batteries. *J. Colloid Interface Sci.*, **342** (2010) 505–512.
315. Q. Zhang, et al., Deep eutectic solvents: syntheses, properties and applications. *Chem. Soc. Rev.*, **41** (2012) 7108–7146.
316. S. Z. Liu, W. Han, B. C. Cui, X. J. Liu, F. L. Zhao, J. Stuart, S. Licht, *J. Power Sources*, **342** (2017) 435.
317. S. Liu, W. Han, B. Cui, X. Liu, H. Sun, J. Zhang, M. Lefler, S. Licht, Rechargeable zinc air batteries and highly improved performance through potassium hydroxide addition to the molten carbonate eutectic electrolyte. *J. Electrochem. Soc.*, **165** (2) (2018) A149–A154.
318. P. Pei, K. Wang, Z. Ma, Technologies for extending zinc-air battery's cycllelife: a review. *Appl. Energy*, **128** (2014) 315–324.
319. S. Martirosyan, *J. Power Sources*, **172** (2007) 984–987.
320. G. Merle, M. Wessling, K. Nijmeijer, Anion exchange membranes for alkaline fuel cells: a review. *J. Membr. Sci.*, **377** (1) (2011) 1–35.
321. P. Sapkota, H. Kim, An experimental study on the performance of a zinc air fuel cell with inexpensive metal oxide catalysts and porous organic polymer separators. *J. Ind. Eng. Chem.*, **16** (1) (2010) 39–44.
322. E. L. Dewi, K. Oyaizu, H. Nishide, E. Tsuchida, Cationic polysulfonium membrane as separator in zinc-air cell. *J. Power Sources*, **115** (1) (2003) 149–152.
323. H. Saputra, R. Othman, A. G. E. Sutjipto, R. Muhida, MCM-41 as a new separator material for electrochemical cell: application in zinc-air system. *J. Membr. Sci.*, **367** (1–2) (2011) 152–157.
324. H. Liu, Y. Liu, J. Li, *Phys. Chem. Chem. Phys.*, **12** (2010) 1685–1697.
325. I. Persson, *Acta Chem. Scand. A*, **36** (1982) 7–13.
326. M. J. Trahan, S. Mukerjee, E. J. Plichta, M. A. Hendrickson, K. M. Abraham, *J. Electrochem. Soc.*, **160** (2013) A259–A267.
327. M. Xu, D. G. Ivey, W. Qu, Z. Xie, *J. Power Sources*, **252** (2014) 327–332.
328. X. Yu and A. Manthiram, Electrochemical energy storage with mediator-ion solid electrolytes. *Joule*, **1** (2017) 453–462.
329. X. Yu, A. Manthiram, A voltage-enhanced, low-cost aqueous iron air battery enabled with a mediator-ion solid electrolyte. *ACS Energy Lett.*, (2017) 1050–1055.

330. S. Licht, B. Cui, J. Stuart, B. Wang, J. Lau, Molten air – a new, highest energy class of rechargeable batteries. *Energy Environ. Sci.*, **6** (2013) 3646.
331. S. Trocino, S. C. Zignani, M. Lo Faro, V. Antonucci, A. S. Aricò, Iron-air battery operating at high temperature. *Energy Technol.*, (2017) 670–680.
332. X. Zhao, X. Li, Y. Gong, N. Xu, K. Huang, *RSC Adv.*, **4** (2014) 22621–22624.
333. M. Berger, O. Tokariev, N. H. Menzler, O. Guillou, M. Bram, *12th European SOFC & SOE Forum Proceedings*, (2016) 215–220.
334. S. Trocino, M. L. Faro, S. C. Zignani, V. Antonucci, A. S. Aricò, High performance solid-state iron-air rechargeable ceramic battery operating at intermediate temperatures (500–650°). *Appl. Energy*, **233–234** (2019) 386–394.
335. A. Inoishi, T. Sakai, Y. W. Ju, S. Ida, T. Ishihara, *J. Power Sources*, **262** (2014) 310–315.
336. A. Inoishi, J. Hyodo, H. Kim, T. Sakai, S. Ida, T. Ishihara, Low temperature operation of a solid-oxide Fe-air rechargeable battery using a  $\text{La}_{0.9}\text{Sr}_{0.1}\text{Ga}_{0.8}\text{Mg}_{0.2}\text{O}_3$  oxide ion conductor. *J. Mater. Chem. A*, **3** (2015) 8260–8264.
337. R. D. McKerracher, C. P. De Leon, R. G. A. Wills, A. A. Shah, F. C. Walsh, A review of the iron-air secondary battery for energy storage. *ChemPlusChem*, (2015) 323–335.
338. X. Zhao, X. Li, Y. Gong, N. Xu, K. Romito, K. Huang, A high energy density all solid-state tungsten-air battery. *Chem. Commun.*, **49** (2013) 5357–5359.
339. X. Zhao, K. Huang, Y. Gong, N. Xu, X. Li, All solid state tungsten-air battery: a new metal-air chemistry. *ECS Meeting Abstracts*, Volume MA2013-02, 533.
340. X. Zhao, Y. Gong, X. Li, N. Xu, K. Huang, A new solid oxide molybdenum-air redox battery. *J. Mater. Chem. A*, **1** (2013) 14858–14861.
341. A. Inoishi, T. Sakai, Y.-W. Ju, S. Ida, T. Ishihara, A rechargeable Si-air solid state oxygen shuttle battery incorporating an oxide ion conductor. *J. Mater. Chem. A*, **1** (2013) 15212–15215.
342. A. Jayakumar, S. Lee, A. Hornés, J. M. Vohs, R. J. Gorte, A comparison of molten Sn and Bi for solid oxide fuel cell anodes. *J. Electrochem. Soc.*, **157** (2010) B365–B369.
343. A. Jayakumar, J. M. Vohs, R. J. Gorte, Molten-metal electrodes for solid oxide fuel cells. *Ind. Eng. Chem. Res.*, **49** (2010) 10237–10241.

344. L. Otaegui, et al., Performance and long term stability of a liquid-tin anode metal-air solid electrolyte battery prototype. *Electrochim. Acta*, **214** (2016) 192–200.
345. S. Sumathi, V. Sethuprakash, W. J. Basirun, I. Zainol, M. Sookhakian, Polyacrylamide-methanesulfonic acid gel polymer electrolytes for tin-air battery. *J. Sol-Gel Sci. Technol.*, **69** (2014) 480–487.
346. G. Cohn, D. Starosvetsky, R. Hagiwara, D. D. Macdonald, Y. Ein-Eli, Silicon-air batteries. *Electrochim. Commun.*, **11** (2009) 1916–1918.
347. G. Cohn, Y. Ein-Eli, *J. Power Sources*, **195** (2010) 4963.
348. G. Cohn, A. Altberg, D. D. Macdonal, Y. Ein-Eli, A silicon-air battery utilizing a composite polymer electrolyte. *Electrochim. Acta*, **58** (2011) 161–164.
349. T. Tsuda, T. Nohira, Y. Nakamori, K. Matsumoto, R. Hagiwara, Y. Ito. *Solid State Ionics*, **149** (2002) 295.
350. R. Hagiwara, T. Hirashige, T. Tsuda, Y. Ito, *J. Fluorine Chem.*, **99** (1999) 1–3.
351. Z. Li, M. S. Pan, L. Su, P.-C. Tsai, A. F. Badel, J. M. Valle, S. L. Eiler, K. Xiang, F. R. Brushett, Y.-M. Chiang, Air-breathing aqueous sulfur flow battery for ultralow-cost long-duration electrical storage. *Joule*, **1** (2017) 306–327.
352. J. Grosse-Austing, C. Nunes-Kirchner, E.-M. Hammer, L. Komsa, G. Wittstock, Study of an unitised bidirectional vanadium/air redox flow battery comprising a two-layered cathode. *J. Power Sources*, **273** (2015) 1163–1170.



Taylor & Francis

Taylor & Francis Group

<http://taylorandfrancis.com>

## **Chapter 8**

# **Electrolytes for Lithium-Sulfur Batteries**

**Maciej Marczewski**

*Faculty of Chemistry, Warsaw University of Technology, Noakowskiego 3,  
00-664 Warszawa, Poland  
maciej.marczewski@pw.edu.pl*

### **8.1 Introduction**

The observed revolution in the area of electromobility creates the need to develop new, more efficient energy storage systems, with electrochemical energy storage (EES) in the leading role. As discussed in the previous chapters, the most commonly used EES systems are lithium-ion batteries (LiBs) [1, 2]. However, LiBs can be hindered by some technical limitations, mainly due to the theoretical capacity of graphite electrode and cathode based mostly on transition metal oxides (560 Wh/kg), and there is a need for the technology development of batteries with a higher energy density. One idea is to replace the graphite electrode for the metallic lithium and metal-oxide cathode with a more capacious sulfur electrode (lithium-sulfur batteries [Li-S]). This helps to obtain a significantly higher theoretical capacity—up to 2500 Wh/kg. Unfortunately, this technology is facing a huge number of principle-related problems

---

*Designing Electrolytes for Lithium-Ion and Post-Lithium Batteries*

Edited by Włodzisław Wieczorek and Janusz Płocharski

Copyright © 2021 Jenny Stanford Publishing Pte. Ltd.

ISBN 978-981-4877-16-9 (Hardcover), 978-1-003-05093-3 (eBook)

[www.jennystanford.com](http://www.jennystanford.com)

[3–6]. Optimizing the electrolyte is one of the most crucial goals in order to improve the Li-S battery in terms of performance, especially in terms of cell cyclability, rate capability, safety, and life span. During the last two decades, the growing interest in the field of electrolyte development for Li-S batteries has led to many improvements and technology breakthroughs, but still not all the problems have been solved.

Li-S batteries are based on the principle of reduction of sulfur (the cathode material) to polysulfide species (PS), which by interacting with lithium cations form lithium sulfide ( $\text{Li}_2\text{S}$ ). During discharge of the battery on the anode (built with metallic lithium) the process of lithium oxidation takes place:  $\text{Li} = \text{Li}^+ + \text{e}^-$ . At the same time, on the cathode, sulfur reduction takes place:  $\text{S} + 2\text{e}^- = \text{S}^{2-}$ . The overall reaction is as follows:  $2\text{Li} + \text{S} = \text{Li}_2\text{S}$ . Because sulfur in nature exists in the form of octasulfur ( $\text{S}_8$ ), it is necessary to modify the overall reaction equation to the following form:  $16\text{Li} + \text{S}_8 = 8\text{Li}_2\text{S}$ . A mechanism of sulfur compound propagation in the electrolyte is described very well by Barghamadi et al. in a review paper [7]. In Li-S cells, various lithium polysulfides with a general formula  $\text{Li}_2\text{S}_x$  ( $2 < x < 8$ ) are formed during the cell discharge process. It is assumed that the elemental sulfur in the solid phase  $\text{S}_8(\text{s})$  is first dissolved in the electrolyte as  $\text{S}_8$  (solvated) and gradually reduce. During cell discharge, lithium polysulfides soluble in common organic solvents ( $\text{Li}_2\text{S}_x$ ,  $4 < x < 8$ ), insoluble in common organic solvents ( $\text{Li}_2\text{S}_x$ ,  $1 < x < 2$ ), and finally lithium sulfide ( $\text{Li}_2\text{S}$ ) appear one after another [8–13].

The presence of these particles in the electrolyte leads to abnormal cell operation in comparison to LIBs. The typical discharge-charge curve for a Li-S cell is dominated by four characteristic regions (Fig. 8.1), related to the following phenomena:

- Reduction of  $\text{S}_8$  to  $\text{S}_8^{2-}$ , which, as mentioned above, is soluble in most of the commonly used organic solvents (Region I; slight reduction in the cell voltage from 2.4 V to 2.2 V versus  $\text{Li}^+/\text{Li}$  observed)
- Reduction of polysulfides to  $\text{Li}_2\text{S}_4$  (Region II; a sharp fall in voltage)

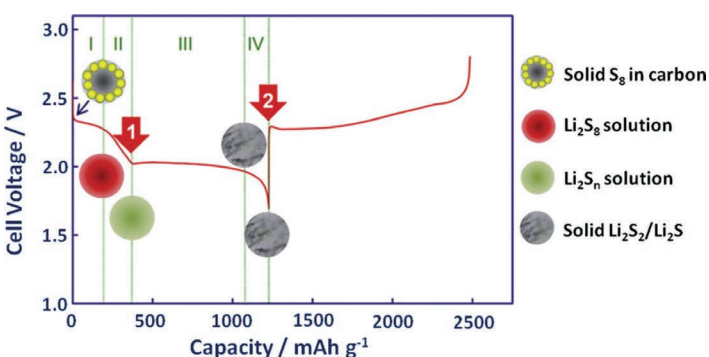


**Figure 8.1** Typical discharge-charge curve for a lithium-sulfur cell [14].

- Further reduction to  $\text{Li}_2\text{S}_2$  and partially to  $\text{Li}_2\text{S}$  (Region III; relatively stable voltage plateau  $\sim 2.1$  V versus  $\text{Li}^+/\text{Li}$ )
- Full reduction to  $\text{Li}_2\text{S}$  (Region IV)

The influence of the described particles on the properties of the Li-S cell is once again very well described by Barghamadi et al. [7]. Firstly, a kind of self-discharge process occurs that is more significant than in LiBs. This is related to the diffusion of soluble sulfur-based species out of the positive electrode to the lithium negative electrode. There, as a result of direct chemical reactions with lithium or during charging, these species undergo a reduction reaction and are deposited as insoluble  $\text{Li}_2\text{S}$  or  $\text{Li}_2\text{S}_2$ . This process results in a permanent loss of active material. What is more, migration of sulfide species has further effects on cell properties.  $\text{Li}_2\text{S}$  and  $\text{Li}_2\text{S}_2$  are highly reduced species and react with the  $\text{S}_x^{2-}$  from the electrolyte to form lower-order polysulfides ( $\text{S}_{x-n}^{2-}$ ). Then these species diffuse back to the positive electrode, where they reoxidize into  $\text{S}_x^{2-}$ . This internal “redox shuttle” process lowers both the available discharge capacity and the efficiency of recharging. As shown, the electrolyte is one of the weakest and most important elements of the Li-S cell. Its composition has influence on the migration processes taking place during charge/discharge and therefore reflects in the cell parameters.

Detailed knowledge about this dissolution process and the polysulfide species formed in the electrolytes is not sufficient.

This slows down the rational design of new electrolytes. Until now, research efforts have mainly been focused on analyzing the electrochemical behavior of lithium polysulfides and identifying the polysulfide intermediate species formed during the Li-S battery cycling process.

## 8.2 Electrolyte Requirements

It is important to highlight that research in the field of Li-S cells was for a long time focused mainly on the electrode materials. But since the last decade, the electrolyte design has become important and led to an increase in the systematic research in this field, helping establish requirements that should be fulfilled by the electrolyte.

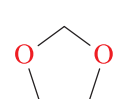
In general, the electrolyte in a Li-S cell should be characterized by ionic conductivity in the range between  $10^{-3}$  S/cm and  $10^{-2}$  S/cm and high values of lithium transference number at room temperature mainly because of its primary function—ionic transport between the electrodes. The required electrochemical stability window in the case of the Li-S cell is  $\sim 2.5$  V, which is way lower than in the case of LiBs ( $\sim 4$  V). The electrolyte should be stable in the presence of metallic lithium. However, this requirement can be overcome by using proper additives. As in the case of LiB technology, the electrolyte should also be characterized by low flammability and low toxicity. One more, very important, requirement is that the electrolyte should have good stability in the presence of polysulfides [15].

Mainly two kinds of electrolytes dedicated to Li-S cells are reported in the literature—liquid and solid—and they are divided into many subgroups. The purpose of this chapter is to show the recent advances in both approaches and highlight the biggest issues for research in this field.

## 8.3 Liquid Electrolytes

Use of liquid electrolytes is justified by the architecture of the cathode materials. Because of the use of large-surface-area carbons

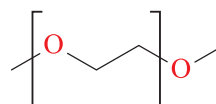
## Ethers



DIOX, DOL

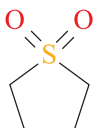


THF

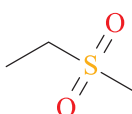


DME (n=1); Gn (n≥2)

## Sulfones

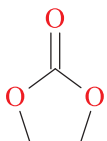


TMS

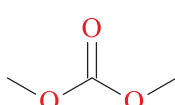


EMS

## Carbonates



EC



DMC

**Figure 8.2** Organic solvents tested for Li-S battery electrolytes.

as the host matrix in the cathode composite materials, liquid electrolytes with good wetting properties are required, characterized by low surface tensions and low viscosities. Several groups of solvents were tested in Li-S cells—carbonates, ethers, sulfones (Fig. 8.2), and ionic liquids (ILs) in different configurations. The most common are binary and ternary mixtures of solvents, but a single-solvent approach is also observed [15].

Typical electrolyte salts used in a Li-S cell are LiTf (LiOTf), LiTFSI, LiPF<sub>6</sub>, LiClO<sub>4</sub>, and LiTDI (Fig. 8.3) [15, 16].

Here a brief description of different classes of solvent-based electrolytes is given, and examples of working electrolytes with crucial parameters are presented in Table 8.1.

**Table 8.1** Characteristics of liquid electrolytes and the corresponding performance in lithium–sulfur cells

Electrolyte composition	Initial discharge capacity ( $\text{mA h g}^{-1}$ )/temperature ( $^{\circ}\text{C}$ )	Residual discharge capacity ( $\text{mA h g}^{-1}$ )/cycles	References
<b>Organic electrolyte</b>			
PEGDME 500 1 M LiTFSI	1200/—	400/40	[38]
TEGDME 0.5 M LiTFSI	330/—	—	[39]
TEGDME/DOL (1/1 v/v) 0.5 M LiTFSI	760/—	—	[39]
TEGDME/DOL (1/1 v/v) 1 M LiTFSI	720/—	460/20	[40]
TEGDME/DOL (33/67 v/v) 1 M LiTFSI + 0.2 M LiNO <sub>3</sub>	900/—	600/20	[41]
TEGDME/DOL (1/1 v/v) + 5% v MA 0.5 M LiTFSI	900/—	—	[39]
TEGDME/DOL (1/1 v/v) + 10% v MA 0.5 M LiTFSI	600/—	—	[39]
TEGDME 1 M LiOTf	400/RT	390/50	[42]
TEGDME/DOL (1/1 v/v) 1 M LiOTf	500/RT	500/50	[42]
TEGDME/DOL (30/70 v/v) 0.5 M LiOTf	—	—	[43]
TEGDME/DOL (70/30 v/v) 0.5 M LiOTf	—	—	[43]
TEGDM/DOL (100/00 v/v) 0.5 M LiOTf	—	—	[43]
TEGDME/DOL (00/100, v/v) 0.5 M LiOTf	—	—	[43]
TEGDME/DOL (1/1 v/v) 1 M LiClO <sub>4</sub>	1000/—	310/20	[40]
TEGDME/DOL (1/1 v/v) 1 M LiOTf	750/—	450/20	[40]
TEGDME 0.98 M LiTFSI DOL 0.5 M LiTFSI	950/30	500/60	[33]
DOL/DME (4/1 v/v) 1 M LiClO <sub>4</sub>	550/—	—	[39]
DOL/DME (2/1 v/v) 1 M LiClO <sub>4</sub>	900/RT	320/20	[44]
			(Contd.)

**Table 8.1** (Continued)

Electrolyte composition	Initial discharge capacity (mA h g <sup>-1</sup> )/ temperature (°C)	Residual discharge capacity (mA h g <sup>-1</sup> )/ cycles	References
<b>Organic electrolyte</b>			
DOL/DME (1/1 v/v) 1 M LiClO <sub>4</sub>	1050/RT	510/20	[40]
DOL/DME (1/2 v/v) 1 M LiClO <sub>4</sub>	1000/RT	500/20	[44]
DOL/DME (2/1 v/v) 1 M LiClO <sub>4</sub>	950/RT	260/20	[44]
DOL/DME (1/1 v/v) 1 M LiClO <sub>4</sub>	750/—	500/20	[40]
DOL/DME (1/1 v/v) 1 M LiTFSI	1000/—	520/20	[40]
DOL/DME (1/1 v/v) 1 M LiOTf	900/—	550/20	[40]
DOL/DME (1/1 v/v) 1 M LiTFSI	1200/RT	450/120	[45]
DOL/DME (1/1 v/v) 0.25 mol kg <sup>-1</sup> LiTFSI + 0.25 mol kg <sup>-1</sup> PYR14TFSI	1000/—	450/200	[46]
DOL/DME (1/1 v/v) 0.25 mol kg <sup>-1</sup> LiNO <sub>3</sub> + 0.25 mol kg <sup>-1</sup> PYR14TFSI	1100/—	500/200	[46]
DOL/DME (1/1 v/v) 0.25 mol kg <sup>-1</sup> LiNO <sub>3</sub> + 0.25 mol kg <sup>-1</sup> TBAOTf	1200/—	500/120	[46]
DME/DEGDME (1/1 v/v) 1 M LiOTf	944/RT	350/50	[42]
DME/DOL (1/1 v/v) 1 M LiTFSI + 2 wt.% LiNO <sub>3</sub>	1300/25	380/1200	[107]
DME/DOL (1/1 v/v) 1 M LiTFSI + 2 wt.% LiNO <sub>3</sub>	900/25	300/1500	[108]
DME/DOL (1/1 v/v) 1 M LiTFSI + 0.5 wt.% LiNO <sub>3</sub>	600/25	400/1000	[109]
DME/DOL (1/1 v/v) 1 M LiTFSI + 2 wt.% LiNO <sub>3</sub>	700/25	600/300	[110]
DME/DOL (1/1 v/v) 1.85 M LiOTf + 0.1 M LiNO <sub>3</sub>	864/25	527/400	[111]

(Contd.)

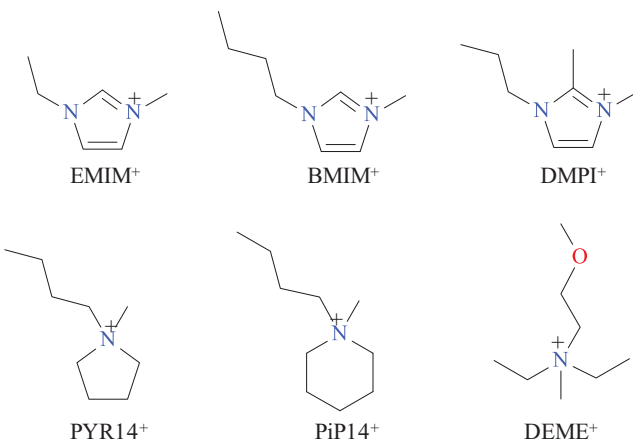
**Table 8.1** (Continued)

Electrolyte composition	Initial discharge capacity (mA h g <sup>-1</sup> )/ temperature (°C)	Residual discharge capacity (mA h g <sup>-1</sup> )/ cycles	References
<b>Organic electrolyte</b>			
DME/DOL (1/1 v/v) 1 M LiTFSI +2 wt.% LiNO <sub>3</sub>	727/25	698/500	[112]
DME/DOL (1/1 v/v) 1 M LiTFSI +2 wt.% LiNO <sub>3</sub>	1000/25	700/500	[113]
<b>Ionic liquid-based electrolyte</b>			
PYR14TFSI/TEGDME (1/1 w/w) 0.2 mol kg <sup>-1</sup> LiTFSI	887/RT	420/20	[47]
PYR14TFS/TEGDME (1/2 w/w) 0.2 mol kg <sup>-1</sup> LiTFSI	—	—	[47]
PYR14TFSI/PEGDME (1/2 w/w) 0.5 M LiTFSI	450/40	250/100	[48]
PYR14TFSI/PEGDME (1/1.5 w/w) 0.5 M LiTFSI	500/40	180/100	[48]
PYR14TFSI: PEGDME (1/1 w/w) 0.5 M LiTFSI	320/40	100/80	[48]
PYR14TFSI/PEGDME (1/0.1 w/w) 0.5 M LiTFSI	—	—	[48]
PYR14TFSI 0.5 M LiTFSI	120/40	20/50	[48]
PYR14TFSI 0.5 mol kg <sup>-1</sup> LiTFSI	720/30	550/50	[32]
PYR14OTf 0.5 mol kg <sup>-1</sup> LiTFSI	650/30	190/50	[32]
PYR13TFSI 0.5 mol kg <sup>-1</sup> LiTFSI	800/30	700/50	[32]
PYR13BETI 0.5 mol kg <sup>-1</sup> LiTFSI	620/30	200/50	[32]
PYR13FSI 0.5 mol kg <sup>-1</sup> LiTFSI	1000/30	50/50	[32]
EMIMTFSI 1 M LiTFSI	1300/—	500/40	[38]
PiP13TFSI 0.5 mol kg <sup>-1</sup> LiTFSI	600/30	520/50	[32]
PiP13TFSI/DME (2/1 v/v) 1 M LiTFSI	1000/—	900/50	[49]
PiP13TFSI 1 M LiTFSI	405/—	320/10	[49]
DEMEBF <sub>4</sub> 0.5 mol kg <sup>-1</sup> LiTFSI	900/30	50/50	[32]
DEMETF <sub>3</sub> 0.5 mol kg <sup>-1</sup> LiTFSI	780/30	650/50	[32]
DEMETF <sub>3</sub> 0.64 M LiTFSI	800/30	580/100	[33]
P2225TFSI 0.5 mol kg <sup>-1</sup> LiTFSI	700/30	500/50	[32]
C <sub>4</sub> dmmiTFSI 0.5 mol kg <sup>-1</sup> LiTFSI	750/30	580/50	[32]

(Contd.)

**Table 8.1** (Continued)

Electrolyte composition	Initial discharge capacity ( $\text{mA h g}^{-1}$ )/temperature ( $^{\circ}\text{C}$ )	Residual discharge capacity ( $\text{mA h g}^{-1}$ )/cycles	References
<b>Solvated ionic liquid</b>			
Li(G4)-TFSI	1100/RT	700/50	[50]
Li(G3)-TFSI	1100/30	700/400	[34]
Li(G3) <sub>4</sub> TFSI	800/30	500/35	[34]
Li(G4)-TFSI/HFE (1/1/4)	1000/30	750/50	[34]
Li(G4)-TFSI	900/30	600/50	[34]
Li(G3)-OTf	280/30	150/100	[51]
Li(G3)-NO <sub>3</sub>	380/30	30/100	[51]
Li(G4)-BETI	700/30	550/100	[51]
Li(G4)-BF <sub>4</sub>	400/30	100/100	[51]

**Figure 8.3** Examples of IL cations implemented in Li-S battery electrolytes.

### 8.3.1 Carbonates

Unlike LiBs, carbonate solvents cannot be used in Li-S cells, mainly due to their incompatibility with most sulfur cathodes. Carbonate can react with soluble polysulfides by a nucleophilic attack on the ether or carbonyl atoms on the carbonate molecules (Fig. 8.4), which leads to a loss of sulfur and electrolyte [17, 18].

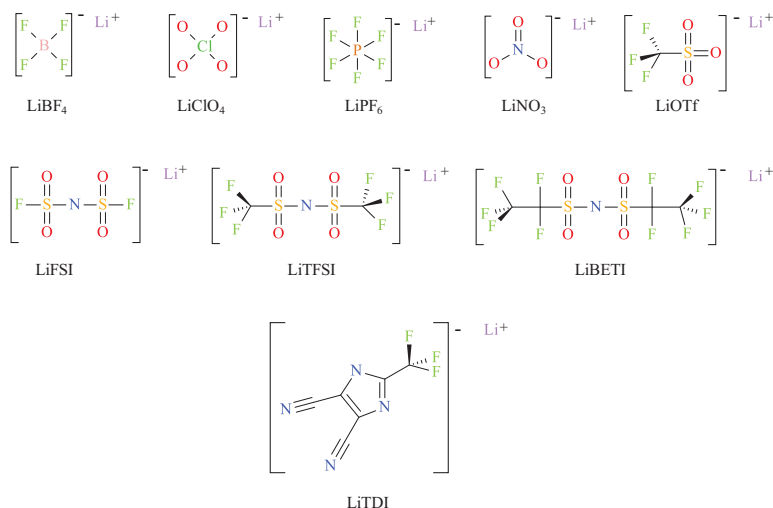


**Figure 8.4** Lithium salts already applied in or of potential use for Li-S battery electrolytes.

The only exception in terms of use of carbonate-based electrolytes is when sulfur is closed in nanopores [17, 19] or covalently bonded on a polymer composite (for instance, sulfurized polyacrylonitrile) [20, 21].

### 8.3.2 Ethers

Ethers are the most commonly used solvents in Li-S battery research. The reason is that they are much more stable toward polysulfides compared, for example, to carbonates. The list of ethers used is very broad—both linear and cyclic, as well as short-chain and polymeric ethers, such as 1,2-dimethoxyethane (DME or G1), tetrahydrofuran (THF), dioxilane (DOL), tetraglyme (TEGDME or G4), triglyme (DGM or G3), partially silanized ethers, and poly(ethylene glycol) dimethyl ether (PEGDME) [15, 22].

The most commonly used solvent mixture is a binary mixture of DME, characterized by a high dielectric constant and a good ability to solvate polysulfides, and DOL, used as a solvent-electrolyte

interphase (SEI) formation agent. Often, instead of DME, a long-chain ether, like TEGDME, is used.

A big drawback of ether-based solvents is the high solubility of polysulfides (up to 10 M solution in THF), which can lead to shuttle problems. This problem can be solved by using specially designed membranes/separators, by electrolytes based on next-generation salts like LiTDI, or by using fluorinated solvents (see Section 8.3.6) [23–26].

Fluorinated ethers are characterized by low melting points, low viscosities, low flammabilities, and poor coordination abilities (fluorine atoms in the structure suppress solvation function due to oxygen atoms) [25, 26]. They can be used as solvents, cosolvents, or additives. The application of fluorinated solvents improves utility parameters. Hydrofluoroether (HFE) used as a cosolvent instead of DME improves the cycling efficiency and reduces capacity fading [25, 26].

The use of ether solvents in the electrolyte offers high initial discharge capacities—from 1100 to 1300 mA h g<sup>-1</sup>—and acceptable residual discharge capacities at the level of 700 mA h g<sup>-1</sup> after 500 cycles or 380 mA h g<sup>-1</sup> after 1200 cycles (Table 8.1). The best results are obtained when the cells are cycled at low currents (0.1 C to 0.25 C).

### 8.3.3 Sulfones

Sulfones have been already used in high-voltage LIBs and were also tested as Li-S battery electrolytes as single solvents, cosolvents, and additives [15, 27–30]. Among the sulfones used for Li-S batteries, the most widely used solvents are tetramethylene sulfone (TMS) and ethyl methyl sulfone.

For example, the difference between the properties of these type of systems and ether systems can be shown on the basis of sulfolane (TMS) and DOL:TEGDME-based electrolytes, which have been studied by Patel et al. by using ultraviolet-visible (UV-vis) spectroscopy [31]. Deconvolution of the UV-vis spectra measured in 1 M LiTFSI in the TEGDME:DOL electrolyte showed a different evolution of polysulfides compared to sulfolane-based electrolytes. This clearly points out that different equilibria may be present

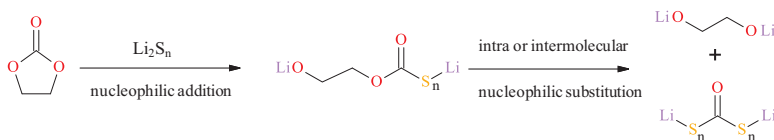


**Figure 8.5** Proposed nucleophilic reaction mechanism of EC with polysulfides.

in the electrolyte during discharge/charge processes for the same cathode composite.

### 8.3.4 Ionic Liquids

ILs are chemical compounds composed entirely of ions (Fig. 8.5), and their properties strictly depend on the interaction between cations and anions (coulombic forces, van der Waals forces, and hydrogen bonds) [32].

IL-based electrolytes for Li-S promise unique properties but have problems with acceptable cell capacities (see Table 8.1). The unique solvation behavior of ILs in Li-S battery electrolytes is especially desirable when the solubility of sulfur and polysulfides affects the battery performance. Park et al. analyzed the solubility of polysulfides in [DEME][TFSI] IL. They stated that the saturation concentration of the most soluble  $\text{Li}_2\text{S}_8$  was 3 orders of magnitude lower compared to that of an organic electrolyte based on TEGDME solvent [33].

The solubility of polysulfides in ILs is a function of the size of the cation:  $[\text{PYR13}]^+ > [\text{PYR14}]^+ > [\text{DEME}]^+ > [\text{PiP13}]^+ > [\text{C4dmim}]^+ > [\text{P2225}]^+$  [32]. Solubility can be increased with higher temperatures, which leads to faster capacity fading during cycling and lower coulombic efficiency, or by adding organic solvents, like TEGDME or PEGDME. Adding a proper amount of organic solvent to the pure IL leads to higher and more stable capacity due to higher conductivity.

Promising direction in research was shown by Dokko et al. with quasi-IL-based electrolytes—solvated ILs (SILs), using G3 and G4 in different ratios versus LiTFSI [34]. SILs are a class of ILs built with a coordinating solvent and salt. Such composition helps raise a chelate

complex that behaves in a manner similar to ILs [114, 115]. SILs suppress PS solubility, which results in a cell with stable capacity.

The use of electrolytes based only on IL and salt binary mixtures offers moderate initial discharge capacities—from 600 to 1300 m Ah g<sup>-1</sup>—and acceptable residual discharge capacities at the level of 500 mA h g<sup>-1</sup>. However, the lifetime of such a cell depends on the chosen composition, ranging from 10 to 50 cycles, which is not acceptable (Table 8.1). The addition of an organic cosolvent to the electrolyte improves the cyclability of the cell (up to 100 cycles) but not the cell parameters. There is visible improvement when SILs are used. The lifetime of the cell is extended by up to 400 cycles.

### 8.3.5 Concentrated Electrolytes

Concentrated electrolytes seem to be very attractive in different cell technologies. In the field of the electrolytes dedicated to Li-S, it is a new and very interesting approach and it seems they can solve many problems of the cell in the near future. These electrolytes are expected to have similar functions as those of ILs in terms of solvation of polysulfides. At this moment, only a few but very promising reports are present in the literature.

It was shown that increasing the LiTFSI concentration from 1 M to 5 M results in improving the coulombic efficiency [35, 36]. Also studies with as high concentration as 7 M LiTFSI in DME:DOL were conducted and such systems can work properly and be characterized by high columbic efficiencies [37].

The major disadvantages of concentrated electrolytes are their increased viscosity and lower conductivity and lithium diffusion rate, which influence the battery performance at high current densities.

### 8.3.6 Novel Approach

Properties of the electrolyte, especially interactions with polysulfides, may be controlled not only by changing solvents and salt concentrations but also by using the proper salt. It was shown that the measured diffusion coefficients of each of the components of Li-S electrolytes composed of different anions (FSI<sup>-</sup>, OTf<sup>-</sup>, TFSI<sup>-</sup>,

and TDI<sup>-</sup>) can be correlated with Li-S cell performance [24]. The various ion–ion and ion–solvent interactions can influence the anion mobility within electrolytes and, thereby, influence the final Li-S cell performance. The correlation between diffusion measurements and the specific capacity reveals that the anion mobility as well as the interaction strength with Li<sup>+</sup> cations are crucial in designing electrolytes for Li-S cells. The higher mobility of an anion (such as FSI<sup>-</sup>) due to weaker interactions with other electrolyte components often leads to the formation of a thicker passivation layer, whereas strongly interacting anions (such as OTf<sup>-</sup>) can accelerate polysulfide dissolution due to their preferential interaction with lithium polysulfides. These predictions are validated by the relatively better cell performance of the TDI<sup>-</sup>-based electrolyte, where the TDI has lower mobility and weak interactions with lithium polysulfide.

In another work, it was confirmed that the use of LiTDI as a supporting electrolyte salt for Li-S batteries effectively decreases the polysulfide solubility, thereby minimizing the polysulfide shuttle mechanism (i.e., which causes a loss of active sulfur material from the cathode and the degradation of the Li metal anode) [23]. Ab initio molecular dynamics simulation reveals that the TDI anion coordination affects the polysulfide disproportion to form a Li<sub>4</sub>S<sub>8</sub> dimer and reduces the solubility. Furthermore, with the incorporation of 0.1% Li<sub>2</sub>S<sub>8</sub> and 0.2 M LiNO<sub>3</sub> additives, excellent Li-S cell performance with cathodes having a high sulfur (3 mgS cm<sup>-2</sup>) loading was obtained using the LiTDI-based electrolyte. Such a cell was cycled for up to 300 cycles with residual discharge capacity at the level of 600 mA h g<sup>-1</sup>.

## 8.4 Solid Electrolytes

As in the case of LiBs, solid electrolytes find application in the Li-S cell technology. They promise not only to be safer than the cells using liquid electrolytes but also to reduce mass and thick [52]. Current research works using solid electrolytes have shown sufficiently high S utilization in the initial cycles; however, the cyclability and areal capacity are still far from the practical requirements. The future

development of this technology needs to overcome the challenges such as low Li-ion conductivity, poor solid-solid contact, lack of in-depth understanding of sulfur redox chemistry in solid electrolytes, and the choice of techniques to probe in detail the interfacial properties.

Starting from the first study on a poly(ethylene oxide) (PEO)-based electrolyte for Li-S cells, several types of solid electrolytes have been investigated. They can be divided into three main categories: those based on pure polymeric components [53–64], ceramic electrolytes [65–82], and composite electrolytes (mix of ceramic and other electrolytes) [83–85]. Properties of solid electrolytes dedicated for Li-S cells are presented in Table 8.2.

**Table 8.2** Characteristics of solid electrolytes and the corresponding performance in lithium-sulfur cells

Electrolyte composition	Initial discharge capacity ( $\text{mA h g}^{-1}$ )/temperature ( $^{\circ}\text{C}$ )	Residual discharge capacity ( $\text{mA h g}^{-1}$ )/cycles	References
<b>Solid polymer electrolyte</b>			
LiTFSI/PEO (1/49 w)	722/90	270/10	[53]
PEO <sub>10</sub> LiTf + Ti <sub>x</sub> O <sub>2x-1</sub> ( $x = 1, 2, 85/15$ , w)	1650/90	490/10	[54]
PEO <sub>20</sub> LiTf + 10 wt.% S-ZrO <sub>2</sub> + Li <sub>2</sub> S	400/70	500/30	[57]
PEO <sub>18</sub> LiTFSI – 10 wt.% SiO <sub>2</sub>	1266/70	823/25	[58]
PEO <sub>6</sub> LiBF <sub>4</sub> – 10 wt.% Al <sub>2</sub> O <sub>3</sub>	1600/80	40/10	[56]
PEO <sub>20</sub> LiTFSI – 10 wt.% $\gamma$ -LiAlO <sub>2</sub>	452/75	184/50	[55]
PEO <sub>20</sub> LiTNFSI	450/60	450/200	[60]
PEO <sub>15</sub> LiTFSI + 10 wt.% HNT	800/25	745/100	[62]
PEO <sub>15</sub> LiTFSI + 6.5 wt.% MIL-53(Al)	1000/60	558/1000	[59]
PEO <sub>15</sub> LiTFSI + 10 wt.% MIL-53(Al)	1450/80	792/50	[61]
PEO <sub>20</sub> LiFSI	900/70	600/50	[63]
PEO <sub>20</sub> LiFSI + 3 vol.% LICGC	1000/70	600/50	[64]

(Contd.)

**Table 8.2** (Continued)

Electrolyte composition	Initial discharge capacity (mA h g <sup>-1</sup> )/temperature (°C)	Residual discharge capacity (mA h g <sup>-1</sup> )/cycles	References
<b>Gel polymer electrolyte</b>			
PEO <sub>20</sub> LiTf + 10 wt.% S-ZrO <sub>2</sub> in EC/DMC + Li <sub>2</sub> S	1200/25	800/30	[89]
LiBF <sub>4</sub> + PVdF-HFP + TEGDME	1450/25	400/10	[89]
LiPF <sub>6</sub> + PVdF-HFP + TEGDME	1500/25	500/10	[97]
LiTf + PVdF-HFP + TEGDME	1200/25	450/10	[97]
LiClO <sub>4</sub> + PEO + TEGDME	320/25	160/10	[86]
PVdF-HFP + LiTFSI + PYR14TFSI	1218/25	818/20	[95]
LiTf + PVdF + TEGDME	1268/22	—	[98]
Cellulose + LiTFSI + TEGDME + DOL + LiNO <sub>3</sub>	730/20	730/60	[87]
PEO <sub>20</sub> LiTf + 10 wt.% ZrO <sub>2</sub> in EC/DMC	600/25	500/20	[83]
PVdF-HFP/PMMA/SiO <sub>2</sub> in LiTFSI-TEGDME	809/25	413/50	[99]
PVdF-HFP/SiO <sub>2</sub> in LiPF <sub>6</sub> -PC/EC/DEC	560/25	300/25	[88]
PVdF-HFP + silicates in LiPF <sub>6</sub> -EC/DEC	900/25	500/300	[100]
PEO <sub>20</sub> LiTf + 10 wt.% ZrO <sub>2</sub> in EC/DMC	200/25	200/80	[90]
PAN/PMMA + LiTFSI/PYR14TFSI/PEGDME	1200/25	900/50	[94]
PMMA/PVdF-HFP in LiPF <sub>6</sub> -EC/DEC	1600/25	1000/110	[91]
<b>Ceramic electrolyte</b>			
80Li <sub>2</sub> S-20P <sub>2</sub> S <sub>5</sub>	1200/25	996/200	[71]
80Li <sub>2</sub> S-20P <sub>2</sub> S <sub>5</sub>	660/25	650/20	[65, 66]
80Li <sub>2</sub> S-20P <sub>2</sub> S <sub>5</sub>	500/25	340/20	[68]
Li <sub>3</sub> PS <sub>4</sub>	1400/60	1200/300	[75]
80Li <sub>2</sub> S-20P <sub>2</sub> S <sub>5</sub>	650/25	650/10	[73]
80Li <sub>2</sub> S-20P <sub>2</sub> S <sub>5</sub>	1000/25	900/20	[72]
60Li <sub>2</sub> S-40P <sub>2</sub> S <sub>5</sub>	1000/25	1100/20	[67]
0.01Li <sub>3</sub> PO <sub>4</sub> -0.63Li <sub>2</sub> S-0.36SiS <sub>2</sub>	900/30	700/20	[70]
75Li <sub>2</sub> S-25P <sub>2</sub> S <sub>5</sub>	1600/30	1400/10	[80]

(Contd.)

**Table 8.2** (Continued)

Electrolyte composition	Initial discharge capacity ( $\text{mA h g}^{-1}$ )/temperature ( $^{\circ}\text{C}$ )	Residual discharge capacity ( $\text{mA h g}^{-1}$ )/cycles	References
Ceramic electrolyte			
$\text{Li}_{3.25}\text{Ge}_{0.25}\text{P}_{0.75}\text{S}_4$	1500/25	900/10	[69]
amorphous $\text{Li}_3\text{PS}_4$	1300/25	1200/50	[79]
60 $\text{Li}_2\text{S}$ -40 $\text{P}_2\text{S}_5$	1300/25	1300/50	[78]
$\beta$ - $\text{Li}_3\text{PS}_4$	1216/60	852/100	[76]
$\text{Li}_2\text{S}$ - $\text{P}_2\text{S}_5$	400/80	400/18	[66]
75 $\text{Li}_2\text{S}$ -25 $\text{P}_2\text{S}_5$	600/80	600/10	[81]
$\text{Li}_{3.25}\text{Ge}_{0.25}\text{P}_{0.75}\text{S}_4$	1600/25	700/30	[74]
70 $\text{Li}_2\text{S}$ -30 $\text{P}_2\text{S}_5$	300/25	250/6	[82]

### 8.4.1 Polymer Electrolytes

Polymeric electrolytes (PEs) can be classified into two categories: solid polymer electrolytes (SPEs) and gel polymer electrolytes (GPEs). In the first electrolyte system, lithium salts are dissolved in high-molecular-weight polymers containing a high concentration of Lewis base groups such as ether ( $-\text{O}-$ ), carbonyl ( $-\text{C}=\text{O}$ ), and cyano ( $-\text{C}\equiv\text{N}$ ), which serve as ligands for coordinating  $\text{Li}^+$  of the dissolved salt, thus offering the necessary solvation energy for the polymer-lithium complex formation. In GPEs, low-molecular-weight components, such as small organic solvents like tetra(ethylene glycol) dimethyl ether, DOL, carbonates, and ILs, are added as plasticizers for improving the ionic conductivity of a polymer electrolyte [54, 86–95]. The composition of the organic solvent mixture affects the gel polymer electrolyte performance.

The use of solid polymer electrolytes offers high and moderate initial discharge capacities (450–1500  $\text{mA h g}^{-1}$ ) and acceptable residual discharge capacities (Table 8.2). The biggest disadvantage of such systems is the working temperature—usually 60°C to 80°C—and the short lifetime of the cell (10–50 cycles). However, some exceptions are presented in Ref. [59]. Gel polymer electrolytes show similar cycling behavior but can be used at room temperature.

### 8.4.2 Ceramic Electrolytes

Another important class of solid electrolytes is the inorganic solid electrolytes, exhibiting higher Li-ion conductivities at operating temperature (e.g.,  $10^{-2}$  S/cm at  $25^\circ\text{C}$  for  $\text{Li}_{10}\text{GeP}_2\text{S}_{12}$ ) compared to SPEs [96]. The reported cycle life for ceramic- and polymer-based cells is mostly less than 200 cycles, while liquid-based cells could maintain more than 1000 cycles with good capacity retention (e.g., up to 1500 cycles with a specific capacity of  $168 \text{ mA h g}^{-1}$  electrode [101]). Solid electrolytes with a relatively long cycle life have been presented in recent studies; however, the cell performance at the end of the cycle life is not competitive with the liquid system.

## 8.5 Additives

Additives play a very important role in the Li-S cells. However, the spectrum of used additives is not as wide as in LiBs [13]. The most studied and used additive in the Li-S cell is lithium nitrate ( $\text{LiNO}_3$ ), which is mainly responsible for the creation and stabilization of the passive SEI layer formed on the surface of the Li anode [102, 103].

$\text{LiNO}_3$  presence in the electrolyte induces the growth of an SEI due to the oxidative nature of  $\text{LiNO}_3$  (Fig. 8.6). The so-formed SEI prevents direct contact between the polysulfides in the electrolyte

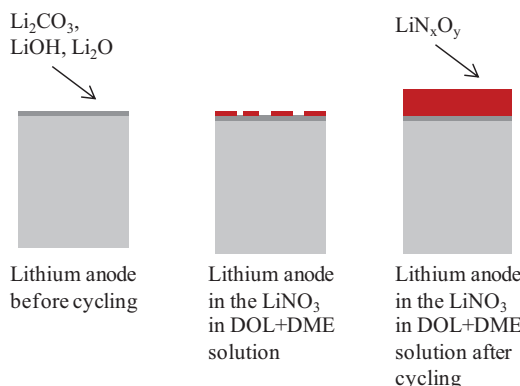


**Figure 8.6** Illustration of the surface film behavior on lithium anode cycling in different electrolyte solutions [103].

solution and the reductive species on the Li electrode. The use of  $\text{LiNO}_3$  has some disadvantages and limitations. During the first discharge,  $\text{LiNO}_3$  was found to be irreversibly reduced at the carbon surface, with a negative impact on the capacity and reversibility of the Li-S battery during subsequent cycles [104]. However, by not discharging the cell further than 1.6 V,  $\text{LiNO}_3$  reduction could be avoided. It was also recommended to use  $\text{LiNO}_3$  as a co-salt rather than as an additive since  $\text{LiNO}_3$  is continuously consumed and thus eventually depleted.

Another group of additives is phosphorous pentasulfide and polysulfides (long-chain lithium polysulfides). During the discharge/charge process, pentasulfide creates a dense and smooth passivation layer between the lithium anode and the electrolyte [105].

Cycling symmetric Li-Li and Li-S cells with 0.2 M  $\text{Li}_2\text{S}_6$  as a co-salt in 0.8 M LiTFSI DOL:DME (1/1 v/v), Xiong et al. demonstrated the

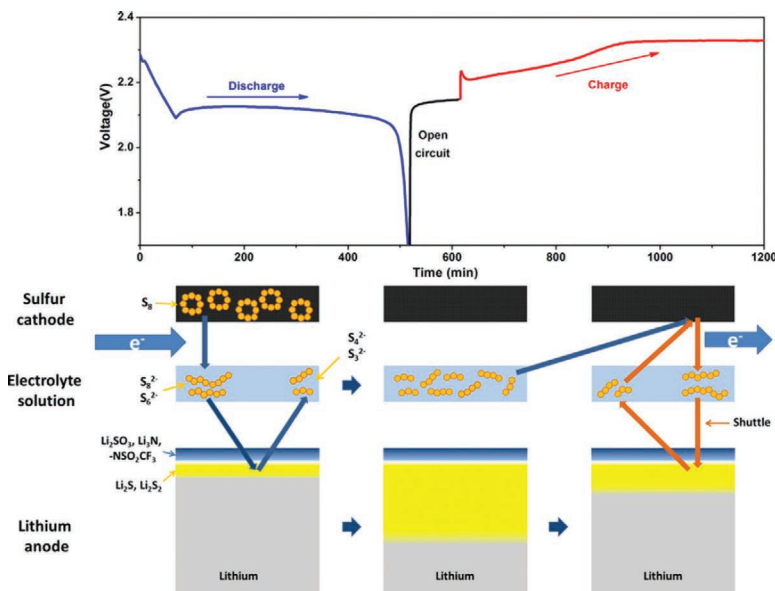


**Figure 8.7** Schematic representation of the surface film behavior on the lithium anode in a lithium-sulfur battery cycled with 0.8 M LiTFSI/0.2 M  $\text{Li}_2\text{S}_6$ /DIOX/DME (1:1 v/v). Redrawn from Ref. [106].

formation of a stable two-layer interface at the lithium metal surface [106].

The top layer consisted of decomposition products of LiTFSI, due to the initial contact with the anode, and the inner lithium sulfide layer was produced from the PS additive (Fig. 8.7). The inner layer prevented continuous reaction of the anode with LiTFSI, but the surface film did not successfully prevent the PS shuttle. However, it was suggested that the top layer could potentially be tailored to prevent the shuttle phenomenon [15, 106].

## 8.6 Summary

Li-S cells are very promising electrochemical storage systems, mainly due to their theoretical working parameters. However, they suffer too many technical issues, which should be solved before they will be commercialized. The biggest issue is related to the proper design of the electrode materials and their compatibility with the electrolyte. In the present chapter, we have focused on the main paths of electrolyte development. It was shown how important the proper choice of the electrolyte components is and how it affects cell parameters. At this moment, an ether-based liquid electrolyte (DOL/DME binary mixture with LiTFSI and LiNO<sub>3</sub> as the additive) is the most commonly used electrolyte and provides the best cell performance.

It seems that a very interesting research path in the near future will be the use of highly concentrated electrolytes, the use of novel salts like LiTDI, and proper design of the electrolyte additives. It is worth highlighting issues that are not included in the chapter but play an important role in Li-S technology—starting from the proper quantity of the used electrolyte (which is in direct correlation with the concentration of soluble polysulfides and thus cell parameters) through properly designed separators to the designing of aqueous electrolytes.

## References

1. M. Armand, J.-M. Tarascon, *Nature*, **451** (2008) 652.
2. J.-M. Tarascon, M. Armand, *Nature*, **414** (2001) 359.
3. P. G. Bruce, S. A. Freunberger, L. J. Hardwick, J.-M. Tarascon, *Nat. Mater.*, **11** (2012) 19.
4. A. Manthiram, Y. Fu, S.-H. Chung, C. Zu, Y.-S. Su, *Chem. Rev.*, **114** (2014) 11751.
5. W. Kang, N. Deng, J. Ju, Q. Li, D. Wu, X. Ma, L. Li, M. Naebe, B. Cheng, *Nanoscale*, **8** (2016) 16541.
6. J. Scheers, S. Fantini, P. Johansson, *J. Power Sources*, **255** (2014) 204.
7. M. Barghamadi, A. S. Best, A. I. Bhatt, A. F. Hollenkamp, M. Musameh, R. J. Rees, T. Rüther, *Energy Environ. Sci.*, **7** (2014) 3902.
8. Y. Zhang, Y. Zhao, K. E. Sun, P. Chen, *Open Mater. Sci. J.*, **5** (2011) 215.
9. K. Kumaresan, Y. Mikhaylik, R. E. White, *J. Electrochem. Soc.*, **155** (2008) A576.
10. C. Barchasz, J.-C. Leprêtre, F. Alloin, S. Patoux, *J. Power Sources*, **199** (2012) 322.
11. X. Ji, L. F. Nazar, *J. Mater. Chem.*, **20** (2010) 9821.
12. Y. Diao, K. Xie, S. Xiong, X. Hong, *J. Electrochem. Soc.*, **159** (2012) A421.
13. R. Dominko, M. U. M. Patel, V. Lapornik, A. Vizintin, M. Kozelj, N. N. Tušar, I. Arćon, L. Stievano, G. Aquilanti, *J. Phys. Chem. C*, **119** (2015) 19001.
14. S. S. Zhang, *J. Power Sources*, **231** (2013) 153.
15. J. Scheersa, S. Fantini, P. Johansson, *J. Power Sources*, **255** (2014) 204.
16. R. Younesi, G. M. Veith, P. Johansson, K. Edström, T. Veggea, *Energy Environ. Sci.*, **8** (2015) 1905.
17. M. Helen, M. A. Reddy, T. Diemant, U. Golla-Schindler, R. J. Behm, U. Kaiser, M. Fichtner, *Sci. Rep.*, **5** (2015) 12146.
18. T. Yim, M.-S. Park, J.-S. Yu, K. J. Kim, K. Y. Im, J.-H. Kim, G. Jeong, Y. N. Jo, S.-G. Woo, K. S. Kang, I. Lee, Y.-J. Kim, *Electrochim. Acta*, **107** (2013) 454.
19. S. Xin, L. Gu, N.-H. Zhao, Y.-X. Yin, L.-J. Zhou, Y.-G. Guo, L.-J. Wan, *J. Am. Chem. Soc.*, **134** (2012) 18510.
20. J. Wang, J. Yang, J. Xie, N. Xu, *Adv. Mater.*, **14** (2002) 963.
21. J. Fanous, M. Wegner, J. Grimminge, Ä. Andresen, M. R. Buchmeiser, *Chem. Mater.*, **23** (2011) 5024.

22. S. Zhang, K. Ueno, K. Dokko, M. Watanabe, *Adv. Energy Mater.*, **5** (2015) 1500117.
23. J. Chen, K.-S. Han, W. A. Henderson, K.-Ch. Lau, M. Vijayakumar, T. Dzwiniel, H. Pan, L. A. Curtiss, J. Xiao, K. T. Mueller, Y. Shao, J. Liu, *Adv. Energy Mater.*, **6** (2016) 1600160.
24. K. Sung Han, J. Chen, R. Cao, N. Nidhi Rajput, V. Murugesan, L. Shi, H. Pan, J.-G. Zhang, J. Liu, K. A. Persson, K. T. Mueller, *Chem. Mater.*, **29** (2017) 9023.
25. W. Weng, V. G. Pol, K. Amine, *Adv. Mater.*, **25** (2013) 1608
26. S. D. Talian, S. Jeschke, A. Vizintin, K. Pirnat, I. Arc?on, G. Aquilanti, P. Johansson, R. Dominko, *Chem. Mater.*, **29** (2017) 10037.
27. K. Xua, C. A. Angell, *J. Electrochem. Soc.*, **149** (2002) A920.
28. R. Dominko, R. Demir-Cakan, M. Morcrette, J.-M. Tarascon, *Electrochem. Commun.*, **13** (2011) 117.
29. V. S. Kolosnitsyn, E. V. Karaseva, D. Y. Seung, M. D. Cho, *Russ. J. Electrochem.*, **38** (2002) 1314.
30. S. Yoon, Y.-H. Lee, K.-H. Shin, S. B. Cho, W. J. Chung, *Electrochim. Acta*, **145** (2014) 170.
31. U. M. Patel, R. Dominko, *ChemSusChem*, **7** (2014) 2167.
32. J.-W. Park, K. Ueno, N. Tachikawa, K. Dokko, M. Watanabe, *J. Phys. Chem. C*, **117** (2013) 20531.
33. J.-W. Park, K. Yamauchi, N. Tachikawa, K. Ueno, K. Dokko, M. Watanabe, *J. Phys. Chem. C*, **117** (2013) 4431–4440.
34. K. Dokko, N. Tachikawa, K. Yamauchi, M. Tsuchiya, A. Yamazaki, E. Takashima, J.-W. Park, K. Ueno, S. Seki, N. Serizawa, M. Watanabe, *J. Electrochem. Soc.*, **160** (2013) A1304.
35. E. S. Shin, K. Kim, S. H. Oh, W. I. Cho, *Chem. Commun.*, **49** (2013) 2004.
36. S. Urbonaite, P. Novák, *J. Power Sources*, **249** (2014) 497.
37. L. Suo, Y.-S. Hu, H. Li, M. Armand, L. Chen, *Nat. Commun.*, **4** (2013) 1481.
38. J. Wang, S. Y. Chew, Z. W. Zhao, S. Ashraf, D. Wexler, J. Chen, S. H. Ng, S. L. Chou, H. K. Liu, *Carbon*, **46** (2008) 229.
39. H.-S. Ryu, H.-J. Ahn, K.-W. Kim, J.-H. Ahn, K.-K. Cho, T.-H. Nam, J.-U. Kim, G.-B. Cho, *J. Power Sources*, **163** (2006) 201.
40. H.-S. Kim, C.-S. Jeong, *Bull. Korean Chem. Soc.*, **32** (2011) 3682.
41. H. S. Kim, T.-G. Jeong, N.-S. Choi, Y.-T. Kim, *Ionics*, **19** (2013) 1795.
42. J.-W. Choi, J.-K. Kim, G. Cheruvally, J.-H. Ahn, H.-J. Ahn, K.-W. Kim, *Electrochim. Acta*, **52** (2007) 2075.

43. D. R. Chang, S. H. Lee, S. W. Kim, H. T. Kim, *J. Power Sources*, **112** (2002) 452.
44. W. Wang, Y. Wang, Y. Huang, C. Huang, Z. Yu, H. Zhang, A. Wang, K. Yuan, *J. Appl. Electrochem.*, **40** (2010) 321.
45. J. Zheng, M. Gu, H. Chen, P. Meduri, M. H. Engelhard, J.-G. Zhang, J. Liu, J. Xiao, *J. Mater. Chem. A*, **1** (2013) 8464.
46. S. S. Zhang, *Electrochim. Acta*, **97** (2013) 226.
47. J. H. Shin, E. J. Cairns, *J. Electrochem. Soc.*, **155** (2008) A368.
48. J. H. Shin, E. J. Cairns, *J. Power Sources*, **177** (2008) 537.
49. L. Wang, H. R. Byon, *J. Power Sources*, **236** (2013) 207.
50. N. Tachikawa, K. Yamauchi, E. Takashima, J. W. Park, K. Dokko, M. Watanabe, *Chem. Commun.*, **47** (2011) 8157.
51. K. Ueno, J.-W. Park, A. Yamazaki, T. Mandai, N. Tachikawa, K. Dokko, M. Watanabe, *J. Phys. Chem. C*, **117** (2013) 20509.
52. X. Judez, H. Zhang, C. Li, G. Gebresilassie Eshetu, J. A. Gonzalez-Marcos, M. Armand, L. M. Rodriguez-Martinez, *J. Electrochem. Soc.*, **165**(1) (2018) A6008.
53. D. Marmorstein, T. H. Yu, K. A. Striebel, F. R. McLarnon, J. Hou, E. J. Cairns, *J. Power Sources*, **89** (2000) 219.
54. J. H. Shin, K. W. Kim, H. J. Ahn, J. H. Ahn, *Mater. Sci. Eng. B*, **95** (2002) 148.
55. X. Zhu, Z. Wen, Z. Gu, Z. Lin, *J. Power Sources*, **139** (2005) 269.
56. S. S. Jeong, Y. T. Lim, Y. J. Choi, G. B. Cho, K. W. Kim, H. J. Ahn, K. K. Cho, *J. Power Sources*, **174** (2007) 745.
57. J. Hassoun, B. Scrosati, *Adv. Mater.*, **22** (2010) 5198.
58. X. Liang, Z. Wen, Y. Liu, H. Zhang, L. Huang, J. Jin, *J. Power Sources*, **196** (2011) 3655.
59. C. Zhang, Y. Lin, J. Liu, *J. Mater. Chem. A*, **3** (2015) 10760.
60. Q. Ma, X. Qi, B. Tong, Y. Zheng, W. Feng, J. Nie, Y. S. Hu, H. Li, X. Huang, L. Chen, Z. Zhou, *ACS Appl. Mater. Interfaces*, **8** (2016) 29705.
61. Y. Zhu, J. Li, J. Liu, *J. Power Sources*, **351** (2017) 17.
62. Y. Lin, X. Wang, J. Liu, J. D. Miller, *Nano Energy*, **31** (2017) 478.
63. X. Judez, H. Zhang, C. Li, J. A. Gonzalez-Marcos, Z. Zhou, M. Armand, L. M. Rodriguez-Martinez, *J. Phys. Chem. Lett.*, **8** (2017) 1956.
64. X. Judez, H. Zhang, C. Li, G. G. Eshetu, Y. Zhang, J. A. Gonzalez-Marcos, M. Armand, L. M. Rodriguez-Martinez, *J. Phys. Chem. Lett.*, **8** (2017) 3473.

65. A. Hayashi, T. Ohtomo, F. Mizuno, K. Tadanaga, M. Tatsumisago, *Electrochim. Commun.*, **5** (2003) 701.
66. A. Hayashi, T. Ohtomo, F. Mizuno, K. Tadanaga, M. Tatsumisago, *Electrochim. Acta*, **50** (2004) 893.
67. N. Machida, K. Kobayashi, Y. Nishikawa, T. Shigematsu, *Solid State Ionics*, **175** (2004) 247.
68. A. Hayashi, R. Ohtsubo, T. Ohtomo, F. Mizuno, M. Tatsumisago, *J. Power Sources*, **183** (2008) 422.
69. T. Kobayashi, Y. Imade, D. Shishihara, K. Homma, M. Nagao, R. Watanabe, T. Yokoi, A. Yamada, R. Kanno, T. Tatsumi, *J. Power Sources*, **182** (2008) 621.
70. T. Takeuchi, H. Kageyama, K. Nakanishi, M. Tabuchi, H. Sakaebi, T. Ohta, H. Senoh, T. Sakai, K. Tatsumi, *J. Electrochem. Soc.*, **157** (2010) A1196.
71. M. Nagao, A. Hayashi, M. Tatsumisago, *Electrochim. Acta*, **56** (2011) 6055.
72. M. Nagao, A. Hayashi, M. Tatsumisago, *Electrochim. Commun.*, **22** (2012) 177.
73. M. Nagao, A. Hayashi, M. Tatsumisago, *J. Mater. Chem.*, **22** (2012) 10015.
74. M. Nagao, Y. Imade, H. Narisawa, T. Kobayashi, R. Watanabe, T. Yokoi, T. Tatsumi, R. Kanno, *J. Power Sources*, **222** (2013) 237.
75. Z. Lin, Z. Liu, W. Fu, N. J. Dudney, C. Liang, *Angew. Chem. Int. Ed.*, **52** (2013) 7460.
76. Z. Lin, Z. Liu, N. J. Dudney, C. Liang, *ACS Nano*, **7** (2013) 2829.
77. M. Agostini, Y. Aihara, T. Yamada, B. Scrosati, J. Hassoun, *Solid State Ionics*, **244** (2013) 48.
78. H. Nagata, Y. Chikusa, *J. Power Sources*, **263** (2014) 141.
79. S. Kinoshita, K. Okuda, N. Machida, M. Naito, T. Sigematsu, *Solid State Ionics*, **256** (2014) 97.
80. T. Yamada, S. Ito, R. Omoda, T. Watanabe, Y. Aihara, M. Agostini, U. Ulissi, J. Hassoun, B. Scrosati, *J. Electrochem. Soc.*, **162** (2015) A646.
81. M. Nagao, A. Hayashi, M. Tatsumisago, T. Ichinose, T. Ozaki, Y. Togawa, S. Mori, *J. Power Sources*, **274** (2015) 471.
82. H. U. Choi, J. S. Jin, J.-Y. Park, H.-T. Lim, *J. Alloys Compd.*, **723** (2017) 787.
83. Q. Wang, J. Jin, X. Wu, G. Ma, J. Yang, Z. Wen, *Phys. Chem. Chem. Phys.*, **16** (2014) 21225.

84. K. Fu, Y. Gong, Y. Li, S. Xu, Y. Wen, L. Zhang, C. Wang, G. Pastel, J. Dai, B. Liu, *Energy Environ. Sci.*, **10** (2017) 1568.
85. X. Yu, Z. Bi, F. Zhao, A. Manthiram, *ACS Appl. Mater. Interfaces*, **7** (2015) 16625.
86. B. H. Jeon, J. H. Yeon, K. M. Kim, I. J. Chung, *J. Power Sources*, **109** (2002) 89.
87. J. R. Nair, F. Bella, N. Angulakshmi, A. M. Stephan, C. Gerbaldi, *Energy Storage Mater.*, **3** (2016) 69.
88. J. L. Wang, J. Yang, J. Y. Xie, N. X. Xu, Y. Li, *Electrochem. Commun.*, **4** (2002) 499.
89. J. Hassoun, B. Scrosati, *Angew. Chem. Int. Ed.*, **49** (2010) 2371.
90. J. Hassoun, Y.-K. Sun, B. Scrosati, *J. Power Sources*, **196** (2011) 343.
91. K. Jeddi, M. Ghaznavi, P. Chen, *J. Mater. Chem. A*, **1** (2013) 2769.
92. K. Jeddi, K. Sarikhani, N. T. Qazvini, P. Chen, *J. Power Sources*, **245** (2014) 656.
93. M. Agostini, J. Hassoun, *Sci. Rep.*, **5** (2015) 7591.
94. M. Rao, X. Geng, X. Li, S. Hu, W. Li, *J. Power Sources*, **212** (2012) 179.
95. J. Jin, Z. Wen, X. Liang, Y. Cui, X. Wu, *Solid State Ionics*, **225** (2012) 604.
96. J. C. Bachman, S. Muy, A. Grimaud, H.-H. Chang, N. Pour, S. F. Lux, O. Paschos, F. Maglia, S. Lupart, P. Lamp, L. Giordano, Y. Shao-Horn, *Chem. Rev.*, **116** (2016) 140.
97. J. H. Shin, S. S. Jung, K. W. Kim, H. J. Ahn, J. H. Ahn, *J. Mater. Sci. Mater. Electron.*, **13** (2002) 727.
98. H.-S. Ryu, H.-J. Ahn, K.-W. Kim, J.-H. Ahn, J.-Y. Lee, *J. Power Sources*, **153** (2006) 360.
99. Y. Zhang, Z. Bakenov, Y. Zhao, A. Konarov, Q. Wang, P. Chen, *Ionics*, **20** (2013) 803.
100. K. Jeddi, Y. Zhao, Y. Zhang, A. Konarov, P. Chen, *J. Electrochem. Soc.*, **160** (2013) A1052.
101. X. Liang, C. Hart, Q. Pang, A. Garsuch, T. Weiss, L. F. Nazar, *Nat. Commun.*, **6** (2015) 5682.
102. D. Aurbach, E. Pollak, R. Elazari, G. Salitra, C. S. Kelley, J. Affinito, *J. Electrochem. Soc.*, **156** (2009) A694.
103. S. Xiong, K. Xie, Y. Diao, X. Hong, *J. Power Sources*, **246** (2014) 840.
104. S. S. Zhang, *Electrochim. Acta*, **70** (2012) 344.
105. Z. Lin, Z. Liu, W. Fu, N. J. Dudney, C. Liang, *Adv. Funct. Mater.*, **23** (2013) 1064.

106. S. Xiong, K. Xie, Y. Diao, X. Hong, *J. Power Sources*, **236** (2013) 181.
107. Op cit n. 101.
108. Q. Pang, X. Liang, C. Y. Kwok, L. F. Nazar, *J. Electrochem. Soc.*, **162** (2015) A2567.
109. C. Zheng, S. Niu, W. Lv, G. Zhou, J. Li, S. Fan, Y. Deng, Z. Pan, B. Li, F. Kang, *Nano Energy*, **33** (2017) 306.
110. G. Zhou, J. Sun, Y. Jin, W. Chen, C. Zu, R. Zhang, Y. Qiu, J. Zhao, D. Zhuo, Y. Liu, *Adv. Mater.*, **29** (2017) 1603366.
111. S.-H. Chung, R. Singhal, V. Kalra, A. Manthiram, *J. Phys. Chem. Lett.*, **6** (2015) 2163.
112. W. Liu, J. Jiang, K. R. Yang, Y. Mi, P. Kumaravadivel, Y. Zhong, Q. Fan, Z. Weng, Z. Wu, J. J. Cha, *Proc. Natl. Acad. Sci.*, **114** (2017) 3578.
113. I. Gomez, D. Mecerreyes, J. A. Blazquez, O. Leonet, H. B. Youcef, C. Li, J. L. Gomez-Camer, O. Bundarchuk, L. Rodriguez-Martinez, *J. Power Sources*, **329** (2016) 72.
114. T. Mandai, K. Yoshida, K. Ueno, K. Dokko, M. Watanabe, *Phys. Chem. Chem. Phys.*, **16** (2014) 8761.
115. D. J. Eyckens, L. C. Henderson, *Front. Chem.*, **7** (2019) 263.

# Index

- acidic aqueous electrolytes 226, 239  
acid salts 226  
acid solutions 239  
activation energy 80, 111, 119, 123  
alkaline electrolytes 198, 207, 224, 243, 251, 253, 255–256  
alkaline solution 198, 232, 252  
all-phenyl complex (APC) 168–169, 176, 178, 183–184  
aluminum 7–8, 11–12, 34, 171, 174, 176, 191, 195, 197, 199–201, 203, 208, 251–253, 265  
    passivate 7, 11, 15–16  
aluminum anode 196, 253–254  
aluminum cation 195  
aluminum chloride 200  
aluminum corrosion 15–16, 252  
amorphous electrolytes,  
    overcooled 93–94  
amorphous polymer 77, 95  
anion mobility 6, 86, 306  
anions 4–6, 9–10, 13–23, 30–33, 43–49, 55–56, 59–60, 62, 74–75, 85–88, 105, 107–108, 155–156, 171, 304–306  
    imidazolate 47–48, 51  
    monovalent 22  
    multivalent 22–23  
    new 32, 45–46  
    transport of 82, 85  
anion size 5–6, 12  
anion structure 5–7, 18, 74  
anode materials 25, 71, 143, 198, 262  
APC, *see* all-phenyl complex  
aprotic solvents 64, 246, 257–258  
Aurbach group 167, 177, 250  
  
batteries 116, 118, 142, 145–146, 150, 192, 195, 197–198, 201–202, 218–219, 221, 241, 243, 249, 293–294  
    anode-based 203, 207  
    iron-air 261–262  
    secondary 152, 200–201, 247  
battery applications 45, 47, 53, 57, 64, 167, 198  
battery chemistries 148, 192  
battery electrolytes 44, 297, 301–304  
BN, *see* boron nitride  
borate 10–11, 218, 255  
boron nitride (BN) 222, 230  
  
calcium 192, 203–205, 251, 265  
capacity 4, 35, 142, 145, 157, 207, 215, 218, 225, 243, 248, 303–304, 306, 310–311  
    acceptable residual discharge 303, 305, 309  
capacity retentions 150  
catalytic properties 7, 32–33

- cathode materials 8, 90, 144, 150, 157, 173, 204, 221, 294, 296  
cathodes 7, 143–145, 169, 173, 176, 197–200, 204, 222–225, 228, 257, 260, 293–294, 297, 304, 306  
catholyte 226, 237–238, 243, 245, 259, 261, 264  
cations 5–6, 14, 16–18, 30–32, 44–46, 49, 51–53, 55, 59, 85, 109, 114–115, 118–119, 177, 304  
multivalent 192–193, 208  
titanium 113, 115  
cation transference numbers 15, 23, 45, 61, 64, 99, 109  
cell 3–4, 6–8, 27–28, 88–90, 157–158, 195–197, 199–201, 206–208, 215–216, 222, 224–225, 247, 294–297, 305–307, 309–312  
battery 111, 113, 248  
electrochemical 166, 265  
electrochemistry-based 260  
lithium-ion 142, 144, 146, 196  
lithium-sulfur 295, 307  
unit 115–116, 120  
cell designs 121, 216, 233, 237–238, 240, 265  
classical 208, 251  
cell discharge 219, 294  
cell electrolytes 202  
cell parameters 295, 305, 312  
cell performance 242, 253, 306, 310  
cell technologies 305–306  
ceramic electrolytes 27, 110–111, 113, 115, 117, 119, 121, 123, 147, 231, 307–308, 310  
ceramic materials 28, 111, 229, 231, 236, 240, 243  
ceramic separators 232, 234, 236–238, 240, 243, 245, 260  
charge carriers 30, 45, 72, 75, 80, 82, 88–89, 106, 111, 199  
charge transport 8, 78–79, 83, 87  
chemical stability 20, 24, 112, 166, 191  
chloride-based electrolytic systems 200  
composite electrolytes 75, 83, 91, 97–98, 101, 234, 307  
conduction process 74, 77–78, 82–83  
conductivity pathways 76, 78–79  
conductivity values 12–13, 25, 27, 78, 83, 92, 94, 96, 102, 109, 120, 230  
coordination ability 43–45, 47, 303  
coordination bonds 74–76, 78, 82, 86, 91  
coordination sphere 44–46, 49, 51, 56, 58  
corrosion inhibitors 208, 251–253, 265  
crystalline materials 44, 73  
crystalline structures 46–47, 50, 52, 55, 60, 65, 144  
crystal structure analysis 46–49, 61–62  
crystal structures 44, 48, 50–51, 54, 59, 61, 66, 112–114, 119, 123, 143  
cubic phase 118–119  
cubic phase stabilization 123  
CV, *see* cyclic voltammetry  
cyclic voltammetry (CV) 172, 177, 182  
decomposition energy 121–122  
dielectric constant 24–25, 29, 74  
discharge 4, 6, 35, 155, 199, 217, 226, 229, 232, 236, 238, 245, 294, 298–301, 307–309  
discharge cycles 90

- discharge products 222, 225, 238, 243–244, 246, 252  
dissociation process 74–75, 108
- EC, *see* ethylene carbonate  
EES, *see* electrochemical energy storage  
electrochemical energy storage (EES) 293  
electrochemical parameters 23, 31, 43, 45, 48, 54, 65–66, 183 better 47–48  
electrochemical performance 145, 150, 200, 227, 234, 243, 266 superior 243, 253  
electrochemical processes 248, 260  
electrochemical properties 14, 16, 44, 152, 154, 174, 191–192, 203  
electrochemical reactions 194, 223, 251, 260, 266  
electrochemical stability 8, 12, 16, 20, 24, 30–32, 72, 95, 100, 105–106, 156, 173, 194, 219, 221 good 96, 185  
electrode components 7  
electrode reactions 6, 91, 143, 157, 192, 194, 197, 223, 258  
electrode surface 6, 89, 221  
electrolyte additives 312  
electrolyte applications 31  
electrolyte components 155, 194, 306, 312  
electrolyte composition 194, 197–198, 205, 244, 255  
electrolyte composition temperature 298–301, 307–309  
electrolyte conductivity 4, 31  
electrolyte decomposition 6–7, 157  
electrolyte design 24–25, 27, 29, 33, 296  
electrolyte development 195, 294, 312  
electrolyte formulations 148, 223, 257  
electrolyte layer 71, 115  
electrolyte/lithium electrode interface 221  
electrolyte materials 110, 112 prospective ceramic 114 solid 121  
electrolyte/metallic electrode interface 195  
electrolyte modification 217, 249  
electrolyte properties 24, 192  
electrolyte solutions 166, 175, 219, 225, 310 best 193 complex ethereal 168 current organic 145 organic 247  
electrolyte system first 309 proper 206  
electrolyte systems 44, 174, 183  
electrolyte viscosity 25, 152  
electron-withdrawing groups 18–20, 31, 109, 171  
EMC, *see* ethyl-methyl carbonate  
energy 4, 80–81, 142, 191, 236, 261 binding 5, 171 lower cation-anion interaction 155  
energy barriers 76, 79–80, 82  
energy density 4, 223–225, 248  
energy storage, electrochemical 293  
ethylene carbonate (EC) 12, 24–26, 28–30, 106, 146–149, 152, 202, 204, 218, 238–239, 241, 251, 257, 297, 304

- ethylene oxide 27, 44, 72, 153, 221, 307  
ethyl-methyl carbonate (EMC) 25–26, 29–30, 35, 149, 241
- fluorine 5–7, 15–16, 20, 155  
free volume 81–82, 85  
functional groups 107–108, 153
- gel electrolytes 73, 75, 153  
gel polymer electrolyte (GPEs) 77, 147, 152, 309  
gel polymer electrolytes 77, 147, 152, 309  
gel-type electrolytes 109, 249  
glass transition temperature 24, 76, 78, 82–83, 92, 94–95, 100  
GPEs, *see* gel polymer electrolyte  
grain boundaries 99, 119, 233
- heterocyclic anions 43, 46–47, 49, 51, 54, 56–57, 59, 64–66  
coordination properties of 65  
high conductivity 14, 34, 72, 99–100, 106, 123, 156, 199  
high ionic conductivity 73, 92, 99, 112, 115, 118, 121, 148, 194, 228, 233  
hybrid electrolytes 235, 239, 259  
hybrid sodium-air cells 243  
hybrid systems 228, 236–237, 240, 242–243  
hydrogen atoms 21–22, 217  
hydrogen evolution 197, 199, 206–207, 256–257  
hydrogen fluoride 7, 15
- imidazolium cations 32, 50–51
- imide 9–10, 12, 14, 17, 22–23, 44, 88, 151, 153, 170, 202, 219, 221–222, 246, 258  
imide salts 32, 248  
inorganic structures 30, 77–78, 91, 98, 100–101  
interactions 5, 7, 16, 18, 72, 75, 92, 98, 108, 155, 194, 249, 304–305  
ion-ion 77–78, 86–87, 101, 103, 105  
interfacial resistivity 229–230, 233  
interfacial stability, chemical 229  
ionic conductivity 3, 5, 19, 21, 28, 72–74, 77, 79, 93–94, 96–100, 102–104, 109–113, 119, 147–148, 151–154  
low 14, 23, 87, 152, 185  
total 21, 33  
values of 78, 83–84, 95, 107, 109, 239
- ionic liquids 50, 73, 75, 77–78, 86, 89, 101, 105–106, 108–109, 146, 151–152, 176, 183, 200, 202
- ion transport 33, 45, 72, 74–79, 81, 94–97, 99, 102, 105–106, 195
- LAGP, *see* lithium aluminum germanium phosphate  
Li anode 235, 237, 240, 310  
Li cations 115, 119  
Li-ion batteries 24, 101, 142, 148  
Li-ion cell electrolytes 32  
Li-ion cell research 9, 11  
Li-ion cells 4, 7–9, 12–14, 16–18, 26, 31, 33, 73–74, 92, 105  
electrolytes for 16, 30–31, 34  
electrolytes in 4, 106  
new generations of 15, 18

- liquid electrolytes 15–16, 30, 46, 65, 74, 110, 116, 122, 144, 147–148, 151–152, 296–299, 301, 303, 305–306
- lithium 9–10, 12–13, 16–17, 19, 45–47, 64–65, 86–88, 104–105, 107–108, 114–115, 141–144, 146–147, 191–192, 217, 265
  - metallic 113, 115, 118, 208, 227, 293–294, 296
- lithium-air 33
- lithium-air batteries 110, 221, 223, 225, 235
  - high-capacity 115, 121
- lithium aluminum germanium phosphate (LAGP) 229–230, 232, 234, 236–237
- lithium anode 15, 231, 235, 310–311
- lithium batteries 71, 221
- lithium cation coordination 55, 97
- lithium cations 14, 17–20, 49–57, 59, 62, 75, 82, 85, 87–88, 91–92, 96–97, 103, 107, 109, 116
  - transport of 4, 86
- lithium coordination sphere 57, 61
- lithium dissociation 108
- lithium electrode 90, 100, 219–220, 227
- lithium electrolytes 176
  - organic 257
- lithium-ion 3, 43, 66, 71, 141, 165, 191, 215, 293
- lithium-ion batteries 146, 293
- lithium-ion battery electrolytes 51
- lithium-ion conductivities 227, 235
- lithium ions 74, 78, 85–88, 98, 105, 109, 114, 123, 149
  - transport of 77–78, 87
- lithium lanthanum titanates 114–115
- lithium loss 120–121
- lithium metal 184, 215, 227–228
- lithium polysulfides 294, 296, 306
- lithium resources 141–142
- lithium salts 3–4, 31–32, 56–58, 64, 66, 72–77, 85, 87, 90, 92, 96, 102–103, 105, 218–219, 265–266
  - amount of 91, 96
  - dissociation of 13, 95, 98
  - high concentrations of 32, 44
  - multivalent 22–23
  - precipitation of 89, 102
- lithium systems 147–149, 157
- lithium transference numbers 85–88, 296
- lithium transport 86, 235–236
- local electrolyte structure 45–46, 63, 65
- lower conductivities 12, 28, 147, 305
  
- MACC, *see* magnesium aluminum chloride complex
- magnesium 165–167, 169, 171, 183, 191–192, 203, 248–249, 261, 265
  - electrodeposition of 167, 185
  - metallic 166–167, 248
- magnesium aluminum chloride complex (MACC) 175–176, 180, 250
- magnesium anodes 166, 169, 248
- magnesium batteries 166, 173, 175, 185
  - electrolytes for 165
- magnesium deposition 177, 184–185
- magnesium electrolytes 177, 183
- magnesium salts 166, 171

- magnitude 76, 88–89, 92, 100, 103, 105–106, 117, 123–124, 229–230, 247, 304
- materials 72, 76–79, 82, 84, 88, 97–98, 100–101, 105–106, 111–112, 114–115, 119–122, 142–143, 231, 234, 254
- active 6–7, 198, 218, 295
- polymeric 74, 111
- melting point 24–25, 28–30, 32, 93, 95–96, 103
- molar ratio 51, 53, 64, 199–202
- Na-ion batteries 142
- Na-ion cells 34, 147–148
- nanowires 98–99
- NaOH aqueous solutions 243, 261
- new electrolytes 169, 171, 296
- new generations 15, 18, 20
- nitrile groups 20, 47, 49, 55–56, 58, 62, 65–66, 96, 220
- nitriles 24, 27, 218, 220, 222, 226
- nitrogen 5, 7, 16–17, 155
- nitrogen atoms 17, 20–21, 48–49, 55–56, 58, 62, 96
- nonaqueous electrolytes 166, 199, 227, 235, 250–251, 266
- novel cell designs 111, 207
- novel electrolyte compositions 226
- oligomeric salts 107, 109
- organic acids 225–226, 257
- organic electrolytes 101, 112, 152, 217, 237, 241, 257, 304
- organic solvents 74–75, 89, 110, 148, 150, 201–202, 218, 222, 236, 250, 257, 294, 297, 304, 309
- common 294
- PC, *see* propylene carbonate
- perfluoroalkyl groups 17, 48–49
- perovskite structure 114–115
- PEs, *see* polymeric electrolytes
- PLD, *see* pulsed laser deposition
- polyelectrolytes 74, 87, 90, 107–109
- polymer chains 73, 76–79, 82–83, 86–87, 91, 96, 100, 102–103, 106, 108–109, 221
- segmental motions of 76, 78, 81
- polymer electrolytes 28, 72–75, 77, 79, 81–83, 86, 88–90, 96–98, 100, 105, 153, 157, 217, 221, 309
- polymeric electrolytes (PEs) 207–208, 217, 257, 309
- Polymer systems 88, 94, 110, 207
- polymer matrix 27, 54, 61, 64–65, 73, 75, 77–78, 83, 85–87, 92, 96–97, 106, 219, 221
- polysulfides 34, 264, 294, 296, 302–305, 310–311
- solubility of 304, 306
- polysulfide species (PS) 294–295, 312
- potassium 191, 203, 246–248, 265
- potassium metal 246–247
- propylene carbonate (PC) 13–14, 25–26, 28–29, 34, 57–58, 91, 147–148, 152, 154, 202–203, 218, 240–241, 247, 251, 257
- protective layer 219, 221, 227, 230–231
- PS, *see* polysulfide species
- pulsed laser deposition (PLD) 123–125
- quantitative models 79, 81, 83
- rechargeable batteries 153, 255

- research groups 9, 102, 166, 173, 175, 250, 254
- room temperature 23, 25, 27–28, 30–31, 33, 74–75, 106–107, 109, 111–113, 116–119, 147, 153–154, 233, 235, 261
- room temperature ionic liquids (RTILs) 200, 221, 246, 257–258
- RTILs, *see* room temperature ionic liquids
- salt complexes 93, 102–103
- salt concentration 28–29, 45–46, 64, 154, 219, 251, 305
- saturated calomel electrode (SCE) 199
- SCE, *see* saturated calomel electrode
- SIBs, *see* sodium-ion batteries
- side chains 5, 92, 94
- sodium 59, 141–146, 148–154, 156–157, 191–192, 203, 242–246, 264–265
- sodium cations 57–59, 64, 66, 112
- sodium cells 143–144, 157–158
- sodium citrate 252
- sodium-ion batteries (SIBs) 58, 66, 141–152, 154, 156–158
- sodium salts 45, 47, 57–60, 64, 66, 148
- solid electrolyte interface formation 144
- solid polymer electrolytes (SPEs) 15, 22, 91, 93, 95, 97, 99, 101, 103, 105, 107, 109, 245, 247, 309–310
- solid-state batteries 71, 112, 118, 121, 125, 235
- solid-state electrolytes 110–111, 122, 125, 227, 240, 260
- ceramic 112, 227
- solvent mixtures 3, 6, 12, 15, 19, 24–26, 28, 30, 34, 148, 248, 302
- solvent molecules 24, 32, 45–46, 49, 65, 109, 194, 217
- space group 114, 116, 119, 230
- SPEs, *see* solid polymer electrolytes
- stable electrolyte system 258
- structural analysis 50, 52, 55–56, 64, 66
- structural motifs 46, 48, 51, 55–56, 58, 64–65
- structural studies 45, 57, 154
- temperature 7–8, 14, 27–29, 56, 62, 76, 80–81, 83, 99, 110, 112, 120, 152, 174
- high 7, 27, 34, 76, 116, 120–121, 123
- low 28, 35, 150
- temperature range 28, 95, 103, 152, 261–262
- tetrahedral sites 116, 119
- thermal stability 4–5, 8, 21, 25, 148, 150, 152, 154, 219, 221–222, 253
- thin films 123, 227, 229
- transference numbers
- high 21, 54
- higher lithium cation 20–22
- high lithium 86–87, 102
- high lithium cation 19, 21
- low lithium cation 12, 15
- units 108–109, 218, 242
- energy conversion 241–242
- vapor pressure 24–25, 150

- WCAs, *see* weakly coordinating anions  
weakly coordinating anions (WCAs) 171, 176
- X-ray diffraction (XRD) 20, 167, 170, 232
- XRD, *see* X-ray diffraction
- zinc 191–193, 206–208, 254–257, 259–260, 265  
zinc-air batteries  
  rechargeable 255  
  secondary 254–255  
zinc salts 257